

CESRL REPORT NO. 77-2

OCTOBER 1977

**THE DESIGN AND BEHAVIOR OF BEAM-
COLUMNS IN UNBRACED STEEL FRAMES**

by

TOKUL KANCHANALAI

AISI PROJECT NO. 189
COLUMN DESIGN IN UNBRACED FRAMES
REPORT NO. 2

DEPARTMENT OF CIVIL ENGINEERING / Structures Research Laboratory
THE UNIVERSITY OF TEXAS AT AUSTIN



THE DESIGN AND BEHAVIOR OF BEAM-COLUMNS
IN UNBRACED STEEL FRAMES

by

Tokul Kanchanalai

This work has been carried out as a part of an investigation
sponsored by the American Iron and Steel Institute,
Project No. 189

Department of Civil Engineering
The University of Texas at Austin
Austin, Texas 78712

October 1977

Report No. 2

A C K N O W L E D G M E N T S

The research project whose results are reported herein was sponsored by the American Iron and Steel Institute. The guidance of the project advisory committee (R. Bjorhovde, W. Hansell, W. LeMessurier, L. Lu, J. Springfield) is greatly appreciated. The testing program was conducted at the Civil Engineering Structures Research Laboratory, Balcones Research Center, The University of Texas at Austin.



A B S T R A C T

Design methods for beam-columns in unbraced frames were investigated both theoretically and experimentally. Theoretical studies were conducted to determine the strength of the beam-columns in symmetrical portal frames and frames containing some columns with pinned connections (leaned frames). The variables in the studies were the slenderness ratio, the relative column-to-beam stiffness, the effect of bending axis, the effect of the residual stress, and the effect of axial load on the pinned-end column in leaned frames. Exact interaction curves were developed for these cases. The results obtained were used as the basis for the comparison with design interaction equations. Three full size two-bay unbraced frames were tested to study the interaction of beam-columns within a frame. The first two specimens were subjected to column loads only and the third specimen was tested under the combined gravity and lateral load.

Another set of tests was conducted to study the spatial behavior and the strength of restrained beam-columns in unbraced frames where there is no experimental data currently available. Three full size biaxially loaded restrained beam-column specimens were tested under the loading and support conditions simulating the actual condition in unbraced frames. The test results were compared with a theoretical prediction and design interaction equations.

The studies indicate that a proposed interaction equation provides an accurate prediction of the strength of a beam-column in planar unbraced frames. The method was also verified by comparing the predicted value with the frame test results. The test results on biaxially loaded restrained beam-columns are in good agreement

with the theoretical prediction. It was found that the current design methods are satisfactory for columns subjected to uniform moment but are very conservative for moment gradient cases. Based on the theoretical and experimental investigation in this study, recommendations for the design of beam-columns in unbraced frames are outlined.

C O N T E N T S

Chapter		Page
1	INTRODUCTION	1
	1.1 Behavior of Structural Frames under Loads . .	2
	1.2 Previous Studies on the Strength and Design of Beam-Columns in Braced Frames	4
	1.2.1 In-plane Behavior	4
	1.2.2 Lateral Torsional Buckling Behavior . .	10
	1.2.3 Biaxial Behavior	17
	1.2.4 Summary	21
	1.3 Previous Studies on the Strength and Design of Beam-Columns in Unbraced Frames	22
	1.3.1 General Review	22
	1.3.2 Present Design Procedures for Columns in Unbraced Frames	25
	1.3.3 Summary	32
	1.4 Scope	32
	1.5 Objective	33
2	THEORETICAL STUDIES	35
	2.1 General	35
	2.2 Method of the Analysis	36
	2.3 Results on the Strength of Beam-Columns in Unbraced Frames	41
	2.4 Discussion of Analytical Results	43
	2.5 Second Order Analysis of Example Frames . . .	46
	2.5.1 Exact Second Order Analysis	47
	2.5.2 P-delta Method of Analysis	49
	2.5.3 Effective Length Approach	52
	2.5.4 Comparison of Second Order Moments . .	54
	2.6 Allowable Stresses and Factor of Safety . . .	55
	2.7 Evaluation of Design Interaction Equations . .	57
	2.8 Effect of the Axial Load Due to the Overturning Effect	62
3	EXPERIMENTAL PROGRAMS	64
	3.1 Design of Test Specimens and Loading Conditions	64
	3.1.1 Unbraced Frame Specimens	65
	3.1.2 Biaxially Loaded Restrained Beam-Columns	67

Chapter	Page
3.2 Material and Member Properties	69
3.2.1 Tension Tests	69
3.2.2 Cross Section Properties	69
3.2.3 Stub Column Tests	70
3.2.4 Residual Stress Measurements	71
4 TWO-BAY UNBRACED FRAMES	72
4.1 Test Setup	72
4.1.1 Details of Test Specimens	72
4.1.2 Loading Apparatus	73
4.2 Instrumentation	74
4.3 Controlled Test	75
4.4 Test Procedures and Test Results	77
4.4.1 Specimen F1	77
4.4.2 Specimen F2	79
4.4.3 Specimen F3	81
4.5 Discussion of Test Results	83
4.5.1 Theoretical Analysis	83
4.5.2 Analytical Model of Test Specimens	84
4.5.3 Behavior of Test Specimens	85
4.6 Comparison of Test Results with Design Equations	90
5 BIAXIALLY LOADED RESTRAINED BEAM-COLUMNS	94
5.1 Test Setup	94
5.1.1 Details of Test Specimens	94
5.1.2 Loading Apparatus	95
5.2 Instrumentation	99
5.3 Controlled Test	101
5.4 Test Procedures and Test Results	102
5.5 Analysis of Test Data	110
5.5.1 Axial Force	110
5.5.2 Displacement	111
5.5.3 Moments at a Cross Section	111
5.6 Discussion of Test Results	114
5.6.1 Theoretical Prediction	114
5.6.2 Analytical Model of Test Specimens	114
5.6.3 Behavior of Test Specimens	116
5.7 Comparison of Test Results with Design Equations	122
6 SUMMARY AND RECOMMENDATIONS	129
6.1 Summary	129
6.2 Design Recommendations	132
6.3 Recommendations for Future Study	135

Chapter	Page
TABLES	137
FIGURES	148
APPENDIX A MOMENT-THRUST-CURVATURE RELATIONSHIPS	292
BIBLIOGRAPHY	294



L I S T O F T A B L E S

Table		Page
1.1	Elastic Second Order Moments in No-Sway Beam-Columns	138
3.1	Mill Material Properties	139
3.2	Summary of Steel Used and Material Testing	139
3.3	Summary of Tension Tests	140
3.4	Member Properties	141
3.5	Summary of Stub Column Tests	142
4.1	Test Results and Theoretical Prediction of Frames Subjected to Gravity Loads	143
4.2	Test Results and Theoretical Prediction of Frame Subjected to Combined Gravity and Lateral Loads	143
4.3	Comparison of Test Results with Design Methods	144
4.4	Contribution of Axial Load and Moment Terms in the Interaction Equations	144
5.1	Characteristics of Restrained Beam-Column Specimens	145
5.2	Test Results and Theoretical Predictions of Restrained Beam-Columns	145
5.3	Comparison of Test Results with Design Methods (Specimens Treated as No-Sway Beam-Columns)	146
5.4	Contribution of Axial Load and Moment Terms in the Interaction Equations	146

Table

Page

5.5	Comparison of Test Results with AISC Method and Effective Length Method (Specimens Treated as Sway Beam-Columns)	147
5.6	Comparison of Test Results with Springfield's Recommendation (Specimens Treated as Sway Beam-Columns)	147

L I S T O F F I G U R E S

Figure	Page
1.1 Load-displacement of a frame	149
1.2 P-delta effect	149
1.3 Behavior of frames under gravity load	150
1.4 Lateral-torsional buckling of beam-columns	151
1.5 Ketter's chart for elastic second order moments in no-sway pinned-end columns	152
1.6 Second order moments in no-sway columns	152
1.7a Elastic second order analysis of no-sway restrained beam-columns (double curvature)	153
1.7b Elastic second order analysis of no-sway restrained beam-columns (single curvature)	153
1.8 Factors to account for the effect of moment gradient on elastic lateral torsional buckling strength of beams	154
1.9 Leaned frame system	154
1.10 Approximate procedure for determining the tangent modulus	155
1.11 Comparison of second order moments at the ultimate strength of beam-columns	155
2.1 Portal frame	156
2.2 Leaned frame	156
2.3 Elastic-plastic stress-strain relationship	156
2.4 Idealized residual stress pattern	156

Figure	Page
2.5	Geometry and compatibility 157
2.6	Equilibrium of portal frame 157
2.7	Moment-rotation relationship of beam with antisymmetrical bending 157
2.8	Equilibrium of leaned frame 157
2.9	Moment-rotation of beam with one end pinned 157
2.10	Moment-thrust-curvature relationship, strong axis bending 158
2.11	Moment-thrust-curvature relationship, weak axis bending 158
2.12	Typical shear resistance-sway relationship of beam-columns in portal frames (strong axis bending) 159
2.13	Typical shear resistance-sway relationship of beam-columns in portal frames (weak axis bending) 160
2.14a	P-delta effect at the maximum strength of beam-columns (strong axis bending) 161
2.14b	P-delta effect at the maximum strength of beam-columns (weak axis bending) 162
2.15a	Maximum strength of beam-columns in portal frames ($G = 0$, strong axis bending) 163
2.15b	Maximum strength of beam-columns in portal frames ($G = 0$, weak axis bending) 164
2.16a	Maximum strength of beam-columns in portal frames ($G = 3$, strong axis bending) 165
2.16b	Maximum strength of beam-columns in portal frames ($G = 3$, weak axis bending) 166
2.17	Effect of axis of bending 167
2.18a	Effect of residual stress ($L_c/r = 40$, strong axis bending) 168

Figure	Page
2.18b Effect of residual stress ($L_c/r = 40$, weak axis bending)	169
2.19a Effect of residual stress ($L_c/r = 60$, strong axis bending)	170
2.19b Effect of residual stress ($L_c/r = 60$, weak axis bending)	171
2.20a Maximum strength of beam-columns in leaned frames ($G = 0$, $L_c/r = 20$, strong axis bending)	172
2.20b Maximum strength of beam-columns in leaned frames ($G = 0$, $L_c/r = 20$, weak axis bending)	173
2.21a Maximum strength of beam-columns in leaned frames ($G = 0$, $L_c/r = 30$, strong axis bending)	174
2.21b Maximum strength of beam-columns in leaned frames ($G = 0$, $L_c/r = 30$, weak axis bending)	175
2.22a Maximum strength of beam-columns in leaned frames ($G = 0$, $L_c/r = 40$, strong axis bending)	176
2.22b Maximum strength of beam-columns in leaned frames ($G = 0$, $L_c/r = 40$, weak axis bending)	177
2.23a Maximum strength of beam-columns in leaned frames ($G = 0$, $L_c/r = 60$, strong axis bending)	178
2.23b Maximum strength of beam-columns in leaned frames ($G = 0$, $L_c/r = 60$, weak axis bending)	179
2.24a Maximum strength of beam-columns in leaned frames ($G = 2$, $L_c/r = 20$, strong axis bending)	180
2.24b Maximum strength of beam-columns in leaned frames ($G = 2$, $L_c/r = 20$, weak axis bending)	181
2.25a Maximum strength of beam-columns in leaned frames ($G = 2$, $L_c/r = 30$, strong axis bending)	182
2.25b Maximum strength of beam-columns in leaned frames ($G = 2$, $L_c/r = 30$, weak axis bending)	183

Figure	Page
2.26a Maximum strength of beam-columns in leaned frames ($G = 2$, $L_c/r = 40$, strong axis bending)	184
2.26b Maximum strength of beam-columns in leaned frames ($G = 2$, $L_c/r = 40$, weak axis bending)	185
2.27a Maximum strength of beam-columns in leaned frames ($G = 2$, $L_c/r = 60$, strong axis bending)	186
2.27b Maximum strength of beam-columns in leaned frames ($G = 2$, $L_c/r = 60$, weak axis bending)	187
2.28 Axial load-shear stiffness relationship	188
2.29 Salem's solutions for elastic stability of leaned frames	188
2.30 Effect of G on the stability of leaned frames . . .	189
2.31 Equilibrium of beam-column as a free body	189
2.32 Methods for determining second order moments . . .	190
2.33 Comparison of second order moments ($G = 0$, $L_c/r = 20$)	191
2.34 Comparison of second order moments ($G = 0$, $L_c/r = 30$)	192
2.35 Comparison of second order moments ($G = 0$, $L_c/r = 40$)	193
2.36 Comparison of second order moments ($G = 0$, $L_c/r = 60$)	194
2.37 Comparison of second order moments ($G = 2$, $L_c/r = 20$)	195
2.38 Comparison of second order moments ($G = 2$, $L_c/r = 30$)	196
2.39 Comparison of second order moments ($G = 2$, $L_c/r = 40$)	197
2.40 Comparison of second order moments ($G = 2$, $L_c/r = 60$)	198

Figure	Page
2.41 Column curves	199
2.42a Comparison of theoretical results with design interaction equations ($G = 0$, $L_c/r = 20$, strong axis bending)	200
2.42b Comparison of theoretical results with design interaction equations ($G = 0$, $L_c/r = 20$, weak axis bending)	201
2.43a Comparison of theoretical results with design interaction equations ($G = 0$, $L_c/r = 30$, strong axis bending)	202
2.43b Comparison of theoretical results with design interaction equations ($G = 0$, $L_c/r = 30$, weak axis bending)	203
2.44a Comparison of theoretical results with design interaction equations ($G = 0$, $L_c/r = 40$, strong axis bending)	204
2.44b Comparison of theoretical results with design interaction equations ($G = 0$, $L_c/r = 40$, weak axis bending)	205
2.45a Comparison of theoretical results with design interaction equations ($G = 0$, $L_c/r = 60$, strong axis bending)	206
2.45b Comparison of theoretical results with design interaction equations ($G = 0$, $L_c/r = 60$, weak axis bending)	207
2.46a Comparison of theoretical results with design interaction equations ($G = 2$, $L_c/r = 20$, strong axis bending)	208
2.46b Comparison of theoretical results with design interaction equations ($G = 2$, $L_c/r = 20$, weak axis bending)	209
2.47a Comparison of theoretical results with design interaction equations ($G = 2$, $L_c/r = 30$, strong axis bending)	210

Figure	Page
2.47b Comparison of theoretical results with design interaction equations ($G = 2$, $L_c/r = 30$, weak axis bending)	211
2.48a Comparison of theoretical results with design interaction equations ($G = 2$, $L_c/r = 40$, strong axis bending)	212
2.48b Comparison of theoretical results with design interaction equations ($G = 2$, $L_c/r = 40$, weak axis bending)	213
2.49a Effect of variable factors of safety, AISC method ($G = 0$, $L_c/r = 40$, strong axis bending)	214
2.49b Effect of variable factors of safety, AISC method ($G = 0$, $L_c/r = 40$, weak axis bending)	215
2.50a Effect of variable factors of safety, P-delta method ($G = 0$, $L_c/r = 40$, strong axis bending)	216
2.50b Effect of variable factors of safety, P-delta method ($G = 0$, $L_c/r = 40$, weak axis bending)	217
2.51a Effect of variable factors of safety, effective length method ($G = 0$, $L_c/r = 40$, strong axis bending)	218
2.51b Effect of variable factors of safety, effective length method ($G = 0$, $L_c/r = 40$, weak axis bending)	219
2.52 Effect of beam length on maximum strength curves	220
2.53 Effect of axial load definitions on maximum strength curves	221
2.54 Typical comparison of design interaction equations for beam-columns in frames with finite beam length	222
3.1 Test arrangement	223
3.2 Two-bay frame buckling in braced and unbraced modes	224
3.3 Selection of L_c/r and G for unbraced frame specimens	225

Figure	Page
3.4 Test program for unbraced frames	226
3.5 Selection of biaxially loaded restrained beam-column specimens	227
3.6 Test program for biaxially loaded restrained beam-columns	228
3.7 Stub column test results	229
3.8 Residual stress patterns	231
4.1 General view of test setup	232
4.2 Beam-to-column connection details	232
4.3 Knife edge support of interior column	233
4.4 Loading system for exterior columns	233
4.5 Tension load cells for exterior columns	234
4.6 Lateral loading system	234
4.7 Instrumentation diagram	235
4.8 Results of Euler test on column C1A	236
4.9 Load-deflection relationship of Specimen F1	237
4.10 Specimen F1 after failure	237
4.11 Variation of column moments with axial loads (Specimen F1)	238
4.12 Variation of beam moments with axial loads (Specimen F1)	240
4.13 Load-deflection relationship of Specimen F2	241
4.14 Yielded zone at midlength region of interior column of Specimen F2	241
4.15 Variation of column moments with axial loads (Specimen F2)	242

Figure	Page
4.16 Variation of beam moments with axial loads (Specimen F2)	245
4.17 Variation of joint rotations with axial loads (Specimen F2)	247
4.18 Load-deflection relationship of Specimen F3	249
4.19 Specimen F3 after failure	250
4.20 Yielded zone at south joint of interior column of Specimen F3	250
4.21 Variation of column moments with lateral load (Specimen F3)	251
4.22 Variation of beam moments with lateral load (Specimen F3)	254
4.23 Analytical models of frame specimens	256
4.24 Typical ΣP -H relationships for Specimen F1 using a limit load technique	257
4.25 Comparison of test and predicted results	258
4.26 Comparison of test and predicted results (nondimensionalized forms)	259
5.1 General view of test setup	260
5.2 End view of test specimens	261
5.3 Components for joint fabrication	261
5.4 Joint fabrication process	262
5.5 End fixtures, exploded view	262
5.6 Column end showing end fixture assembly	263
5.7 Gravity load simulator	263
5.8 Movement of top pin of simulator during sway	264
5.9 Mechanism for preventing twist at the midlength section	264

Figure	Page
5.10 Joint loading apparatus	265
5.11 Dial gage arrangement for measuring displacements .	265
5.12 Instrumentation diagram	266
5.13 Results of Euler test on Specimen BC-1	267
5.14 Load-displacement relationship at the midlength (Specimen BC-1)	268
5.15 Variation of column moments with axial force (Specimen BC-1)	269
5.16 Variation of restraining moments with axial force (Specimen BC-1)	270
5.17 Deflected shapes of Specimen BC-1 at the maximum load	270
5.18 Load-displacement relationship at the midlength (Specimen BC-2)	271
5.19 Variation of column moments with loads (Specimen BC-2)	273
5.20 Variation of restraining moments with loads (Specimen BC-2)	274
5.21 Deflected shapes of Specimen BC-2 at the maximum load	275
5.22 Load-displacement relationship at the midlength (Specimen BC-3)	276
5.23 Variation of column moments with loads (Specimen BC-3)	278
5.24 Variation of restraining moments with loads (Specimen BC-3)	280
5.25 Deflected shapes of Specimen BC-3 at the maximum load	281
5.26 Specimen BC-1 after failure	282
5.27 Specimen BC-2 after failure	282

Figure	Page
5.28 Yielded zone at south joint after failure, Specimen BC-2	283
5.29 Yielded zone at north joint after failure, Specimen BC-2	283
5.30 Yielded zone at midlength after failure, Specimen BC-2	284
5.31 Yielded zone at south joint after failure, Specimen BC-3	284
5.32 Axial force in test specimen	285
5.33 Displacement components of a cross section	285
5.34 Moments at a cross section in untwist and twist coordinates	286
5.35 Comparison of column moments based on the equilibrium and strain data analysis (Specimen BC-1)	287
5.36a Comparison of test and predicted results (Specimen BC-1)	289
5.36b Comparison of test and predicted results (Specimen BC-2)	290
5.36c Comparison of test and predicted results (Specimen BC-3)	291

N O M E N C L A T U R E

A	= area of cross section
a_1, a_2, a_3	= undetermined coefficients in the equation for determining the strain on a plane surface
B	= flange width
B_1	= amplification factor for end moment arising from loading that does not cause sway
B_2	= amplification factor for end moment arising from loading that causes sway
b	= distance between dial gages across the flange of biaxially loaded restrained beam-column specimens
b_o	= distance parallel to the strong axis of the cross section measured from the weak axis to the point of contact with dial gages
C_b	= factor applied to the uniform critical moment of a beam to account for the moment gradient for the lateral torsional buckling behavior
C_c, C'_c	= the slenderness ratio corresponding to the start of inelastic buckling
C_m, C_{mx}, C_{my}	= factor applied to the larger end moment in a beam-column to account for the moment gradient for the in-plane behavior
C_w	= warping constant of cross section
c	= half depth or half width of cross section, for bending about the strong or weak axis, respectively
c_i	= distance of the center of element i from the centroidal axis of cross section
D	= depth of cross section
d	= distance between dial gages across the web of biaxially loaded restrained beam-column specimens
d_o	= distance parallel to the weak axis of cross section measured from the strong axis to the point of contact with dial gages
d_1, d_2, d_3, d_4	= dial gage readings at flange tips of biaxially loaded restrained beam-column specimens

E	= Young's modulus of elasticity
E_{st}	= strain hardening modulus
E_t	= tangent modulus
F	= axial force in beam-columns
F_a, F'_a	= allowable buckling stress for centrally loaded columns (the prime denotes the quantity being based on the effective length factor; otherwise it is based on the actual column height)
F_b, F_{bx}, F_{by}	= allowable bending stress of member considered as a beam
$F_{b,cr}$	= allowable critical bending stress for lateral torsional buckling of member considered as a beam
F_{cr}	= buckling stress, not including the factor of safety
F_e, F_{ex}, F_{ey}	= Euler buckling stress, based on the actual column height, divided by the factor of safety
F'_e	= Euler buckling stress, based on the effective slenderness ratio in a sway mode, divided by the factor of safety
F_{rc}	= maximum compressive residual stress in the flanges
F_y	= yield strength of material
f_a	= computed axial stress
f_b, f_{bx}, f_{by}	= computed bending stress
G	= modulus of elasticity in shear = relative column-to-beam stiffness
G_e	= modified relative column-to-beam stiffness to account for inelasticity of columns
H, H_x, H_y	= applied wind load (x and y denote the strong and weak directions, respectively)
I, I_b, I_c	= moment of inertia of cross section (subscripts b and c denote beam and column, respectively)
I_y	= moment of inertia about the weak axis of cross section
i	= index
J	= torsional constant of cross section
K	= effective length factor
K_b, K_c	= stiffness factor = EI/L (subscripts b and c denote beam and column, respectively)

- K_s = elastic first order sway stiffness of an unbraced bent
 \bar{K}_{si} = elastic first order sway stiffness contributed by column "i" in an unbraced bent
 L, L_b, L_c = length of member (subscripts b and c denote beam and column, respectively)
 L'_c = half of the total length of beam-column specimens
 M = first order end moment
 M^* = second order end moment
 M_1 = smaller first order end moment
 M_{1x}, M_{1y} = moments at the joint of biaxially loaded restrained beam-column specimens (x and y indicate that the moments are about the strong and weak axes, respectively)
 M_2 = larger first order end moment
 M_{2x}, M_{2y} = moments at the midlength of biaxially loaded restrained beam-column specimens (x and y indicate that the moments are about the strong and weak axes, respectively)
 M_{AB}, M_{BA} = moment at end A and end B, respectively, of member AB in a slope deflection equation
 M_b, M_c = end moments in beam and column, respectively, in the inelastic analysis of unbraced portal frames and leaned frames
 M_{cr} = critical moment of beam, accounting for the moment gradient, due to lateral torsional buckling
 M_{cr}^* = elastic critical moment of beam, in pure bending, due to lateral torsional buckling
 M_{end}^* = second order end moment for which a girder and a connection in unbraced frames should be designed
 M_{eq} = equivalent uniform moment in beam-column, for the lateral torsional buckling behavior
 M_{js}, M_{jw} = applied joint moments about the strong and weak axes, respectively, of biaxially loaded restrained beam-column specimens
 M_m = inelastic critical moment of beam, in pure bending, due to lateral torsional buckling

- M_{NS} = first order end moment due to loading which does not cause sway
- M_p = plastic moment capacity
- M_{pc}, M_{pcx}, M_{pcy} = reduced plastic bending strength, due to the presence of axial load
- M_{px}, M_{py} = plastic moment capacity about the strong and weak axes of section, respectively
- M_{rx}, M_{ry} = moments in restraining beams, in the strong and weak directions, respectively, of biaxially loaded restrained beam-column specimens
- M_{SW} = first order end moment due to loading which causes sway
- M_t = torsional moment
- M_x = first order moment, about the strong axis of member
 = moment about the strong axis in the x-y system of coordinates, transformed from M_ξ and M_η
- M_y = first order moment, about the weak axis of member
 = moment about the weak axis in the x-y system of coordinates, transformed from M_ξ and M_η
 = moment corresponding to first yield = $\eta S \sigma_y$
- M_η = moment about the weak axis in the ξ - η system of coordinates
- M_ξ = moment about the strong axis in the ξ - η system of coordinates
- m = moment nondimensionalized by M_p
- n = integer
- P = applied axial load
- P_1, P_2 = applied axial load on rigidly jointed column and on pinned-end column, respectively
- P_{cr} = buckling strength of column based on the actual height
- P'_{cr} = buckling strength of column based on the effective length factor
- P^*_{cr} = buckling strength, accounting for inelasticity of column, determined by applying the ratio of the tangent modulus at a particular level of axial load to the modulus of elasticity, to P'_E

- P_E, P_{Ex}, P_{Ey} = Euler load (x and y indicate that the buckling loads are about the strong and weak axes, respectively)
- P'_E, P'_{Ex}, P'_{Ey} = elastic buckling load based on the effective length factor (x and y indicate that the buckling loads are about the strong and weak axes, respectively)
- P_s, P_w = stub loads in the strong and weak directions, respectively, of biaxially loaded restrained beam-column specimens
- P_y = axial load at complete yielding of cross section
- P = axial load nondimensionalized by P_y
- q = ratio of the smaller to the larger first order end moments
- R_s, R_w = forces in the restraining bars, in the strong and weak directions, respectively, of biaxially loaded restrained beam-column specimens
- r, r_x, r_y = radius of gyration of cross section (subscripts x and y denote the strong and weak axes, respectively)
- S = elastic section modulus
- S_1, S_2, S_3 = stability functions accounting for the reduction of stiffness due to axial load in the slope deflection equations
- s, s_s = displacement of centroid and the average displacement of flange tips of cross section, respectively, in the strong direction with respect to the untwist coordinates, measured from the unloaded position of biaxially loaded restrained beam-column specimens
- V = shear resistance of the rigidly jointed column in leaned frames
- V_2 = shear resistance required for the stability of leaned column
- V_i = shear resistance contributed by column i in an unbraced bent
- w, w_s = displacement of centroid and the average displacement of flange tips of cross section, respectively, in the weak direction with respect to the untwist coordinates, measured from the unloaded position of biaxially loaded restrained beam-column specimens

Z	= plastic section modulus
α	= ratio of the axial load on leaned column to the axial load on the rigidly jointed column
β	= twist of cross section about the centroid measured from the unloaded position of biaxially loaded restrained beam-column specimens = a parameter defined as $\beta = L_c \sqrt{P/EI_c}$
Δ	= sway deflection at the column top in portal frames and leaned frames = deflection at the midlength of columns in unbraced frame specimens, measured from the unloaded position
Δ_o	= sway at the column top in portal frames and leaned frames determined by a first order elastic analysis
Δ_{el}	= sway at the column top in portal frames and leaned frames determined by a second order elastic analysis
Δ_i, Δ_{i-1}	= sway at the column top in portal frames and leaned frames during the i^{th} and the $i-1^{\text{th}}$ iterations of a second order elastic analysis
ΔA_i	= incremental area i of cross section
ϵ	= strain
ϵ_i	= strain at element i of cross section
ϵ_o	= strain at the centroid of cross section
ϵ_{ri}	= residual strain at element i of cross section
ϵ_{st}	= strain at the start of strain hardening
ϵ_y	= strain at first yielding
η	= exponent on the moment terms in Chen's strength-type interaction equation
η_i	= distance along the weak axis, in the ξ - η system of coordinates, to a point on cross section
$\theta, \theta_b, \theta_c$	= end rotation (subscripts b and c denote beam and column, respectively)
θ_A, θ_B	= rotation at end A and end B of a member in a slope-deflection equation
θ'	= angle between a tangent to the top of the column and the chord connecting the ends of column
$\lambda_1, \lambda_2, \lambda_3$	= ratios of the actual factor of safety to the basic factor of safety of 1.67

ν	= factor applied to moment terms in Pillai's interaction equation
ξ	= exponent on the moment terms in Chen's stability-type interaction equation
ξ_i	= distance along the strong axis, in the ξ - η system of coordinates, to a point on cross section
Σ	= symbol for summation
σ_i	= normal stress at element i of cross section
σ_{rc}	= maximum compressive residual stress in the flanges
σ_{rt}	= maximum tensile residual stress in flanges, uniform tensile cooling stress in web
σ_u	= ultimate strength of material
σ_y	= static yield strength of material
τ	= ratio of the tangent modulus to Young's modulus of elasticity
ϕ	= curvature nondimensionalized by the curvature at initial yielding, ϕ_y
$(\phi_x)_{av}$	= average curvature about the strong axis, determined from the measured strain data in biaxially loaded restrained beam-column specimens
ϕ_y	= curvature corresponding to first yielding of cross section
$(\phi_y)_{av}$	= average curvature about the weak axis, determined from the measured strain data in biaxially loaded restrained beam-column specimens



CHAPTER 1

INTRODUCTION

In modern steel buildings, the structural frame serves to support the load which is transmitted from the functional elements of the structure. The load acting on the structure may be classified as the static gravity force arising from the dead load and the live load and the dynamic force due to wind or earthquake. The latter is usually acting laterally and for design purposes is considered as an equivalent static load applied at the joints. The applied load on the building is resisted by the frame which is an assemblage of beams and columns interconnected at the joints. Beams are the members which resist the load primarily in bending. On the other hand, columns carry predominantly the axial load transmitted from the beams and may also carry bending moments arising from unbalanced gravity load or from the wind load.

A frame may be classified as braced or unbraced. Braced frames are ones in which the resistance to the lateral load and the lateral stiffness are provided by the vertical bracing system containing diagonal X or K bracing and/or shear walls. It is usually assumed that bending moments are not introduced into the frame by the lateral loads. The other class of frames called unbraced frames do not contain any lateral supporting system and must rely on the bending stiffness of the columns and beams to resist the load and to provide the lateral stiffness of the frames.

Braced and unbraced frames may be further classified as planar or space frames. A planar frame is constrained to deform in the plane of the frame by the out-of-plane bracing; in this case,

all the connections in the perpendicular direction to the plane of the frame are flexible connections so that no bending moment can be transmitted to the columns. The space frame behavior arises if the girder-to-column connections in the out-of-plane direction are rigid. In this case, the columns are subjected to combined gravity load and biaxial moments. The sway movement of the joints in the out-of-plane direction depends on the presence of bracing in that direction.

1.1 Behavior of Structural Frames under Loads

The response of a planar frame can be described by referring to a load-displacement relationship, as shown in Fig. 1.1. The frame is subjected to the gravity and lateral loads applied proportionally. A point on the load displacement curve represents an equilibrium configuration of the frame. As the load increases, the axial force and moments increase. The increase in bending moment is due to two effects; the first part arising from the applied load is called primary moment whereas the second part, called the secondary moment, is attributed to the effect of the axial force acting through the deflected shape of the columns in braced frames or through the relative displacement of the joints in unbraced frames (see Fig. 1.2). For loading below the elastic limit, the frame will return to the undeformed state if the loads are removed. As the load increases beyond the elastic limit, yielding occurs at some location in the frame which results in a reduction in the stiffness of the frame. This causes the deflection to increase at a faster rate than the load until the maximum load is reached. Beyond the maximum load, the P-delta effect is significantly increased and the frame has to unload to maintain the equilibrium. This type of failure is called in-plane inelastic instability and commonly occurs in a frame that carries high axial

load^{18*} in which the P-delta effect is significant.

Two other extreme modes of failure of a frame are mechanism failure and frame buckling. The former occurs in a frame which carries low axial load and relatively high beam loads. In this case, moment redistribution takes place after the first plastic hinge has formed in a highly stressed region. As the load increases, more plastic hinges develop until the frame fails as a mechanism. Frame buckling, on the other hand, occurs in a symmetrical frame subjected to symmetrical gravity load. Figure 1.3 shows the load displacement characteristics of braced and unbraced frames subjected to gravity load with and without the presence of primary bending moment.

As discussed above, for braced and unbraced frames subjected to high axial load, failure is generally due to in-plane instability of the beam-columns and usually occurs before the plastic strength of the frame is attained. Another kind of instability of a beam-column may occur when it is not fully braced laterally. When the load is increased to the critical level, lateral torsional buckling may occur before the in-plane instability is reached. The beam-column which has been deflecting in the plane of the frame starts to move laterally and is accompanied by twist of the cross section (Fig. 1.4). A more general case is for an unbraced space frame; in this case, the beam-column may sway in any direction. If the frame is loaded in the strong plane, there is the possibility that, at the critical load, lateral torsional buckling of a beam column may occur which is analogous to sidesway buckling of an unbraced planar frame. If the space frame is loaded in a proportional manner, a joint will start to displace obliquely from the beginning of loading. The failure of a beam-column may be due to instability with combined deflection and twist of the member along the column height. In addition to inelastic instability and lateral torsional buckling,

*Superscript numbers indicate references in the Bibliography.

local buckling of the plate element of the cross section may be the cause of failure of the member and the frame. However, this phenomenon usually takes place when the moment approaches the plastic moment. For beam-columns subjected to high axial load, inelastic instability and lateral torsional buckling are the more general causes of failure.

Any form of instability reduces the maximum strength and the ductility of the frame. In the plastic design method, where the maximum load of the frame is of interest, beam-columns must be designed so that instability does not occur before the strength of the frame is attained. On the other hand, in the allowable stress design method, the maximum strength of a member corresponds to the limit of structural usefulness. This may be attributed to instability in the beam-column or a plastic hinge having formed in a beam with some partial redistribution of moment beyond the first hinge. Therefore, for economic consideration, beam-columns should be designed so that instability does not occur before the beam reaches its plastic strength. Instability of beam-columns is caused by the P-delta effect and yielding which is more significant in an unbraced frame than in a braced frame. This study is concerned with the design of columns in unbraced frames. However, the next sections will discuss the previous work relating to the strength and design of columns in both braced and unbraced frames.

1.2 Previous Studies on the Strength and Design of Beam-Columns in Braced Frames

1.2.1 In-plane Behavior. There have been extensive theoretical studies on the strength of isolated beam-columns and these studies were summarized by Johnston.²⁸ The problems of pinned-end columns loaded with equal end moments and with the moment applied at one end were studied by Galambos and Ketter.¹⁹ The method of solution was based on integrating the moment-thrust-curvature

relationship using a Newmark integration scheme to satisfy the equilibrium and boundary conditions. The effect of residual stress was considered and the results were presented in the form of interaction curves relating the axial force and the applied end moment which causes instability. The analytical results were compared with the available test results and the approximate interaction equations. Additional study on similar problems was conducted by Ketter.³⁰ Analytical results were obtained for columns subjected to equal and unequal end moments with the ratio varying from $-1.0 < q < 1.0$ (q is the ratio of the smaller end moment to the larger end moment, being positive when the end moments cause the column to bend in single curvature). In addition to the loading condition with end moments, the solution of pinned-end columns subjected to a concentrated load at midspan was also studied. All the results were presented in the form of interaction curves. Within the elastic limit, Ketter also developed the expression for determining the maximum elastic second order moment within the span of the member for various ratios of end moments and this was presented in the form of a chart (see Fig. 1.5). This figure shows the variation of the amplification factor as the ratio P/P_E increases (P_E is the Euler load). The amplification factor is the ratio of the maximum second order moment within the span of the member to the larger end moment.

In 1960, Ojalvo⁴⁶ developed a method to determine the strength of beam-columns based on the restrained column theory. The response of the column subjected to end moments was presented in the form of end moment-end rotation curves and the nomograph⁴⁷ and the ultimate strength tables of these beam-columns were also available.²⁰

Besides the loading with unequal end moments, beam-columns that are subjected to a concentrated load at the midspan and to uniformly distributed load with both ends pinned or fixed were solved by Lu and Kamalvand⁴⁰ using the restrained column theory technique.

The results were presented in the form of interaction curves between the axial force and the ultimate lateral load. Chen¹⁰ has conducted further studies on pinned-end beam-columns subjected to equal end moments and a concentrated lateral load. The solutions were obtained for wide flange columns bent about the strong and the weak axes with and without the presence of residual stresses.

All the studies discussed except Lu and Kamalvand's study⁴⁰ have considered only isolated beam-columns with simply supported ends, while columns in real structures occur as part of the frame. Levi, Driscoll, and Lu³⁵ studied the strength of columns in continuous frames which led to the subassemblage method of plastic design for no-sway frames. In this method the response of the joint is constructed from the response of the columns and the restraining beams based on equilibrium of moments and compatibility of the joint rotation. The strength of the subassemblage is adequate if the resisting moment of the joint is larger than the applied joint moment.

With regard to experimental studies, there were extensive tests on eccentrically loaded beam-columns with equal and unequal end moments. Part of these results has been used to compare with the theoretical studies.¹⁹ Tests on restrained beam-columns were conducted by Lay and Galambos³³ to verify the validity of the subassemblage method. The column was subjected to a constant axial load and increasing joint moments. All the specimens were bent in single curvature and the results confirmed the validity of the subassemblage method. Experiments on restrained columns subjected to a constant axial load and a concentrated lateral load were conducted by English and Adams¹⁴ and Carpenter.⁹ The test results were compared with the theoretical prediction using the elastic-plastic method of analysis and with the design interaction equations. The comparison was found to be in good agreement. Sheninger and Lu⁵⁵ conducted tests on no-sway subassemblages with three-story

continuous columns. The loading was designed so that the middle column was bent in single and double curvatures.

The strength of isolated beam-columns in the previous theoretical studies was generally presented in the form of interaction curves which relate the axial force and the end moment at failure for a given slenderness ratio. The in-plane failure results from inelastic instability or due to the plastic strength being reached. The failure is controlled by instability when the maximum moment occurs within the span of the member for a beam-column subjected to end moments. In this case, as the axial load increases, the moment will increase due to the P-delta effect. As yielding takes place, the stiffness of the member reduces which causes the column to deflect further and this results in a larger P-delta moment. On the other hand, for the loading that causes the maximum moment to occur at the end of the beam-column, there is no P-delta effect and the member can develop its maximum plastic strength, M_{pc} , at the end. Regardless of which type of failure occurs, the column must have been loaded into the inelastic range resulting in an extensive degree of yielding.

For design application, interaction equations provide a convenient means of expressing the relationship between the axial load and the moment. To apply this method for the design of an isolated column, the second order moment is estimated from the end moment and is then checked with the interaction equations:²⁸

$$\frac{P}{P_{cr}} + \frac{M^*}{M_p} = 1.0 \quad (1.1)$$

where

$$M^* = \frac{C_m}{1 - \frac{P}{P_E}} M \quad (1.2)$$

and

$$\frac{P}{P_y} + \frac{0.85 M}{M_p} = 1.0 \quad (1.3)$$

In Eqs. 1.1 and 1.3, P and M are the axial load and the larger end moment ; P_{cr} is the buckling strength of the column; P_y is the yield load; and M_p is the fully plastic strength. Equation 1.3 controls when M^* occurs at the end; that is, $M^* = M$ (see Fig. 1.6). In fact, Eq. 1.3 implies that the end cross section develops the reduced plastic hinge capacity. It is noted that Eq. 1.2 has been derived initially for an elastic beam-column subjected to equal end moments causing the column to bend in single curvature. In this case, C_m can be expressed more accurately as $C_m = 1 + 0.23P/P_E$; ⁴ however, it is considered to be unity in most design specifications. For columns subjected to unequal end moments, $C_m = 0.6 + 0.4 q$. In the current AISC Specification, ¹ a limit of C_m to be not less than 0.4 is specified. The comparison of the predicted second order moments determined from Eq. 1.2 with the chart derived from the exact elastic second order analysis ³⁰ is shown in Fig. 1.5 for various ratios of end moments. It may be seen that the predicted second order moment is conservative for double curvature and is unconservative for single curvature. Therefore, the limitation of $C_m \nless 0.4$ for $q < - 0.5$ (double curvature) yields the predicted second order moment to be more conservative for the in-plane behavior. In fact, this limit applies for lateral torsional buckling (to be discussed later). In Fig. 1.5 it may also be noted that for columns subjected to unequal end moments, the maximum moment occurs at the end of the member (i.e., $M^* = M$) at low level of the axial load.

The accuracy of interaction equation 1.1 has been compared with theoretical analysis and experimental results and it was found that it predicts the actual strength accurately. ²⁸ It should be observed that M in Eqs. 1.1 and 1.3, as well as in the interaction curves, ^{19,30} is the end moment at failure. Therefore, for the structure that is designed by the plastic design method, these two

equations can also be used to check the strength of the column. In fact, Eqs. 1.1 and 1.3 are recommended by the current AISC Specification for the plastic design procedure (Sec. 2.4) with Eq. 1.1 modified to take into account the possibility of lateral torsional buckling.

In a braced frame that is designed by the allowable stress design method, the column end moments are obtained from a first order analysis of the frame at the service load level. The current AISC Specification (Sec. 1.6) recommends the use of Eqs. 1.1 and 1.3 written in the allowable stress forms as

$$\frac{f_a}{F_a} + \frac{C_m f_b}{\left(1 - \frac{f_a}{F_e}\right) F_b} \leq 1.0 \quad (1.4)$$

$$\frac{f_a}{0.6F_y} + \frac{f_b}{F_b} \leq 1.0 \quad (1.5)$$

Usually for no sway columns, the buckling strength, F_a , and F_e in Eq. 1.4 are based on the actual column height ($K = 1.0$). The determination of the second order bending stress

$$\frac{C_m f_b}{1 - f_a/F_e}$$

is based on the assumption that the first order bending stress f_b does not change as axial load is applied. In fact, as the axial load on the column increases, the column end moment is reduced. A study on the amplification factor for restrained no sway columns subjected to joint moments and for columns with different boundary conditions subjected to lateral load was conducted⁶⁹ and some results are shown in Fig. 1.7 and Table 1.1. It can be seen that for restrained columns the column end moment, M , decreases as the axial load increases and the girder moment increases; this is different from an unrestrained column where the column end moment remains

constant. The amplification factor gives a reasonable prediction of the maximum second order column moment if P_E is based on the effective length ($K < 1.0$). Therefore, using P_E based on the actual column height overestimates the extent of the elastic second order moment. For restrained columns loaded laterally, both the end moment and the interior moment increase due to the P-delta effect; in the cases studied, the moment at the end is the maximum. This is in contrast with the simply supported beam-column where the interior moment always controls.

The buckling strength P_{cr} in Eq. 1.1 is based on the actual column height. However, for restrained columns, the buckling strength increases due to the effect of restraint. It is felt that using P_{cr} based on $K = 1$ does not change the result significantly. The slenderness ratio of columns commonly encountered is in the range that buckling occurs inelastically. In this zone the buckling strength is not very sensitive to the effective length factor. Therefore, the design of no sway columns according to the allowable stress design method with the use of Eqs. 1.4 and 1.5, is generally conservative.

1.2.2 Lateral Torsional Buckling Behavior. When a beam-column is bent about its strong axis and is laterally unbraced, lateral torsional buckling may occur before the in-plane plastic strength is attained. The theoretical and experimental research that is available considered only the cases of no sway columns. The early theoretical work on the elastic lateral torsional buckling was attributed to Timoshenko⁶⁰ who derived the differential equations and solved the problem of a beam-column subjected to equal end moments. The ends of the column were simply supported with respect to bending and torsion. Salvadori^{52,53} applied the energy method to solve beams and beam-columns of I cross section subjected to equal and unequal end moments. The effect of weak axis restraint was also investigated. It was found that the difference in the

elastic critical moment due to the effect of weak direction restraint was not significant for all column lengths and end moment ratios under consideration, except for the complete double curvature ($q = -1$) case where the weak axis restraint increases the critical moment appreciably.

The elastic critical moment of I shape beams subjected to uniform moment may be expressed as⁶⁰

$$M_{cr}^* = \frac{\pi}{KL} \sqrt{EI_y GJ + \frac{\pi^2}{(KL)^2} EI_y EC_w} \quad (1.6)$$

where G = modulus of elasticity in shear, J = torsional constant, and C_w = warping constant.

Based on Salvadori's study, the critical moment for beams subjected to other ratios of end moments causing a straight line, moment gradient is larger than the case of uniform moment and this may be determined from

$$M_{cr} = C_b M_{cr}^* \quad (1.7)$$

where C_b is a modifying factor. Salvadori found that C_b is fairly constant for most of the practical length and the degree of weak axis restraint and depends mainly on the end moment ratio of the beam. C_b may be expressed as

$$C_b = 1.75 - 1.05q + 0.3q^2 \leq 2.5 \quad (1.8a)$$

or

$$C_b = \frac{1}{0.6 + 0.4q} \leq 2.5 \quad (1.8b)$$

The relationship between C_b and q is shown in Fig. 1.8. The dashed and broken curves correspond to the maximum and the minimum values of C_b considering the various combination of length and boundary conditions. It may be seen that for $q > 0$, C_b has a single relationship. However, for $q < 0$, C_b is sensitive to the length and the condition of support in the lateral direction. The solid curve

appears to be the average values of C_b in the double curvature range. It may be seen that the limit 2.5 in Eq. 1.8 is the average value of C_b for $-1.0 < q < -0.5$. The AISC Specification specifies this limit to be 2.3, which corresponds to the minimum value of C_b in this range.

Salvadori's study of elastic lateral torsional buckling was also extended to beam-columns and the results were presented in the form of interaction curves between the axial load and the larger first order end moment for various ratios of $q (= M_1/M_2)$. It was well understood that for beam-columns with the I shape cross sections, the compressive stress reduces the torsional rigidity of the member which is commonly known as the Wagner effect.²⁵ Salvadori took this into consideration when he compared two sets of solutions in which the Wagner effect was and was not considered. The relationship of the axial load and the larger end moment at the onset of lateral torsional buckling was reasonably proportional for most values of q when the Wagner effect is considered. Massonnet⁴² also studied the elastic lateral torsional buckling of beam-columns subjected to unequal end moments using the energy method as Salvadori did. He recommended the following interaction equation, based on Salvadori's and his results:

$$\frac{P}{P'_{Ey}} + \frac{M_{eq}}{M_{cr}^* \left(1 - \frac{q+1}{2} \frac{P}{P_E}\right)} = 1.0 \quad (1.9)$$

In Eq. 1.9, P'_{Ey} is the elastic buckling strength based on the effective slenderness ratio ($K < 1.0$) about the weak axis of the member; and M_{cr}^* is the elastic critical moment of the member considered as a beam and subjected to uniform moment. M_{eq} is the equivalent uniform first order moment about the strong axis of the member and the factor

$$\frac{1}{1 - \left(\frac{q+1}{2}\right) \frac{P}{P_E}}$$

is intended to account for the action of the axial load acting through the transverse deflection prior to buckling. This factor is empirically adjusted for the moment gradient by introducing $(q+1)/2$ as the coefficient of P/P_E . Massonnet has recommended that the equivalent moment factor may be expressed as

$$\frac{M_{eq}}{M_2} = \sqrt{0.3(1 + q^2) + 0.4q} \quad (1.10)$$

It has been shown that M_{eq}/M_2 in Eq. 1.10 is very close to the reciprocal of Salvadori's expression for C_b (Eq. 1.8).

The interaction equation for elastic lateral torsional buckling given by Eq. 1.9 was confirmed by tests conducted by Hill and Clark.²⁵ Aluminum column specimens were tested with equal end eccentricity about the strong axis. The boundary conditions were pinned about the strong axis and fixed about the weak axis. All specimens failed by lateral torsional buckling at a stress below the proportional limit. From the experimental study, it was evident that the Wagner effect was significant and must be considered in the theoretical prediction. The test results were found to be in good agreement with the predicted strength using Eq. 1.9 (with $q = 1.0$ and $M_{eq} = M$) when the P-delta effect prior to buckling was accounted for.

The theoretical studies and the design equation discussed were limited to elastic lateral torsional buckling. In real structures, a member may fail by lateral torsional buckling after partial yielding has occurred in the member as a result of in-plane bending; this is called inelastic lateral torsional buckling. Galambos¹⁶ and Fukumoto¹⁵ have investigated the problems of wide flange columns subjected to equal end moments and one end moment respectively. In their studies, the effect of residual stress was considered and the member ends were simply supported with respect to the strong axis and the weak axis and warping was

permitted. The critical moment at the onset of lateral torsional buckling was based on the tangent modulus theory. More extensive theoretical studies on inelastic lateral torsional buckling of beam-columns with single span and three span continuous columns were conducted.³⁷ The critical moment was predicted based on the tangent modulus and the reduced modulus theories and the post buckling strength was also determined. The parameters included in the study were the effect of weak axis bending and warping restraints and the end moment ratios. It was found that the presence of warping restraint slightly improves the critical moment of the columns with pinned ends about the strong axis. The effect of weak axis bending restraint is not significant for columns with $L/r_x < 60$; however for longer columns, the weak axis restraint may increase the critical moment appreciably. It was observed that short columns with $L/r_x < 40$ may develop a larger degree of post buckling strength.

The strength of beam-columns which fail by lateral torsional buckling in the inelastic range was given by Massonnet⁴² and may be expressed in the form

$$\frac{P}{P'_{cr}} + \frac{M_{eq}}{\left(1 - \frac{P}{P_E}\right) M_m} = 1.0 \quad (1.11)$$

Equation 1.11 is similar in form with the previous Eq. 1.9 except for the terms P'_{cr} and M_m . The coefficient, $\frac{q+1}{2}$, for P/P_E was removed for simplicity, being on the conservative side. Massonnet suggested that P'_{cr} be based on the largest slenderness ratio considering the effective length factor and using the tangent modulus buckling load. For steel columns, the basic column strength defined by CRC, which includes the effects of residual stresses can be used to calculate P'_{cr} . The critical moment M_m , being the inelastic

lateral buckling strength of a beam under pure bending may be determined as the product of the inelastic critical stress and the plastic section modulus.

Equation 1.11 has been compared with test results on I-shape columns subjected to unequal end moments which failed by inelastic lateral torsional buckling.⁴² The comparison was found to be reasonable and Eq. 1.11 predicted results which were mostly on the safe side. Galambos in his discussion to the paper by Massonnet made a comparison between Eq. 1.11 and his exact analysis on columns of W8x31 and W14x142 shapes with the slenderness ratios varying from $20 < L/r_x < 120$.¹⁶ For these cases, Eq. 1.11 predicted more conservative results as L/r_x increased.

Lay, Aglietti and Galambos³⁴ conducted a series of tests on unrestrained unbraced beam-columns and one restrained unbraced specimen. The axial load was applied and held constant while the joint loading was increased until failure occurred. The test result on the restrained unbraced column was compared with the similar specimen which was braced to prevent lateral torsional buckling. There was a 15 percent reduction in the unbraced column end moment at failure. The comparison of the test results with the prediction from Eq. 1.11 was also examined. In the comparison, P'_{cr} was computed from the CRC basic column strength curve based on the largest effective slenderness ratio. The results were found to be in good agreement.

The AISC Specification recommends Eq. 1.11 for the design of no-sway unbraced beam-columns for plastic design, but it is written in the form

$$\frac{P}{P_{cr}} + \frac{C_m M}{\left(1 - \frac{P}{P_E}\right) M_m} \leq 1.0 \quad (1.12)$$

In this equation $C_m = 0.6 + 0.4q$, but not less than 0.4. Austin⁴ examined the C_m factor which was used in conjunction with the in-plane behavior and found a close relationship with Massonnet's expression for the equivalent moment factor and with the reciprocal of Salvadori's C_b factor if the limit 0.4 is imposed. The determination of P_{cr} is based on CRC basic column strength considering the largest slenderness ratio ($K = 1$) and M_m is based on the straight line critical moment of the beam under pure bending and is expressed as

$$M_m = \left(1.07 - \frac{\frac{L}{r} \sqrt{F_y}}{3160}\right) M_p \quad (1.13)$$

It should be noted that Eq. 1.12 controls when the maximum second order moment occurs within the span of the member. When the maximum moment occurs at the end, AISC recommends the design to be based on Eq. 1.3.

For the allowable stress design method, Yura⁶⁹ recommended the same form of the equation to be used irrespective of where the maximum second order moment occurs. These equations may be expressed as

$$\frac{f_a}{F_a} + \frac{C_m f_b}{\left(1 - \frac{f_a}{F_e}\right) F_{b,cr}} = 1.0 \quad \begin{array}{l} \text{(maximum} \\ \text{moment} \\ \text{within span)} \end{array} \quad (1.14)$$

$$\frac{f_a}{F_a} + \frac{f_b}{C_b F_{b,cr}} = 1.0 \quad \begin{array}{l} \text{(maximum} \\ \text{moment at} \\ \text{end)} \end{array} \quad (1.15)$$

where F_a is the critical stress based on the largest slenderness ratio and F_e is the elastic Euler stress about the strong axis.

1.2.3 Biaxial Behavior. As discussed earlier, in a no-sway space frame, the gravity load on the beams which are framed rigidly to the columns in the strong and weak axes causes biaxial moments in the column in addition to the axial load. Up to the present time, most of the theoretical and experimental researches have been conducted on isolated pinned-end columns subjected to eccentrically applied load about the strong and the weak axes. Chen and Santathadaporn¹¹ summarized the previous research prior to 1968. The ultimate capacity of wide flange columns subjected to biaxial eccentric loadings was studied at New York University by Birnstiel and Michalos.⁶ The theory was improved to reduce the amount of work necessary to obtain a solution by Harstead, Birnstiel and Leu.²⁴ Columns were assumed to be initially straight and untwisted. Residual stress present prior to loading and strain reversal were considered in the study. The end cross sections may be either free to warp or prevented from warping. The results show that in one example, the end warping restraint increases the ultimate load by 12 percent. The residual stress was found to have a significant influence on the deformational response and the ultimate carrying capacity of the columns. Marshall and Ellis⁴¹ and Pillai and Ellis⁵⁰ have presented the results of the ultimate load capacity of eccentrically loaded tubular columns. Santathadaporn and Chen⁵⁴ have used the tangent stiffness method to analyze biaxially loaded columns with end rotational restraints. The initial curvature of the column and the presence of residual stress were taken into account. Milner and Gent^{23,44} presented both analytical and experimental studies on no-sway restrained columns subjected to initial beam loads and an increase in axial load. The effect of strain hardening, strain reversal, and consideration of torsional moment were studied in the analysis and verified with the experimental investigation; however, the effect of residual stress was not taken into account. It is concluded that strain

hardening and strain reversal must be considered in the analysis if a reliable estimate of the collapse load is to be obtained. The effect of torsional moment is found to be not significant. Vinnakota⁶¹ mentioned that he has developed a computer program capable of solving biaxially loaded beam-columns with rotational, directional, and torsional end restraints. Recently Mitchell⁴⁵ has developed a method of analysis using three-dimensional discrete element models to analyze biaxially loaded beam-columns. Rotational, directional, and torsional restraints may be input at the ends of the member and along the nodes within the member; therefore, sway columns may be analyzed. However, the effects of residual stress, strain reversal, and the end warping restraint are not considered. The internal torsional moment is assumed to be proportional to the St. Venant torsional rigidity only.

There have not been many experimental studies on the behavior of biaxially loaded restrained beam-columns. Most of the available tests were limited to only study the behavior and strength of beam-columns of H and I shaped sections subjected to biaxially eccentric load.^{7,12,31} Some experiments on biaxially eccentrically loaded square tubular columns have been conducted in Canada.⁴¹ Milner and Gent⁴⁴ conducted experiments on small-scale no-sway columns restrained by elastic beams in two directions and the test results were used to corroborate their theoretical prediction, as was discussed earlier. In all of these test programs, the specimens failed by excessive bending about the weak axis.

For design application, CRC²⁸ recommended the plane surface equation for predicting the strength of isolated columns subjected to biaxially eccentric load

$$\frac{P}{P_{cr}} + \frac{C_{mx} M_x}{\left(1 - \frac{P}{P_{Ex}}\right) M_m} + \frac{C_{my} M_y}{\left(1 - \frac{P}{P_{Ey}}\right) M_{py}} \leq 1.0 \quad (1.16)$$

This equation is basically an extension of the recommendation for uniaxial unbraced no-sway columns bent about the strong axis. The addition of the weak axis bending term does not consider the presence of any torsional moment in the member. The amplification terms are calculated with respect to the respective planes of bending and P_{cr} is based on the largest slenderness ratio.

Equation 1.16 produces inconsistent results for the case of tubular columns. Pillai⁵⁰ has modified the CRC equation to the following form which was reported to give good correlation with the test results on square tubular columns

$$\frac{P}{P_{cr}} + \nu \left\{ \frac{C_{mx} M_x}{\left(1 - \frac{P}{P_{Ex}}\right) M_m} + \frac{C_{my} M_y}{\left(1 - \frac{P}{P_{Ey}}\right) M_{py}} \right\} = 1.0 \quad (1.17)$$

where

$$\nu = \frac{\sqrt{(C_{mx} M_x)^2 + (C_{my} M_y)^2}}{C_{mx} M_x + C_{my} M_y}$$

Equations 1.16 and 1.17 give identical results for the case of uniaxial bending. The difference in the prediction is attributed to the value ν which depends on the ratio of $C_{mx} M_x / C_{my} M_y$, that is, the ratio of the equivalent uniform moments about the strong and the weak axes not considering the effect of axial load acting through the deflection. When $C_{mx} M_x / C_{my} M_y$ is unity so that $\nu = 1/\sqrt{2}$, the largest difference in the predicted strength results. Recently, Tebedge and Chen⁵⁹ have proposed new interaction equations in the form of curved surfaces for the loading that causes the maximum moment to occur within the span of the member (stability control) and at the end of the member (strength control). The equations may be expressed as, for stability control,

$$\left[\frac{C_{mx} M_x}{\left(1 - \frac{P}{P_{cr}}\right) \left(1 - \frac{P}{P_{Ex}}\right) M_m} \right]^{\xi} + \left[\frac{C_{my} M_y}{\left(1 - \frac{P}{P_{cr}}\right) \left(1 - \frac{P}{P_{Ey}}\right) M_{py}} \right]^{\xi} = 1.0 \quad (1.18)$$

and, for strength control,

$$\left(\frac{M_x}{M_{pcx}}\right)^\eta + \left(\frac{M_y}{M_{pcy}}\right)^\eta = 1.0 \quad (1.19)$$

In these equations M_{pcx} and M_{pcy} are the reduced plastic moments about the strong and the weak axes in the presence of axial load, respectively, η is the exponent which depends on P/P_y level and ξ depends on P/P_y and the width-to-depth ratio of the cross section. The other terms have the same meaning as before. In view of Eq. 1.19, which is actually the equation for the biaxial plastic strength of the cross section, the recommendation allows the column to develop a plastic hinge when the loading causes the maximum moment at the end of the member. This is applicable for a structure designed by the plastic design method. For structures designed according to the allowable stress method, Eq. 1.19 is not applicable because an elastic analysis is used to determine the end moments. The 1969 AISC provision on plastic design has no recommendation related to biaxial bending in beam-columns because the research work leading to the design equations such as Eqs. 1.18 and 1.19 was not completed at that time. It recommended the following interaction equations to be used in the allowable stress design provision; for stability control

$$\frac{f_a}{F_a} + \frac{C_{mx} f_{bx}}{f (1 - \frac{a}{F_{ex}}) F_{bx}} + \frac{C_{my} f_{by}}{f (1 - \frac{a}{F_{ey}}) F_{by}} = 1.0 \quad (1.20)$$

and for strength control,

$$\frac{f_a}{0.6F_y} + \frac{f_{bx}}{F_{bx}} + \frac{f_{by}}{F_{by}} = 1.0 \quad (1.21)$$

The comparison of the predicted strength using different recommended interaction equations with the test results on eccentrically loaded unrestrained columns was conducted by Springfield

and Hegan.⁵⁸ It was found that the CRC equation is generally conservative and using Pillai's equation improved the result significantly. Chen's equation is found to be reliable for most of the specimens having H-shape sections and tends to be conservative for specimens having I-shape sections.

1.2.4 Summary. This section discussed the previous theoretical and experimental research that are available regarding the strength of no-sway beam-columns and the development of the design recommendations. The design equations for planar behavior and lateral torsional buckling were developed independently but were found to be similar in form. For laterally unbraced beam-columns, lateral torsional buckling usually controls the design. The extension to biaxial bending problems did not consider the effect of torsional moment. The interaction equations are applicable to beam-columns in plastically designed planar frames because at the ultimate load, a plastic hinge usually forms in the beam and has no restraining effect on the column. On the other hand, the beam-column in the structure designed according to the allowable stress design procedure is restrained by an elastic beam. As a result, there is a relaxation of the column end moment back to the beam. To be proper, the determination of F_a , F_{ex} and F_{ey} should be based on the effective length factor ($K < 1$). However, the specification suggests that the design be based on the column height which leads to a conservative result. It is felt that this is reasonable (using $K=1$) provided that the slenderness ratio is in the zone that the buckling strength is inelastic. There are extensive theoretical and test results that have been used as the basis for comparison with the design equations for in-plane instability, lateral torsional buckling, and biaxial behavior of no-sway beam-columns.

1.3 Previous Studies on the Strength and Design of Beam-Columns in Unbraced Frames

1.3.1 General Review. In unbraced frames where relative sway between the column ends may occur during loading, the P-delta effect results in a more adverse effect in terms of the stiffness and the strength of the columns than in braced frames. Since the stability of unbraced frames depends solely on the stiffness of the columns and the framing girders, the reduction of stiffness due to P-delta effect is an important consideration in column design in unbraced frames. There has not been much theoretical and experimental study on the strength and behavior of columns in unbraced frames and on the development of design equations for predicting the strength of the columns. Some previous research investigated the stability of unbraced portal frames with and without primary bending moments in the columns.^{38,39} Lu developed a numerical method to solve the sidesway frame buckling problem assuming that no strain reversal occurs in the partially yielded beam. The frame was solved initially as a no-sway frame subjected to trial values of gravity load and the stiffnesses of the beam and the columns were determined. The frame was then assumed to deflect laterally for a small amount of sway and, with the instantaneous stiffness computed, a horizontal force required for the equilibrium could be determined. Several values of gravity load were tried and the stability load was determined as the limit load at which no horizontal force is present. McNamee and Lu⁴³ considered the effect of strain reversal in the solution of inelastic sidesway buckling of multistory frames. Laosirichon³² conducted theoretical and experimental studies on the effect of beam yielding on the stability of columns in frames loaded by gravity load and on the strength of beam-columns in frames subjected to combined gravity and lateral load. It was confirmed that there is no significant reduction of the buckling load or the strength of the column if

the beam is loaded slightly above the yield moment level. Only when the beam is loaded to the plastic moment level did a severe reduction in column strength occur. However the reduction is gradual because of the effect of inelastic unloading on the windward end of the beam and the strain hardening on the leeward end.

The studies on the stability of unbraced frames discussed so far were conducted on symmetrical frames subjected to symmetrical gravity load. Salem⁵¹ has studied the elastic stability of unbraced frames where columns have unequal stiffnesses and are subjected to unequal column loads. Some of the frames studied contained a "leaned" column, which is a column framed to the beam by means of a flexible connection (see Fig. 1.9). In this case, the leaned column has no lateral stiffness and the frame must depend on the rigidly framed column for its stability. The studies by Salem provide the evidence that in an unbraced frame, columns with larger stiffness can provide potential bracing to other columns in the same story with less stiffness. Based on Salem's work, Yura⁶⁷ has illustrated that the assessment of the stability of an unbraced frame must consider the total buckling strength of each individual column in the story. There is one limitation, however, that a column cannot carry a load higher than its own capacity in the no-sway mode. If this is the case, the individual column failure will occur before sidesway buckling of the frame. The other feature of Yura's study is the effect of yielding in the columns prior to buckling. Based on the CRC basic column strength, inelastic buckling occurs when the effective slenderness ratio is in the range that results in a buckling load of $P/P_y > 0.5$. The restraining effect of the beam offered to the joint may be characterized by the parameter G

$$(G = \frac{EI_c/L_c}{EI_b/L_b}) .$$

As the column is partially yielded uniformly along the length, the beam becomes more effective in restraining the joint; therefore, the

effective length of the column is reduced. As a result the buckling load of the column is higher than that calculated on the basis of elastic G . It was suggested that in determining the effective length factor, G should be adjusted for the inelasticity of the columns such that

$$G_e = \frac{E_t}{E} G \quad (1.22)$$

where E_t is the tangent modulus of elasticity which may be approximated from the basic column strength curve (Fig. 1.10)

$$\frac{E_t}{E} \approx \frac{F'_a}{F'_e} \quad (1.23)$$

A theoretical study on the strength of beam-columns in single story unbraced frames with pinned bases subjected to combined gravity and lateral loads was conducted by Yura and Galambos.⁷⁰ An algebraic expression for the moment rotation relationship of a no-sway column subjected to one end moment was obtained by curve fitting to exact data. The equation for the shear resistance-sway relationship was established to satisfy the equilibrium and compatibility conditions; this relationship was then differentiated to obtain the strength and the corresponding sway at the maximum load. The results were obtained for strong axis columns with different slenderness ratios and two extreme values of G . Levi, Driscoll and Lu³⁶ determined the behavior of restrained columns in multi-bay frames permitted to sway by constructing the shear resistance-sway relationship using the moment-rotation of the no-sway restrained columns. This is essentially the basic step for what is called the sway subassemblage method for designing unbraced frames according to plastic design procedures.

The inelastic behavior of frames is generally complicated because of the nonlinear effects due to material yielding and due to the geometric nonlinearity. To predict the behavior accurately,

all the mechanical properties of steel must be considered, including the effects of residual stress, strain hardening and strain reversal. In the past, the behavior of a frame or its subassemblage was predicted by the elastic-plastic method of analysis. This method assumes all the members are elastic except at the plastic hinge locations which are confined to a point. With the use of discrete element models, as was investigated by Oral⁴⁸, the spread of yielding and several characteristics of steel can be considered and a more accurate prediction of the frame behavior can be developed.

The experimental studies on unbraced frames are limited in number. Yen, et al.⁶⁶ conducted tests to determine the buckling strength of single story unbraced frames with the presence of primary moments. The purpose was to verify the theoretical studies by Lu.³⁸ Later, McNamee and Lu⁴³ investigated the stability of multi-story frames. Arnold, Adams and Lu² studied the behavior and strength of a single story, one bay fixed base frame subjected to a constant gravity load and an increasing lateral load. Yarimci⁶⁴ carried out experiments on three story, one bay and three story, two bay unbraced frames subjected to combined gravity and lateral loads. In these specimens the magnitude of load on each column is equal; therefore, the effect of potential bracing by the other columns cannot be examined. In fact, the level of column loads in the test frames under combined loading is small so that the P-delta effect is relatively insignificant. These few tests were used to verify methods of inelastic structural analysis rather than check design procedures.

1.3.2 Present Design Procedures for Columns in Unbraced Frames. The design procedure for beam-columns in unbraced frames depends on whether the plastic design method or the allowable stress design method is used. The procedure based on the plastic design method will be discussed briefly whereas more details will

be given for design by the allowable stress procedure. In the plastic design method, the frame is generally designed story by story. Each story is subdivided into exterior and interior sub-assemblages. The columns are designed so that the strength of the story is adequate to resist the ultimate load with an acceptable sway limit. This is achieved by determining the response of the story based on the ultimate strength and stiffness of the sub-assemblages. The details of the method may be found in the references on the plastic design method.^{3,13}

In the allowable stress design procedure, only the strength of an individual beam-column is of interest, since redistribution of moment is not considered when axial loads are significant. The moments and axial loads are obtained from an elastic structural analysis. Interaction equations are used to design the beam-columns and are expected to account for material nonlinearities (residual stress, initial imperfection).

1.3.2.1 Unbraced Planar Frames. AISC Method. The 1969 AISC specification recommends the same interaction equations for both no-sway columns and columns permitted to sway. Equations 1.4 and 1.5 may be expressed in terms of strength of the member as:

$$\frac{P}{P'_{cr}} + \frac{0.85M}{\left(1 - \frac{P}{P'_E}\right) M_P} = 1.0 \quad (1.24)$$

$$\frac{P}{P_y} + \frac{M}{M_P} = 1.0 \quad (1.25)$$

In the AISC method, first order elastic analysis is used to determine bending moments in the frame. P and M in Eqs. 1.24, 1.25 are the axial load and the larger first order end moment in the columns respectively. AISC recommends $C_m = 0.85$ for beam-columns permitted to sway. P'_{cr} and P'_E are the buckling strength and the elastic buckling strength based on the effective length factor in a sway mode ($K > 1.0$). When the column is braced only

at the joints, lateral torsional buckling must be considered. As has been shown for no-sway columns, the interaction equation for lateral torsional buckling has the same form as the equation for the in-plane behavior except that P'_{cr} is based on the largest effective slenderness ratio and P'_E is always the elastic buckling load in the plane of bending; M_p is replaced by the critical moment for beam under pure bending. It should be noted that the AISC equations for sway columns are not derived and the concept of the buckling strength of the story is not considered. The first order moment is used to design the girder; this leads to unconservative design since the P delta effect increases the moment in the column as well as in the beam.

P-delta Method. A new design method for beam-columns in unbraced frames, called the P-delta method, was proposed by Wood, Beaulieu, and Adams^{62,63} and has been recommended in the 1976 SSRC Guide.²⁹ In this method, the P-delta effect is taken into account by using an elastic second order analysis to determine the moments in the frame. In a true elastic second order analysis, complication arises because the reduction in the bending stiffness of the member due to the presence of axial force must be considered. An approximate second order analysis is proposed whereby the frame is initially analyzed using the first order elastic analysis to obtain the sway displacement. The overturning effect of $P\Delta$ is represented as a sway force of $\Sigma P\Delta/L$ which is applied to the frame as a fictitious wind load, and the frame is reanalyzed in this manner until convergence is obtained. The moments that are determined from the second order analysis have included the secondary moment due to the P-delta effect. It is recommended that the columns be designed in the same way as the no-sway column. In the previous section, it has been discussed that for braced frames, columns may be conservatively designed by considering K to be unity. Therefore, the design of a sway column may be based on the

following equations written in terms of the strength of the member:

$$\frac{P}{P_{cr}} + \frac{C_m M^*}{\left(1 - \frac{P}{P_E}\right) M_P} = 1.0 \quad (1.26)$$

$$\frac{P}{P_y} + 0.85 \frac{M^*}{M_P} = 1.0 \quad (1.27)$$

where $C_m = 0.6 + 0.4q \geq 0.4$

In these equations, M^* is the larger column end moment determined from the second order analysis. It should be noted that where Eq. 1.27 controls, M^* will correspond to the plastic moment of the cross section ($M^* = M_{pc}$). It is felt that this will lead to unconservative design because the analysis to determine M^* is based on the elastic analysis; therefore, the P-delta effect has been underestimated. Figure 1.11 shows the envelope obtained by analyzing the frame at the load corresponding to the strength of the column using an elastic second order analysis. Therefore, the following equation should be used for the case of strength control:

$$\frac{P}{P_y} + \frac{M^*}{M_P} = 1.0 \quad (1.28)$$

The justification of Eqs. 1.26 and 1.28 needs to be verified by comparison with exact theoretical results. The design for lateral torsional buckling is the same as in Sec. 1.2.2 for no-sway columns.

The P-delta method recommends the design of the girder be based on the second order moment which is more proper than the AISC method.

Effective Length Method. In the investigation on the strength of single story frames⁷⁰ subjected to combined gravity and lateral loads, it was observed that, for bending about the strong axis, the column end moment curve at the instability limit follows the M_{pc} curve closely until the buckling load is approached.

Therefore, there is not much interaction between the buckling and the bending strength. Furthermore, it was understood from the study on the stability of unbraced frames that the maximum load that can be carried by a column is the buckling load in the no-sway mode and the stability of unbraced frames should be assessed from the buckling strength of the system. Based on the results of these studies, Yura proposed the following linear interaction equation:⁶⁹

$$\frac{P}{P_{cr}} + \frac{M^*}{M_p} = 1.0 \quad (1.29)$$

where

$$M^* = \frac{M}{1 - \frac{\sum P}{\sum P'_E}}$$

where P_{cr} is based on $K = 1.0$, $\sum P'_E$ is the sum of the elastic buckling load of all the columns in the bent considering K as in a sway mode ($K > 1.0$), and M is determined from the first order elastic analysis of the frame. The method described above is similar to the treatments in the current ACI Code⁷² and in Ref. 73. Initially, the inelasticity of the columns⁶⁷ due to high axial load was taken into account by adjusting $\sum P'_E$ in the amplification term of Eq. 1.29 such that

$$\sum P^*_{cr} = \sum [P'_E \tau(P)] \quad (1.30)$$

where

$$\tau(P) = \frac{E_t(P)}{E}$$

being the tangent modulus of elasticity corresponding to the axial load on the column to the elastic modulus of elasticity. If $\sum P^*_{cr}$ is used in Eq. 1.29 for $\sum P'_E$, the equation also checks the buckling strength of the frame as well as the limit where $\sum P = 0$. However, it was felt that the consideration of the adjustment for inelasticity of the column may lead to confusion in the design practice. Therefore, a separate check for the stability of the system is

suggested as follows:

$$\Sigma P = \Sigma P'_{cr} \quad (1.31)$$

when P'_{cr} is the buckling strength of individual columns considering the effective length factor in a sway mode. The amplification factor

$$\frac{1}{\left(1 - \frac{\Sigma P}{\Sigma P'_E}\right)}$$

for the larger end moment (first order) has been derived for a frame subjected to a lateral load. For frames that are subjected to concurrent beam load and wind load, this factor may overestimate the extent of the second order moment. Isbell²⁷ has conducted an investigation of the approximate second order moments. It was found for the combined loading case that the first order end moments may be separated into two components, those resulting from loads which do not cause sway and from loads which cause sway displacement. This may be expressed as

$$M^* = B_1 M_{NS} + B_2 M_{SW} \quad (1.32)$$

where

$$B_1 = \frac{C_m}{1 - \frac{P}{P_E}} \geq 1.0$$

$$B_2 = 1 - \frac{\Sigma P}{\Sigma P'_E}$$

The first term of Eq. 1.32 is intended to represent the maximum second order moment due to gravity load which may occur at the end or within the span of the member. The second term is due to wind load which always occurs at the end of the member; M^* may be slightly conservative for $B_1 > 1.0$. Further it is recommended that the girder design be based on the amplified end moment, i.e.,

$$M^*_{end} = M_{NS} + B_2 M_{SW} \quad (1.33)$$

To design for lateral torsional buckling, it is speculated that

P_{cr} , P'_{cr} are based on the largest slenderness ratio and $C_b M_m$ is used in place of M_p in Eq. 1.29.

1.3.2.2 Unbraced Space Frames. An unbraced space frame is one in which there is no bracing in any direction and the column-to-beam connections are moment resisting so that the columns are subjected to biaxial moments. For design, the currently available recommendation is the AISC method. The AISC Specification has extended the same interaction equations for columns in no-sway frames to columns in sway frames. These equations may be referred to again, as follows:

$$\frac{P}{P'_{cr}} + \frac{0.85M_x}{\left(1 - \frac{P}{P'_{Ex}}\right)M_m} + \frac{0.85M_y}{\left(1 - \frac{P}{P'_{Ey}}\right)M_{py}} = 1.0 \quad (1.34)$$

$$\frac{P}{P_y} + \frac{M_x}{M_{px}} + \frac{M_y}{M_{py}} = 1.0 \quad (1.35)$$

In these equations, M_x and M_y are the larger end moments obtained from first order elastic analyses; P'_{cr} is the buckling load based on the largest slenderness ratio ($K > 1.0$, usually the weak axis controls). The other terms have the same meaning as before. Equation 1.34 is based on the CRC equation (Eq. 1.16), except that C_{mx} and C_{my} are specified to be 0.85 and the effective length factors in a sway mode are used to determine P'_{cr} , P'_{Ex} , and P'_{Ey} .

Recently, Springfield⁵⁶ suggested a design recommendation which is essentially using the same concept as the P-delta method in planar frames combined with Chen's biaxial interaction equations. It is suggested that the frame be analyzed by a second order elastic analysis to obtain the column moments about the strong and the weak axes. These second order moments are substituted into Chen's equations as in the design of columns in no-sway frames (see Eqs. 1.18 and 1.19).

1.3.3 Summary. The previous theoretical and experimental studies on the strength of beam-columns in unbraced frames were discussed in this section. The studies that were available were limited to planar behavior and adequate bracing was assumed out of the plane so that no failure due to lateral torsional buckling was possible. Three design approaches were discussed (the current AISC method, P-delta method, and the effective length method), all of which use interaction equations. It was mentioned that the AISC equations as currently used for columns in unbraced frames are not derived and are merely extended from the case of no-sway columns. The AISC method does not consider the increase in girder moments due to second order effects. In the P-delta method, the second order moments are obtained from an elastic second order analysis. The P-delta method does consider the secondary girder moments in a very efficient manner. The effective length method correctly considers the concept of the buckling strength of the story for determining the second order moments.

1.4 Scope

Based on the discussions in Secs. 1.2 and 1.3, it may be seen that the design of beam-columns in no-sway frames is well understood. There have been numerous theoretical and experimental studies that have been used to verify the design interaction equations for all modes of behavior. Although these equations were developed for unrestrained beam-columns, they have been applied satisfactorily for the design of beam-columns in continuous braced frames.

On the other hand, the design of beam-columns in unbraced frames is the subject of controversy even for planar behavior. The complication arises because the design cannot just consider an individual column as in no-sway frames. Referring to Eqs. 1.24, 1.26, and 1.28, the intent of the moment term is to determine the elastic second order moment. Whether the first order moment with an amplification factor or an approximate second order analysis is used is

immaterial; the main problem relates to the form of the interaction equations to be used. The justification of any equations can be established by comparing the equations with theoretical and experimental results which are currently very meager. For planar behavior, only the solution of a single restrained column permitted to sway is available.^{36,70} These studies only considered bending about the strong axis of the column. The behavior about the weak axis of the member should be investigated if the design method is general and is to be developed for biaxial bending. Tests on biaxially loaded beam-columns, at least in no-sway frames, show that the specimens always fail about the weak axis. A study of unbraced frames with columns of unequal stiffnesses and subjected to combined gravity and lateral loads is necessary. A special case concerns the problem of leaned frames where a rigid frame has to provide the stability to the frames with flexible connections. These types of frames are becoming increasingly popular in construction practice⁵⁷ and they may be represented by the model, as shown in Fig. 1.9.

Theoretical studies on lateral torsional buckling of restrained columns in unbraced frames with and without sway bracing in the perpendicular direction to the plane of the frame and on the behavior of beam-columns in unbraced space frames are necessary before rational design equations may be proposed. Referring to the experimental studies, few experiments have been conducted on unbraced frames. The loading condition did not show the effect of columns with unequal stiffnesses. There have been no experimental studies on the behavior and strength of sway restrained columns in unbraced space frames.

1.5 Objective

It may be seen that there are several areas regarding the behavior and strength of columns in unbraced frames required to justify any design method. The main purpose of this study is to

provide theoretical solutions and experimental results for use in developing future design recommendations for beam-columns in unbraced frames. The theoretical study will be focused on two aspects:

(1) The development of ultimate strength curves for a variety of unbraced frames so that the accuracy of any suggested interaction equations can be evaluated.

(2) The determination of exact second order elastic moments for comparison with the P-delta analysis and the amplification factor approach.

Experimental studies will be conducted on full-size specimens in the following areas:

(1) Unbraced frames with columns having unequal stiffnesses. Two loading conditions will be studied, gravity load only and combined gravity load and wind load. The purpose is to verify the concept that the buckling strength of an unbraced frame is approximately equal to the summation of each individual column strength in the sway mode and to justify the current recommended design equations.

(2) Biaxially loaded restrained beam-columns permitted to sway. The purpose is to provide data on the behavior of beam-columns in unbraced space frames and to justify the current design recommendation.

CHAPTER 2

THEORETICAL STUDIES

2.1 General

In continuous frames proportioned according to the allowable stress design procedure, the limit of structural usefulness occurs when the strength of a critical member is reached. The additional load-carrying capacity of a frame due to the redistribution of moment beyond the first plastic hinge formation is not considered (except that a partial redistribution of moment is allowed according to AISC Specification Sec. 1.5.1.4). The strength of a beam-column is attained when the moment at a cross section reaches M_{pc} or when instability (either in-plane or lateral torsional buckling) occurs. For design application, the strength of the beam-column is represented by interaction equations which relate the axial load and the first order column end moment. It has been indicated that the interaction equations for beam-columns in unbraced frames are merely extended from the case of beam-columns in no-sway frames. There are limited theoretical solutions⁷⁰ that can be used for comparison with the design equations. The purpose of this chapter is first to provide extensive results on the strength of beam-columns in some unbraced frames, and second to evaluate the accuracy of the design interaction equations. The results of the analysis of example frames are used as the basis for such comparison. Only the in-plane behavior of the frame is considered.

Consider the portal frame in Fig. 2.1, which represents a lower story of multistory unbraced frames. The frame is symmetrical in geometry and all connections are rigid. Two equal axial loads

are applied at the column tops as well as a concentrated lateral load at the beam-to-column joint. The axial loads represent gravity load from the upper stories and the lateral load simulates wind load. The stability of the frame is controlled by sidesway buckling. Since the geometry and the loading are symmetrical, the columns reach their individual buckling capacity simultaneously. Figure 2.2 shows a typical leaned frame consisting of a column rigidly connected to the beam and a column with a pinned connection. The load on the pinned column represents the load on all the leaned columns in the system (see Fig. 1.9). In a sway buckling mode, the column with the simple connection has no lateral stiffness and the stability of the system must rely on the stiffness of the rigidly framed column and beam. This type of framing system is found to be economical and has been used frequently in practice.⁵⁷ Yet, the current AISC Specification has no provision for the design of columns in this type of frames.

The unbraced frame models in Figs. 2.1 and 2.2 are used throughout this study. In these models, moment redistribution does not occur because the frame will become a mechanism as soon as a plastic hinge is formed. Therefore, the maximum load of the frame is the load at which the strength of the beam-column is reached. Yura and Galambos⁷⁰ determined the strength of frames similar to those shown in Fig. 2.1. In their studies, the columns were bent about the strong axis and the results were presented mainly for the slenderness ratio of 40. In this study, the strength of beam-columns will be determined for various slenderness ratios and relative column-to-beam stiffnesses for both strong and weak axes. The presence of residual stress is considered. The effect of loads on the leaned column on the strength of frames will be examined.

2.2 Method of the Analysis

The columns in unbraced frames shown in Figs. 2.1 and 2.2 are made of W8x31 section conforming to ASTM A36 steel. This

column shape has been used extensively by previous researchers.¹⁸ The stress-strain relationship of the material is shown in Fig. 2.3, where the yield strength, $\sigma_y = 36$ ksi and the modulus of elasticity, $E = 29000$ ksi. The idealized residual stress distribution that is used in this study is shown in Fig. 2.4. This pattern of residual stress is typical for rolled W shapes and is a result of uneven cooling process.²⁶ The beam is assumed to remain elastic because the strength of the beam-column is of interest in this study. It is not desirable that the frame fails due to a plastic hinge formed in the beam.

Figure 2.5 shows a beam-column in a deformed configuration. The geometry of the sway displacement and the end rotation of the column and the compatibility condition of the joint may be expressed as

$$\theta_c = \frac{\Delta}{L_c} - \theta' \quad (2.1a)$$

and
$$\theta_b = \theta_c \quad (2.1b)$$

in which θ_b and θ_c are the angles between the tangent at the end of the beam and column with the original position; θ' is the rotation between the tangent at the column top and the chord; Δ is the sway displacement; and L_c is the column length.

Referring to Fig. 2.6, assume that if the beam is very long compared to the length of the column, the difference in the column loads which is attributed to the overturning effects of the wind and the P-delta effect of the column loads is not significant. Therefore, the axial loads in both columns may be considered to be equal to the applied load at the column top. The shear force in each column is $H/2$ due to symmetry, where H is the applied wind load. The equilibrium condition of the columns under the action of end moment, axial force, and shear force, and the joint equilibrium condition require that

$$M_c = VL_c + P\Delta \quad (2.2a)$$

and

$$M_c = M_b \quad (2.2b)$$

The idealized moment-rotation characteristic of the beam subjected to equal end moments causing reverse curvature is (see Fig. 2.7):

$$M_b = \frac{6EI_b}{L_b} \theta_b \quad (2.3)$$

In Eqs. 2.2 and 2.3, M_c and M_b are end moments in the column and the beam; V and P are the shear force and the axial force in the column, respectively; I_b is the moment of inertia; and L_b is the length of the beam.

In view of Eqs. 2.2b, 2.3, and 2.1b, the sway displacement may be determined from Eq. 2.1a, as follows:

$$\frac{\Delta}{L_c} = \frac{M_c}{6EI_b/L_b} + \theta' \quad (2.4)$$

Nondimensionalizing all the terms in Eq. 2.2a by M_p , the plastic moment of the cross section, and with some manipulation of the axial load term leads to

$$\frac{HL_c}{2M_p} = \frac{VL_c}{M_p} = \frac{M_c}{M_p} - \left(\frac{rA}{Z} \right) \frac{P}{P_y} \frac{L_c}{r} \frac{\Delta}{L_c} \quad (2.5)$$

where all section properties are related to the bending axis.

The equilibrium and compatibility conditions for leaned frames in Fig. 2.2 are formulated in a similar manner, except that the rotational stiffness of the beam is $3EI_b/L_b$ and that part of the shear resistance of the rigidly jointed column is used up to overcome the overturning effect of axial load on the pinned column. Consider the structure in Fig. 2.8 in a sway configuration defined by Δ , the axial force on the leaned column produces an overturning

moment of $P_2 \Delta$. Thus, the shear resistance that must be provided by the rigidly jointed column becomes

$$V_2 = \frac{P_2 \Delta}{L_c} \quad (2.6)$$

In view of Eq. 2.4, the sway displacement of the leaned frame is given by

$$\frac{\Delta}{L_c} = \frac{M_c}{3EI_b/L_b} + \theta' \quad (2.7)$$

For the shear resistance of the rigidly joint column V , the wind load that can be applied to the frame is equal to the effective shear resistance defined by the following equation:

$$H = V - V_2 \quad (2.8)$$

Equation 2.8 may be expressed in nondimensionalized form, in view of Eq. 2.5, as

$$\frac{HL_c}{M_p} = \frac{VL_c}{M_p} - \frac{P_2 \Delta}{M_p} = \frac{M_c}{M_p} - \left(\frac{rA}{Z} \right) \frac{P_1}{P_y} \frac{L_c}{r} \frac{\Delta}{L_c} - \frac{P_2 \Delta}{M_p} \quad (2.9)$$

It is to be noted that in the development of Eq. 2.9, it has also been assumed that $L_b \gg L_c$ so that the change of the axial force due to the overturning effect is not significant.

In order to determine Δ and H in Eqs. 2.4, 2.5, 2.7, and 2.9, the moment-rotation characteristics (M_c vs θ') of the columns must be known. This relationship can be obtained for a given slenderness ratio and a specified axial load by numerically integrating the moment-thrust-curvature relationship of the cross section and satisfying the boundary conditions. The details of the procedure may be found in Ref. 19. The moment-thrust-curvature

relationship can be determined numerically by dividing the cross section into a series of grid elements. The axial force and moment are computed by integrating the elemental force and moment over the cross section using the assumed stress-strain relationship and residual stress distribution, and satisfying the equilibrium and compatibility conditions. The details for calculating the moment-thrust-curvature relationship are given in Appendix A. Figures 2.10 and 2.11 show typical moment-thrust-curvature relationships for strong and weak axis bending. The moment and the curvature are non-dimensionalized by the moment at initial yielding M_y ($M_y = S \times \sigma_y$) and the curvature at initial yielding ϕ_y ($\phi_y = 2\epsilon_y/c$), respectively. It may be observed that the reduction in flexural rigidity of the cross section due to the presence of residual stresses is more pronounced for weak axis bending than for strong axis bending. The results of the computed relationship are in good agreement with others.^{19,48}

After the moment-rotation characteristics of the column have been established, the shear resistance (or the effective shear resistance)-sway relationship may be determined for a particular value of G from Eqs. 2.4 and 2.5 for portal frames and from Eqs. 2.7 and 2.9 for leaned frames. These relationships represent the equilibrium positions of the frame. For the portal frames and the leaned frames in the present study, the applied wind load H produces an elastic first order moment at the column top equal to $HL_c/2$ and HL_c , respectively. Therefore, Eqs. 2.5 and 2.9 may be interpreted as being the relationship between the first order column end moment and the sway deflection. The typical solutions of the portal frames are shown in Figs. 2.12 and 2.13 for the columns bent about the strong and the weak axes, respectively. The maximum strength of beam-columns corresponds to the peak of the shear resistance-sway relationship. This peak is defined as the instability limit if the column end moment, M_c , does not reach M_{pc} at the maximum load.

For columns with low slenderness ratio and low axial load, instability may not occur. Instead, a plastic hinge (moment reaches M_{pc}) may form at the top of the column and the frame fails by a plastic mechanism.

The results that are shown in Figs. 2.12 and 2.13 are for frames subjected to a constant level of axial loads. If the first order moment corresponding to the peak value of the shear resistance-sway relationship is plotted as a function of the axial load, an interaction curve is obtained. Typical interaction curves are shown in Fig. 2.14a and 2.14b for frames with columns bent about the strong and the weak axes, respectively. In these plots, the solid curves represent the nondimensionalized column end moment, M_c/M_p , and the dashed curves show the nondimensionalized first order end moment, $HL_c/2M_p$. It may be observed that for low axial load ($P/P_y < 0.15$), the frames fail as a plastic mechanism. Inelastic instability governs for the higher level of axial load.

2.3 Results on the Strength of Beam-Columns in Unbraced Frames

The portal frames and the leaned frames shown in Figs. 2.1 and 2.2 were analyzed for a wide range of column slenderness ratios and two extreme values of G corresponding to a rigid and a very flexible beam restraints. For leaned frames, the analysis was conducted for several values of α , which is defined as the ratio of the load on the pinned-end column to the load on the rigidly jointed column. In both classes of frames, bending about the strong and the weak axes of the column is considered. The effect of residual stresses on the strength of beam-columns is examined in some of the portal frames. The results of the ultimate strength analysis are presented in the form of interaction curves where the nondimensionalized first order moment, $HL_c/2M_p$ or HL_c/M_p , at the maximum

strength of the beam-columns is plotted against the nondimensionalized axial load, P/P_y .

Results on the strength of beam-columns in portal frames are given in Figs. 2.15 to 2.19. The slenderness ratio is a parameter in these interaction curves and it varies between $L_c/r = 20$ to $L_c/r = 80$. Two values of G considered are $G = 0$ and $G = 3.0$. The effective length factors corresponding to these extreme values of G with the bottom end of the column pinned ($G = \infty$) are 2.0 and 2.92, respectively. This gives a range of the effective slenderness ratios from $KL_c/r = 40$ ($K = 2.0$, $L_c/r = 20$) to $KL_c/r = 234$ ($K = 2.92$, $L_c/r = 80$). For the results shown in Figs. 2.15 and 2.16, the residual stress is taken into account. In order to examine the effect of residual stress on the strength of beam-columns, an analysis was conducted on portal frames with $L_c/r = 40$ and $L_c/r = 60$. In this analysis, the moment-thrust-curvature relationship with no residual stress was input. The results of this study are compared with those that consider the effect of residual stress in Figs. 2.18 and 2.19.

Results on the strength of the rigidly framed column in leaned frames are given in Figs. 2.20 to 2.27. In each plot, G and L_c/r are constant and the variable is α . In these results, the residual stress is considered in the analysis. The slenderness ratio and G vary from $L_c/r = 20$ to $L_c/r = 60$, and $G = 0$ to $G = 2.0$. The effective length factors corresponding to this range of G are $K = 2.0$ to $K = 3.25$. It should be noted that the results for columns in leaned frames for the case where there is no load on the pinned-end column, $\alpha = 0$, are the same for columns in portal frames, provided that one-half of the G value in leaned frames is used in portal frames. This results from the fact that the stiffnesses of the restraining beams are $3EI_b/L_b$ for leaned frames and $6EI_b/L_b$ for portal frames.

In portal frames and leaned frames in the present study, it has been assumed that the beam is very long compared with the height of the column. Consider a leaned frame subjected to constant column loads P and αP and a lateral load H (see Fig. 2.2). At the equilibrium position, suppose that the sway deflection of the frame is Δ , the overturning moment due to the column loads and the lateral load is $HL_c + (1 + \alpha)P\Delta$. This results in an increase in the axial load in the leeward column and a decrease in the axial load in the windward column of equal magnitude. The change of axial load due to the overturning moment is $[HL_c + (1 + \alpha)P\Delta]/L_b$. Therefore, the axial load in the leeward column is $P + [HL_c + (1 + \alpha)P\Delta]/L_b$. In usual design practice, an elastic first order analysis is used to analyze the frame. This neglects the overturning effect due to the column loads; therefore, the axial load in the leeward column is $P + HL_c/L_b$. It may be seen that the plots of interaction curves depend on the definition of the axial load. With the assumption that $L_b \gg L_c$, the change of axial load due to the overturning effect is small and the axial load may be considered to be equal to the applied column load. The effect of beam length will be discussed later in Sec. 2.8.

2.4 Discussion of Analytical Results

Figures 2.15 and 2.16 show the effect of slenderness ratios on the strength of beam-columns for bending about the strong and the weak axes. Generally the strength decreases as the slenderness ratio increases. It may be observed in these figures that for $HL_c/2M_p$ larger than 0.1, and for L_c/r larger than 40, the relationship between the first order moment and the axial load is approximately linear. In the vicinity of the stability load, the change in moment occurs faster, especially for weak axis bending than for strong axis bending. This behavior can also be seen in Fig. 2.17, which shows the comparison of the strength of beam-columns having the same L_c/r and G and are bent about the strong and the weak axes.

Generally, the strength is lower when bending occurs about the weak axis. This is attributed to the deterioration of bending stiffness, which is faster for weak axis bending than for strong axis bending. For columns with a small slenderness ratio, the strength with respect to the plastic moment of the cross section is higher for weak axis bending when the column load is less than about 65 percent of the buckling load.

The effect of residual stresses can be seen in Figs. 2.18 and 2.19. The reduction of strength due to residual stress is larger for the weak axis and for stiff restraint. For $L_c/r = 40$ and $G = 0$, the effective slenderness ratio is 80. The reduction in buckling strengths is 15 percent and 23 percent of P_y for strong and weak axis bending, respectively. The residual stress effect decreases as the level of axial load decreases and as the slenderness ratio increases.

Referring again to Figs. 2.12 and 2.13, which show typical shear resistance-sway relationships for strong and weak axis bending for $L_c/r = 40$, it can be observed that the shear stiffness reduces considerably as G increases from 0 to 3.0. For strong axis bending, the nondimensionalized shear stiffnesses

$$\left(\frac{HL_c}{2M_p} / \frac{\Delta}{L_c} \right)$$

at $P/P_y = 0.2$ for $G = 0$ and $G = 3.0$ are 53.1 and 16.6, respectively; at $P/P_y = 0.5$, the stiffnesses for $G = 0$ and $G = 3.0$ are 37.6 and 3.6. The sway at the maximum strength also is affected by G . With $G = 0$, the strength at $P/P_y = 0.2$ is reached at Δ/L_c less than 0.02, while Δ/L_c is about 0.04 for $G = 3.0$. This range of sway is similar for strong and weak axis bending. The significant effect of residual stress for weak axis bending at high axial load may be seen in Fig. 2.13. The typical relationship between the axial force and primary and secondary moments at the maximum strength for the case of $L_c/r = 40$ is shown in Fig. 2.14. The plots also show the plastic moment of

the cross section in the presence of axial load. At a given axial load level, the difference between the column end moment and the primary moment is the moment that is caused by the P-delta effect. This is more significant for weak axis bending with small restraint; for example, at $P/P_y = 0.3$ with $G = 3.0$, the P-delta moment for strong and weak axis bending amounts to $0.4M_p$ and $0.54M_p$, respectively (M_p is with respect to the bending axis). A significant difference in the behavior of the frames with respect to the bending axis can also be observed. For strong axis bending, the column end moment curves follow the M_{pc} curve for most of the axial load level. The deviation from the M_{pc} curve is rather sudden as the buckling load is approached. The deviation occurs at a rather low level of axial load for weak axis bending.

The effect of load on the leaned column is shown in Figs. 2.20 to 2.27. In general, the reduction in shear strength of the frames is appreciable. The reduction in axial load capacity of the rigidly jointed column at the frame stability limit can be determined by considering the shear equilibrium of the structure in Fig. 2.8. At the instant of buckling, an infinitesimal sway displacement, Δ , is assumed. The shear required for equilibrium of the pinned column is $\alpha P \Delta / L_c$ which must be supplied by the rigidly jointed column. The frame reaches the stability limit when the initial shear stiffness $(V/\Delta)_{\Delta \rightarrow 0}$ is equal to $\alpha P / L_c$. This may be illustrated by referring to Fig. 2.28, where the initial shear stiffness and the load on the pinned column are plotted as a function of the load on the rigidly jointed column. All the quantities are nondimensionalized by P_y . It may be noted that in the inelastic zone ($P/P_y > 0.7$), the shear stiffness depends on the axis of bending. The frame reaches the stability limit at the axial load level defined by the intersection of the $\alpha P / P_y$ line (radial line) and the $V L_c / P_y \Delta$ line (sloping line). As an example, for a frame having $L_c / r = 40$ and $G = 0$ and with $\alpha = 2.0$, the critical axial load that

can be carried by the rigidly jointed column is $P/P_y = 0.47$ (the ordinate of point A). This result can be verified by considering Salem's solution in Fig. 2.29. For the example considered, $P_1/P_2 = 0.5$, giving $(P_1 + P_2)/2P_E = 0.141$ or $P_1/P_y = 0.47$ ($\sigma_y = 36$ ksi and $E = 29000$ ksi are used for computing the results in Fig. 2.28). The results in Fig. 2.28 may be presented in another form, as shown in Fig. 2.30, where the buckling strength (such as point A) is plotted as a function of α . The buckling strength, P , is nondimensionalized by P'_E , the elastic buckling load in which the effective length factor is taken into account. In the elastic range and the case for large G , the result coincides with the solution $\Sigma P/\Sigma P'_E = 1.0$.⁶⁷ For curve A with $G = 0$ and $L_c/r = 40$, inelastic buckling starts at $P/P'_E = 0.57$, which corresponds to $P/P_y = 0.7$.

2.5 Second Order Analysis of Example Frames

As mentioned in Chapter 1, the current AISC Specification takes into account the P-delta effect in columns in frames permitted to sway indirectly by amplifying the larger column end moment obtained from the first order analysis by the expression of $0.85/(1 - P/P'_E)$. On the other hand, in the P-delta method of design, the secondary effect is considered directly in the second order analysis. For leaned frames, the direct application of the AISC procedure leads to an unconservative prediction of the second order moment because the P-delta effect due to the axial load on the pinned column is not considered. The secondary effects in leaned frames can be taken into account if the second order analysis is performed, or if the effective length method is used; that is, to consider the strength of the story in the amplification factor. The purpose of the study in this section is to examine the accuracy of the approximate methods (P-delta method and the effective length method) for determining P-delta effects in portal frame and leaned

frame examples. An exact elastic second order analysis is used as the basis for the comparison.

2.5.1 Exact Second Order Analysis. Consider an elastic beam-column, as shown in Fig. 2.31. The deformation of the members are end rotations and the relative end translation. By means of the slope deflection equations,⁸ in which the effect of axial force on the stiffness of the member is considered, the end moments M_{AB} and M_{BA} are expressed in terms of deformations as

$$M_{AB} = S_1 K_c \theta_A + S_2 K_c \theta_B - (S_1 + S_2) K_c \frac{\Delta}{L_c} \quad (2.10a)$$

and

$$M_{BA} = S_2 K_c \theta_A + S_1 K_c \theta_B - (S_1 + S_2) K_c \frac{\Delta}{L_c} \quad (2.10b)$$

where

$$S_1 = \frac{1 - \beta \cot \beta}{\frac{2 \tan \beta/2}{\beta} - 1}$$

$$S_2 = \frac{\beta \operatorname{cosec} \beta - 1}{\frac{2 \tan \beta/2}{\beta} - 1};$$

$$\beta = L_c \sqrt{\frac{P}{EI_c}}$$

and
$$K_c = \frac{EI_c}{L_c}$$

For the case that end B is pinned, $M_{BA} = 0$ and θ_B can be solved in terms of θ_A and Δ/L_c ; Eq. 2.10a then becomes

$$M_{AB} = S_3 K_c \theta_A - S_3 K_c \frac{\Delta}{L_c} \quad (2.11)$$

where
$$S_3 = \frac{\beta^2}{1 - \beta \cot \beta} = \left\{ 1 - \left(\frac{S_2}{S_1} \right)^2 \right\} S_1$$

For every member in a rigid frame, end moments can be expressed in terms of end deformations; compatibility requires that the end rotations of members that frame into a common joint are the

same. Equilibrium conditions, i.e., joint moment equilibrium and shear equilibrium for the story, are used to solve for the unknown joint displacements.

For the portal frames shown in Fig. 2.1, the unknown joint displacements are θ_B and Δ/L_c , considering antisymmetric bending in the beam. The joint moment equilibrium and the shear equilibrium of the story are

$$M_{BA} + M_{BC} = 0 \quad (2.12)$$

$$\frac{HL_c}{2} + M_{BA} + PL_c \frac{\Delta}{L_c} = 0 \quad (2.13)$$

Expressing moments M_{BA} and M_{BC} in terms of joint displacements and substituting into the equilibrium equations leads to two simultaneous stiffness equations which can be written in matrix form as

$$\begin{bmatrix} S_3 K_c + 6K_b & -S_3 K_c \\ -S_3 K_c & S_3 K_c - PL_c \end{bmatrix} \begin{Bmatrix} \theta_B \\ \frac{\Delta}{L_c} \end{Bmatrix} = \begin{Bmatrix} 0 \\ \frac{HL_c}{2} \end{Bmatrix} \quad (2.14)$$

In Eq. 2.14, $K_b = EI_b/L_b$. Solving Eq. 2.14 for θ_B and Δ/L_c and substituting into the slopedeflection equations yields the end moments. Because the axial force in the column is not exactly equal to the applied axial load, due to the shear force in the beam, a few cycles of iteration are required to adjust the level of axial force, but the change is usually not significant.

The problem can be approached similarly for the leaned frames in Fig. 2.2. Consider the equilibrium of the whole frame; knowing that there is no moment at the real hinge leads to two unknown joint displacements, θ_B and Δ/L_c . The stiffness of the beam with one end hinged is $3K_b$. In view of the equilibrium equations

$$M_{BA} + M_{BC} = 0 \quad (2.15)$$

$$\text{and} \quad HL_c + M_{BA} + \Sigma PL_c \frac{\Delta}{L_c} = 0 \quad (2.16)$$

the problem is reduced to the following matrix equations

$$\begin{bmatrix} S_3 K_c + 3K_b & -S_3 K_c \\ -S_3 K_c & S_3 K_c - \Sigma PL_c \end{bmatrix} \begin{Bmatrix} \theta_B \\ \frac{\Delta}{L_c} \end{Bmatrix} = \begin{Bmatrix} 0 \\ HL_c \end{Bmatrix} \quad (2.17)$$

and the end moments are obtained the same way as in portal frames.

2.5.2 P-delta Method of Analysis. In the P-delta method of elastic second order analysis, the reduction of member stiffness due to axial load is not considered. Referring to Fig. 2.32 which shows an unbraced frame subjected to combined gravity and lateral loads, the P-delta analysis starts by analyzing the structure by first order elastic theory to obtain sway displacement Δ_0 . With this sway displacement, a fictitious lateral load which is equal to $\Sigma P \Delta_0 / L_c$ is added to the applied lateral load. The structure is reanalyzed, also by first order elastic theory, each time a new fictitious load is computed. The analysis continues until the sway displacement does not change from the previous cycle within a specified tolerance. The final end moments obtained include the P-delta effect. When the axial load approaches the stability load of the frame or when the frame is flexible, the convergence is usually slow.⁶²

The formulation of the equilibrium equations is the same as in the exact second order analysis except that S_3 is equal to 3, the value for members in flexure, and the overturning moment is transposed to the load side. Thus for the portal frame examples, the equilibrium equations become

$$\begin{bmatrix} 3K_c + 6K_b & -3K_c \\ -3K_c & 3K_c \end{bmatrix} \begin{Bmatrix} \theta_B \\ \frac{\Delta_i}{L_c} \end{Bmatrix} = \begin{Bmatrix} 0 \\ \frac{HL_c}{2} + P\Delta_{i-1} \end{Bmatrix} \quad (2.18)$$

in which Δ_i and Δ_{i-1} denote the sway displacement in the current and the previous iterations, respectively. For the first iteration, $P\Delta_{i-1}$ is not considered.

Similarly, equilibrium equations for the leaned frames are

$$\begin{bmatrix} 3K_c + 3K_b & -3K_c \\ -3K_c & 3K_c \end{bmatrix} \begin{Bmatrix} \theta_B \\ \frac{\Delta_i}{L_c} \end{Bmatrix} = \begin{Bmatrix} 0 \\ HL_c + \Sigma P\Delta_{i-1} \end{Bmatrix} \quad (2.19)$$

Alternatively, since the approximate analysis uses first order theory and the fictitious lateral load simulating the overturning effect due to gravity load is added to the applied load, results from successive iterations are proportional to those from the first order analysis under the applied lateral load alone. Therefore, an expression to determine the second order moments can be formulated readily. Consider the unbraced bent in Fig. 2.32b, under the application of H. Define the sway displacement of the bent as determined by first order elastic theory by Δ_o , the sway stiffness of the bent is

$$K_S = \frac{H}{\Delta_o} \quad (2.20)$$

The fictitious load due to gravity load and sway Δ_o is $\Sigma P\Delta_o/L_c$. In the second cycle, the sway displacement of the bent becomes

$$\Delta_1 = \Delta_o + \frac{(\Sigma P\Delta_o/L_c)}{K_S} \quad (2.21)$$

Similarly, for the i^{th} cycle

$$\Delta_i = \Delta_o + \frac{(\Sigma P \Delta_{i-1} / L_c)}{K_S} \quad (2.22)$$

When the solution converges, $\Delta_i \approx \Delta_{i-1} = \Delta$; in view of Eq. 2.22, the final sway can be expressed as

$$\Delta = \frac{\Delta_o}{1 - \frac{\Sigma P}{K_S L_c}} \quad (2.23)$$

The actual loading on the frame is adjusted to the modified lateral load $H^* = (H + \Sigma P \Delta / L_c)$, or using Eq. 2.23

$$H^* = \frac{H}{1 - \frac{\Sigma P}{K_S L_c}} \quad (2.24)$$

Therefore, if shear force on column i produced by the applied load H is V_i , so that the first order moment in the column is $V_i L_c$, then the second order moment becomes

$$M^* = \frac{V_i L_c}{1 - \frac{\Sigma P}{K_S L_c}} \quad (2.25)$$

It should be noted that the true shear in the column is not equal to $V_i (1 - \Sigma P / K_S L_c)$; instead, it is obtained from equilibrium of the column taken as a free body with end moment M^* given by Eq. 2.25. The buckling load of the frame is the load at which the stiffness of the bent vanishes. The sway stiffness of the bent in the presence of axial load is H/Δ and, in view of Eq. 2.20 can be expressed as

$$\frac{H}{\Delta} = \frac{H}{\Delta_o} \left(1 - \frac{\Sigma P}{K_S L_c} \right) = K_S \left(1 - \frac{\Sigma P}{K_S L_c} \right) \quad (2.26)$$

Therefore, in the P-delta method of analysis, the frame reaches the stability limit when

$$\Sigma P = K_S L_c \quad (2.27)$$

For example frames used in this chapter, the full sway stiffnesses for the cases of portal frames and leaned frames are $K_S = 6EI_c / (G + 2)L_c^3$ and $K_S = 3EI_c / (G + 1)L_c^3$, respectively; the second order moments at the column tops for portal frames are

$$\begin{aligned} M_c^* &= \frac{HL_c}{2[1 - (G + 2)L_c^2 P / 6EI_c]} \\ &= \frac{HL_c}{[1 - \frac{\pi^2(G + 2)}{6K^2} \frac{P}{P'_E}]} \end{aligned} \quad (2.28)$$

and for leaned frames

$$\begin{aligned} M &= \frac{HL_c}{[1 - (G + 1)L_c^2 \Sigma P / 3EI_c]} \\ &= \frac{HL_c}{[1 - \frac{\pi(G + 1)}{3K^2} \frac{\Sigma P}{P'_E}]} \end{aligned} \quad (2.29)$$

In Eqs. 2.28 and 2.29, K is the effective length factor and P'_E is the elastic buckling load based on the effective column length.

2.5.3 Effective Length Approach. Consider the bent in Fig. 2.32c being subjected to gravity load only. At the instant of sidesway buckling, the nomograph method for determining effective length¹ assumes that the beam deforms antisymmetrically from which the stiffness is known to be $6EI_b / L_b$. If it is assumed further that the deformation configuration of the frame due to the lateral load is similar in shape to the case at the instant of bifurcation, then the first order sway displacement of the frame and shear force at column i , V_i is related by

$$\Delta_o = \frac{V_i}{\bar{K}_{Si}} = \frac{V_i L_c^3 (G + 2)}{6EI_c} \quad (2.30)$$

in which \bar{K}_{Si} is the sway stiffness contributed by column i . Equilibrium in the horizontal direction requires that the sum of shear forces is equal to the applied lateral load. Using Eq. 2.30, the horizontal shear load can be expressed as

$$H = \Delta_o \sum \bar{K}_{Si} = \Delta_o K_S \quad (2.31)$$

or

$$V_i = H \frac{\bar{K}_{Si}}{K_S} \quad (2.32)$$

The second order sway displacement is related to the first order displacement by

$$\Delta = \frac{\Delta_o}{1 - \frac{\sum P}{\sum P'_E}} \quad (2.33)$$

where $\sum P'_E$ is the sum of the elastic buckling loads of all columns with rigid joints in the bent based on the individual effective lengths.

Assuming that each rigidly jointed column carries the P-delta moment of the story in proportion to its first order sway stiffness, the second order moment of column i , using Eqs. 2.30 and 2.33, becomes

$$M^* = V_i L_c + \sum P \Delta \frac{\bar{K}_{Si}}{K_S} = V_i L_c \left[1 + \frac{\frac{\sum P}{K_S L_c}}{1 - \frac{\sum P}{\sum P'_E}} \right] \quad (2.34)$$

In view of Eq. 2.30 and $K_S L_c = \sum \bar{K}_{Si} L_c = \sum P'_E [6K^2/\pi^2(2+G)]$, the term $6K^2/\pi^2(2+G)$ varies between 1.22 and 1.00 for the range of $0 < G < 10.0$, which can be conservatively taken to be unity. Thus, Eq. 2.34 becomes

$$M^* = \frac{V_i L_c}{1 - \frac{\Sigma P}{\Sigma P'_E}} \quad (2.35)$$

For the frames under consideration, the second order moments for the portal frames and the leaned frames are given by

$$M^* = \frac{HL_c}{2[1 - \frac{P}{P'_E}]} \quad (\text{portal}) \quad (2.36)$$

and

$$M^* = \frac{HL_c}{1 - \frac{\Sigma P}{\Sigma P'_E}} \quad (\text{leaned}) \quad (2.37)$$

In general, the stability load of the frame predicted by this method is

$$1 - \frac{\Sigma P}{\Sigma P'_E} = 0$$

or

$$\Sigma P = \Sigma P'_E \quad (2.38)$$

2.5.4 Comparison of Second Order Moments. The results of the study on approximate second order analysis techniques for frames are shown in Figs. 2.33 to 2.40. A computer program was written for analyzing the frames exactly by the slope deflection method. The plots show the comparison of second order moments obtained by the exact second order analysis, the P-delta approach, the effective length method, and the current AISC expression. Several values of G , L_c/r and α were chosen. The ordinate of the plots, M^*/M , which is the ratio of the second order moment at the column top to the moment obtained by first order analysis, is defined as the amplification factor. The AISC expression for the amplification factor is equal to $0.85/(1 - P/P'_E)$. Since the

behavior is elastic, the amplification factor for the column having the same G and L_c/r is independent of the bending axis.

For the case of $\alpha = 0$, results for portal frames are the same as for leaned frames for $G = 0.5$ times that of the latter (see Fig. 2.2). It can be seen that the P-delta method is unconservative at high axial load when the beam is very stiff ($G = 0$). The unconservativeness decreases as the value of G increases. The effective length method gives conservative estimates of second order moments. The prediction almost coincides with the exact second order analysis. The AISC expression is slightly unconservative for all cases; this is due to the factor 0.85.

When there is load on the pinned column, results from the P-delta method of analysis are unconservative, but much less than the case when $\alpha = 0$. The effective length method gives conservative results; as α increases, the method becomes more conservative. The AISC method should not be used for these leaned cases; the results show that the method is very unconservative.

The P-delta analysis leads to slightly unconservative results because the method does not consider the reduction of stiffness due to axial load while the exact analysis does. In leaned frames, the effective length method replaces the shear demand by the pinned columns as an equivalent axial load. This produces more moment area for rigidly jointed columns⁶⁷ whereas the P-delta method superimposes two linear moment diagrams corresponding to first and second order moments. The plots indicate that both the P-delta method and the effective length method give similar results and are applicable to both portal and leaned frames.

2.6 Allowable Stresses and Factor of Safety

It was discussed in Chapter 1 that interaction equations in the current AISC design specification are given in terms of

allowable stresses. In these equations, different factors of safety for F'_a , F'_e , and F'_b are used. Referring to Fig. 2.41, the allowable stress for inelastic buckling is based on the CRC basic column strength curve for both strong and weak axis buckling. Buckling in the inelastic range is assumed to occur when $KL_c/r < C_c$ ($C_c = \pi \sqrt{2E/F_y}$) and is represented by a parabola joining point A ($F_{cr}/F_y = 1.0$ at $KL_c/r = 0$) to point C ($F_{cr}/F_y = 0.5$ at $KL_c/r = C_c$). When the effective slenderness ratio is larger than C_c , buckling is governed by the Euler strength. The allowable stresses for axially loaded columns are

$$F'_a = \frac{F_y \left[1 - \frac{1}{2} \left(\frac{KL_c/r}{C_c} \right)^2 \right]}{\frac{5}{3} + \frac{3}{8} \frac{KL_c/r}{C_c} - \frac{1}{8} \left(\frac{KL_c/r}{C_c} \right)^3} \quad KL_c/r < C_c \quad (2.39)$$

$$F'_a = F'_e = \frac{149,000}{(KL_c/r)^2} \quad KL_c/r \geq C_c \quad (2.40)$$

In these equations, the prime denotes that the value depends on the effective slenderness ratio. The factor of safety for F'_a is given by the expression in the denominator of Eq. 2.39, which depends on KL_c/r . The factor of safety varies from 1.67 to 1.92 for the range of KL_c/r between 0 and C_c . For F'_a corresponding to $KL_c/r > C_c$, a constant factor of safety of 1.92 is used. For all KL_c/r , F'_e is defined by Eq. 2.40.

It should be mentioned that inelastic buckling strength depends on the bending axis. For $F_{rc}/F_y = 0.3$, inelastic buckling occurs when $P/P_y > 0.7$. The solid lines between points A and B represent the true buckling strengths based on the tangent modulus theory. For strong axis buckling, it may be approximated by a

parabola (curve S). A straight line (curve W) gives a close approximation to the weak axis buckling strength curve.²⁶

The allowable stress for bending about the strong axis of a compact section is given by

$$F_b = 0.66F_y \quad (2.41)$$

This is based on the plastic strength of the cross section. Since the shape factor of most wide flange sections is about 1.12, the allowable bending moment becomes $0.6M_{px}$, giving the factor of safety of about 1.67. This factor of safety is used for all strong axis bending situations, even when the section is noncompact. When bending occurs about the weak axis, AISC specifies an allowable bending stress of

$$F_b = 0.75F_y \quad (2.42)$$

Since the shape factor of a W-shape bent about the weak axis is 1.5, the allowable bending moment is $0.5M_{py}$, yielding the factor of safety of 2.0.

2.7 Evaluation of Design Interaction Equations

In this section, the design interaction equations will be evaluated by comparing the predicted strength of beam-columns in example frames with the results determined from the inelastic analysis. Although the computed and allowable stresses are generally used in the interaction equations, it is convenient to express the computed stresses in terms of axial load and moments at the overload level equal to the factor of safety times the working load and the allowable stresses as the strengths of the member. Since AISC allows different factors of safety, as discussed in the previous section, it is simpler to express the computed force and

moments as the ratio of the basic overload quantities at a factor of safety of 1.67. Thus, the design interaction equations given in Sec. 1.3 become

(a) AISC Method

$$\text{Stability: } \frac{\lambda_1 P}{P'_{cr}} + \frac{0.85}{1 - \frac{\lambda_2 P}{P'_E}} \frac{M}{M_P} \leq 1.0 \quad (2.43a)$$

$$\text{Strength: } \frac{P}{P_y} + \frac{M}{M_P} \leq 1.0 \quad (2.43b)$$

(b) P-delta Method

$$\text{Stability: } \frac{\lambda_1 P}{P_{cr}} + \frac{C_m}{1 - \frac{\lambda_2 P}{P_E}} \frac{M^*}{M_P} \leq 1.0 \quad (2.44a)$$

$$\text{Strength: } \frac{P}{P_y} + \frac{M^*}{M_P} \leq 1.0 \quad (2.44b)$$

(c) Effective Length Method

$$\text{Stability: } \frac{\Sigma \lambda_1 P}{\Sigma P'_{cr}} \leq 1.0 \quad (2.45a)$$

$$\text{Strength: } \frac{\lambda_2 P}{P_{cr}} + \frac{1}{1 - \frac{\lambda_3 \Sigma P}{\Sigma P'_E}} \frac{M}{M_P} \leq 1.0 \quad (2.45b)$$

In these equations, λ_i are the ratios of the actual factor of safety used to the basic factor of 1.67. M^* is obtained from a second order analysis and the prime denotes the buckling loads in which the effective length factor in a sway mode is considered. It should be noted that the axial load, P , in the interaction equations is different for AISC and the effective length methods, and the P-delta method. Generally the axial load to be used in the equations is the applied load plus the load due to the overturning

effect considering the direction of the applied wind load. Since AISC and the effective length methods are based on the first order analysis, for the portal frame studied, the axial load in the column is $P + HL_c/L_b$. The P-delta method is based on the second order analysis. In this case the axial load that is used in the interaction equations is $P + (HL_c + \Sigma P \Delta_{e1})/L_b$, where Δ_{e1} is the sway obtained from the elastic second order analysis. The comparison of results in this section assumes that $L_b \gg L_c$, so that the force due to the overturning effect is not significant. Its effect depends on the length of the beam, which will be discussed in the next section.

The comparisons of various design interaction equations are shown in Figs. 2.42 to 2.48 for several slenderness ratios, G , and several α values. In these plots the effective slenderness ratio varies between 40 and 130. The comparisons are shown for both strong and weak axis bending. In each plot the results from the analysis discussed in Sec. 2.3 that considers the effect of residual stress and inelastic behavior are compared with the interaction equations. The plots in Figs. 2.42 to 2.48 do not consider the difference in the factor of safety, i.e., all λ_1 are unity and the buckling strength terms P_{cr} , P'_{cr} are based on curves S or W shown in Fig. 2.41.

For $\alpha = 0$, which is also the case of portal frames, the AISC equations are generally conservative. Although the comparison of elastic second order moment methods reveals that AISC expressions are slightly unconservative, the stability type interaction equation which is based on the buckling strength that considers the effective length factor makes the interaction equation conservative. The difference between the exact curve and the AISC curve is significant for large slenderness ratios and $G = 2.0$ (see Fig. 2.48). The strength of a very short column ($L_c/r_y = 20$) that is bent about the weak axis is much higher than that predicted by interaction equations, especially for low axial load.

Generally, the P-delta method and the effective length method predict strengths which are higher than the actual strength, especially for high axial load on columns with stiff end restraints. At the same axial load level, the unconservativeness is greater for weak axis bending. This is due to the effect of residual stress, which causes a greater reduction in stiffness when bending occurs in the weak axis than for strong axis bending. The effective length method gives better results than the P-delta method, because the estimate of the extent of second order moment is more conservative. Note that the P-delta method and the effective length method use different limits for the axial load term in Eq. 2.44b and use different limits for the axial load term in Eq. 2.44b and Eq. 2.45b, respectively. This results in a large difference between the P-delta method and the effective length method for high axial loads (see Figs. 2.44 and 2.45 as the examples). For frames where buckling occurs in the elastic range, the amplification factor in Eq. 2.45b checks the stability limit while the P-delta method converges to the load defined by Eq. 2.27. When buckling occurs in the inelastic range, the cutoff as defined by Eq. 2.45a provides a means to reduce the unconservativeness. It is to be noted that the stability limit defined by Eq. 2.45a does not necessarily coincide with the results from the inelastic analysis. This is attributed to two reasons. First, the design buckling strength is based on curve S or W, rather than the true strength curves (see Fig. 2.41). Second, the maximum strength analysis generally yields the stability limit higher than that based on the tangent modulus theory (from which the curves in Fig. 2.41 are derived). In any case, Eq. 2.45a gives a conservative prediction of buckling load (see Fig. 2.46 as an example).

When $\alpha > 0$, the AISC equation does not apply. The effective length method predicts better results than the P-delta method. Large discrepancies can be observed for medium length columns with

rigid restraint. The effective length method is conservative for predicting the buckling strength for $G = 0$. This behavior can be explained by referring to Fig. 2.29. The actual buckling strength for $G = 0$ is higher than for the design that uses the $\Sigma P \leq \Sigma P'_{cr}$ concept. The difference in the two methods decreases as G increases.

For columns with soft restraints, strength usually occurs at large sway displacement. It can be observed in Figs. 2.12 and 2.13 that the sway stiffness for large G is small; the ultimate strength is reached at $\Delta/L_c = 0.04$. In such a case, the deflection at working load would be excessive. Therefore, in the design of columns with flexible restraints, deflection at working load should be checked to be within the limit, e.g., $\Delta/L_c = 0.002$.

The effect of variation in the factor of safety in the interaction equations can be seen in Figs. 2.49 to 2.51. The comparisons of all design methods for the case of $G = 0$ and $L_c/r = 40$ are shown. In these plots the CRC basic column strength equation is used for both strong and weak axes. Thus, the stability limit is different from that shown in the previous plots. Also shown are the theoretical results for the case of no residual stresses. For weak axis bending, curve "D" corresponds to using $0.75F_y$ as the strength implied by the current AISC Specification. Strengths at overload level of 1.67 are matched with the theoretical results. It can be seen that using high values of factor of safety for axially loaded columns leads to more conservativeness in the current AISC method. It improves the results for the effective length method and the P-delta method. In fact, from the comparisons shown in Figs. 2.42 to 2.48, using the effective length method with the uniform factor of safety will lead to a satisfactory design. It should be noted that variations in the factor of safety result in rather a large scatter of solutions. This scatter is greater than the differences which occur among the various design approaches themselves using a

constant factor of safety. Therefore, significant attention to the effect of variation in the factor of safety should be paid by specification writers.

2.8 Effect of the Axial Load Due to the Overturning Effect

In the previous sections of this study, it has been assumed that the length of the girder is very long compared to the length of the columns. Therefore, the axial load arising from the overturning effect is not significant. In order to examine the effect of the girder length, a maximum strength analysis was conducted on a leaned frame. The length of the girder is selected to be equal to the length of the column. It is felt that this proportion is the minimum in practice and would show the largest effect of the overturning force. Figure 2.52 shows the interaction between the applied column loads and the wind load at the maximum strength of the frame. The column has $L_c/r = 40$ and $G = 0$ and is bent about the strong axis. The solid curve is the result for $L_b \gg L_c$ and the dashed curve is for $L_b = L_c$. The reduction of the applied column load due to the variation of beam length is not very significant and occurs mainly in the low column load region.

For a typical leaned frame subjected to combined column load and wind load, shown in Fig. 2.2, the axial load on the column to be substituted into the interaction equation is slightly different, depending on whether the first order or the second order structural analysis is used. In the AISC and the effective length methods, the axial load is $P + HL_c/L_c$, while in the P-delta method the axial load would be $P + (HL_c + \Sigma P\Delta_{el})/L_b$. It seems that the P-delta method is conservative as far as the axial load to be used is concerned, especially for leaned frames with relatively high load on the pinned column. To examine the significance of the secondary axial load $\Sigma P\Delta_{el}/L_b$, refer to Fig. 2.53. At the maximum load of

the frame, the column loads are P and αP and the wind load is H . The plots show the interaction of the axial load on the rigidly jointed column with the wind load in nondimensionalized forms. The solid curve is a true axial load in the column based on the inelastic analysis. The long and short dashed curves are the loads based on the first and second order elastic analyses and the broken curve is the applied column load. For $\alpha = 0$, the difference between the first and second order axial loads is not significant. For $\alpha = 2.0$, there is some effect due to the secondary axial load. As an example, at $P = 75.03$ kips ($P/P_y = 0.23$), $P + HL_c/L_b = 77.85$ kips and $P + (HL_c + \Sigma P\Delta_{el})/L_b = 80.31$ kips, the difference is in the order of 3 percent of P .

Figure 2.54 shows a typical comparison of design interaction equations for the leaned frame with $L_b = L_c$. In these comparisons the effect of secondary axial load is considered in the first term of the interaction equations. The first order axial load $(P + HL_c/L_b)/P_y$ is plotted as the ordinate. It may be observed that the effective length method generally gives a closer prediction of the maximum strength than the P-delta method.

CHAPTER 3

EXPERIMENTAL PROGRAMS

3.1 Design of Test Specimens and Loading Conditions

The purposes of the experimental study were to provide some data on the behavior of beam-columns in unbraced frames and to compare the strength of the beam-column test specimens with theoretical prediction and design interaction equations. Three unbraced frames and three biaxially loaded restrained beam-columns were tested. The specimens were full-size and the geometry in each type of structure was the same; only the loading conditions were different and were designed to simulate the actual conditions encountered in practice. The geometry and loading conditions of the specimens were selected so that the test results, when presented in the interaction diagrams, would be in the region that shows any difference between design methods clearly.

In testing the structures in which there is relative joint translation, difficulty arises because the gravity loading system must be designed to displace with the structure while maintaining the original line of action. To overcome this problem, a structure with twice the length of the actual structure and having identical boundary conditions at both ends is tested instead (see Fig. 3.1). This makes use of symmetry about the plane passing through the middle of the structure. With this testing arrangement, the joints at both ends of the structure do not translate so that the loading system can be designed to be fixed in position. The middle plane, which corresponds to the base of the real structure, translates with respect to both ends. This technique was used by Laosirichon³²

in the experimental study to determine the effect of beam yielding on the column strength. Another feature of the testing facility is that the plane of the structure is horizontal. Column load was applied against the reaction brackets which were prestressed to the testing slab.

3.1.1 Unbraced Frame Specimens. The general layout of the two-bay frame that was used with the test setup discussed is shown in Fig. 3.2. The frame was initially studied with column axial loads only and the specimen is shown at the state of bifurcation in the braced (Fig. 3.2a) and unbraced modes (Fig. 3.2b). The midlength of the columns is connected by links so that the displacement of all three columns is compatible. The links are also used for transmitting shear forces between columns in the combined gravity and lateral load test. Also shown in the figures are the charts for determining the effective length factor as a function of the column-to-beam stiffness, G , at the end and the boundary condition at the midlength section. These charts were constructed from the alignment charts for braced and unbraced modes of buckling. One of the objectives of the frame test is to verify the theory that the stability of an unbraced frame is approximately equal to the sum of the potential buckling strength of the individual columns in the sidesway mode; yet the load on each column must be less than the strength in braced frames. For the test, the loading arrangement was planned so that a column could carry higher load than its own buckling capacity in the sway mode, because of the potential bracing effect provided by other lightly loaded columns. In the design of the frames, the ranges of L/r and G were studied to determine the combination that gives a large difference in the buckling strength in the two modes to ensure that failure will not occur as an individual column before the frame reaches stability load. The result of the study on L/r and G is shown in Fig. 3.3, considering that the columns were bent about the weak axis. For each specified value of

G and L/r , the effective length factors for braced and unbraced cases were determined and the buckling strengths were obtained from the column curve in Fig. 3.3a. The difference in strength between the braced and unbraced modes is plotted as the ordinate in Fig. 3.3b. It can be seen that the slenderness ratio of 100 leads to the desirable result as G increases. The reason can be explained by referring to Fig. 3.3b. At an L/r of 100, the effective slenderness ratio in the unbraced case is likely to fall in the elastic buckling range, while that for the braced case is on the inelastic curve. This yields a large difference in the buckling strength. With the values of G and L/r so obtained, several cross sections were examined and the final design of the frame is shown in Fig. 3.4. The column and beam sections are $W8 \times 17$ and $M4 \times 13$; the lengths of columns and beams between the centerline of the joints are 20 ft., 11 in. and 8 ft., 6 in., respectively. All members are bent about the weak axis; therefore, lateral bracing to prevent lateral torsional buckling is not required. The slenderness ratio of the column from the joint to the midlength is 102 and G at the ends are 1.79 and 0.89 for exterior and interior columns, respectively. These values are based on section properties in the AISC Manual.

The next step was to design the loading on the frame. For the first two specimens, several trials of load arrangements were studied. The suitable loading scheme would be such that all columns are loaded to 70 kips; the loads on the exterior columns are maintained at this value while the load on the interior column is increased until failure occurs. The third frame was planned to study the design interaction equations for combined gravity and lateral loading, where strength of individual columns is not reached simultaneously. This is accomplished by loading the columns to different levels and maintaining the axial load. The lateral load is then applied until instability is reached. The effect of the magnitude of load on each column on the distribution of moments in

the structure was studied by means of an elastic second order analysis. It was decided to load the exterior columns to 50 kips and the interior column to 80 kips before the application of the lateral load to failure.

3.1.2 Biaxially Loaded Restrained Beam-Columns. The column cross section was first selected such that the width-to-depth ratio is small so as to increase the possibility of lateral torsional buckling if it would occur. It was decided to use W10x21 section, which has the B/D ratio of 0.58. The length of the column is restricted to the distance between the reaction beams, which is about 20 ft. The selection of the slenderness ratio and G with respect to both axes of bending were based on the interaction equations considering the specimen as two independent planar problems. Figure 3.5 shows the plots using AISC-type equations (Eqs. 1.24 and 1.25). The buckling strength about the weak axis controlled the axial load term. Two extreme values of G , corresponding to rigid and no restraints at the joint, were determined. It may be seen that the effect of the variation of G on the strength is confined to a narrow band for strong axis bending and is significant for weak axis bending. The specimen designed consists of a column made of W10x21 section and restraining beams in the strong and weak directions are fabricated from W8x20 and W5x18.5 shapes. The dimensions of the specimen are shown in Fig. 3.6, in which G for the strong and weak directions at the joint is 1.20 and 0.24, respectively.

In the design interaction equations, the three components of member forces that determine the strength of the beam-column are axial force and moments in two directions. It was planned to load each specimen with two force components to a certain level and to increase the other component until failure occurs. Preliminary study on the level of axial force and moments about the strong and the weak axes of the column was accomplished by

referring to the currently used design interaction equations (see Eqs. 1.16, 1.17, and 1.18) treating the specimen as a no-sway beam-column symmetrically restrained by beams at both ends. The first order elastic analysis was used to determine column end moments due to applied joint moments or to applied wind load.

The testing program for biaxially loaded restrained beam-columns is summarized in Fig. 3.6. The first specimen was planned for the study of the behavior and the strength of columns subjected to axial force and moments due to gravity load in two directions. This type of moment arises from unbalanced beam loads in actual unbraced frames and is conveniently simulated by applying the load by a stub cantilever.³³ For the specimen under consideration, the joint moment produces uniform first order moment diagram in the column. The symbols M_{js} and M_{jw} refer to joint moments applied about the strong and weak axes, respectively. In this specimen the joint moments are held constant and the column load P is increased to failure. In the second specimen, the two force components that are held constant are axial force and moment about the strong axis due to joint moment. The moment due to wind load in the weak direction is increased to failure. In the third specimen, axial force and moment about the weak axis, due to joint moment, are applied to the column and the specimen is loaded to failure by the wind load in the strong direction. The results of the preliminary study indicated that the initial levels of column end moments (due to joint moments) should be $M_x/M_{px} \approx 0.15$ and $M_y/M_{py} \approx 0.08$. These values were based on an axial force of $0.4P_y$; this level of axial force was selected so that the moment components would not be too small. With the levels of axial load and column end moments selected, the corresponding joint moments are $M_{js} \approx 520$ kip-in. and $M_{jw} \approx 220$ kip-in.

3.2 Material and Member Properties

For the unbraced frame and biaxially loaded restrained column specimens, the material for the columns is structural carbon steel conforming to ASTM A36. For beams, high strength low alloy columbian-vanadium steel, ASTM A572 Grade 50, is used so that higher elastic behavior of the restraint can be obtained. To minimize differences in materials, each shape was rolled from the same heat. The chemical composition and the mechanical properties of the steel from the mill reports are shown in Table 3.1. Steel was purchased in stock length of 40 or 50 ft. Table 3.2 shows the descriptions of steel lengths that were used for various components of the specimens and the type of material tests performed. The material properties were determined from the remaining part of the length. Four types of tests and measurements were performed: tension tests, cross section measurements, stub column test, and residual stress measurement.

3.2.1 Tension Tests. Tension tests were made for most of the length. Usually three coupons, two from the opposite flanges and one from the middle of the web, were cut from one section. This enables the bending and axial load capacity to be calculated if the section properties are measured. The results of the tension tests are shown in Table 3.3; static yield strength, σ_y , ultimate strength, σ_u , percent of elongation in 8 in., strain hardening modulus, E_{st} , strain at yield strength, ϵ_y , and strain at strain hardening, ϵ_{st} , are given. It can be seen that the web material usually has higher yield strength and much longer yield plateau than the flange material. The flange coupon has larger strain hardening modulus. This is typical for the sections which were cold-straightened by the rotarizing process. The tensile properties from different lengths of the same shape are quite consistant.

3.2.2 Cross Section Properties. The cross section dimensions were measured at the two ends of each member cut from each

length using a micrometer and a graduated scale. The average measured dimensions and the measured material properties are used to calculate cross section properties, i.e., the area and the moment of inertia, plastic moment of the cross section, and the yield load. These calculated properties and the nominal values from the AISC Manual are listed in Table 3.4. The section properties are in good agreement with those given in the AISC Manual.

3.2.3 Stub Column Tests. The purpose of the stub column tests is to establish the stress-strain curve in compression for the entire cross section and to determine if there are any appreciable residual stresses in the members that are used for columns. A high level of residual stress will lead to localized yielding at a load less than the cross section yield load, P_y . This reduces the proportional limit and the effective EI of the cross section. The tests were carried out on three specimens, two from the W8x17 section and one from the W10x21 section. The stub column specimens were 30 in. long and the end surfaces were machined flat. Before the test, the cross section measurement was also taken and the specimen whitewashed so that the progress of yielding could be observed. Specimens were tested in a 400-kip screw-type testing machine and the testing procedure followed the method recommended in the SSRC Guide.²⁹ The axial load-axial strain relationship for the three specimens is shown in Fig. 3.7. The plots revealed that there was high compressive residual stress in the steel because the deviation from linearity occurred at about 70 percent of the yield load. First yielding was observed in the web, so the high compressive residual stress in the web would be expected. This was verified by the residual stress measurements presented in the next section. The average yield load from the two specimens of W8x17 section is 198.5 kips and that of W10x21 section is 248.5 kips. These loads are within 4.5 percent and 1 percent of the calculated yield loads using the cross section dimensions and the yield

strength from the tension tests. The results of the stub column test and the relevant properties of the specimens were summarized in Table 3.5.

3.2.4 Residual Stress Measurements. Residual stresses were measured in two specimens, one from W8x17 section and the other from W10x21 section, by the method of sectioning.²⁶ The specimens were prepared from the remaining length that was used for stub column specimens. The distribution of residual stress of the two cross sections is shown in Fig. 3.8. It can be observed that the web contains high compressive residual stress and the distribution is reasonably parabolic. The flange portion has small residual stress and in some instances the flange tip is in tension. The distribution of residual stress in the flange is irregular. This pattern is typical for rotarized cross sections. The low residual stress level in the flange is a favorable characteristic as far as column strength is concerned, because full flexural rigidity EI is effective for high levels of axial load. The actual distribution of residual stresses was used for the theoretical predictions of the test behavior.

CHAPTER 4

TWO-BAY UNBRACED FRAMES

4.1 Test Setup

4.1.1 Details of Test Specimens. All unbraced frame specimens were identical in geometry. Steel sections which were used to fabricate columns and beams were W8x17 and M4x13, respectively, and all members were bent about the weak axis. The length of the columns between the centerline of the joints was 20 ft., 11 in., and that of the beam was 8 ft., 6 in. (see Fig. 3.3 and Fig. 4.1). All beam-to-column connections were moment resisting end plate connections in which 1 in. end plates were welded to both ends of the beam, which in turn were bolted to the web of the columns by means of 15/16 in. ASTM A325 high strength bolts, as shown in Fig. 4.2. The connections were designed to transmit the plastic moment of the beam or the reduced plastic moment of the column cross section at the maximum axial load. The linkages between the midlength of the columns were made of two 2 in. x 2 in. x 1/4 in. angles and were connected to the web of the columns by bolting to a small tee section; this connection could transmit only shear forces between the exterior and the interior columns. At the ends of the interior column were welded 1/2 in. end plates to which a 1-7/8 in. grooved-plate fixture could be fastened, as shown in Fig. 4.3. Cold rolled pins 1-3/4 in. in diameter were welded to each flange of the exterior columns at the joint location. Each pin was reinforced with two triangular plates welded to the pin and to the flanges of the column. A 1/4 in. stiffener plate was welded across the web of the column on the outside of each exterior

column joint. These pins were used for connecting the tension ram fixtures, as shown in Fig. 4.4.

4.1.2 Loading Apparatus. The plane of the frame is horizontal and the weight of the frame was supported by bents made of 4 in. x 4 in. x 1/4 in. angles which were bolted to the testing slab; rollers were used underneath the frame in order to minimize the friction. Axial load on the interior column was applied by a 100-ton hydraulic ram acting against a reaction beam at one end of the column and a load cell was placed between the end plate and the reaction beam at the other end of the column. The ram and the load cell were supported on a platform and were braced against movement in any direction. A spherical end fixture was placed between the ram and the reaction beam to align the load. A similar arrangement was used at the other end of the interior column. The reaction beams were supported by two reaction brackets which were prestressed to the test slab by means of 3 in. anchor bolts. During loading, the ram load was transmitted to the column through the fixture consisting of a knife edge mounted on the ram piston and the grooved plate which was bolted to the column end plate, as shown in Fig. 4.3.

A self-contained loading system was used for the application of axial load on the exterior columns. The system consists of a 5 in. bore hydraulic tension ram, a 1-1/2 in. loading bar of high strength steel, and a load cell connected in series (see Figs. 4.4 and 4.5). Load cells in the system were made of high strength aluminum bars and were calibrated to measure the load in the line. The fixture at the ends of the system consisted of a knuckle in which the eye was mounted with two roller bearings which fitted to the pins that were welded to the flanges of the column. Bearings were used to minimize the friction between the pin and the knuckle that would restrain the joint from rotation. Each exterior column was loaded with two tension rams and the hydraulic hoses for all four rams were connected to a common manifold. The axial load on

the columns was maintained by two pumps; one pump was used for the interior column and the other was used to operate all tension rams for loading the exterior columns.

The lateral loading system which was used in Specimen F3 consisted of a Universal load cell connected by means of threaded rods to the auxiliary frame on one side and to a nut which was welded to a plate on the other side, as shown in Fig. 4.6. This plate was bolted to the web of an exterior column opposite the tee connection of the lateral linkages. By tightening the nuts which were used to lock the threaded rod to the auxiliary frame, the frame was forced to displace a specified distance; the force which was developed in the threaded rods could be measured by the load cell.

4.2 Instrumentation. The interior column load was measured by a 240-kip compression load cell and each exterior column load was monitored by tension load cells connected in series to the 1-1/2 in. loading bars. The compression load cell was considered accurate to within 0.3 kip and the tension load cells were accurate to within 0.03 kip. During the test, the pressure in the hydraulic lines to the rams was also measured by pressure transducers as well as by pressure gages. The pressure records provide a mean to check the magnitude of load in the columns. The load indicated by the pressure readings was within 3 percent of that given by the load cells. All loads used in the results were taken from the load cells, since these were considered to be more accurate. The lateral load was measured by a Universal load cell calibrated to 30 kips and was considered accurate to within 0.02 kip.

Strain data were recorded by means of W80 electrical strain gages having the gage factor of 2.12. These gages were placed at four stations within the elastic zones of each member. At each station there were four gages bonded to the flange surface at 1/4 in.

from the flange tip. From the strain data, the moment at a cross section can be computed knowing the modulus of elasticity and moment of inertia of the cross section. The probable error in the strain recording system corresponds to a moment of 0.23 kip-in. For beams, moments at the strain gage locations are used to determine the shear force and the beam moments at the joints based on equilibrium. For columns, the deflection at the strain gage locations and at the joints must be determined in order that equilibrium of the column, which includes the effect of axial force acting through the displaced configuration of the structure, can be established. Strain gages were also placed at two stations of an unloaded column member and these recorded strains were used as temperature compensation.

Deflection of the columns was measured by 0.001 in. dial gages mounted on stands. Rotation of the joints and the midlength of the columns was measured from the differential movement of two points on an arm which was clamped to the top flange of the members. The deflection of the interior column was also recorded from a transit sighting on scales. This provided a check on dial gage readings. Figure 4.7 shows the arrangement of the instrumentation for all specimens. Due to the large amount of instrumentation to be recorded during the test, strain gages and exterior column load cell gages were connected to a remote switching unit of a VIDAR data acquisition system so that the strain data could be recorded automatically during each load stage. The pressure dial gages, pressure transducers, and interior column load cell were monitored and the displacement data were taken manually during the test.

4.3 Controlled Test

Before the main tests on the unbraced frames were conducted, a test was performed on one of the exterior columns as an isolated member. The purpose of the test was to check the loading system

and to evaluate the significance of friction in the pin connection. The member was acting as an Euler column and remained elastic throughout the test. Both tension rams were connected to the same pump; the axial load and the deflection of the column at the mid-length and at the joints were recorded. Figure 4.8 shows the results of the Euler test in the form of an axial load-centerline deflection plot and the Southwell plot. The Southwell method is a technique to determine the buckling load from the experimental data of an elastic column having initial load eccentricity. If the ratio of the centerline deflection measured from the unloaded position of the column to the axial load, Δ/P , is plotted as the ordinate and the deflection is plotted as the abscissa, it was found that the relationship is linear.⁶⁰ The buckling load of the column is the inverse of the gradient of the straight line and the intersection with the deflection axis gives the magnitude of the initial eccentricity of the load with respect to the straight position of the column. The Southwell method is advantageous because it does not require the column to be loaded to the buckling load level. The method gives reliable results if the maximum axial load level is not less than 80 percent of the actual buckling load.⁶⁹

In this test the maximum applied load was 33.2 kips. The Southwell plot yielded a buckling load of 35.5 kips and the Euler load based on the modulus of elasticity of 29500 kips is 34.5 kips. The difference between the experimental buckling load and the theoretical buckling load was 2.9 percent, which may be attributed to friction at the pin, error in the modulus of elasticity, and experimental errors in measuring the load and the deflection. The initial eccentricity determined from the Southwell plot was 0.098 in., compared with the measured eccentricity of 0.125 in. This is attributed to the effect of the pins being eccentric to the center of the web plane and the initial shape of the column.

This test indicated that the friction effect, if any, was less than 3 percent.

4.4 Test Procedures and Test Results

4.4.1 Specimen F1. This specimen was loaded with column loads only to simulate the condition of unbraced frames under gravity loading. The initial deflected shapes of the columns were measured by stretching a string between the joints and measuring the offset to the flange. The magnitude of the out-of-straightness was: left exterior column, 0.07 in. to the east; right exterior column, 0.23 in. to the west; and the interior column, 0.11 in. to the east. Initially all columns were loaded equally to a load of 70 kips. Thereafter, the exterior columns were held at constant load and the interior column load was increased until ultimate load was obtained. Figure 4.9 shows the behavior of Specimen F1 throughout the history of loading. The controlling displacement parameter is the deflection of the midlength of the columns. This deflection was measured from the position in the unloaded state. Load stages 2 to 12 corresponded to the proportional application of column loads. Although the rams on the exterior columns were operated from the same pump, the loads on each column differed slightly. At the end of load stage 12, the loads on the two exterior columns were 70.1 and 67.0 kips, a difference of about 4 percent. Up to load stage 15 there were no apparent yield lines. First yield lines occurred at the top flange of the interior column adjacent to the end plate at the south end, which was due to the welding residual stresses. The stiffness of the frame between load stages 15 and 16 decreased rapidly. At the end of load stage 16, extensive yield lines occurred at a distance about 30 in. from the midlength towards the south joint of the interior column. The deflected shape of the interior column was not symmetrical; the curvature seemed to concentrate at the yielded zone in which the deflection was

larger than that at the midlength. The maximum load on the frame of 269.1 kips was reached at load stage 16, where the interior column carried 132.7 kips. Beyond load stage 16, the frame could not carry higher load and failure occurred suddenly by sidesway deflection. After the frame stopped moving, the deflection at the midlength was measured by the transit and was found to be 2.4 in. The loads dropped to 61.2 and 58.3 kips for the exterior columns and 110.8 kips for the interior column. The total load on the frame was 230.1 kips; this corresponds to a reduction of 14.5 percent from the maximum load. The equilibrium path during instability could not be obtained and is shown dashed in the load displacement curve. Figure 4.10 shows the deflected shape of the frame before the specimen was unloaded. It could be observed that the deflected shape of the interior column was not symmetrical about the midlength. The frame was unloaded and by inspection extensive yielding occurred in the compression zones of the interior column. These zones were at about 8 in. from both joints and along the length between the middle strain gage locations. The section where yield lines formed earlier seemed to have reached plastic moment capacity. At this section, yield lines penetrated to the web junction. There was no distress in the beams nor in the exterior columns except some yielding at the top of the web below the pins due to high crippling stresses.

The strain data that were recorded during the test by VIDAR acquisition system were in voltage units. By knowing the change in strain due to temperature and the system drift, the data were converted into strain due to applied loads, from which bending moments at strain gage locations could be computed. A computer program was written to calculate the moments at the ends of the members, given the moments at the strain gage locations, the axial force, the distance between gages and the ends, and the deflection at these points. The moments at various locations of the frame throughout

the history of loading are plotted in Figs. 4.11 and 4.12. These moments were low up to load stage 15. Thereafter, the increase was rather sudden. The moments at the assumed points of symmetry are shown on the same plot, which indicates that the behavior of the frame is not truly symmetrical; however, the difference is not significant. From the results of the calculated moments it is indicated that the equilibrium of moments at the joints checks very well to within 7 percent of M_p . The column loads indicated by load cells agree to within 10 percent of those calculated from strain gage data.

4.4.2 Specimen F2. This test was conducted to confirm the frame stability load of Specimen F1. At the end of test F1 the deflected shape of the interior column was not symmetrical. It was found that the roller on the screw jack near the north end that was used to support the dead weight of the interior column was very tight. This may have restrained the column from deflection and may have raised the frame stability load. Since the beams and the exterior columns were still elastic, and could be reused, it was decided that the specimen would be retested; only the interior column need be replaced. The initial shapes of all columns were measured and the magnitude of the initial out-of-straightness was: left exterior column, 0.26 in. to the east; right exterior column, 0.28 in. to the east; and interior column, 0.2 in. to the east. As a precaution against sudden failure due to bifurcation the lateral loading unit was attached to the left exterior column, but the nut which was used to lock the threaded rod to the auxiliary frame was kept loose so that there was no lateral load exerted on the structure. The sequence of loading was the same as Specimen F1. Figure 4.13 shows the load displacement behavior of Specimen F2. Load stages 2 to 11 corresponded to the proportional increase of all column loads. The frame deflection started to increase as the loads increased. This behavior was different from the previous

specimen because the initial deflection was larger and all columns were bent in the same direction. At the end of load stage 11, all columns were loaded to about 70 kips. The deflection of the frame was 0.67 in., compared with 0.1 in. for Specimen F1. From load stage 11, the load on the exterior columns was held constant while that on the interior column was increased independently. The first yield lines were observed after load stage 16 at the middle of the flange of the interior column, adjacent to the end plate on the south end. The frame reached the instability limit after load stage 17, where the maximum load was 233.6 kips; this corresponded to a reduction of 13.2 percent from the maximum load of Specimen F1. Beyond this stage, the deflection of the frame increased while carrying virtually no additional load. As the deflection increased further due to the loss of stiffness of the frame, column shortening caused the ram pressure to drop. Consequently, the column loads decreased and the frame was in equilibrium state on the unloading part of the load displacement curve. After load stage 18, yield lines occurred extensively on the interior column between the midlength and the strain gage location on the compression side as well as at a distance of 24 in. from the north joint. The yielded zone at the midlength region of the interior column penetrated about 2 in. from the flange tip. Figure 4.14 shows the yielded portion near one of the strain gage stations on the interior column. Yield lines on the exterior columns were rather symmetrical but not as extensive as the interior column. It was observed that as the ultimate load was approached the exterior columns moved in opposite directions in the north-south (longitudinal) direction, resulting in a racking-type action; this movement increased faster beyond the ultimate load. The deflected shape of the interior column was similar to that of Specimen F1, being unsymmetrical with respect to the midlength section. The frame was unloaded after load stage 20.

The moments in the member components of the frame are shown in Figs. 4.15 and 4.16. These figures show the moments at the ends and at the midlength of the columns and at the ends of the beams. The moments at the locations of assumed symmetry are in good agreement and the change in moments occurred gradually as the loads increased. The equilibrium of moments is checked at every joint for all loading stages and the error is found to be within 8 percent of the plastic moment capacity of the column. Figure 4.17a and 4.17b shows the variation of the exterior joint rotations of the frame with axial loads. The change of the rotations of the interior column joints and the midlength section of all columns with axial loads is shown in Fig. 4.17c and 4.17d. It may be seen that for exterior columns, the joints at the north end rotate less than the joints at the south end. This is attributed to the racking movement of the frame tending to satisfy the equilibrium condition. The exterior column on the left is moving longitudinally to the south direction and the one on the right is moving northwards. For the interior column, the north joint rotates less than the south joint and in the opposite sense until the maximum load is approached; this is also attributed to the racking motion of the frame. At the maximum load and in the unloading range, the rotation of the north joint changes to the same sense as that of the south joint. This may be attributed to the switch in the mode shape as yielding occurs when the axial load is high.

4.4.3 Specimen F3. In this specimen, 50 and 80 kip axial loads were applied proportionally to the exterior and interior columns, respectively, during this first loading stage. After this, the column loads were to be kept constant while the lateral load was applied to the structure. This scheme of loading simulates the combined gravity and wind loading in real structures. For this test, two end stops were set up at the north end of the exterior columns to prevent excessive racking action of the frame as the

load approached the ultimate condition. The initial deflection of the columns was: left exterior column, 0.13 in. to the east; right exterior column, 0.07 in. to the east; and interior column, 0.13 in. to the west. The lateral load displacement characteristic of the frame is shown in Fig. 4.18. Load stages 1 to 7 corresponded to the proportional application of axial loads. At the end of load stage 7, the loads on the exterior columns were 54.7 kips and 53.6 kips, a difference of 2 percent, while the interior column load was 79.9 kips. After load stage 7, the axial loads were held constant by manually controlling the hydraulic pumps while the lateral load was applied. The deflection that is shown in Fig. 4.18 was measured from the initial unloaded position of the midlength of the columns. The initial behavior of the frame between load stages 7 and 11 was elastic and the relationship between the lateral load and the deflection was reasonably linear at low level of wind load. First yielding occurred after load stage 12, at a distance of 5 in. from both joints of the exterior columns. These yield lines were localized and were probably due to residual stresses arising from welding of the triangular plate to the pin. After load stage 13, there were some slight yield lines at about 5 in. from the south joint of the interior column; elsewhere the frame appeared to remain elastic. Yield lines appeared within a distance of 13 in. on either side of the midlength of the interior column after load stage 14 and propagated along the length during load stage 15. At the end of load stage 16, both exterior columns started to yield along the midlength to a distance of 14 in. on either side. There was relatively little yielding at all of the joints except at the south joint of the interior column where early yielding was observed. This was probably due to high localized residual stresses. The maximum lateral load carried was 2.25 kips and was reached after load stage 14. The deflection at the maximum strength was 2.43 in., corresponding to a sway index (Δ/L_c) of

0.019. The ratio of the load at the stage just before first yielding (load stage 11) to the maximum load was 0.67. After the maximum load was reached, the frame unloaded quickly, indicating an instability type of failure. The deformed shape of the frame is shown in Fig. 4.19, which appeared to be symmetrical. The frame was unloaded after load stage 18. The unloading was carried out in two steps. First, the lateral load was released and, second, the axial loads on all columns were released. Figure 4.20 shows typical yield lines at the south joint of the interior column at the end of load stage 18.

The moments at the ends of the members and at the midlength of all columns were plotted as a function of lateral load and are shown in Figs. 4.21 and 4.22. It can be seen that the rate of increase in moments with the wind load was larger for the loading stages than for the unloading stages. The moments at the point of symmetry in the beams were in very good agreement, while there was some discrepancy in column moments. Generally, the equilibrium of moments at the joints is checked to within 10 percent of the plastic strength of the columns. Also, the axial load in the columns indicated by strain gage data is in good agreement with that measured by the load cells to within 10 percent.

4.5 Discussion of Test Results

4.5.1 Theoretical Analysis. A theoretical prediction of the behavior of the test specimens was made using a computer program, FRAME 99, for the inelastic analysis of planar steel frames which was developed previously.⁴⁸ This computer program accounts for all the nonlinear effects due to material properties, support and geometry changes, and inelastic unloading caused by strain reversals in the inelastic ranges. The method of analysis which was the basis for the computer program consists of an iterative nonlinear inelastic member solution nested within an iterative nonlinear solution

for the frame joint displacements using the tangent stiffness technique. A member is divided into a series of discrete elements. A cross section of the member consists of fibers in which the material properties are characterized by independent stress-strain relationships. Trial joint displacements are assumed and the structure is analyzed by the two-fold integration scheme until the equilibrium, compatibility, and boundary conditions are satisfied.

The stability of the frames in this study is determined by the limit load technique suggested by Oral.⁴⁸ In this technique a small value of sway deflection is assumed and the lateral load required to produce this displacement is determined for several trial values of gravity load. The critical value of gravity load is the one which requires no lateral load to produce the specified sway displacement. Generally, the critical load is determined by linear interpolation between the corresponding values of gravity load and lateral load.

For frames subjected to combined gravity and lateral loads, the relationship between the lateral load and sway displacement can be obtained directly for the loading portion of the response. For the unloading portion, the computer program provides a deformation control option to establish the equilibrium position in this region. A linear spring with very large stiffness is introduced at a monitor joint in the direction of the required displacement. With a specified value of deflection, the program can determine the required load for equilibrium. This option is also useful for determining the frame stability load by the limit load technique discussed.

4.5.2 Analytical Model of Test Specimens. The model of the specimens that was used for theoretical analysis is shown in Fig. 4.23. To reduce the computer time, half of the actual frame was solved. The plane of symmetry at the midlength of all columns was replaced by roller supports which were free to displace

laterally but were completely restrained against vertical movement and rotation. The end support of the interior column was restrained against lateral translation but was allowed to displace vertically and to rotate freely. This corresponds to the knife edge support in the actual structure. The ram loads on the exterior columns were represented by externally applied load. The numbers of discrete elements that were specified for columns and beams were 40 and 30, respectively, giving about a 3 in. length to each discrete element. From the results of previous experimental studies,^{2,14,33} the yield zone did not occur at the center of the joint, but appeared at some distance away; this is due to the stiffening effect of the joint. This effect was simulated in the model by specifying a certain distance from the joint to remain elastic irrespective of the stress level. In the analysis, one discrete element was specified to account for the size of all joints. Since the location of the rotational spring is at quarter point within a discrete element, the length of specified elastic element from the center of the joint was 3.75 in. The linearly elastic elements were also specified for the portion of the interior column between the end plate and the center of the joint. The actual material and cross section properties were input for all the members. The elastic-plastic stress-strain relationship with strain hardening, which was obtained from the tension coupon test, was input separately for the flanges and the web. The measured residual stress distribution was input for all columns. For beams, no residual stresses were specified. This was justified because the test results revealed that the beams were elastic. In fact, the level of residual stress in the beam flanges would be low, since the members had been rotarized. The initial imperfection of the columns was also taken into account in the analysis.

4.5.3 Behavior of Test Specimens. The stability load of Specimen F1 was obtained analytically by specifying a small sway

deflection of 0.25 in.; this corresponds to a sway index of 0.002. Since it was required to determine the buckling capacity of the frame, the initial imperfection of the frame was taken as zero. In the test, the axial loads on the external columns were held constant after load stage 12. However, there was some slight variation in loads during succeeding load stages before bifurcation occurred. Therefore, the average values of loads were input, i.e., 70.2 kips on the left and 66.9 kips on the right exterior columns. Several interior column loads were tried until the horizontal load required to keep the frame in equilibrium was zero. The stability load of the frame at this specified deflection is 281 kips. The frame was also analyzed for other specified values of sway deflections, as shown in Fig. 4.24. The post-buckling strengths of the frame and the corresponding sway deflections were shown on the same plot of the test results in Fig. 4.9. The post-buckling strength curve was extrapolated to give the stability load of 285.3 kips at the onset of sway buckling. The ratio of axial load to the yield load of the individual columns at the instant of buckling was 0.37 and 0.35 for the exterior columns and 0.75 for the interior column. These values were based on the calculated yield load using material properties from the tension test. The maximum test load of Specimen F1 was 269.1 kips; this was 94 percent of the theoretical sway buckling load. The determination of experimental buckling loads of Specimens F1 and F2 using Southwell technique was conducted. The test buckling loads were found to be 289.6 kips for Specimen F1 and 279.2 kips for Specimen F2. This agrees to within 3 percent of the theoretical buckling load.

In determining the buckling strength of columns in unbraced frames using the nomograph, the stiffness that a restraining beam provides to the joint is $6EI_b/L_b$, which is the result of the assumption that the beam is bent antisymmetrically. The buckling strength of individual columns of the test specimen, based on the design

alignment chart, was determined by considering the exterior and the interior subassemblages as shown in Fig. 4.23. The beam length in each subassemblage is half of that in the real frame and the far end of the beam is pin-supported so that the stiffness of the restraint equals to $6EI_b/L_b$. Since the effective slenderness ratio of the column in the subassemblages is in elastic buckling range, the buckling load can be determined by performing a stability analysis of the beam-column.⁶⁰ The vanishing of the determinant of the stiffness characteristics of the system leads to the buckling load. The joint size is considered by specifying some distance from the joint to be rigid. The range of the buckling load for the column in the exterior subassemblage is 87.7 to 89.6 kips, and that for the column in the interior subassemblage is 102.8 to 106.1 kips, from which the buckling strength of the frame becomes 278.1 to 285.3 kips. The limits depend on whether the joint size is considered or not. The results from the limit load technique agree with the sum of the individual column strengths within less than 2 percent.

In the test, the average load on the exterior columns was 76.5 percent of their own buckling strengths; therefore, there was some reserve to provide a bracing effect for the highly loaded interior column. At the maximum test load, the load on the interior column was 132.7 kips, which was 25 percent higher than the capacity considered as the individual column. It was observed that the stiffness of the frame decreased appreciably after load stage 15. Yielding occurred at a distance of 30 in. from the midlength towards the south joint of the interior column. This was due to the effect of combined axial force and bending moment as the deflection increased. The deflected shape of the interior column became noticeably unsymmetrical after load stage 15. This may be attributed to the level of interior column axial load which approached the buckling strength in the braced mode, which was nominally equal to

$P = 142.3$ kips (see Fig. 3.1); however, the effect of deterioration of stiffness of the frame in the unbraced mode was dominating, which caused the sudden sidesway movement. Table 4.1 shows a summary of the test results and the comparison with the theoretical prediction.

The theoretical behavior of Specimen F2 was determined. In this specimen the initial imperfection was larger than Specimen F1 and the structure deflected from the start of loading. In the analysis, the initial imperfection was input and the loads corresponding to several loading stages were applied to the structure from which the analysis yielded the deflection. After instability was reached, the limit load technique was used to determine the solutions in the unloading zone for the specified displacements of 1.6, 2.0, and 2.4 in. The theoretical result is shown in Fig. 4.13 and can be seen to be in very good agreement with the test behavior. The moments at various locations in the frame are also plotted in Figs. 4.15 and 4.16 for comparison. Generally, the results are in reasonable agreement with the theoretical prediction. Joint rotations from the analytical results were also shown in Fig. 4.17; the predicted values overestimate the test results.

The plastic strength was not reached at any location in Specimen F2. The reduced plastic moment due to the presence of axial load of all columns was calculated for various load stages. At the instability limit of the frame, the axial loads in the two exterior columns and the interior column were 65.2, 62.1, and 106.3 kips, and the corresponding plastic moment capacities were 161.0, 161.3, and 144.4 kip-in. These values of M_{pc} were based on simple plastic theory, but different yield strengths in the flanges and the web were considered. The behavior of this specimen was controlled by the stiffness characteristics of the frame. First yield lines observed at the south end of the interior column were probably due to welding residual stress at the end plates and did not seem to affect the general behavior of the frame. Extensive yielding

occurred along the central portion of the interior column after load stage 17 and was the cause of the deterioration of stiffness of the frame. The column load could not be maintained as the deflection increased. The yield lines in the interior column were spreading relatively uniformly over the middle portion.

The theoretical prediction for Specimen F3 is shown in Fig. 4.18. The comparison of the experimental and theoretical behavior is in reasonable agreement. The predicted maximum load was 2.30 kips, compared with the test result of 2.25 kips, a difference of 2.2 percent. The deflection at maximum load for the predicted and the test results was 2.10 in. and 2.47 in., respectively. The initial sway stiffness was obtained by using a least square fit to the data in the loading stages before first yielding occurred, and was found to be 1.27 kip-in. The predicted result of the initial sway stiffness was 1.58 kip-in., which overestimated the actual stiffness. This may be attributed to the fact that the beams were framed to the web of the columns. When the wind load was applied, the flexibility of the web plate causes some localized end rotation in the beams. As a result, the stiffness of the frame is reduced.

The moments from theoretical prediction are shown in Figs. 4.21 and 4.22. For the section at midlength of all columns, the predicted values underestimated the extent of the measured moment for loads below ultimate load. The comparison for the beams was in good agreement in the loading stages but the measured moments were overestimated by the predicted results in the unloading stages. In reference to the load-deflection relationship, first local yield lines were observed after load stage 12, at a distance of 5 in. from both joints of the exterior columns. This was followed by yielding at 5 in. from the south joint of the interior column after load stage 13. At these stages there was a gradual decrease of the frame stiffness. Yielding in the middle portion occurred between

load stages 13 and 14, which reduced the stiffness appreciably, and the frame could not carry higher load beyond load stage 14. There was little evidence of moment redistribution because instability was reached very soon after yielding occurred in the middle of the interior column. After instability was reached, stiffness decreased further as a result of yield lines propagating along the length of the middle portion of the interior as well as the exterior columns; this caused further reduction in the lateral load. At the maximum levels of axial loads in the columns, the reduced plastic moment capacities of the sections were: left exterior column, 161.9 kip-in.; right exterior column, 162.1 kip-in.; and interior column, 158.9 kip-in. It can be seen that the moment levels at all locations of the frame were below M_{pc} , except at the midlength of the right exterior column. The behavior of this specimen was controlled by instability, due to the secondary effect of axial loads. Table 4.2 shows the summary of test results of Specimen F3 and the theoretical predictions.

4.6 Comparison of Test Results with Design Equations

In Specimens F1 and F2, where the column design is governed by stability of the frame, the current AISC method requires each column to have a capacity equal to its individual buckling strength, which is based on the effective length in the unbraced mode. With this approach, the interior column would be allowed to carry the axial load of 106.1 kips (Sec. 4.5.3). The results from the test and the analytical studies revealed that the interior column can carry an axial load at least 25 percent higher than the suggested value when the other columns in the frame were loaded to 76.5 percent of their own buckling strengths. The results provide the evidence that the stability of the system is equal to the sum of the individual column strengths.

The methods of design of columns in unbraced frames subjected to combined axial force and bending moment were discussed in Chapter 2. The interaction equations in terms of the ultimate strength were given by Eqs. 2.43 to 2.45. Without considering the difference in factors of safety for axial load and bending moments, the interaction equations can be written as follows:

AISC Method:

$$\text{Stability } \frac{P}{P'_{cr}} + \frac{0.85}{1 - P/P'_E} \frac{M}{M_p} \leq 1.0 \quad (4.1a)$$

$$\text{Strength } \frac{P}{P_y} + \frac{M}{M_p} \leq 1.0 \quad (4.1b)$$

P-delta Method:

$$\text{Stability } \frac{P}{P_{cr}} + \frac{C_m}{1 - P/P_E} \frac{M^*}{M_p} \leq 1.0 \quad (4.2a)$$

$$\text{Strength } \frac{P}{P_y} + \frac{M^*}{M_p} \leq 1.0 \quad (4.2b)$$

Effective Length Method:

$$\text{Stability } \frac{\Sigma P}{\Sigma P'_{cr}} \leq 1.0 \quad (4.3a)$$

$$\text{Strength } \frac{P}{P_{cr}} + \frac{1}{1 - \Sigma P/\Sigma P'_E} \frac{M}{M_p} \leq 1.0 \quad (4.3b)$$

In these equations, M is the larger end moment determined by a first order elastic theory; M^* is the larger end moment determined by the P-delta method of analysis; other terms have the same meaning as discussed in Chapter 2. The buckling strengths P_{cr} and P'_{cr} are based on the elastic buckling curve, since it is felt that at the slenderness ratio of the effective slenderness ratio under

consideration, buckling still occurs in the elastic range due to the low value of residual stress in the flange tip of the W8x17 section.

Figures 4.25 and 4.26 show the plot of the relationships between the axial load and the first order end moment, as suggested by several design methods for the exterior and the interior columns in Specimen F3. Only the left exterior column was considered because it carried slightly higher load than the right column. In Fig. 4.25, the quantities are in absolute units, while those in Fig. 4.26 are in nondimensionalized form. The solid line represents the AISC method; the P-delta method and effective length method are shown in short dashed line and long dashed line, respectively. In determining the design curves for the P-delta and effective length methods, the ratios of the axial loads are kept in the same proportion as in the test. For the proportions and levels of axial loads on the columns, the applied wind load is controlled by the capacity of the interior column. The predicted wind loads by various design methods are compared with the test result in Table 4.3. It may be seen that the AISC method gives a very conservative prediction of the maximum wind load (134.4 percent conservative), because it considers only the individual column strength in determining the amplification factor. In the P-delta method, the result is 20 percent unconservative and is controlled by the strength-type equation (Eq. 4.2b). It should be noted that the limitation on C_m to be not less than 0.4 is not used, since this study deals with the planar behavior. It is found that if this limit is used ($C_m \geq 0.4$), the predicted result becomes 3.7 percent conservative and Eq. 4.2a controls. The test result agrees well with the effective length approach, which is 8.7 percent conservative. The contribution of axial load and bending moment terms in the interaction equations is summarized in Table 4.4. As an example, for the interior column the magnitudes of the axial load and moment terms are 0.747 and

0.253 for the AISC method, 0.418 and 0.582 for the P-delta method, and 0.575 and 0.425 for the effective length method.

CHAPTER 5

BIAXIALLY LOADED RESTRAINED BEAM-COLUMNS

5.1 Test Setup

5.1.1 Details of Test Specimens. Figure 5.1 shows the general view of the test setup and Fig. 5.2 shows an end view of the test specimen. All the test specimens were identical and the test program has been summarized in Fig. 3.6. The W10x21 column was cut to a length of 22 ft., 3 in. and the length of the column between the centerline of the joint is 20 ft., 8 in. In order to use the same beams for all three tests, bolted beam-to-column connections were used. The design method given in Ref. 71 indicated that the flanges of the W10x21 column were too thin to support the bolt forces in the tension zone of the moment connection. Column flange bending by the bolt forces was minimized by the box-type connection shown in Figs. 5.3 and 5.4. The joint was fabricated by welding the flange tips of two 15 in. long tee sections to the edges of the column flange and welding the stem of the tees to the column web. Before the tees were welded, 15/16 in. holes were drilled in the web of the column and in the tee sections. Threaded rods 10 in. long were cut from a 7/8 in. diameter A4140 steel bar. These rods were used as fasteners for the restraining beams and the stub cantilevers in the weak direction. Spacers were used between the inside face of the tees and the column web to reduce bending of the tee plates, since they spanned across the web which was about 9 in. deep. These spacers were cut from a 1 in. diameter extra strong pipe with both ends being machined flat. The fasteners for the restraining beams and the cantilever stubs which were framed to the flanges of the column were 7/8 in. A325 bolts and nuts which were

tack welded to 1/2 in. x 2 in. x 15 in. washer plates. These washer plates were used to increase the punching shear capacity of the column flanges. After the joints were fabricated, the ends of the columns were squared, to which 1/2 in. x 10 in. x 12 in. end plates were welded. The restraining beams in the strong direction were cut from W8x20 to a length of 8 ft. A 1-1/4 in. x 5-3/4 in. x 15 in. end plate was welded to one end of the beam. The restraining beams in the weak direction were cut from W5x18.5 to a length of 6 ft., 10 in. to which a 1 in. x 7-1/2 in. x 12 in. end plate was welded. All the beams were bent about the strong axis.

5.1.2 Loading Apparatus. The column was tested in the horizontal plane, which was temporarily supported by bents made of 1/4 in. x 4 in. x 4 in. angles. The end section of the specimen simulates the boundary condition at the floor level of the real structure and the midlength section represents a fixed base. In the actual structure, the fixed base does not twist nor displace in any direction. The cross section at the floor level may translate relative to the base and rotate about either axis, but twisting is prevented by the rigid floor action. In the testing arrangement, the end fixtures prevented the end sections from translating and twisting, whereas the midlength section is free to translate in the plane of the cross section, but twisting was prevented by a linkage mechanism. Considering the cross section at the midlength of the column as a plane of symmetry, the deformations of the specimen in the test setup simulate the deformations of a column in a frame unbraced in both principal directions.

The axial loading system was the same as for the interior column in the unbraced frame tests. Column load was applied by a 100 ton hydraulic ram which was operated by a pump. A load cell on the opposite end was used to monitor the load and served as the reaction. The ram load acted against the W30x116 reaction beams,

which were supported by the reaction brackets that have been prestressed to the test slab by means of 3 in. diameter anchor bolts.

The end fixtures were designed to allow column shortening and free end rotation of the column but to prevent twisting of the end cross sections. Warping of the flanges was prevented due to the welding of the tees along the edges of the column flanges. The end fixtures consisted of two 1 in. x 6 in. x 6 in. plates with a hardened steel cup inserted and a 2 in. diameter hardened steel ball, as shown in Fig. 5.5. One of the plates was attached to a 1/2 in. x 16 in. x 16 in. plate by means of 1/2 in. diameter bolts which, in turn, was mounted to the ram piston. The other plate was bolted to a 1-1/2 in. x 12 in. x 12 in. plate and the column end plate with 3/4 in. bolts. Two 1/2 in. holes were drilled and tapped on each edge of the 1-1/2 in. x 12 in. x 12 in. plate, so that a 1/2 in. x 3 in. x 7 in. plate with two circular guides could be attached. The circular guides have an 8 in. radius of curvature and are concentric to the center of the ball. The guides on all four sides of the 1-1/2 in. x 12 in. x 12 in. plate were supported by flat plates which were welded to a bent made of W6x20 sections. Figure 5.6 shows the view of the end fixture assembly.

During loading the circular guides slide along the flat plates to accommodate the shortening of the column and rotate in the two orthogonal directions about the center of the ball. Twisting of the cross section was prevented by bearing of the two circular guides against the flat plate on each side. Only two sides of the fixture were supported by the bent during movement; the other two moved away from the supporting flat plates. Any resistance to rotation of the cross section was due to friction between the surfaces of the hardened steel cup and steel ball and between the surfaces of the circular guides and the flat plates. The

significance of the restraining effect due to friction was examined indirectly by performing an Euler test on Specimen BC-1 before the main test was carried out, and the results will be discussed in Sec. 5.3. The bents that were used to support the fixture at both ends of the column were braced to increase the stability.

In Specimens BC-2 and BC-3, the lateral load was applied at the midlength section by means of a 5 in. bore tension ram acting integrally with a gravity load simulator⁶⁵ and measured by a tension load cell, as shown in Fig. 5.7. The lateral loading system was attached to the midlength section with a knuckle-pin-clevis fixture. The purpose of the simulator was to maintain the load in the vertical direction as the cross section displaced upward and laterally. The simulator was designed for a capacity of 20 kips and a sway movement of 8 in. on either side of the central position. A test on the strength and the kinematic behavior of the simulator was carried out before the main test series. Figure 5.8 shows the vertical movement of the top pin as the simulator swayed. It can be seen that the elevation of the pin is practically constant within a 6 in. range of sway. The base beam of the simulator was attached to two 12 in. columns which were bolted to the test slab. It was to be noted that the simulator was in the inverted position from the tests at Lehigh University and exerted an upward force on the column.

Figure 5.9 shows the details of the mechanism which was attached to the midlength section of all specimens. It consisted of two pairs of parallel links which were pin-connected to the stem of the tee sections cut from a W6x20 beam. The middle tee sections were bolted back to back. Each link consisted of two 22 in. long 1/4 in. x 2 in. x 2 in. angles separated by pipe spacers. The mechanism prevented twisting by exerting the resisting couple to the cross section, but did not restrain the horizontal and vertical movement of the cross section.

A self-contained system was used to apply the joint loadings in the strong and weak directions, which were operated by separate hand pumps. The system consisted of a 5 in. bore tension ram, a 1-1/2 in. loading bar, and a 1-1/2 in. aluminum load cell connected in series. The system was attached to the ends of the cantilever stubs on both sides by means of a pin and a knuckle (see Fig. 5.10). Since the joint rotation in one direction causes the stub to twist in the other direction, each knuckle in the loading bar was fitted with a spherical bearing in order to minimize any twisting moment developed. The stub in the strong direction consisted of two 8x13.75 channels welded to a 1-1/4 in. x 8 in. x 15 in. end plate. The channels were separated back to back to house the knuckle fixture. In the weak direction of the specimen, the stub was made of two 5 x 9 channels welded to a 1 in. x 7-1/2 in. x 12 in. end plate. The length of the stub in the strong direction measured from the outside of the end plate to the center of the pin was 26-3/4 in., and the lever arm of the stub load with respect to the centroid of the specimen was 31-3/4 in. The corresponding length of the stub in the weak direction was 12-7/8 in., and the lever arm to the centroid of the specimen was 16-1/4 in.

During the joint loading and wind loading stages, the moment diagram in the restraining beams was linear with the tension on the outside of the cross section. The reaction at the far end of the restraining beams was provided by attaching a tension bar to the beam at both ends of the column. In the strong direction, a 1-1/2 in. tension bar was used and a 7/8 in. tension bar was used in the weak direction. Each bar was connected to a tension load cell and a turnbuckle was used so that some adjustment in length could be made. A knuckle-pin-clevis fixture was used for the connection at the beam. The length of the restraining beam in the strong direction measured from the outside of the end plate to the centerline of the tension bar was 91 in., so that the distance from the

centroid of the column to the reaction was 96 in. The corresponding lengths for the restraining beam in the weak direction were 76-5/8 in. and 80 in., respectively.

The design of the restraining beams did not require any lateral bracing. However, as a precaution, intermediate lateral bracing was provided for the vertical beam. The bracing consisted of a pair of tension rods. One end of a rod was attached to channels which were clamped to the restraining beam. The other end of the rod was locked to a slotted angle bent. The rod could slide freely in the slot, thus exerted no in-plane restraining force to the beam. In the horizontal direction, the horizontal beam was supported on angle bents. These bents could be used to provide bracing for the beam if necessary.

5.2 Instrumentation

The test specimens were equipped with three categories of instrumentation for measuring the applied loads and restraining forces, the displacements, and the strain data.

A 240 kip load cell was used to monitor the column load, which was accurate to 0.30 kip, based on 5 μ in./in. probable error of the strain recording apparatus. The 70 kip load cells, made of 1-1/2 in. high strength aluminum bars, were used to measure the stub loads in the strong and weak directions, the force in the tension bar in the strong direction, and the lateral load for Specimen BC-3 (applied in the strong direction). These load cells were considered accurate to 0.03 kip. The lateral load for Specimen BC-2 (applied in the weak direction) and the force in the tension bar in the weak direction were measured by the aluminum cylinder load cells having the capacity of 10 kips. These had an accuracy of 0.02 kip. In addition to the load cells, the pressure in the hydraulic lines was also recorded by pressure gages and pressure transducers which provided a check on the applied loads.

In all tests the loads that were indicated by the load cells and by the pressure agreed to within 3 percent. Load cell data were used in all data reduction.

Strains were recorded at four stations in the elastic zone of the column and in one of the restraining beams in each direction. The strain was also recorded on an unloaded member to be used as temperature compensation. At each station, four W80 strain gages were bonded to the face of the flanges at $1/4$ in. from the flange tips. The strain data were used to calculate the moments at the stations. The strain gages on the beams were used as a check on the force in the tension bars. The computed moments in the column, together with the measured displacements, were used to calculate the moments at the ends of each segment about the strong and weak axes of the cross section. This will be discussed in Sec. 5.5.

During loading, a cross section of the column could displace in any direction. The column could also twist at all sections except the ends and the midlength, where twisting was restricted by the test fixture. The instrumentation was designed to measure the vertical and the horizontal components of the displacement of the flange tips and the detail is shown in Fig. 5.11. The flange tips were clamped with three light $1/16$ in. x $9/16$ in. x $7/8$ in. aluminum channels by means of set screws. The flange and the web of the channel were attached with a 1 in. long set screw with a cap nut. The plunger of a 0.001 in. dial gage was attached with $2-1/4$ in. x $2-1/4$ in. thin aluminum plates. A set of four dial gages was used to measure the movements of the flange tips. With the recorded movements of the flange tips and the dimension of the cross section, the vertical and horizontal components of the displacement of the centroid and the twist of the cross section could be determined. The twist of the cross section at eight stations was also measured with

three inclinometers. Two of the inclinometers were left in place at the midlength station and at an end station and the other was used to record the twist at other stations during loading. By turning the micrometers fitted to the inclinometer, keeping the bubble level, the change in the amount of tilt could be determined to give the angle of twist.

The rotation of cross sections adjacent to the joints was measured by recording the movement of the rotation arms clamped to the specimen using 0.001 in. dial gages and piano wire extensions. The rotation arms were clamped to the cross section 4 in. from both ends. Figure 5.12 shows the arrangement of various instrumentation on the test specimens.

5.3 Controlled Test

In order to check the loading system and to evaluate the significance of friction between the steel ball and the hardened steel cup, an Euler test was conducted on the column used for Specimen BC-1 before the main test. In this test the restraining beams and the loading stubs were not bolted to the column; therefore, the column behaved as a pinned-end column. The column was aligned with a transit, so that there was no end eccentricities. The ram load and the centerline deflection were measured for each stage of loading. The applied load was in the range that kept the stress in the column within the elastic limit. Figure 5.13 shows the results of the Euler test, which are presented in the form of an axial load-centerline deflection plot and a Southwell plot. The centerline deflection shown was measured from the unloaded position of the column. The maximum load applied in the test was 38.4 kips. The least square curve fitting method was used to establish the Southwell line from the data points in which the load was within 80 percent of the calculated Euler load. The test buckling load determined by the Southwell method was 45.1 kips, whereas the

buckling load determined from the Euler formula with $E = 29500$ ksi was 43.0 kips. The calculated initial eccentricity was 0.298 in., compared to the measured eccentricity of 0.37 in. The ratio of the test buckling load and the calculated Euler load was 1.05. This reflected the possible effect of friction between the ball and the cup and between the circular surfaces of the steel pieces attached to the edges of the fixture plate and the flat guides of the bent. Some of the difference could also be attributed to the variation in the modulus of elasticity and to experimental errors in taking measurements. The effect of friction in the ball and cup fixture was larger than the knife edge fixture discussed in Chapter 4 ($P_{\text{Southwell}}/P_{\text{Euler}} = 1.03$) as it should be. This magnitude did not seem uncommon and the effect of friction was not as significant for specimens in the combined axial load and flexure test as it was for specimens in the stability test.

5.4 Test Procedures and Test Results

All columns were tested horizontally and were oriented in the north-south direction. In Specimens BC-1 and BC-2, the web of the column was parallel to the floor slab, whereas in Specimen BC-3 the column was rotated 90° so that the web becomes perpendicular to the floor slab. The restraining beams in the strong direction were designated as BS1 and BS2, and those in the weak direction were designated as BW1 and BW2. The numbers 1 and 2 refer to the north and south beams, respectively (see Fig. 3.6). The specimens were aligned with a transit sighting on a scale, so that the line of action of the axial load coincided with the centroid of the cross section. The tie rods at the far ends of the restraining beams were tightened to reduce the sag by turning the turnbuckles. The load cells in the rods were monitored so that the force in the strong direction rod was 0.1 kip and that in the weak direction rod was 0.042 kip before applying the external loads. These prestress forces introduce

moments in the column about 5 percent of the yield moment, M_y . The sweep and the camber of the column were measured by the transit and the initial twist of the cross sections along the length with respect to the north end of the column was measured by an inclinometer. During loading stages, load cells, pressure transducers, and pressure gages were monitored. All strain gage wires were connected to the VIDAR data acquisition system and the displacement data were recorded manually.

Specimen BC-1. The loading sequence for this specimen was to apply the stub loads in the strong and the weak directions to the predetermined levels and then to increase the column axial load to failure while maintaining the stub loads constant. The column load and the joint loads were operated by three independent hand pumps. Figure 5.14 shows the load-displacement behavior of Specimen BC-1. The displacement parameters were the lateral deflection in the weak direction, w , the lateral deflection in the strong direction, s , and the twist of the cross section at the midlength, β . These displacements were measured from the unloaded position of the column. The initial deformation of the column at the midlength section was: camber = 0.08 in. to the east, sweep = 0.1 in. downward, and twist = 0.016 radians clockwise with respect to the cross section at the north end. The analysis of the experimental data will be discussed in the next section (Sec. 5.5). The axial force, F , in the column was the sum of the applied column load, the stub loads, and the forces in the tie rods. Initially, a small column load of 5 kips was applied to seat the column. Load stages 1 to 5 corresponded to the application of the weak axis stub load. At the end of load stage 5, the stub load was 13.8 kips. This corresponded to M_{jy} of 224.4 kip-in. From load stages 5 to 10, the stub load in the strong direction was increased to the level of 16.4 kips and the corresponding M_{jx} was 521 kip-in. Beyond load stage 10, only the column load was increased and M_{jx} and M_{jy} were kept constant. As the

column load was increased, w increased faster than s . First yield lines were observed after load stage 19 at the bottom flange tip on the east side of the midlength section, which was the location of maximum combined stresses. The yield lines were generally distributed symmetrically about the centerline of the cross section. After load stage 21, significant yield lines extended to a distance of about 30 in. from the midlength section and penetrated to the flange-web junction. Yield lines also started to form at both ends of the column at the top flange tip on the east side. The maximum axial force of 132.3 kips was reached at this load stage. The displacement of the centroid of the midlength section at the maximum load was: $s = 0.63$ in., $w = 2.13$ in., and $\beta = 0.021$ rad. in the clockwise direction when facing south. Twist at the midlength section did occur and was larger than the twist at other stations. The change in twist with load followed similar trends as the lateral deflection. Beyond load stage 21, the specimen began to unload gradually, while w and β increased rapidly. Yield lines after load stage 22 propagated to a distance 24 in. from the north end and 12 in. from the south end. The column was unloaded after load stage 23.

Figure 5.15 shows the moments about the strong and the weak axes of the column at the north joint and at the midlength section. The moments in the restraining beams BS and BW are shown in Fig. 5.16. These moments were obtained from the analysis of the load and the displacement data based on the equilibrium condition of the specimen (discussed in Sec. 5.5). The column moments plotted were the components parallel to the untwisted coordinates which passed through the centroid of the cross section. After both stub loads were applied ($F \approx 40$ kips), it can be seen that as the column load increased, the end moments decreased while the moments in the restraining beams increased. The relaxation of the end moments was much faster for M_{ly} than for M_{lx} . The sign of M_{ly} was even

reversed when the axial force was about 80 kips. In the strong direction, the end moment, M_{1x} , was almost constant at low load. As the maximum load was approached, the relaxation of M_{1x} started to occur. The change in moments occurred rapidly near and beyond the maximum load. The sketches of the deflected shape of the column at the maximum load are shown in Fig. 5.17. At low loads, the deflected shape was in single curvature for both directions. At the maximum load, the y-y deflection developed a double curvature while the x-x deflection was still in the single curvature.

Specimen BC-2. The loading condition for this specimen simulated the case of a frame subjected to gravity load acting on the beam in the strong direction and wind load acting in the weak direction. The stub loading system in the weak direction was not attached to the specimen. The sequence of loading was to apply the stub load about the strong axis of the cross section to the same level as in Specimen BC-1, and then the column load was increased so that the axial force in the column was about 90 kips ($F/P_y = 0.37$). After that, P and M_{jx} were held constant while the simulator load was increased until failure occurred. The web of the column was in the horizontal plane, as in Specimen BC-1. The initial deformation at the midlength section was: camber = 0.06 in. to the east, sweep = 0.35 in. downward, and twist = 0.031 rad. clockwise with respect to the north end. Figure 5.18 shows the load-displacement characteristics of Specimen BC-2. Initially, a small axial load of 5 kips was applied to the column. This was followed by the application of the stub load in the strong direction. The stub load after load stage 6 was 16.4 kips and the corresponding joint moment, M_{jx} , was 520.4 kip-in. Between load stages 6 and 13, the column load was increased in stages to 71 kips, which gave an axial force of 91 kips. Beyond load stage 13, only the wind load was applied. The first yield lines were observed at both ends of the column adjacent to the box

joint after load stage 19. These yield lines extended about 1/2 in. down the top of the flange on the east side. The first occurrence of yield lines at the ends rather than at the midlength was probably due to the effect of the residual stresses and to the fact that the moment resulting from the dead weight tended to reduce the total moment at the midlength. After load stage 20, yield lines started to form at the bottom flange tip of the midlength section and spread to a distance of 10 in. on either side of the centerline. The yielding at the midlength section caused a rapid deterioration of the stiffness of the specimen. The maximum wind load of 2.99 kips was reached after load stage 23, at which some yielding on the west side at both ends started to form. The yielding on the west side was less extensive than on the east side. At the maximum load, $w = 2.45$ in. and $s = 0.61$ in. After this stage, the column unloaded rapidly as the deflection increased, indicating an instability type failure. After load stage 25, the ends of the column yielded extensively on the east side. The yield lines penetrated about 2 in. into the web at the north end adjacent to the box. From Fig. 5.18 it can be seen that the column deflected mainly in the weak direction. The strong axis deflection was about 0.5 in. after the end of the stub load and the change was very small throughout the test. The twist at the midlength was very small prior to the application of wind load and started to increase as the wind load was increased. The twist occurred in a clockwise direction when looking in the positive direction (southward). The magnitude at the maximum wind load was 0.013 rad. The specimen was unloaded after load stage 25.

The moments at the joint and at the midlength of the column are shown in Fig. 5.19, and the restraining moments are shown in Fig. 5.20. The moments in the strong direction stayed relatively constant with increasing wind load until the first yielding occurred; after that they started to decrease. The relaxation of M_{1x} at the

joint caused an increase in the restraining moment, M_{rx} (see Fig. 5.20). It can be observed that before the application of wind load the restraining moment in the weak direction, M_{ry} , was negative. The sketches of the deflected shape of the column are shown in Fig. 5.21. At the maximum load, the x-x deflection was in single curvature, whereas the y-y deflection was in double curvature.

Specimen BC-3. The loading condition for this specimen simulates a column in a frame subjected to gravity load acting on the beam which is framed to the column in the weak direction and the wind acting in the strong direction. In this specimen, the column was rotated 90° from the previous specimens, so that the web of the column was perpendicular to the floor. The loading stub in the strong direction was not attached to the specimen. The sequence of loading was to apply a stub load in the weak direction to the same level as in Specimen BC-1 and increase the column load so that the axial force was 90 kips. The column load and the stub load were maintained and only the simulator load was increased until failure occurred. The initial deflection of this specimen at the midlength section was: camber = 0.15 in. downward, sweep = 0.25 in. to the east, and the twist was 0.024 rad. clockwise with respect to the north end. Figure 5.22 shows the load-displacement characteristics of Specimen BC-3. A small axial load of 5 kips was applied initially and the weak axis stub load was applied between load stages 1 to 6. At the end of load stage 6, the stub load was 13.9 kips, which corresponded to M_{jy} of 225.4 kip-in. The column load was increased to 74.3 kips between load stages 6 and 13. At load stage 13 the axial force in the column was 90.6 kips. During the stub and column loading stages, the valve controlling the flow of oil to the simulator was left open so that there would be no lateral force acting on the column. However, the load cell indicated that there was a small load in the order of 30 lbs. The simulator load was increased from load stage 13. The first yield lines were

observed after load stage 20 at the bottom flange of the midlength section on the east side. After load stage 23 the yielding extended 15 in. on each side of the midlength. At this stage, yielding at both ends next to the box joint on the west side was also observed. The stiffness of the specimen in the strong direction did not change much between load stages 20 and 23. However, the yielding significantly affected the stiffness in the weak direction. Before yielding occurred there was practically no change in the deflection in the weak direction. The weak axis deflection started to increase after the first yielding occurred at the midlength section. The stiffness in the weak direction deteriorated faster when the end sections also yielded. After load stage 24, yielding penetrated into the web at about 6 in. on either side of the midlength. Beyond load stage 24, the specimen deflected in the weak direction much greater than in the strong direction, due to the loss of stiffness. The maximum wind load of 18.6 kips was reached at load stage 25. At load stage 26 the deflection in the strong direction was 1.55 in. and that in the weak direction was 2.25 in. There was extensive yielding along the midlength section and at the ends. The extensive yield lines also formed on the tension side and in the web at the midlength section, indicating that a plastic hinge capacity was reached at this section. There were some yield lines in the web close to the top flange junction at the north end. A slight unloading occurred at load stage 26. Beyond this load stage the specimen failed suddenly due to buckling laterally in the west direction until it was rested against the stopper plates. Equilibrium was obtained when the simulator load was reduced to 3.2 kips and the axial load was decreased to 82.5 kips. The deflection of the specimen was obtained by means of a transit. The strong axis deflection reduced to 0.63 in. and the weak axis deflection increased to 3.44 in. The specimen was unloaded after this stage. Figure 5.22(c) and (d) shows the change in the twist of the midlength section with load. The twist

increased rapidly as the maximum load was approached and the value at the maximum wind load was found to be 0.014 rad. in the counter-clockwise direction when looking toward the south direction. The twist at other stations along the length of the column also increased as the load increased. Although the midlength section is prevented from twisting by the linkage mechanism, it was observed that the twist at this section was larger than that at other stations. However, the magnitude of twist up to the maximum load is very small (less than 1 degree); the occurrence of twist at the midlength section may be attributed to the imperfection of the pins in the mechanism. This will be discussed further in Sec. 5.6. In Fig. 5.23 it can be observed that after the first yielding occurred ($H_x \approx 12$ kips), there was a slight bend in the strong axis moment at the midlength section, indicating that the moment started to redistribute to the stiffer cross sections at the ends. Near the maximum load, this moment decreased faster. The weak axis moments at the end and at the midlength remained constant up to first yielding when they started to increase gradually. As the maximum load was approached, the rate of increase was faster. Figure 5.24 shows the load-restraining moment relationships. The variation shows a similar trend as the moments at the ends of the column. The deflected shape of the column at the maximum wind load is shown in the sketches in Fig. 5.25.

For all the test specimens, the yield lines at the ends formed next to the end of the box joints. There were no yield lines in the stub portion between the joint and the fixture. This indicated that the stub portion was acting as an elastic segment and the joint contributed to strengthen the load-carrying capacity of the column. Specimens BC-1 and BC-2 failed by inelastic instability, and Specimen BC-3 failed due to flexural buckling about the weak axis. This was associated with a very small twist of the cross section. Figures 5.26 and 5.27 show the views of Specimens BC-1 and BC-2 at the end of the tests. The typical yielding patterns at the joints and at the midlength section of Specimen BC-2 are shown

in Figs. 5.28 to 5.30. Figure 5.31 shows yield lines at the top flange of the south joint of Specimen BC-3 after failure.

5.5 Analysis of Test Data

5.5.1 Axial Force. During the loading stages, the applied column load, the stub loads, and the simulator load were measured by means of load cells. In addition, the pressure in the hydraulic lines was also recorded by means of pressure gages and pressure transducers. The loads indicated by the load cells and by the pressure transducers generally were in good agreement to within 3 percent. The loading scheme of the test specimens gave rise to the tension force in the tie rods attached to the end of the restraining beams. The force in the tie rods was the shear force in the beams and it increased the axial force in the column. The restraining moments were obtained in two ways. First, the force in the tie rod was measured by the tension load cell. The moment at any cross section of the beam was equal to the product of the tie rod force and the distance to that cross section. At a cross section of the beam, about 12 in. from the face of the connection, four strain gages were attached, enabling the moment to be determined directly. The moments determined from these two independent records agreed to within 2 percent. The axial force in the column at any load stage was equal to (see Fig. 5.32):

$$F = P + P_s + P_w + R_s + R_w \quad (5.1)$$

in which F is the axial force in the column; P is the applied column load; P_s and P_w are the stub loads in the strong and weak directions, and R_s and R_w are the forces in the restraining beams in the strong and weak directions, respectively. The force F acting through the deflection caused the secondary moments in the column.

5.5.2 Displacement. At each cross section, four dial gages were used to record the horizontal and vertical movements of the flange tips. Referring to Fig. 5.33, the twist of the cross section could be determined from a pair of the dial gage readings and the distance between the gages. If d_1 , d_2 , d_3 , and d_4 are the dial gage readings, then the twist can be computed from the following formula:

$$\beta = \frac{d_1 - d_2}{b} \quad (5.2a)$$

or

$$\beta = \frac{d_3 - d_4}{d} \quad (5.2b)$$

An additional record of twist was obtained from the inclinometer readings which were taken at the strain gage locations, the midlength section, and the end sections. It was found that the twist computed from the pair of dial gages across the web was in good agreement with the inclinometer readings. This was because the accuracy was about twice that of using the pair of gages across the flange. In the analysis of the data, the twist that was obtained from Eq. 5.2b was used. After the twist is determined, the displacement of the centroid of the cross section can be computed from the dial gage readings, as follows:

$$w = w_s + b_o(1 - \cos \beta) \quad (5.3)$$

$$s = s_s + d_o(1 - \cos \beta) \quad (5.4)$$

in which w_s and s_s are the average weak axis and strong axis deflections of the flange tips, respectively; b_o and d_o are the distances between the centroid and the points where the displacements were measured.

5.5.3 Moments at a Cross Section. Strain gages were attached to the cross sections of the column in the elastic zone.

The moments about the strong and weak axes of the cross section with respect to the local coordinates passing through the centroid of the cross section were computed from the equations:

$$M_{\xi} = EI_x (\varphi_x)_{av} \quad (5.5a)$$

$$M_{\eta} = EI_y (\varphi_y)_{av} \quad (5.5b)$$

where $(\varphi_x)_{av}$ and $(\varphi_y)_{av}$ were the average curvatures with respect to the strong and weak axes of the cross section. They were computed as the difference of the average strains at the opposite faces of the section divided by the distance across the faces. Equations 5.5a and 5.5b made use of the assumption that a plane section before bending remained plane after bending. This assumption could be verified if it could be shown that the strain at any point on a cross section was on a common plane of strain. The equation that defines the strain at a point which has the coordinates (ξ_i, η_i) is:

$$a_1 \xi_i + a_2 \eta_i + a_3 \epsilon_i = 1.0 \quad (5.6)$$

where ϵ_i is the strain at point "i" of the cross section. The undetermined coefficients a_1 , a_2 , and a_3 could be obtained from the strain values at three points and their coordinates.

At each loading stage and for each cross section, three values of strain were used to compute the coefficients a_1 , a_2 , and a_3 and the calculated strain at the fourth point was compared with the measured strain. The comparison showed very good agreement near the maximum load (within 8 percent). After the equation of the strain has been established, a more convenient way to determine M_{ξ} and M_{η} without using Eq. 5.5 was to divide the cross section into small grid elements. The axial force and the bending moments could be determined from the following equations:

$$F = E \sum \epsilon_i \Delta A_i \quad (5.7a)$$

$$M_{\xi} = E \sum \epsilon_i \xi_i \Delta A_i \quad (5.7b)$$

$$M_{\eta} = E \sum \epsilon_i \eta_i \Delta A_i \quad (5.7c)$$

where ΔA_i was the area of a grid element and ξ_i and η_i were its coordinates. The moments computed from Eq. 5.7b and 5.7c were in reference with the local coordinates. They could be transformed to the untwisted coordinates (see Fig. 5.34):

$$M_x = M_{\xi} \cos \beta + M_{\eta} \sin \beta \quad (5.8a)$$

$$M_y = -M_{\xi} \sin \beta + M_{\eta} \cos \beta \quad (5.8b)$$

From the known axial force, the displacements of the centroid, the moments at two strain gage locations, and the distance between the strain gage locations, the shear force could be determined. The moments at the joint and at the midlength section of the column were then calculated from the moments at the strain gage stations using the equilibrium condition.

The moments at the end and at the midlength of the column could be determined from the equilibrium condition without using the moments from the strain gage data. Since the restraining moments were measured at each loading stage, the end moments in the column could be determined from the equilibrium of moments at the joint. The problem was reduced to an eccentrically loaded beam-column. The moments at the midlength section could then be extrapolated from the moments at the column end. Figure 5.35 shows the typical comparison of the end moments and the moments at the midlength of Specimen BC-1 based on the equilibrium condition and on the extrapolation of the moments obtained from the strain data. The results appear to be in reasonable agreement. In the plots of the test results discussed in Sec. 5.4, only the moments based on the equilibrium condition were shown.

5.6 Discussion of Test Results

5.6.1 Theoretical Prediction. Mitchell⁴⁵ developed the computer program BMCOL71 for the analysis of biaxially loaded beam-columns. The solution is based on a discrete element model in which the beam-column is divided into a number of discrete elements. The method of solution is based on the tangent stiffness iteration of the load displacement relationship of the member. The program was developed for an initially straight column with no residual stresses. Strain hardening can be considered, but the program does not take into account the strain reversal. The end restraints can be simulated by inputting external linear rotational springs at the member joints; therefore, only elastic restraint can be considered. The resisting torsional moment is assumed to be proportional to the rate of change of the angle of twist

$$M_t = GJ \frac{d\beta}{d\ell} \quad (5.9)$$

therefore, the warping resistance is neglected. In the program a displacement at a joint can be specified by inputting a very stiff spring in that direction. The solution to a problem is the equilibrium state of the member and the maximum strength can be obtained by incrementing the load parameter until the solution fails to converge. The program BMCOL71 was used extensively to determine the theoretical prediction of the strength of the test specimens.

5.6.2 Analytical Model of Test Specimens. A test specimen was simulated as a straight beam-column, 22 ft., 10 in. long, which was the distance between the center of the balls. The column was divided into forty elements so that each element was 6.85 in. long. One end of the column was pinned and the other end was supported on the roller; this permitted free end rotation and axial shortening. A no-twist boundary condition at the end cross sections was specified. In the test specimen, the centerline of the joint was 13 in. from

the center of the ball and the edge of the box was another 7-1/2 in. from the centerline of the joint. This joint size was taken into account by specifying three elements to behave elastically at any stress level. The cross sections of the box and of the column were input as four rectangular plates and as three plates, respectively. Separate stress-strain characteristics were specified for the flanges and the web. Since the specimen was in a horizontal plane, the weight of the column was acting prior to the application of the external load. Therefore, the first loading condition of each specimen was in fact the column subjected to its weight, in which the solution could be obtained from the simple beam formula. After the initial stage, linear springs were input about the strong and weak axes of the cross section at the end of the second discrete element and the column was subjected to an axial load of 5 kips. The magnitude of the spring stiffness was 65100 kip-in./rad. about the strong axis and 27730 kip-in./rad. about the weak axis. This spring stiffness was computed from $3EI_b/L_b$, which was the stiffness of the beam where the far end was pinned. The actual sequence of loading was input for each specimen. Since the beam restraint was represented as the rotational spring, the axial force rather than the column load was input and the applied joint moments were input as couples. For each specimen, two cases were solved. In one case, the cross section at the midlength was allowed to twist freely while in the other case a no-twist boundary condition was specified. The purpose was to determine if the twist of the midlength section had any effect on the strength of the column.

For Specimen BC-1 the strength was determined by incrementing the axial force using 10 kip increments at low loads and 2 kip increments as the maximum load was approached. For Specimen BC-2 the control of the deflection at the mid section was used so that the unloading path of the load displacement characteristic could be obtained. For Specimen BC-3 the solution did not converge when

the control of deflection was used. Therefore, the wind load was incremented instead. The theoretical behavior is plotted on the same figures as the test results and is shown dashed. The comparison of the theoretical and the experimental behaviors will be discussed in the next section.

5.6.3 Behavior of Test Specimens. The predicted behavior of the test specimens that is shown in the plots of the test results was obtained from the analysis in which twist at the mid-length section was prevented. It was found that for Specimens BC-1 and BC-2 the occurrence of twist at the midlength section did not affect the response of the column nor reduce the maximum load. For Specimen BC-3, which was loaded primarily about the strong axis, the predicted failure load was much lower when it was assumed that twist was not restrained. This will be discussed later in this section.

Referring to the test results of Specimen BC-1 in Figs. 5.14 to 5.16, the end moments were: $M_{1x} = 134.8$ kip-in. ($M_{1x}/M_{px} = 0.141$) and $M_{1y} = 18.0$ kip-in. ($M_{1y}/M_{py} = 0.078$) at the end of stub loadings (load stage 10). The moments at the midlength section were: $M_{2x} = 147.2$ kip-in. ($M_{2x}/M_{px} = 0.154$) and $M_{2y} = 23.4$ kip-in. ($M_{2y}/M_{py} = 0.102$). As the axial load was increased, M_{1x} and M_{1y} decreased, but the rate of decrease of M_{1y} was faster than that of M_{1x} . This was reflected in the rate of increase of the restraining moment M_{ry} as compared to M_{rx} . The relaxation of the end moments was also reported in the small scale restrained column tests conducted by Milner and Gent.⁴⁴ It was found that the reversal of end moments occurred at a low axial load for slender columns. For columns with low slenderness ratio, the reversal occurred near the maximum load. The test specimens in this study were slender with $L_c/r_y = 187$ ($L_c =$ total length of column) and $G_{x-x} = 0.59$ and $G_{y-y} = 0.14$ based on a no-sway model. The end moment M_{1y} was relaxed to zero and the sign reversed at

an axial force of 80 kips, which was at 60 percent of the maximum load. This means that there was a point of inflection within the span of the column at loads higher than 80 kips. Consequently, the restraining moment M_{ry} after the reversal of M_{ly} became larger than the applied joint moment, M_{jy} . The relaxation of the end moment in the strong direction, M_{1x} , occurred slowly until the maximum load was approached, when it decreased rapidly. The moments at the midlength, M_{2x} and M_{2y} , increased with the load, but M_{2x} decreased near the maximum load. The maximum axial force in the column was 132.3 kips ($F/P_y = 0.54$). The reduced plastic moments of the cross section (based on the simple plastic theory) at this load were $M_{pcx} = 561.4$ kip-in. and $M_{pcy} = 209.3$ kip-in. The moment, M_{2y} , almost reached the plastic moment capacity after the maximum load had been reached. The failure of this specimen was due to inelastic instability. The first yielding was observed at the axial force of 131.5 kips, which was within a few percent of the maximum load. This indicated that there was not much redistribution of moments between first yield and maximum strength. The theoretical prediction of the maximum load was 128 kips, when the twist at the midlength section was prevented, and 125 kips when the twist was allowed. The predicted strength was within 97 percent of the test maximum load. The predicted behavior slightly underestimated the lateral deflection, but in general was in good agreement with the observed behavior. In the test, the twist at the midlength section at the maximum load was 0.021 rad. compared to 0.113 rad. (at 125 kips) for the analysis that allowed twist. The predicted value seems to be too large, however, since the torsional moment developed in the column was small. The largest torsional moment at the maximum load was 2.0 kip-in.

In Specimen BC-2 (Figs. 5.18 to 5.20), the predicted deformation response agreed very well with the test results, especially for the strong axis deflection. The theory overestimated the moments about

the weak axis and underestimated the moments about the strong axis. At the end of the stub loading stages, the moments about the strong axis were $M_{1x} = 164.5$ kip-in. ($M_{1x}/M_{px} = 0.172$) and $M_{2x} = 171.9$ kip-in. ($M_{2x}/M_{px} = 0.180$). Although M_{jx} was at the same level as Specimen BC-1, the column moments were about 30 kip-in. higher than those in Specimen BC-1. This was attributed to the lower restraining moment ($M_{rx} = 359$ kip-in.) in Specimen BC-2 than in Specimen BC-1 ($M_{rx} = 387$ kip-in.) at the end of the stub loadings ($M_{jx} = 521$ kip-in.). The axial force at the maximum wind load was 93.8 kips and the corresponding $M_{pcx} = 731$ kip-in. and $M_{pcy} = 223.8$ kip-in. At the maximum wind load the column moments were lower than the plastic moment capacity. The failure was due to inelastic instability about the weak axis. The predicted maximum wind load was 2.8 kips, which underestimated the test value by 6.3 percent. The predicted deflection at the maximum load was within a few percent of the experimental value. The analysis that allowed twist at the midlength section yielded the same maximum load and identical behavior. With regard to twisting of the cross section, the magnitude of twist at the midlength section was very small during the initial loading stages. It occurred in the counterclockwise direction looking along the positive axis of the column (southward). As the wind load increased, the twist became clockwise. This agreed with the analysis that allowed twist, except that the predicted twist was very large. At the maximum wind load, the actual twist was 0.015 rad. compared with the predicted value of 0.183 rad. The large value of the predicted twist may be attributed to the fact that Mitchell neglected warping torsional stiffness in his analysis.

In Specimen BC-3 (see Figs. 5.22 to 5.24), the predicted behavior overestimated the lateral deflection during the initial loading stages and this effect amplified during the wind loading stages. The analysis also overestimated the moments about both axes at the ends. At the end of the stub loadings ($M_{jy} = 225$ kip-in.),

the moments about the weak axis were $M_{1y} = 22.5$ kip-in. ($M_{1y}/M_{py} = 0.098$) and $M_{2y} = 29.1$ kip-in. ($M_{2y}/M_{py} = 0.127$). The restraining moment in the weak direction was 203 kip-in. compared to 191 kip-in. for Specimen BC-1. The axial force at the maximum wind load was 96.9 kips, in which the reduced plastic moment capacities were $M_{pcx} = 716.2$ kip-in. and $M_{pcy} = 223.4$ kip-in. It can be observed that M_{2x} at the maximum load was 850 kip-in., which exceeded M_{pcx} by 18.7 percent. At this load stage the central 12 in. of the column was yielded extensively and the yield lines also formed in the web. It indicated that this portion reached the strain hardening region which contributed to the increase in the moment above M_{pcx} . The end moment, M_{1x} , at the maximum load was 297 kip-in., which was still below M_{pcx} . In this specimen the first yield lines were observed at the wind load 11.7 kips, which was at 63 percent of the maximum load. The rate of change of M_{2x} decreased slightly after the first yield. This was different from the previous two specimens which were loaded mainly about the weak axis. There, the rate of change of M_{2y} increased when the first yield occurred. It was observed that the reduction in the strong axis moments occurred rapidly as the maximum load was approached. The decrease in the rate of change of M_{2x} in Specimen BC-3 was due to the redistribution of the moment. This specimen failed by flexural buckling about the weak axis. As the maximum load was approached, the compression flange at the midlength may have been completely yielded. At this stage the stiffness about the weak axis was significantly reduced because of the yielding. Beyond the maximum load the stiffness in the weak direction was not adequate to resist the second order moment and flexural buckling occurred. The theoretical analysis predicted a maximum wind load of 13.5 kips when the twist at the midlength section was restrained and 6 kips when the twist was allowed. The predicted response showed the similar trends with the test results that the lateral deflection increased rapidly as the wind load increased. The Mitchell result

was conservative by 27.5 percent, which was probably due to the fact that the analysis neglected the elastic unloading of the yielded compression flange. Milner and Gent⁴⁴ compared the theoretical prediction with their test results on biaxially loaded small scale restrained columns and reported that strain reversal increased the predicted strength significantly. As a check on the experimental results, the shear forces in the column in the strong and the weak axes, which were obtained from the consideration of equilibrium only, were compared with those computed from the strain data. It was found that the two procedures compared very favorably (within 8 percent). This indicated that the simulator did not restrain the lateral movement of the column prior to buckling.

Regarding the twist at the midlength section, the observed twist was in the clockwise direction during the initial loading stages. As the wind load was applied, the twist changed to counterclockwise (looking southward). The same behavior was indicated from the analysis. The twist at the maximum wind load of 18.6 kips was 0.013 rad. compared with 0.107 rad. at 6 kips for the analysis that allowed twist.

It has been observed that twisting at the midlength section actually occurred for all specimens, although the linkage mechanism was used to prevent the twist. This behavior was examined by plotting the twist versus the deflection in the weak direction for Specimens BC-1 and BC-2 and the twist versus the deflection in the strong direction for Specimen BC-3. In Specimen BC-1, the slope of the twist-weak axis deflection plot is flatter when the twist is approaching 0.02 rad. (1.14 degrees). This means that, due to the imperfection of the mechanism, if any, the mechanism was not very effective in restraining twist of the cross section until a twist of about 0.02 rad. was reached. In Specimen BC-2, twisting at the instability limit was less than 0.02 rad.; the mechanism may not have been effective. In Specimen BC-3, the twist before flexural buckling took place was close to 0.02 rad. When buckling occurred,

the mechanism could have been effective in preventing any further twist. Therefore, it may be concluded that the mechanism is effective in minimizing twist at the midlength section.

It is of interest to determine the strength of the test specimens in planar loading to evaluate the reduction in the maximum load when there is moment in the other direction. Mitchell's program was used for this study and the loading of the specimens was as follows. Specimen BC-1 was subjected to M_{jy} of 225 kip-in. and the axial load was increased to failure. In Specimen BC-2 and Specimen BC-3, the axial load of 93 kips was input and maintained at this level; the control of deflection technique was used by incrementing the deflection to about 4 in. It was found that the maximum axial load in Specimen BC-1 was 130 kips and the weak axis deflection at this load was less than that for biaxial loading. This was anticipated because the column should be stiffer for uniaxial bending. In Specimen BC-2, the maximum theoretical wind load was 2.93 kips and occurred at the same deflection as the biaxial specimen. The maximum wind load in Specimen BC-3 was found to be 22.7 kips. The load-displacement curve had a long plateau which was the result of strain hardening. When the specimens were loaded primarily about the weak axis, there was not much decrease in the strength due to biaxial load. However, the biaxial effect was significant when bending occurred mainly about the strong axis.

In the theoretical analysis, the shift in the shear center as yielding penetrated into the cross section was not taken into account. When the member is elastic, the shear center coincides with the centroid of the cross section. As the compression flange yields, the shear center shifts towards the tension flange. Therefore, an error was introduced in determining the torsional moment because the shift in the shear center was neglected. It was thought that this effect did not significantly change the prediction of the

maximum strength because the torsional moment is small compared with the bending moments about the strong and weak axes.

5.7 Comparison of Test Results with Design Equations

In Chapter 1 it has been discussed that the design of biaxially loaded no-sway beam-columns is generally based on the CRC equations and Chen's equations. For convenience, these equations may be referred to again, as follows:

$$\text{CRC: } \frac{P}{P'_{cr}} + \frac{C_{mx} M_x}{\left(1 - \frac{P}{P'_{Ex}}\right) M_m} + \frac{C_{my} M_y}{\left(1 - \frac{P}{P'_{Ey}}\right) M_{py}} = 1.0 \quad (5.10a)$$

$$\frac{P}{P_y} + \frac{M_x}{M_{px}} + \frac{M_y}{M_{py}} = 1.0 \quad (5.10b)$$

$$\text{Chen: } \left[\frac{C_{mx} M_x}{\left(1 - \frac{P}{P'_{cr}}\right) \left(1 - \frac{P}{P'_{Ex}}\right) M_m} \right]^{\xi} + \left[\frac{C_{my} M_y}{\left(1 - \frac{P}{P'_{cr}}\right) \left(1 - \frac{P}{P'_{Ey}}\right) M_{py}} \right]^{\xi} = 1.0 \quad (5.11a)$$

$$\left[\frac{M_x}{M_{pcx}} \right]^{\eta} + \left[\frac{M_y}{M_{pcy}} \right]^{\eta} = 1.0 \quad (5.11b)$$

where $\xi = 0.4 + P/P_y + B/D$

and $\eta = 1.6 - \frac{P/P_y}{2 \ln(P/P_y)}$

Equation 5.10a has been modified by Pillai⁴⁹ to the following form and is usually applicable for tubular beam-columns:

$$\frac{P}{P'_{cr}} + \nu \left[\frac{C_{mx} M_x}{\left(1 - \frac{P}{P'_{Ex}}\right) M_m} + \frac{C_{my} M_y}{\left(1 - \frac{P}{P'_{Ey}}\right) M_{py}} \right] = 1.0 \quad (5.12)$$

$$\text{where } \nu = \frac{\sqrt{(C_{mx} M_x)^2 + (C_{my} M_y)^2}}{C_{mx} M_x + C_{my} M_y}$$

The moments M_x , M_y in Eqs. 5.10 to 5.12 are first order moments and the amplification factors $C_{mx}/(1 - P/P'_{Ex})$ and $C_{my}/(1 - P/P'_{Ey})$ account for the secondary effect of axial load acting through the eccentricity of the deflected shape of the member. The terms P'_{cr} , P'_{Ex} , and P'_{Ey} should be based on the effective length factor in the no-sway mode ($K < 1.0$), but generally K is conservatively taken as 1.0 in design practice.

For beam-columns in unbraced frames, the design is generally based on AISC Specification or alternatively the recently proposed Springfield recommendation⁵⁶ may be used. According to the AISC Specification, the interactions are extended from the case of no-sway beam-columns (Eq. 5.10). The only differences are that the terms P'_{cr} , P'_{Ex} , and P'_{Ey} are based on the effective length in the sway mode ($K > 1.0$) and C_{mx} and C_{my} are 0.85. The Springfield recommendation uses the same concept as the P-delta method in unbraced planar frames. The moments M_x and M_y are determined by the P-delta analysis and the member is treated as a no-sway beam-column. Chen's equations (Eq. 5.11a and 5.11b) are used to check the strength of the member.

The restrained beam-column specimens under this study may be considered as no-sway columns with a length between the joints of 20 ft., 8 in. and symmetrical beam restraints at both ends. They may also be considered as beam-columns permitted to sway with a length half of the distance between the joints. One "end" is treated as a fixed base (this is actually the midlength section of

the actual specimen) and the other end is restrained by beams about the strong and the weak axes. The strength of the specimens will be considered as no-sway beam-columns first, and then the treatment as sway beam-columns will be discussed.

Considering the specimens as no-sway restrained beam-columns, the stub loading produces a uniform first order moment diagram so that $C_m = 1.0$, while the wind load produces a moment gradient in the member where $C_m = 1 - 0.18 P/P'_E$. For this study, the effective length factor in the no-sway mode is used to determine P'_{cr} , P'_{Ex} , and P'_{Ey} . The test specimens have effective slenderness ratios $KL_c/r_x = 39.2$ and $KL_c/r_y = 102.1$ ($L_c =$ total length of the column). The elastic buckling loads in the plane of bending are $P'_{Ex} = 1164.7$ kips and $P'_{Ey} = 173.1$ kips. In determining the buckling strength of the test specimens, the effective slenderness ratio about the weak axis controls. Due to a low value of residual stress in the flange of the W10x21 section, the buckling strength, $P'_{cr} = 173.1$ kips, is based on the elastic buckling load. The term M_m in Eqs. 5.10a, 5.11a, and 5.12 accounts for the reduction of plastic strength due to lateral torsional buckling of the beam-column considered as a beam. In the AISC Specification, the equation for M_m is given as:

$$M_m = \left[1.07 - \frac{L'_c/r_y \sqrt{\sigma_y}}{3160} \right] M_{px} \leq M_{px} \quad (5.13)$$

where $L'_c =$ the unbraced length of the member.

Equation 5.13 applies for a column with uniform first order moment diagram. However, the specification does not specify any modification for the moment gradient case. In determining the unbraced length to be used in Eq. 5.13, half of the total length instead of the whole length is used, since the midlength section was prevented from twisting.

Table 5.3 shows the comparison of the actual strength of the member and the strength predicted by the interaction equations. For all of the test specimens, the stability-type equations always controlled. For Specimens BC-1 and BC-2, the maximum moment in the column is less than the plastic moment at the maximum load of the assemblage. Therefore, this load corresponds to the maximum strength of the column and is used to compare directly with the results from the interaction equations. For Specimen BC-3, however, there is some redistribution of moments in the column before the maximum load of the assemblage is attained. In order to exclude the strength of the assemblage due to moment redistribution beyond the first hinge, the load at which the observed moment at the midlength section just reaches the biaxial plastic hinge capacity is considered to be the strength of the member. This limit state is based on Chen's equation for a biaxial plastic hinge of the cross section (Eq. 5.11b). At each loading stage the moments M_x and M_y at the midlength section, which is the location of the maximum moment, were checked with Eq. 5.11b and the load at which Eq. 5.11b was satisfied is considered to be the limit of structural usefulness. The maximum wind load that Specimen BC-3 carried was 18.6 kips and the load that corresponds to the formation of the first plastic hinge was found to be 16.7 kips.

The ratios of the test results to the predicted results are given in Table 5.3 and range from 1.18 to 1.27 for Specimen BC-1, 2.41 to 3.21 for Specimen BC-2, and 2.50 to 3.39 for Specimen BC-3. The interaction of the first order moments and the axial load, as given by various design equations, is shown graphically in Fig. 5.36. The CRC equation gives the most conservative results. Pillai's equation gives results between Chen's and the CRC equations, except when the ratio $C_{mx} M_x / C_{my} M_y$ is close to unity so that ν approaches $1/\sqrt{2}$. In this region, Pillai's recommendation is higher than that given by Chen's equation. For Specimen BC-1, the level of

conservativeness for all equations is in the same order of magnitude as indicated in the comparisons made by Springfield and Hegan⁵⁸ with previous experiments. Specimen BC-1, which was subjected to applied joint moments about the strong and the weak axes of the column, produces a uniform first order moment diagram just as in the tests on unrestrained beam-columns. However, the relaxation of the column end moments to the beams is not accounted for in the interaction equations. This leads to a conservative prediction of the strength. For Specimens BC-2 and BC-3, the predicted results are very conservative. This is attributed to the effect of moment gradient which is produced by the applied wind load. The use of M_m for the strong axis bending term seems to be conservative for these two specimens. If the limit for lateral torsional buckling of the member with no axial load is considered, the critical moment should be $C_b M_m$. For a moment diagram in double curvature, this critical moment is controlled by M_{px} .

The contribution of the terms involving the axial load and bending moments about the strong and the weak axes in the interaction equations is summarized in Table 5.4 for all three specimens. As an example, for the CRC equation the axial load term contributes 0.6 for Specimen BC-1, and about 0.55 for Specimens BC-2 and BC-3. The contributions from the moments about the strong and the weak axes are 0.191 and 0.208 for Specimen BC-1, 0.189 and 0.268 for Specimen BC-2, and 0.249 and 0.189 for Specimen BC-3.

In the above comparison M_m was used as the bending strength about the strong axis. If the bending strength about the strong axis is taken as $C_b M_m = M_{px}$, the predicted strength increases by 8 percent for Specimen BC-2 and by 26 percent for Specimen BC-3. It may be concluded that M_m has a large effect when bending occurs mainly about the strong axis.

The test specimens can also be considered as beam-columns in unbraced space frames. If the AISC procedure is used, the first

order moments are used in the interaction equations. The terms P'_{cr} , P'_{Ex} , and P'_{Ey} are based on half of the total length with K determined from a sway mode. These quantities will be exactly the same if they are based on the total length with K determined from a no-sway mode. However, the AISC procedure would use $C_{mx} = C_{my} = 0.85$ for the sway case and M_m is used as the limiting bending strength about the strong axis. The comparison between the tests results and the AISC recommendation is given in Table 5.5. In this table the prediction by CRC is taken from the no-sway case (Table 5.3) for comparison. The comparison indicates that the capacity of Specimens BC-2 and BC-3 are significantly underestimated by the AISC interaction equations. A comparison of the CRC and AISC results indicates that there is some difference between the calculated capacities depending on whether the specimen is treated as a sway or no-sway column. If a design method is truly rational, both approaches should produce the same result. The treatment as a sway frame produces less conservative results.

In Chapter 2, a method of design called the effective length method was described in which the buckling strength is based on the actual slenderness ratio (L'_c/r_x or L'_c/r_y where L'_c is half of the total length). This method has also been applied to the biaxial problem. The terms C_{mx} and C_{my} are taken to be unity since the maximum second order moment occurs at the end (in this case, the midlength section). The comparison of the predicted strength is shown in Table 5.5. There is not much difference between the AISC and effective length approaches.

Table 5.6 shows the predicted strength of the test specimens if they are treated as sway beam-columns and Springfield's recommendation is used. In this table Chen's prediction for the no-sway approach is taken from Table 5.3 for comparison. For Springfield's prediction, the terms P_{cr} , P_{Ex} , and P_{Ey} are based on the actual slenderness ratios considering as half of the total length and using

$K = 1.0$. The terms C_{mx} and C_{my} are computed from $C_m = 0.6 + 0.4q$ and M_m is used as the bending strength about the strong axis. (If the limit $C_m > 0.4$ is imposed, this alters the result of Specimen BC-2 from 3.25 kips to 2.15 kips. The limit on C_m does not control for Specimen BC-1 and Eq. 5.11b governs the design of Specimen BC-3).

A comparison of Chen's (no-sway) and Springfield's (sway) solutions shows considerable difference in both Specimens BC-2 and BC-3, which indicates that Springfield's suggestion is questionable. Although Springfield's recommendation apparently gives a good prediction of the test results to within 20 percent for Specimen BC-1, and 10 percent for Specimens BC-2 and BC-3, its concept should be discussed. For Specimens BC-1 and BC-2, the stability-type equation, Eq. 5.11a, controls. This means that the maximum moment occurs between the midlength section and the joint. The true elastic second order analysis and the test results indicate that the midlength is the section where the maximum moment occurs. Thus, the strength-type equation (Eq. 5.11b) should not be used to check the moment at the midlength section only. For Specimen BC-3, the strength-type equation controls the design and is used to check the moment condition at the midlength section. This is correct conceptually but there is one questionable aspect. Equation 5.11b is the condition of biaxial plastic hinge in which yielding has occurred in the member but in design, an elastic analysis is used to obtain the second order moment. Thus, Springfield's recommendation is close to the test results for Specimens BC-2 and BC-3 because of compensating factors, conservative no-sway Chen's equations coupled with an unconservative analysis and C_b factor.

CHAPTER 6

SUMMARY AND RECOMMENDATIONS

6.1 Summary

A theoretical and experimental study on the strength and behavior of beam-columns in unbraced frames has been presented. The main purpose has been to provide data for comparison with design methods over a wide range of problems. In the theoretical study, the strength of beam-columns in single story unbraced portal frames and leaned frames was determined with respect to several parameters. The results were compared with the predicted strength using the existing AISC and P-delta methods and the effective length method.

Three full size, two-bay unbraced planar frames were tested to study the leaned column concept. Also, full size biaxially loaded restrained beam-columns were tested under loading and support conditions simulating the actual condition in unbraced frames. The test results were compared with the theoretical prediction and the design interaction equations. The results of the analytical and experimental studies may be summarized as follows:

(1) The strength of beam-columns in single story pinned-base symmetrical portal frames was determined for a wide range of slenderness ratios ($20 < L_c/r < 80$) and relative ratios of column-to-beam stiffness ($0 < G < 3.0$). This corresponds to the effective slenderness ratios between 40 and 230. The results were obtained for bending about the strong and weak axes of the column and with and without the presence of residual stresses. It was found that the strength depends largely on the combined effect of L_c/r and G , i.e., on the effective slenderness ratio. For columns with the same values of L_c/r and G and subjected to the same axial load, the

reduction in strength due to the residual stresses is more pronounced when bending occurs about the weak axis than about the strong axis of the member. It was observed that for weak axis bending, the relative strength of short columns ($L_c/r < 30$) with respect to M_p is higher than those bent about the strong axis. This occurs at axial loads below 60 percent of the buckling load and is attributed to the relatively more favorable relationship between axial load and plastic bending strength (see Fig. 2.14).

(2) Frames with leaned columns were solved for a wide range of L_c/r ($20 < L_c/r < 60$) and G ($0 < G < 2.0$), so that the range of the effective slenderness ratio is between 40 and 195. The value of α generally varies between 0 and 3.0. In general, there is an appreciable reduction in beam-column strength due to the load on the pinned column. At the stability limit of leaned frames, the ratio of the reduced buckling load to the full elastic buckling load of the rigidly jointed column is inversely proportional to α , when buckling occurs in the elastic range. In the inelastic range, this ratio may be approximated to be linearly proportional to α .

(3) A comparison of exact elastic second order moments with those predicted by the effective length method and the P-delta method shows that both methods give good results, especially for flexible frames and when axial loads are less than about 50 percent of the frame buckling load. The effective length method gives better results for high axial load and large restraints.

(4) Maximum strength interaction curves developed from the inelastic analysis were compared with the design interaction equations suggested by the AISC Specification, the P-delta method, and the effective length method (see Sec. 2.7). The comparison shows that for $\alpha = 0$, the AISC method is generally conservative; it tends to be very conservative for columns with soft restraints. It may

be unconservative in some cases, e.g., for $L_c/r = 30$ and $G = 0$ with strong axis bending. The current AISC method does not have any provision for the design of columns in leaned frames. The effective length method gives a close prediction of strength, although it is slightly unconservative for weak axis bending. In leaned frames, the effective length method always yields a conservative prediction of the buckling load. The P-delta method is generally unconservative, especially for weak axis bending when the axial load is high.

(5) The manner in which factors of safety are used with the interaction equations can have a greater effect than the differences which occur among the various design methods themselves.

(6) The experimental results on unbraced frames were in very good agreement with the theoretical prediction and gave a strong verification of the leaned frame concept. For Specimens F1 and F2, the experimental buckling loads of the frames are within 3 percent of the theoretical buckling loads (using the limit load technique) and the sum of the buckling strength of individual columns in a sway mode. The interior column of Specimen F1 can carry the load 25 percent higher than its isolated capacity; this is attributed to the potential bracing effect of the lightly loaded exterior columns. The maximum load capacity and the behavior of Specimens F1 and F2 are considerably different, due to the initial imperfection of the frames. For Specimen F3, which is subjected to combined gravity and lateral loads, the strength is within 3 percent of the theoretical prediction. The test results are also in good agreement with the predicted value using the effective length method (9 percent conservative). The P-delta method gives a result that is 20 percent unconservative. If the AISC method is used, the predicted value was found to be 134 percent conservative.

(7) Experiments on biaxially loaded restrained beam-columns were conducted on three identical specimens but with different loading conditions. The results compared favorably with Mitchell's theoretical prediction. For Specimens BC-1 and BC-2, the strength is within 7 percent of the predicted value. For Specimen BC-3, the predicted strength is 38 percent conservative. This is attributed to the fact that the theoretical analysis does not consider the elastic unloading of the yielded fibers. The comparison of the test results with the design equations was studied by treating the specimens as no-sway (based on the total length) and sway (based on half of the total length) restrained beam-columns. In both cases the predicted results were in reasonable agreement for Specimen BC-1 (about 20 percent conservative) and were very conservative for Specimens BC-2 and BC-3. This was due to the fact that the interaction equations were developed for eccentrically loaded columns bent in single curvature. The wind load in Specimens BC-2 and BC-3 produces moment gradient which causes a higher strength.

(8) The experimental methods and testing fixtures used in the experiments were very satisfactory.

6.2 Design Recommendations

The results of the theoretical and experimental studies on unbraced frames show that the design of a beam-column in unbraced planar frames can be based on the following interaction equations:

$$\frac{P}{P_{cr}} + \frac{M^*}{M_p} \leq 1.0 \quad (6.1a)$$

and

$$\frac{\sum P}{\sum P'_{cr}} \leq 1.0 \quad (6.1b)$$

Equation 6.1a checks the strength and stability of a member and Eq. 6.1b checks the stability of the frame. The buckling strength of the column, P_{cr} (Eq. 6.1a), is based on the actual column height

and P'_{cr} (Eq. 6.1b), is based on the effective slenderness ratio in a sway mode. The second order moment M^* may be determined from the first order moment with an amplification factor (see Eq. 1.32) or it may be obtained by analyzing the frame using the P-delta method of analysis.

When the sway beam-column is braced laterally at the joints, and the member is bent about the strong axis, a separate check for lateral torsional buckling of the member must be considered by the following interaction equation:

$$\frac{P}{P'_{cr}} + \frac{M^*}{C_b M_m} \leq 1.0 \quad (6.2)$$

where

$$C_b M_m \leq M_{px}$$

In this equation P'_{cr} is the buckling strength about the weak axis considering the effective length in the no-sway mode or conservatively using the story height. The second order moment M^* is in the plane of bending (about the strong axis). The limit on the bending strength is $C_b M_m$, which is the critical moment of the member considered as a beam (see Eqs. 1.8 and 1.13 for the expressions for C_b and M_m). It should be noted that the AISC Specification specifies M_m to be the critical bending strength. This leads to a certain degree of conservativeness because the effect of moment gradient is not considered.

Referring to Chapter 1, the design of biaxially loaded beam-columns in unbraced frames is based on the AISC method and Springfield's recommendation. The comparison of the test results with the design methods was studied in Chapter 5 (Sec. 5.7) using these approaches. In addition, the test results were compared with the effective length method and with the methods that treat the specimens as no-sway beam-columns. It was found that the AISC method gives results which are in good agreement with other approaches, but Springfield's

recommendation yields inconsistent results. In view of this study and the studies in Chapter 2 on frames with leaned columns, it is recommended that the design of biaxially loaded beam-columns in unbraced frames should be based on either of the following methods:

$$\text{AISC Method: } \frac{P}{P'_{cr}} + \frac{0.85M_x}{\left(1 - \frac{\Sigma P}{\Sigma P'_{Ex}}\right) C_b M_m} + \frac{0.85M_y}{\left(1 - \frac{\Sigma P}{\Sigma P'_{Ey}}\right) M_{py}} \leq 1.0 \quad (6.3a)$$

$$\frac{P}{P_y} + \frac{M_x}{M_{px}} + \frac{M_y}{M_{py}} \leq 1.0 \quad (6.3b)$$

$$\frac{\Sigma P}{\Sigma P'_{cr}} \leq 1.0 \quad (6.1b)$$

Effective Length Method:

$$\frac{P}{P_{cr}} + \frac{M_x}{\left(1 - \frac{\Sigma P}{\Sigma P'_{Ex}}\right) C_b M_m} + \frac{M_y}{\left(1 - \frac{\Sigma P}{\Sigma P'_{Ey}}\right) M_{py}} \leq 1.0 \quad (6.4)$$

$$\frac{\Sigma P}{\Sigma P'_{cr}} \leq 1.0 \quad (6.1b)$$

The terms P'_{cr} and P_{cr} in Eqs. 6.3a and 6.4 are based on the largest KL_c/r and L_c/r , respectively. It should be observed that the amplification factors in Eqs. 6.3a and 6.4 have accounted for the loads on the leaned columns. Eq. 6.1b should also be checked in the AISC method, especially in the leaned frame system.

According to the AISC specification, the design of girders and connections is based on the first order moment. Since the column end moment has been increased due to the P-delta effect, the girders and the connections should also be designed for the second order end moment (see Eq. 1.33).

In summary, the following steps are recommended for the design of beam-columns in unbraced frames.

(1) Determine M^* from Eq. 1.32 or from an elastic second order analysis.

(2) Design girders and connections for the second order end moment given by Eq. 1.33.

(3) For planar behavior, design beam-columns using Eq. 6.1 and check Eq. 6.2 if the members are not fully braced laterally.

(4) For biaxially loaded beam-columns, the design should be based on Eq. 6.3 or 6.4 and Eq. 6.1b.

(5) A uniform factor of safety of 1.67 (or 1.3 for the combined gravity and lateral loads) should be used to determine the allowable buckling load and the allowable moments in the interaction equations (Eqs. 6.3 and 6.4). In the case of frame buckling (Specimen F1 of the unbraced frame tests), a higher factor of safety of, for example, 1.92 should be used in Eq. 6.1b.

6.3 Recommendations for Future Study

The design of beam-columns in unbraced frames for the planar behavior can be recommended with confidence. Although elastic beams were considered in this study, a previous study³² showed that slight beam yielding did not affect the strength of beam-columns significantly. However, there was not much research concerning the lateral torsional buckling behavior and the spatial behavior of beam-columns in unbraced frames. The test results on biaxially loaded restrained beam-columns in this study served to provide the exploratory data. Mitchell's program with some modification could provide a very useful analytical tool for further theoretical study. At present, the program requires a lot of computer time to obtain a solution for the strength of the member and some difficulties in the convergence of the solution are often encountered. Besides, several features of steel structures are not taken into

account. The recommendations for the future study can be summarized as:

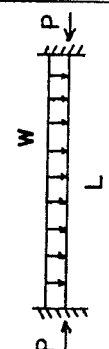
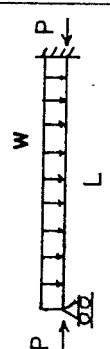
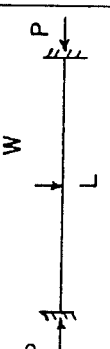
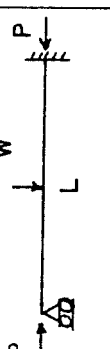
(1) The algorithm of Mitchell's program should be investigated to improve the efficiency in computer time and to overcome the convergence problem. Further modifications of the program should be studied so that the program can take into account the initial curvatures of the column, strain reversal, the presence of residual stresses, the warping boundary condition, and the more exact treatment of torsional analysis. The shifting of the shear center as the cross section is yielded should be considered, if this is feasible for the discrete element model. The program should also be extended to solve the spatial behavior of the frame so that the effect of beam yielding may be studied. With these modifications, the extensive parametric studies relating to the lateral torsional buckling and the biaxial behavior of beam-columns can be conducted. Emphasis should be placed on loading conditions producing moment gradient in the columns, since the present design recommendation grossly underestimates the actual strength for these cases.

(2) Additional experimental programs on biaxially loaded restrained beam-columns should be investigated. The study should be planned to consider the effects of the slenderness ratio and the relative column-to-beam stiffness in two directions and the loading path. It is felt that a test with a constant axial load and an oblique wind load would be desirable.

(3) The design interaction surfaces should be studied and compared with the results of the parametric studies and the experiments.

T A B L E S

TABLE 1.1 ELASTIC SECOND ORDER MOMENTS IN NO-SWAY BEAM COLUMNS

Loading Condition	Effective Length Factor	M_{end} (First Order)	M_{end}^*/M_{end}	
			Exact	Approximate
	0.5	$wL^2/12$	$\frac{3(\tan u - u)}{u^2 \tan u}$	$\frac{1 - 0.39 P/P'E}{1 - P/P'E}$
	0.7	$wL^2/8$	$\frac{\tan u - u}{\frac{1}{2} u^2 (\frac{1}{2u} - \frac{1}{\tan 2u})}$	$\frac{1 - 0.39 P/P'E}{1 - P/P'E}$
	0.5	$wL/8$	$\frac{2(1 - \cos u)}{u \sin u}$	$\frac{1 - 0.19 P/P'E}{1 - P/P'E}$
	0.7	$3/16 WL$	$1.6 \frac{\tan u}{u} - 0.6 \sec u \frac{\lambda(u)}{\psi(u)}$	$\frac{1 - 0.3 P/P'E}{1 - P/P'E}$

NOTE: (1) $u = \frac{L}{2} \sqrt{\frac{P}{EI}}$

(2) $\lambda(u) = 2(1 - \cos u)/u^2 \cos u$

(3) $\psi(u) = \frac{3}{2u} \left(\frac{1}{2u} - \frac{1}{\tan 2u} \right)$

(4) M_{end} and M_{end}^* are the elastic first and second order end moments, respectively.

(5) Maximum moment occurs at the end of the member for all cases.

TABLE 3.1 MILL MATERIAL PROPERTIES

Section	Use	ASTM Designation	Mill Yield Stress ksi	Mill Ult. Tensile Stress ksi	Elong. 8 in. %	Mill Chemical Analysis					
						C	Mn	P	S	Si	Cb
W8x17	Column	A36-70A	47.8	65.1	29.0	.16	.55	.010	.025	.03	
W10x21	Column	A36-70A	46.6	62.2	31.5	.13	.48	.010	.019	.06	
W8x20	Beam	A572-73	58.9	73.5	30.0	.15	.89	.010	.019	.04	.012
W5x18.5	Beam	A572-73	54.9	68.3	28.0	.15	.80	.010	.020	.03	.011
M4x13	Beam	A572-73	54.9	68.3	28.0	.15	.80	.010	.020	.03	.011

TABLE 3.2 SUMMARY OF STEEL USED AND MATERIAL TESTING

Length Number	Section	Main Test	Member Number	Use	Number of Property Testing				Cross Section Measurement
					Tension Flange	Coupon Web	Stub Column	Residual Strain Measurement	
L1	W8x17	Frame	C1A, C1C	Column	2	1	1	1	6
L2	W8x17	Frame	C1B, C2B	Column			1	1	6
L3	W8x17	Frame	C3A, C3C	Column	2	1			4
L11	W8x17	Frame	C3B	Column	2	1			2
L4	W10x21	Restrained Col.	C1, C2	Column	2	1	1	1	6
L5	W10x21	Restrained Col.	C3	Column	2	1			2
L6	M4x13	Frame	B1, B2, B3, B4	Beam	2	1			8
L8	W8x20	Restrained Col.	BS1, BS2	Beam	2	1			4
L9	W5x18.5	Restrained Col.	BW1, BW2	Beam	2	1			4

TABLE 3.3 SUMMARY OF TENSION TESTS

Section	Length Number	Specimen	σ_y ksi	ϵ_y^*	ϵ_{st}	E_{st} ksi	σ_{ult} ksi	Elongation in 8 in., %
W8x17	L1	Flange	37.8	.00128	.01140	442	62.4	28.2
		Flange	37.7	.00127	.01378	356	--	29.7
		Web	40.6	.00137	.02450	345	61.7	32.9
	L3	Flange	37.5	.00127	.01368	475	61.9	28.0
		Flange	37.8	.00128	.01550	458	61.8	28.5
		Web	40.7	.00137	.02740	279	61.2	34.6
	L11	Flange	37.2	.00126	.01090	397	61.3	--
		Flange	38.3	.00129	.01630	412	61.5	27.9
		Web	41.4	.00140	.02610	226	60.6	31.4
	Average	Flange	37.7	.00128	.01359	423	61.8	28.5
	Web	40.9	.00139	.02600	283	61.2	33.0	
W10x21	L5	Flange	39.1	.00132	.01069	429	61.1	23.7
		Flange	40.0	.00135	.01263	383	61.2	22.7
		Web	39.6	.00134	.02602	236	59.3	31.6
	Average	Flange	39.5	.00134	.01166	406	61.1	23.2
	Web	39.6	.00134	.02602	236	59.3	31.6	
M4x13	L6	Flange	48.5	.00164	.01203	406	69.6	26.6
		Flange	48.6	.00164	.01062	399	69.9	27.2
		Web	50.1	.00169	.02228	323	69.5	26.7
	Average	Flange	48.5	.00164	.01132	402	69.7	26.9
	Web	50.1	.00169	.02228	323	69.5	26.7	
W8x20	L8	Flange	51.2	.00173	.00718	462	74.7	24.7
		Flange	51.3	.00173	.00597	502	75.1	23.9
		Web	53.5	.00181	.02701	279	71.9	22.6
	Average	Flange	51.2	.00174	.00657	482	74.9	24.3
	Web	53.5	.00181	.02701	279	71.9	22.6	
W5x18.5	L9	Flange	47.6	.00161	.00925	475	69.5	26.2
		Flange	47.5	.00160	.01274	410	69.0	28.9
		Web	47.8	.00161	.02491	329	66.7	28.6
	Average	Flange	47.5	.00161	.01099	442	69.2	27.5
	Web	47.8	.00161	.02491	329	66.7	28.6	

$$*\epsilon_y = \sigma_y / E \quad (E = 29500 \text{ ksi})$$

TABLE 3.4 MEMBER PROPERTIES

Section	Source	b in.	d in.	t _f in.	t _w in.	A in. ²	I _x ⁴ in. ⁴	I _y ⁴ in. ⁴	Z _x ³ in. ³	Z _y ³ in. ³	P _y kip	M _{px} kip-in.	M _{py} kip-in.
W8x17	Measured	5.257	8.04	.308	.223	4.89	56.03	7.46	15.59	4.35	189.8	597.5	164.2
	AISC	5.250	8.00	.308	.230	5.01	56.60	7.44	15.90	4.36	180.4	572.4	157.0
W10x21	Measured	5.765	9.96	.341	.246	6.21	107.36	10.90	24.20	5.81	245.7	956.6	229.4
	AISC	5.750	9.90	.340	.240	6.20	107.00	10.80	24.10	5.77	223.2	867.6	207.7
M4x13	Measured	3.97	3.96	.389	.245	3.87	10.54	4.06	6.13	3.11	188.8	298.4	151.1
	AISC	3.94	3.81	.371	.254	3.81	10.50	3.36	6.06	2.74	190.5	303.0	137.0
W8x20	Measured	5.326	8.17	.384	.254	5.97	70.62	9.68	19.40	5.56	310.0	1001.4	285.2
	AISC	5.268	8.14	.378	.248	5.89	69.40	9.22	19.10	5.37	294.5	955.0	268.5
W5x18.5	Measured	5.067	5.068	.427	.273	5.48	25.07	9.26	11.25	5.56	260.5	534.9	264.1
	AISC	5.025	5.12	.420	.265	5.43	25.40	8.89	11.30	5.39	271.5	565.0	269.5

TABLE 3.5 SUMMARY OF STUB COLUMN TESTS

	Unit	W8x17 L1	W8x17 L2	W10x21 L4
Length	in.	30	30	30
Area	in. ²	4.85	4.96	6.22
Average σ_y (flange)	ksi	37.7	37.7	39.5
Average σ_y (web)	ksi	40.9	40.9	39.6
P_y (calculated)	kip	188.2	192.6	246.3
P_y (measured)	kip	195.7	201.3	248.5
$\frac{P_y \text{ (calculated)}}{P_y \text{ (measured)}}$.962	.957	.991
Error	%	3.8	4.3	0.9

TABLE 4.1 TEST RESULTS AND THEORETICAL PREDICTION OF FRAMES SUBJECTED TO GRAVITY LOADS

Specimen	Experimental Ultimate Load				Theoretical Ultimate Load	Type of Failure
	Left Exterior Column	Interior Column	Right Exterior Column	ΣP		
	(kips)	(kips)	(kips)	(kips)	(kips)	
F1	69.8	132.7	66.5	269.1	285.3	Bifurcation
F2	65.2	106.3	62.1	233.6	235.0	Instability

TABLE 4.2 TEST RESULTS AND THEORETICAL PREDICTION OF FRAME SUBJECTED TO COMBINED GRAVITY AND LATERAL LOADS

Specimen	ΣP kip	H_{\max} kip		Δ at H_{\max} in.		K_s kip/in.		Type of Failure
		Test	Theory	Test	Theory	Test	Theory	
F3	186.4	2.25	2.30	2.47	2.10	1.27	1.58	Instability

TABLE 4.3 COMPARISON OF TEST RESULTS WITH DESIGN METHODS

Specimen	H_{max} kips				$\frac{H_{max} \text{ (Test)}}{H_{max} \text{ (Predicted)}}$		
	Test	AISC	P-delta	Effective Length	AISC	P-delta	Effective Length
F3	2.25	0.96	2.81	2.07	2.344	0.802	1.087

TABLE 4.4 CONTRIBUTION OF AXIAL LOAD AND MOMENT TERMS IN THE INTERACTION EQUATIONS

Specimen	Column	Quantity	Interaction Equation		
			AISC	P-delta	Effective Length
F3	Exterior	Axial Load	0.610	0.288	0.396
		Moment	0.370	0.722	0.614
	Interior	Axial Load	0.747	0.418	0.575
		Moment	0.253	0.582	0.425

TABLE 5.1 CHARACTERISTICS OF RESTRAINED BEAM-COLUMN SPECIMENS

Specimen	L_c in.	$G = \frac{EI_c/L_b}{EI_b/L_b}$		Slenderness Ratio			
				$\frac{L_c}{r_x}$	$\frac{KL_c}{r_x}$	$\frac{L_c}{r_y}$	$\frac{KL_c}{r_y}$
		Strong Axis	Weak Axis				
BC-1	124	1.18	0.28	29.8	39.2	93.6	102.1
BC-2	124	1.18	0.28	29.8	39.2	93.6	102.1
BC-3	124	1.18	0.28	29.8	39.2	93.6	102.1

* L_c is the length from center of joint to midlength.

TABLE 5.2 TEST RESULTS AND THEORETICAL PREDICTION OF RESTRAINED BEAM-COLUMNS

Specimen	Strength (kips)	Test	Theory			$\frac{\text{Test}}{\text{Theory}^*}$	Mode of Failure
			$\beta_{\mathcal{L}} = 0$	$\beta_{\mathcal{L}} \neq 0$	Uniaxial		
BC-1	F	132.3	128.0	125.0	130.0	1.03	Instability
BC-2	H_y	2.99	2.80	2.82	2.93	1.07	Instability
BC-3	H_x	18.6	13.50	6.0	22.70	1.38	Flexural Buckling

*Theory is based on $\beta_{\mathcal{L}} = 0$ analysis.

TABLE 5.3 COMPARISON OF TEST RESULTS WITH DESIGN METHODS
(SPECIMENS TREATED AS NO-SWAY BEAM-COLUMNS)

Specimen	Type of Strength	Test Results kips	CRC kips	Pillai kips	Chen kips	$\frac{\text{Test}}{\text{CRC}}$	$\frac{\text{Test}}{\text{Pillai}}$	$\frac{\text{Test}}{\text{Chen}}$
BC-1	F	132.3	104.0	108.5	112.5	1.27	1.22	1.18
BC-2	H _y	2.99	0.93	1.24	1.21	3.21	2.41	2.47
BC-3	H _x	16.7	4.93	5.54	6.67	3.39	3.07	2.50

TABLE 5.4 CONTRIBUTION OF AXIAL LOAD AND MOMENT TERMS
IN THE INTERACTION EQUATIONS

Specimen	Quantity	Interaction Equation		
		CRC	Pillai	Chen
BC-1	Axial Load	0.6	0.627	--
	Moment x-x	0.191	0.171	0.424
	Moment y-y	0.208	0.198	0.575
BC-2	Axial Load	0.542	0.542	--
	Moment x-x	0.189	0.155	0.301
	Moment y-y	0.268	0.294	0.695
BC-3	Axial Load	0.560	0.560	--
	Moment x-x	0.249	0.257	0.704
	Moment y-y	0.189	0.174	0.309

TABLE 5.5 COMPARISON OF TEST RESULTS WITH AISC METHOD
(SPECIMENS TREATED AS SWAY BEAM-COLUMNS)

Specimen	Strength Component	Test Results (kips)	Predicted Results			Test Results		
			CRC	AISC	Effective Length Method	CRC	AISC	Effective Length Method
BC-1	F	132.3	104.0	110.0	115.0	1.27	1.20	1.15
BC-2	H _y	2.99	0.93	1.09	1.12	3.21	2.74	2.67
BC-3	H _x	16.7	4.93	6.43	6.60	3.39	2.60	2.53

TABLE 5.6 COMPARISON OF TEST RESULTS WITH SPRINGFIELD'S RECOMMENDATION
(SPECIMENS TREATED AS SWAY BEAM-COLUMNS)

Specimen	Strength Component	Test Results (kips)	Predicted Results		Test Results	
			Chen	Springfield	Chen	Springfield
BC-1	F	132.3	112.5	111.2	1.18	1.19
BC-2	H _y	2.99	1.21	3.25	2.47	0.92
BC-3	H _x	16.7	6.67	15.5	2.50	1.08

F I G U R E S

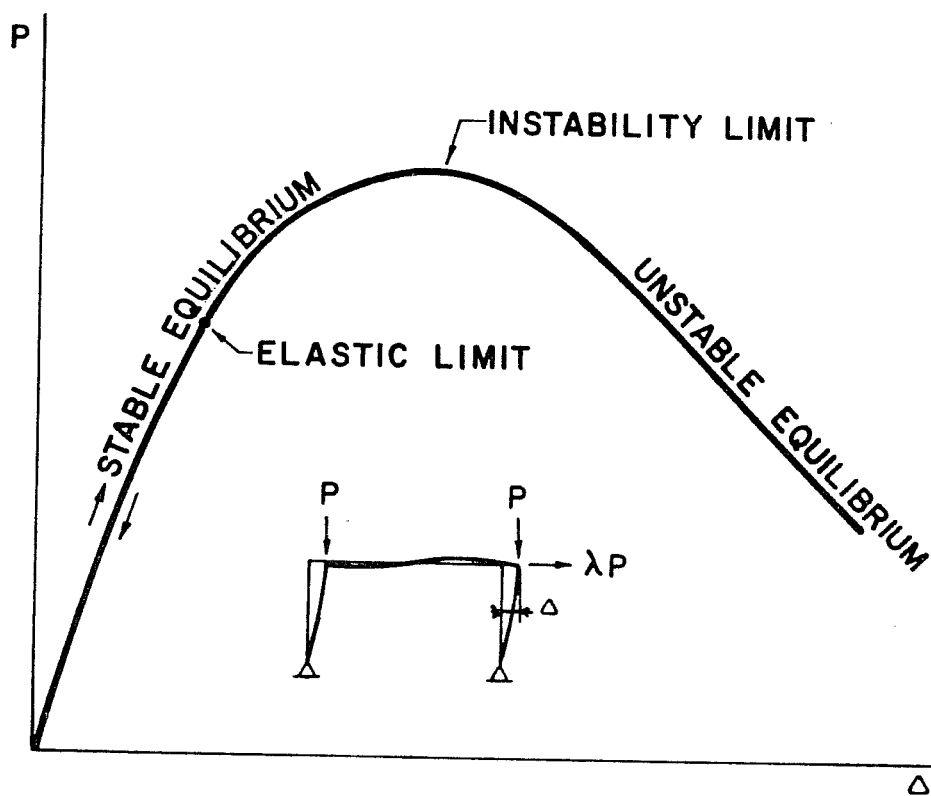


Fig. 1.1 Load-displacement of a frame

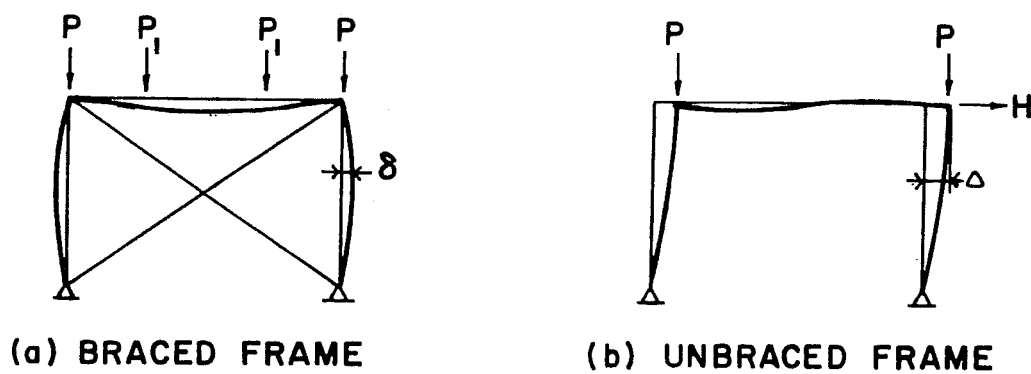


Fig. 1.2 P-delta effect

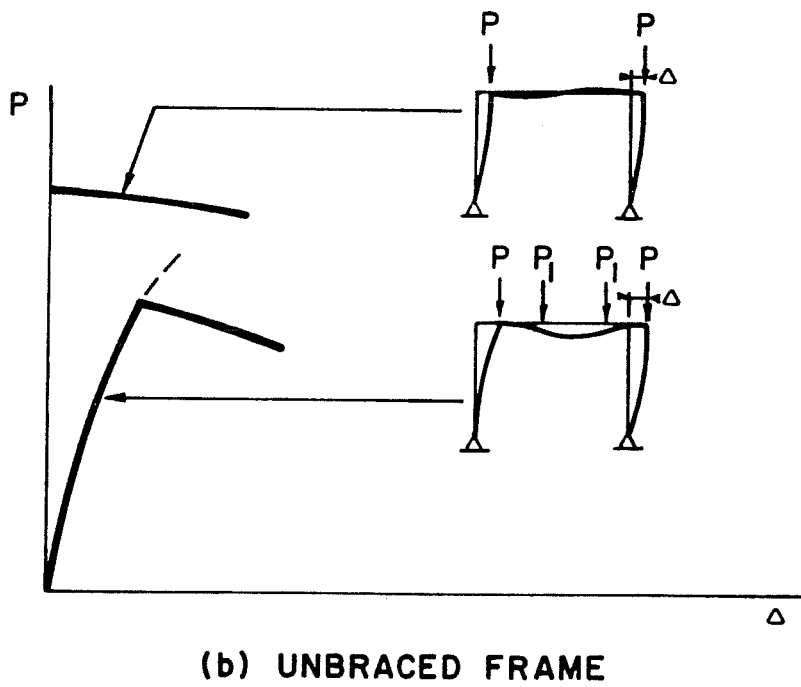
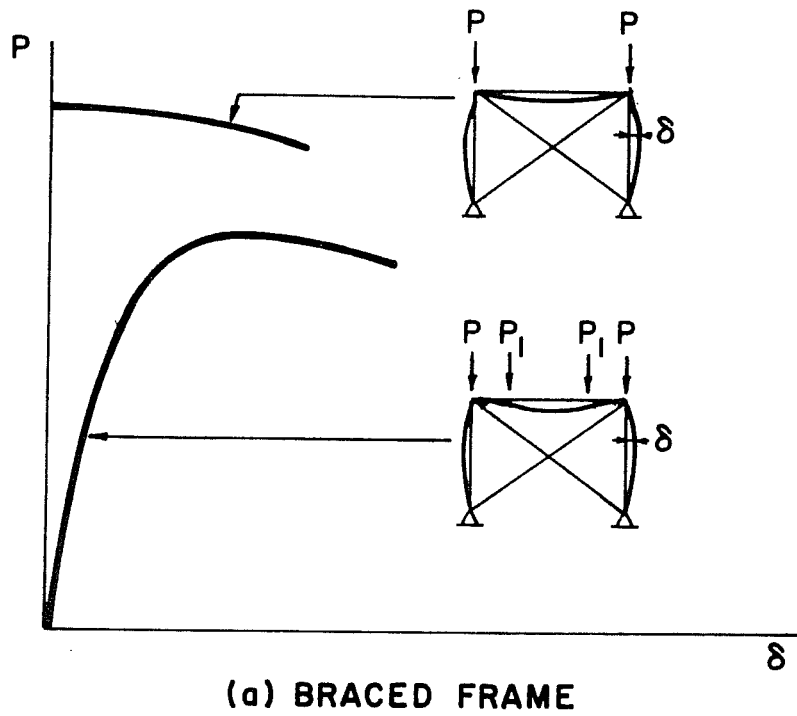


Fig. 1.3 Behavior of frames under gravity load

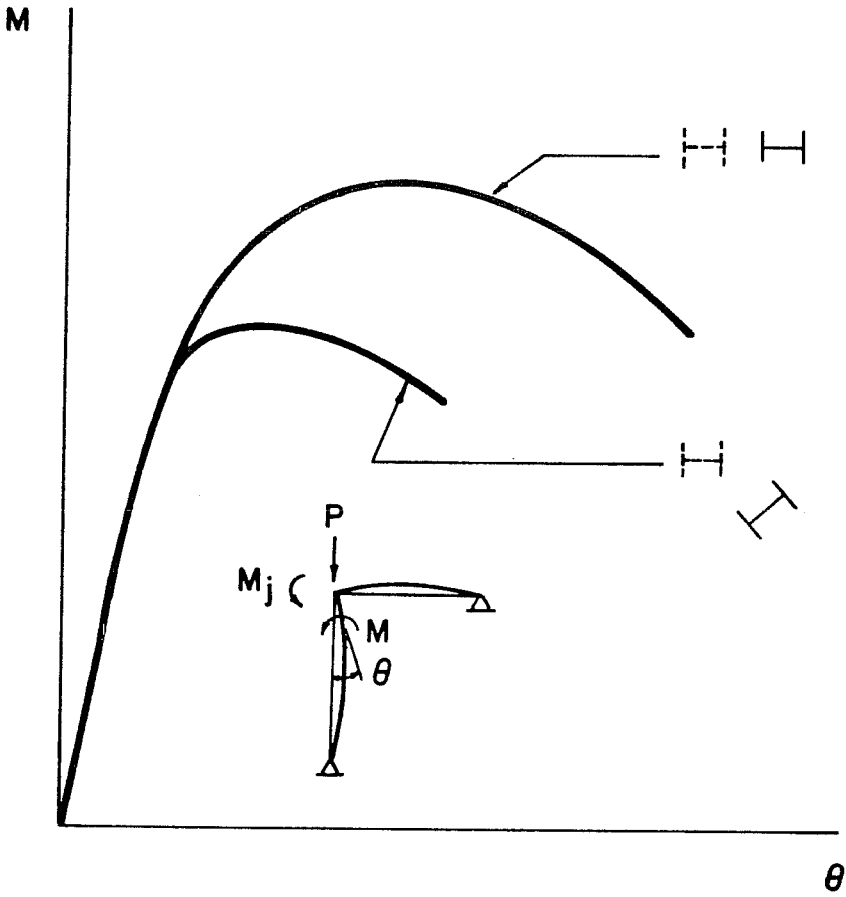


Fig. 4.1 Lateral-torsional buckling of beam-columns

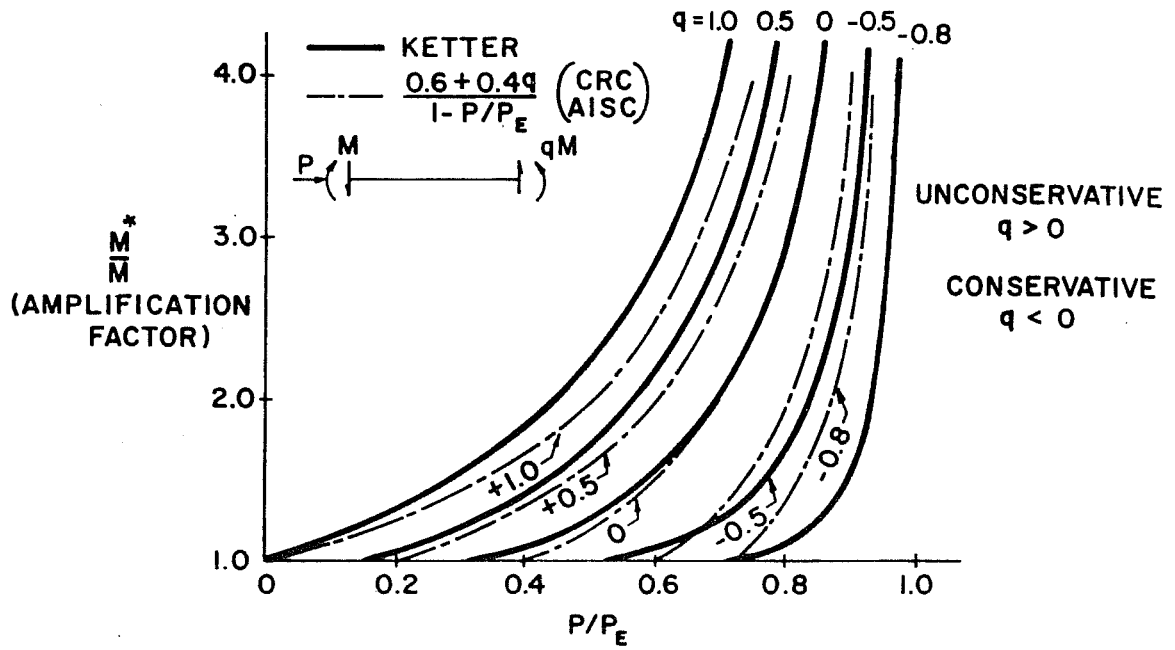


Fig. 1.5 Ketter's chart for elastic second order moments in no-sway pinned-end columns

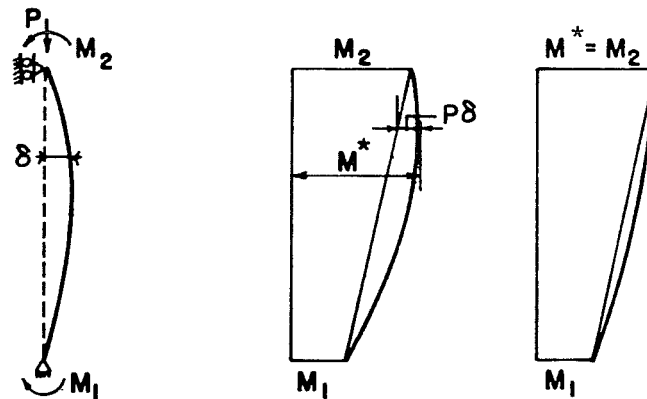


Fig. 1.6 Second order moments in no-sway columns

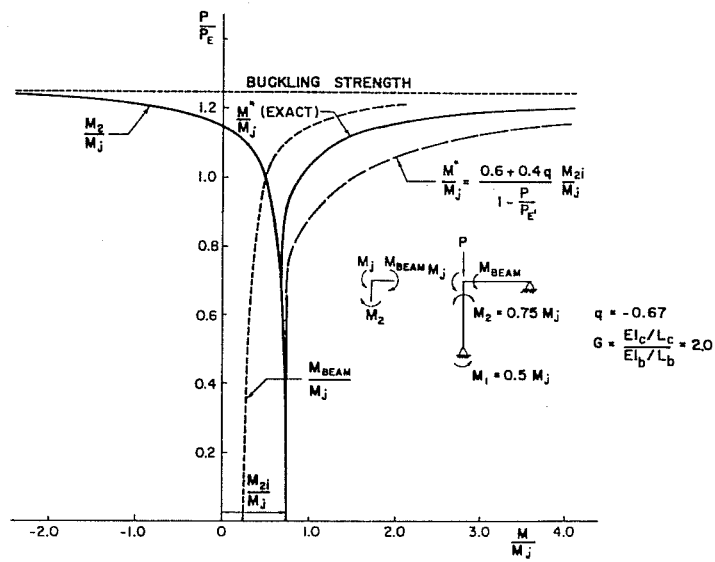


Fig. 1.7a Elastic second order analysis of no-sway restrained beam-columns (double curvature)

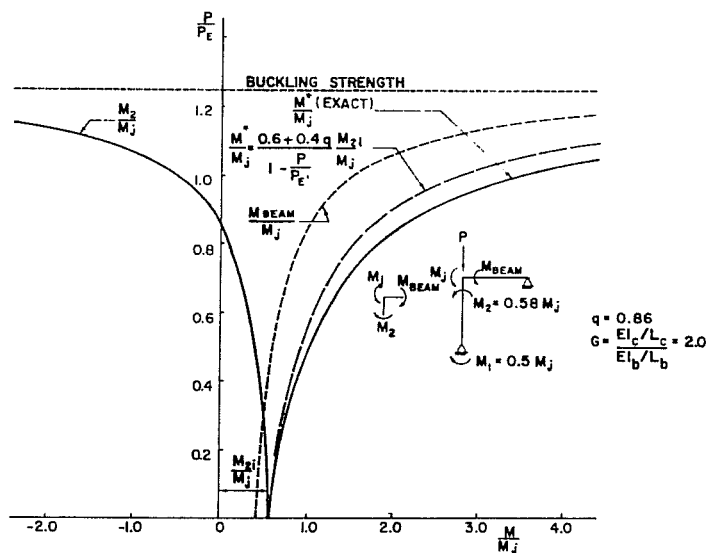


Fig. 1.7b Elastic second order analysis of no-sway restrained beam-columns (single curvature)

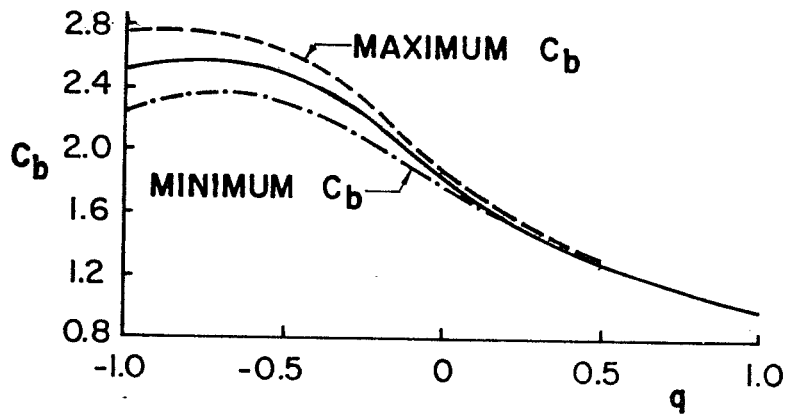


Fig. 1.8 Factors to account for the effect of moment gradient on elastic lateral torsional buckling strength of beams

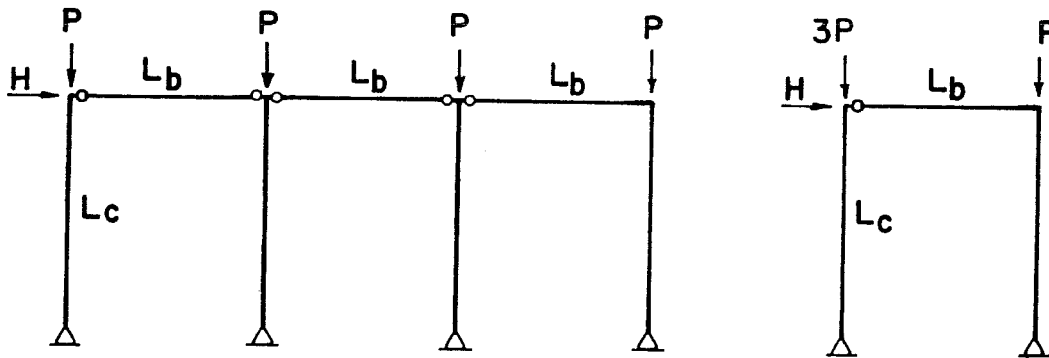


Fig. 1.9 Leaned frame system

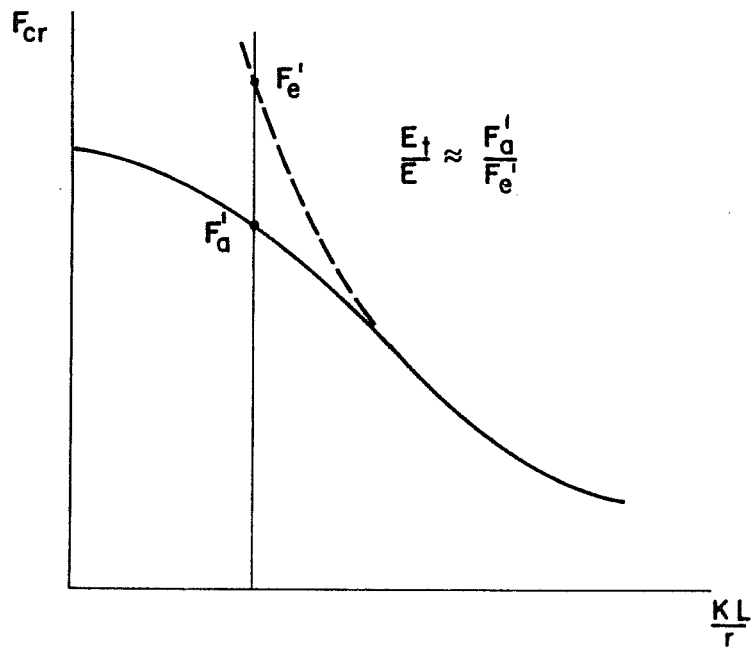


Fig. 1.10 Approximate procedure for determining the tangent modulus

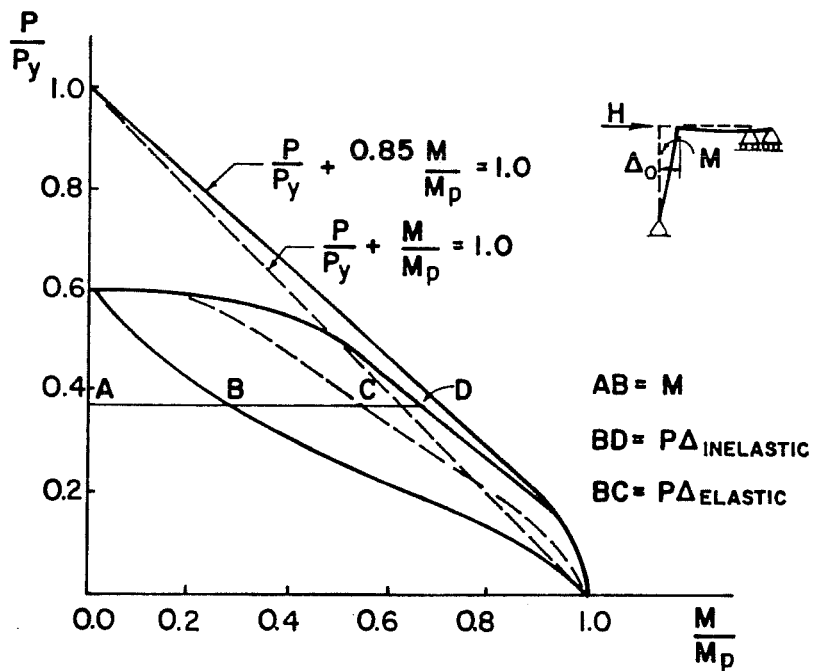


Fig. 1.11 Comparison of second order moments at the ultimate strength of beam-columns

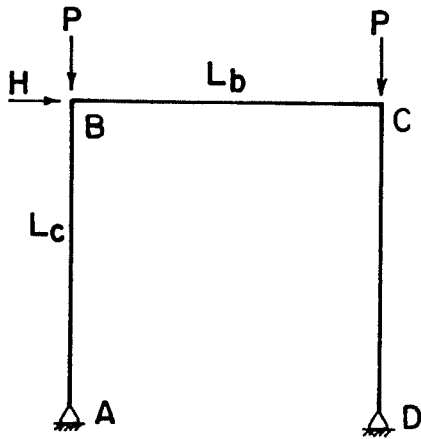


Fig. 2.1 Portal frame

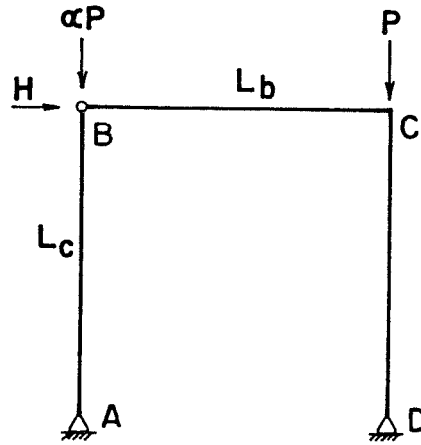


Fig. 2.2 Leaned frame

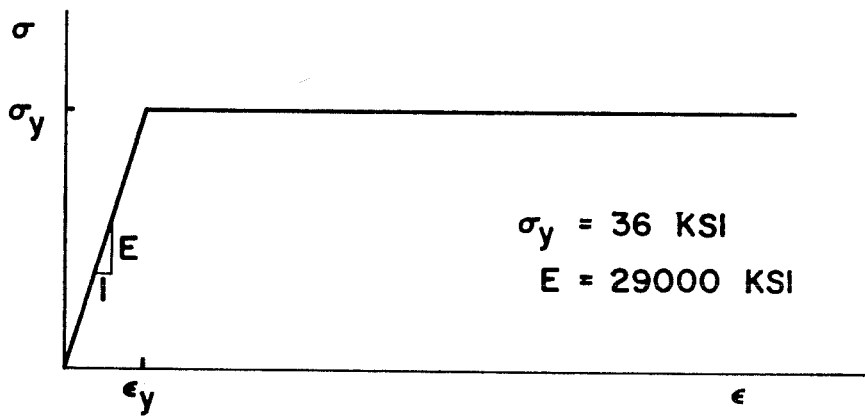


Fig. 2.3 Elastic-plastic stress-strain relationship

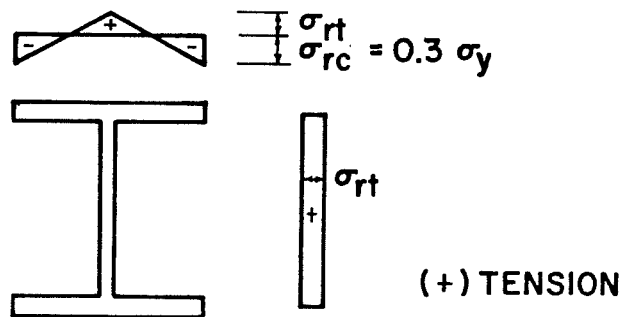


Fig. 2.4 Idealized residual stress pattern

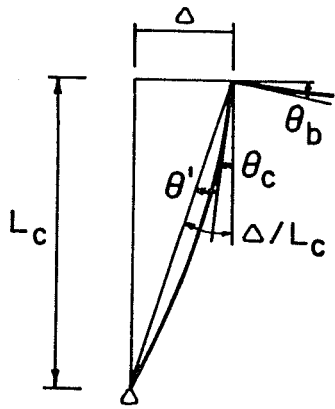


Fig. 2.5 Geometry and compatibility

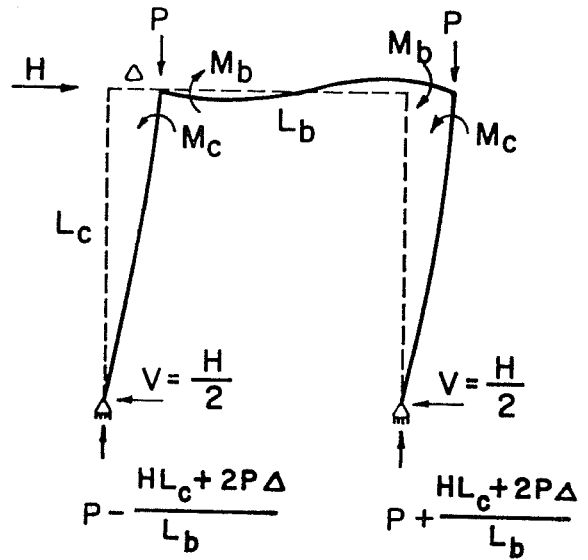


Fig. 2.6 Equilibrium of portal frame

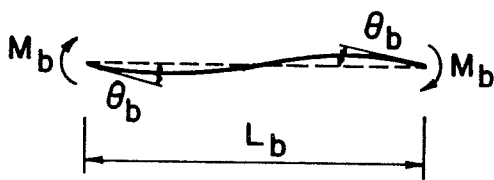


Fig. 2.7 Moment-rotation relationship of beam with antisymmetrical bending

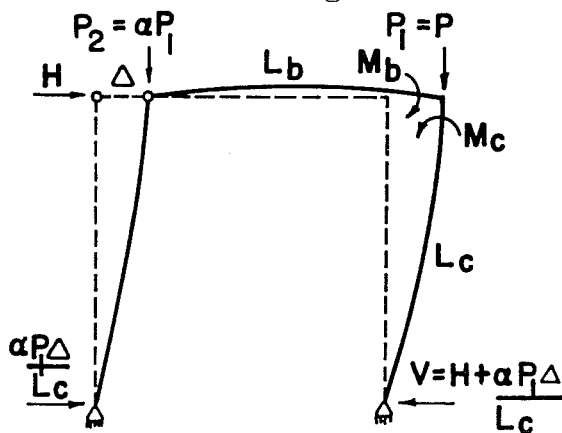
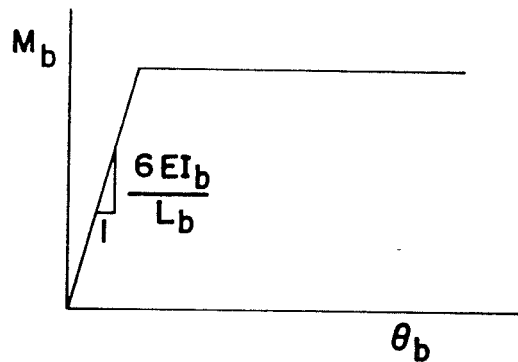


Fig. 2.8 Equilibrium of leaned frame

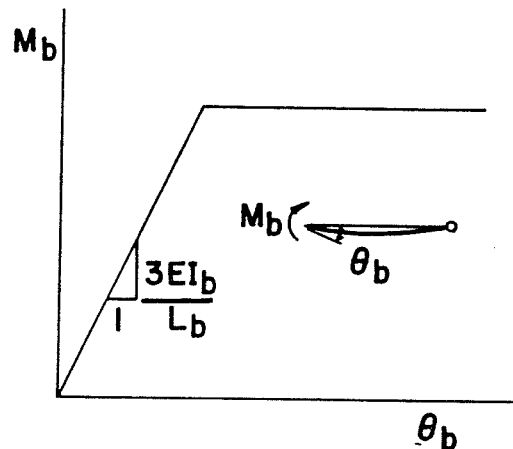
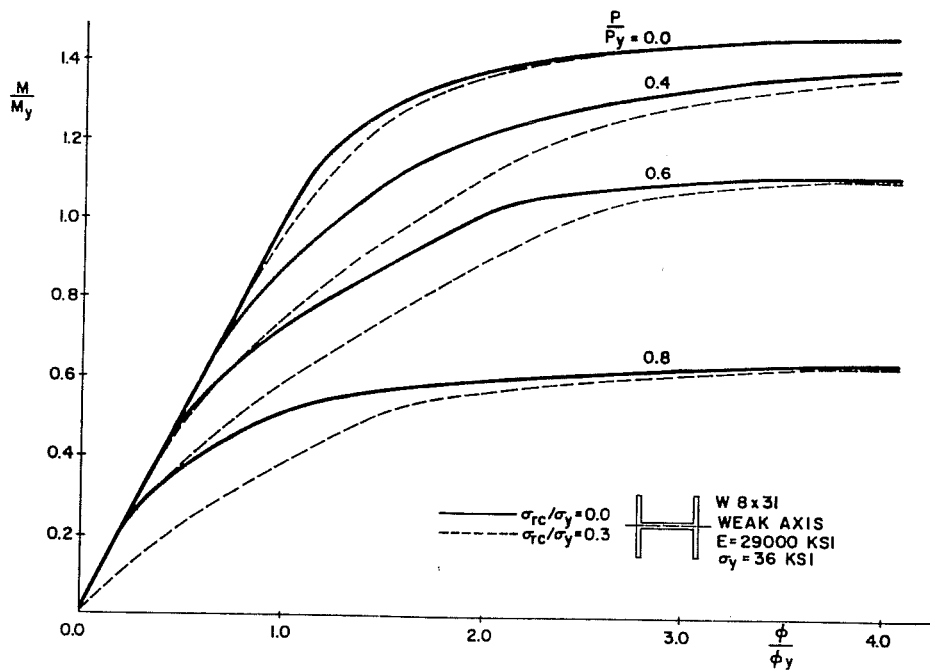
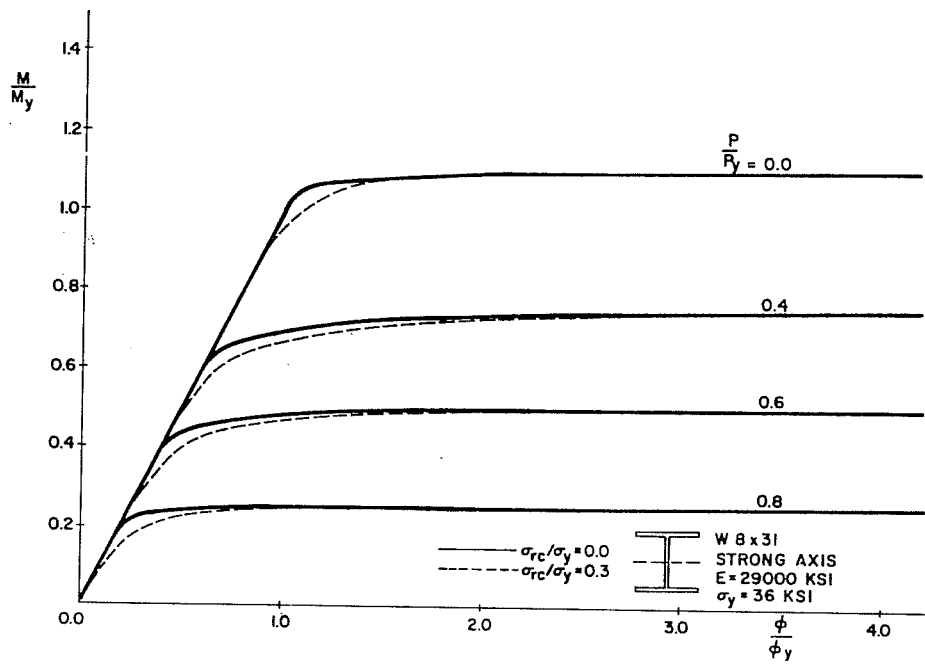


Fig. 2.9 Moment-rotation of beam with one end pinned



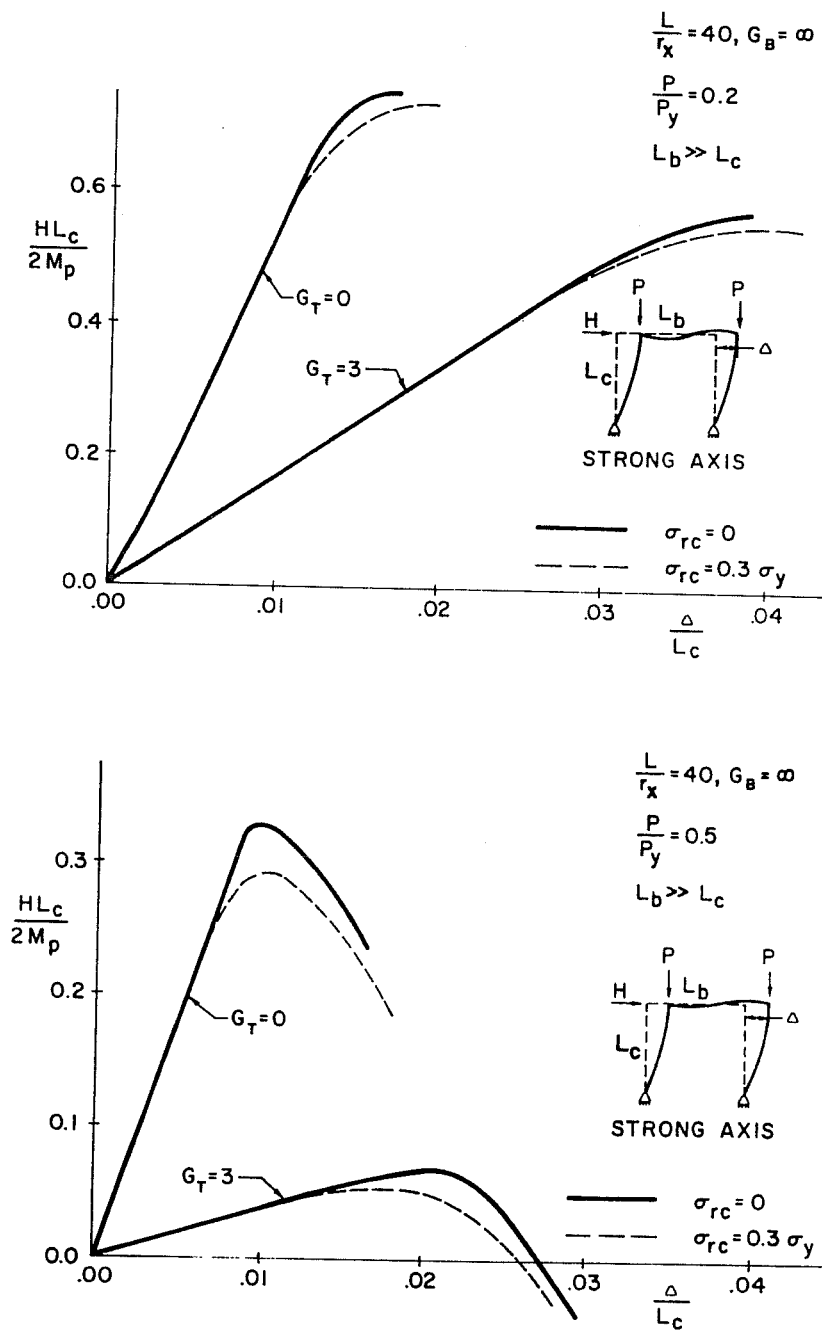


Fig. 2.12 Typical shear resistance-relationship of beam-columns in portal frames (strong axis bending)

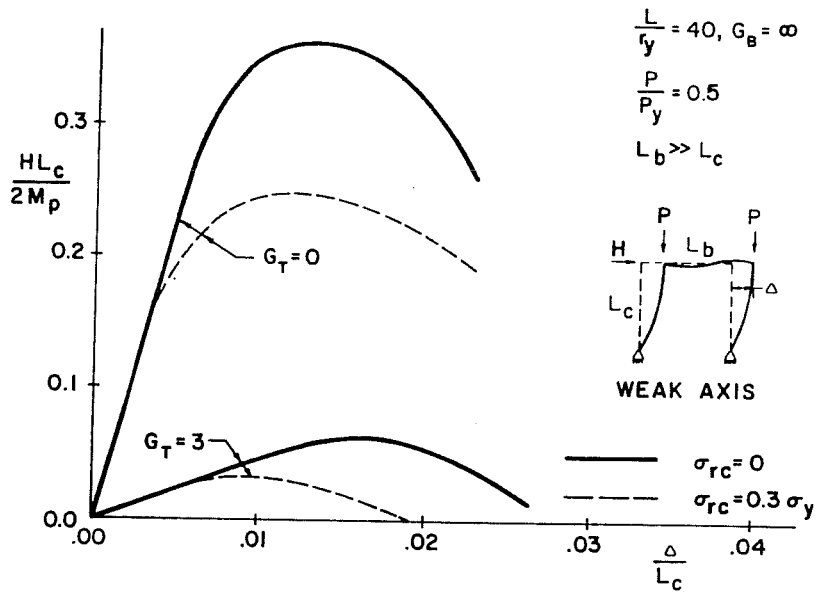
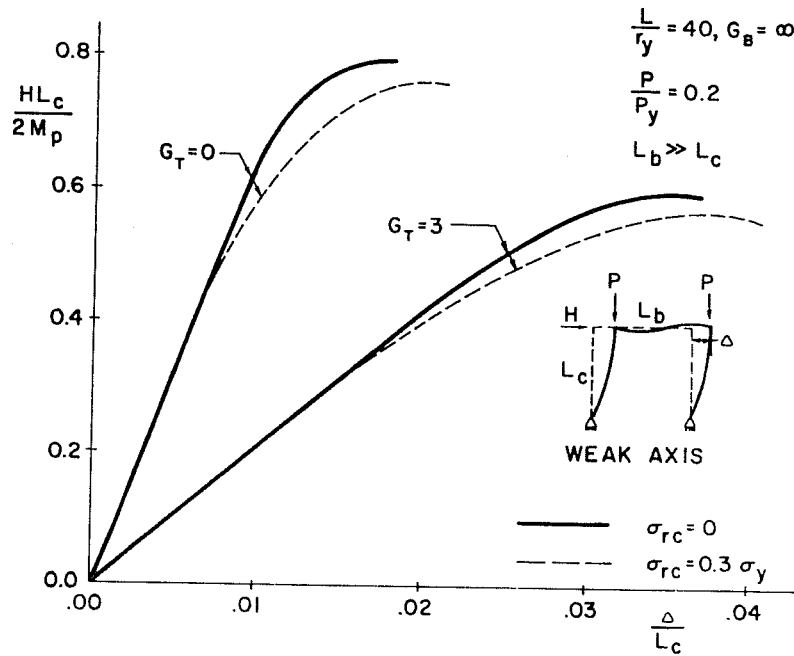


Fig. 2.13 Typical shear resistance-sway relationship of beam-columns in portal frames (weak axis bending)

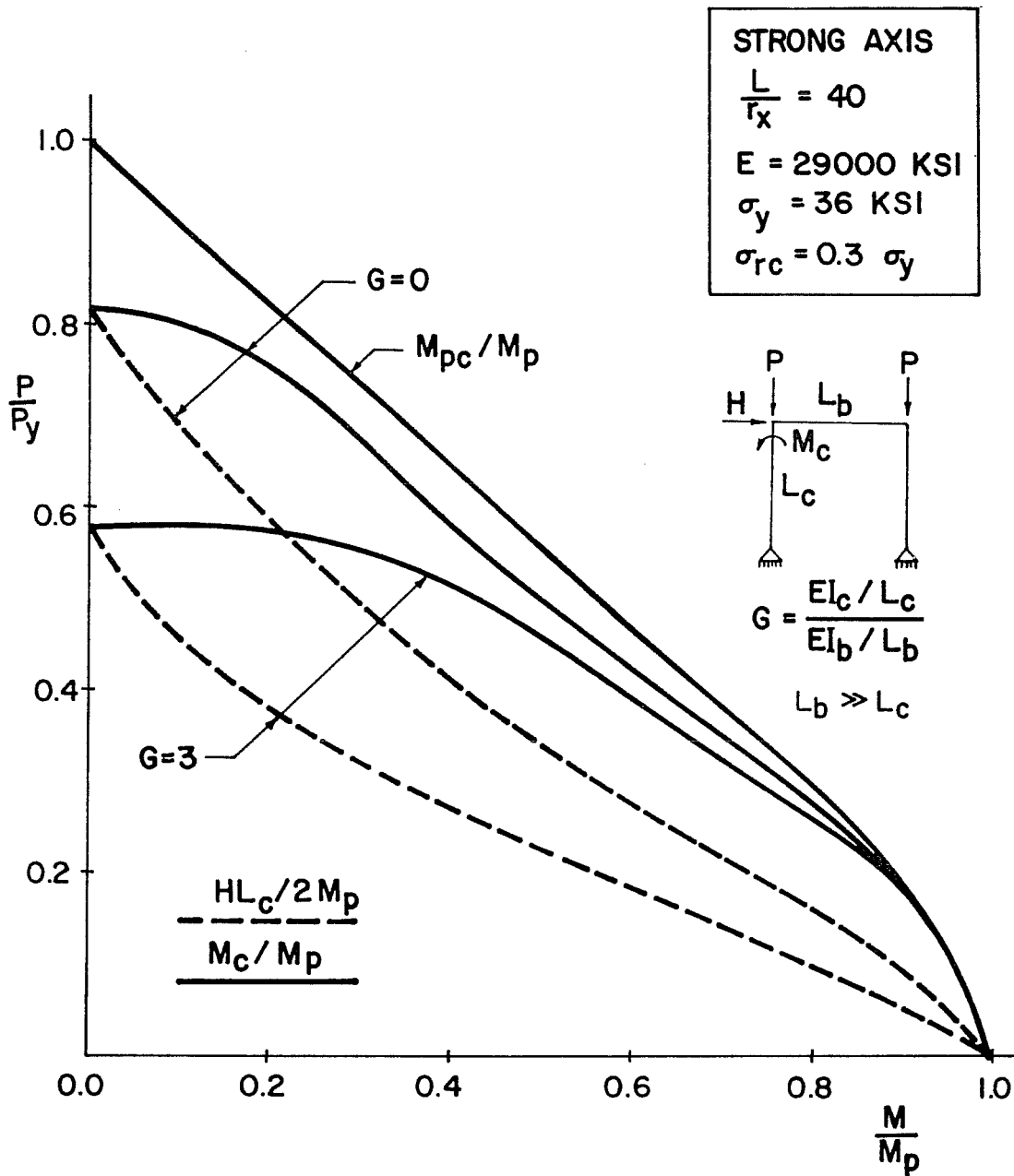


Fig. 2.14a P-delta effect at the maximum strength of beam-columns (strong axis bending)

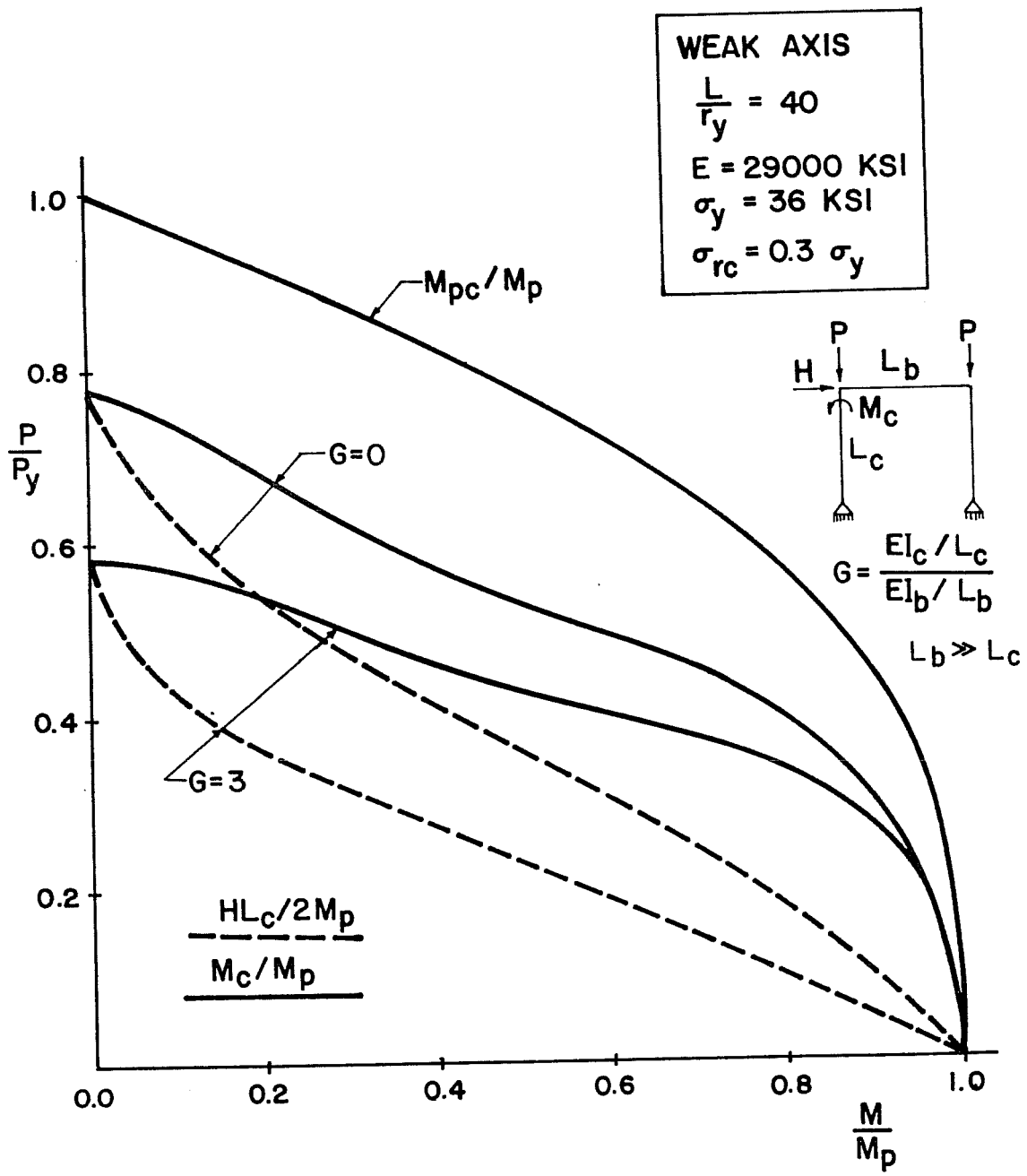


Fig. 2.14b P-delta effect at the maximum strength of beam-columns (weak axis bending)

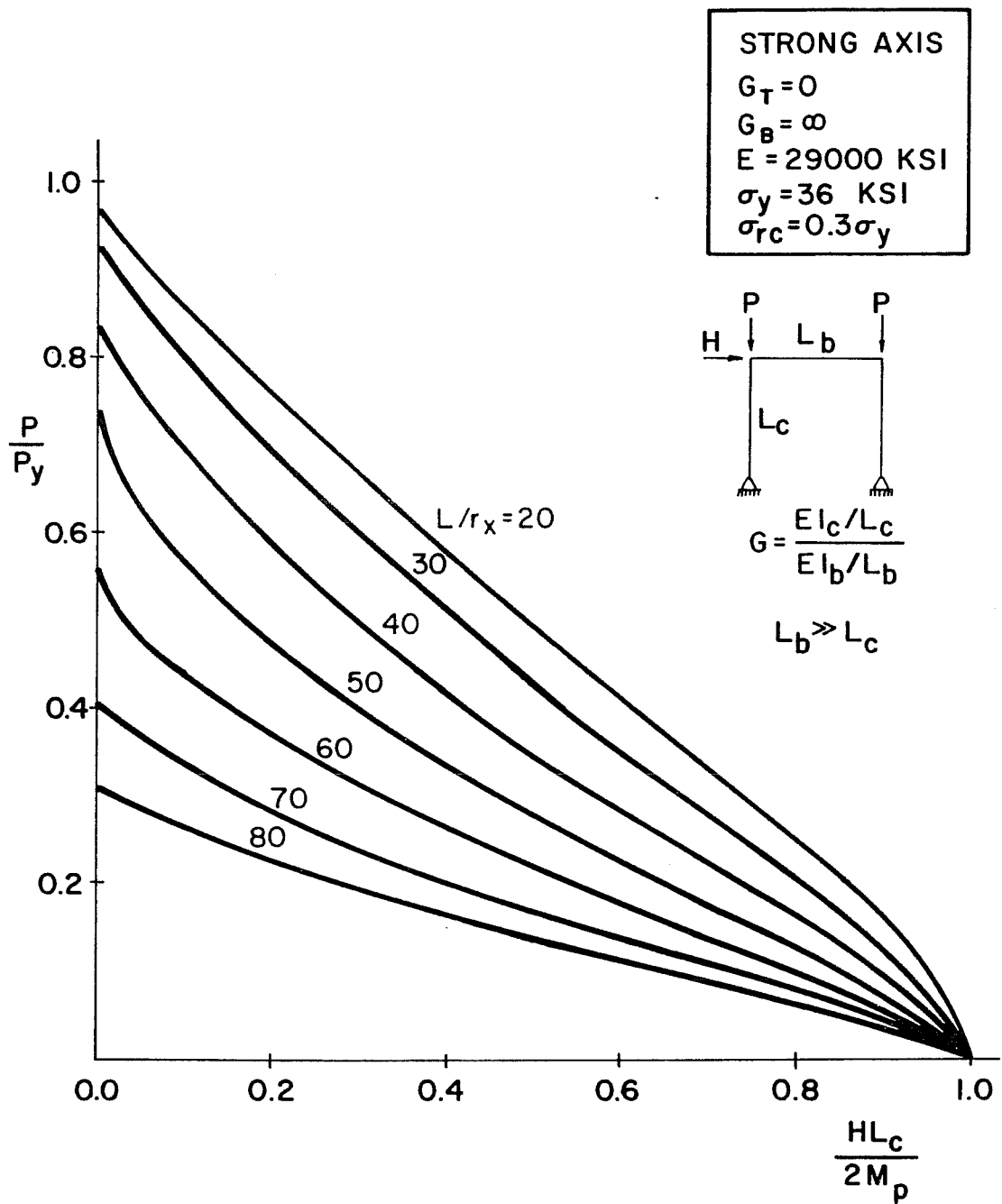


Fig. 2.15a Maximum strength of beam-columns in portal frames
($G = 0$, strong axis bending)

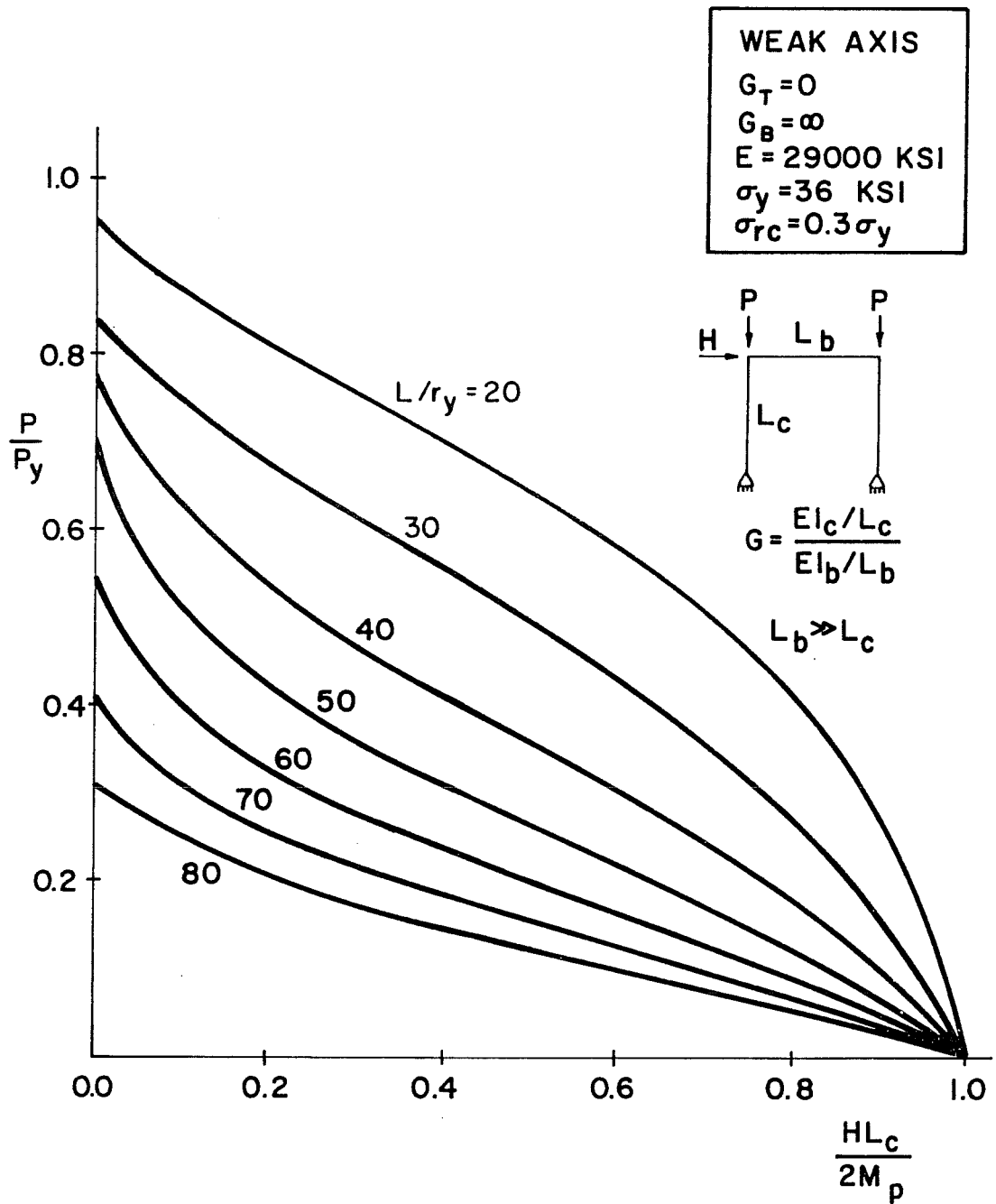


Fig. 2.15b Maximum strength of beam-columns in portal frames
($G = 0$, weak axis bending)

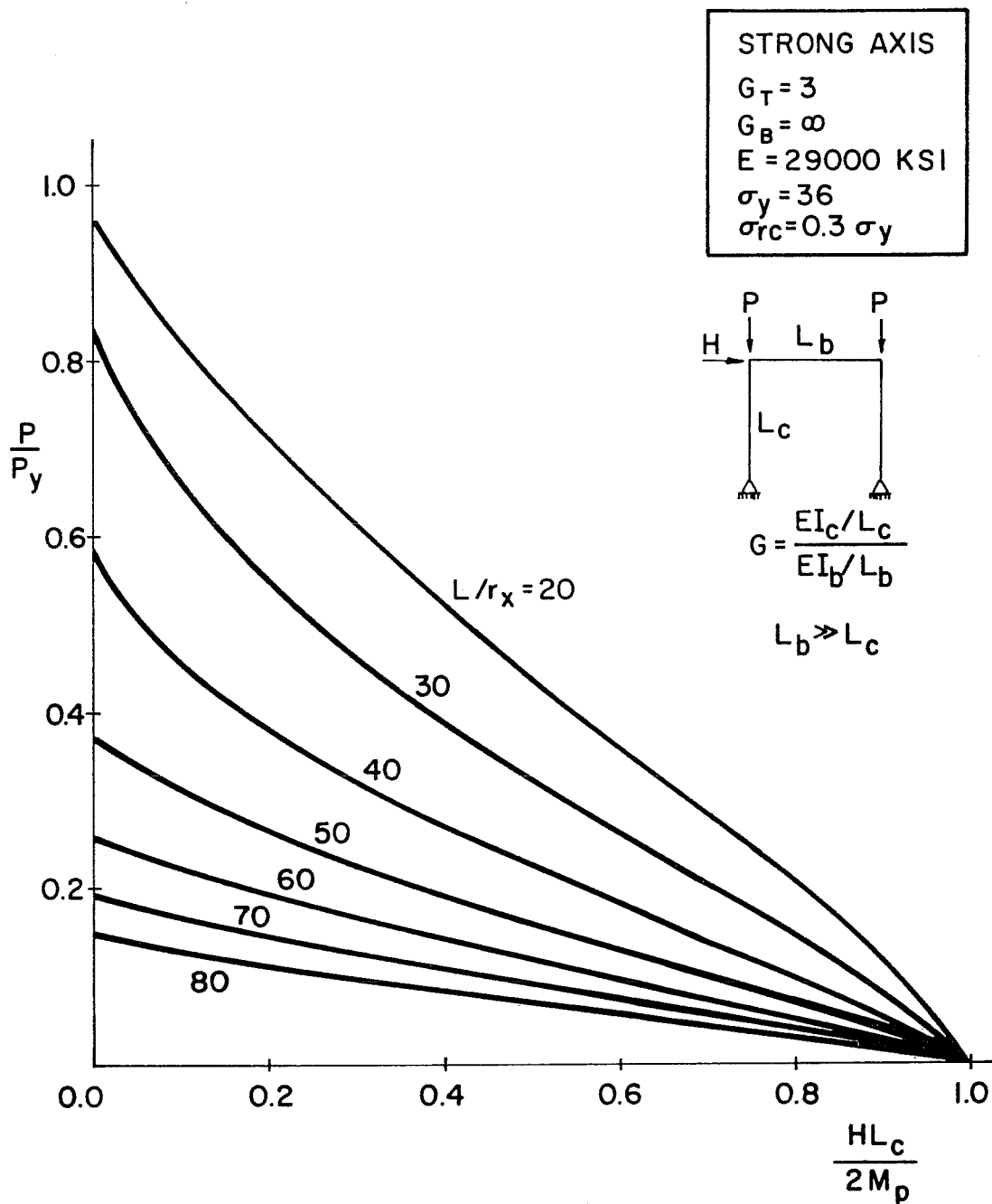


Fig. 2.16a Maximum strength of beam-columns in portal frames
($G = 3$, strong axis bending)

WEAK AXIS
 $G_T = 3$
 $G_B = \infty$
 $E = 29000 \text{ KSI}$
 $\sigma_y = 36 \text{ KSI}$
 $\sigma_{rc} = 0.3 \sigma_y$

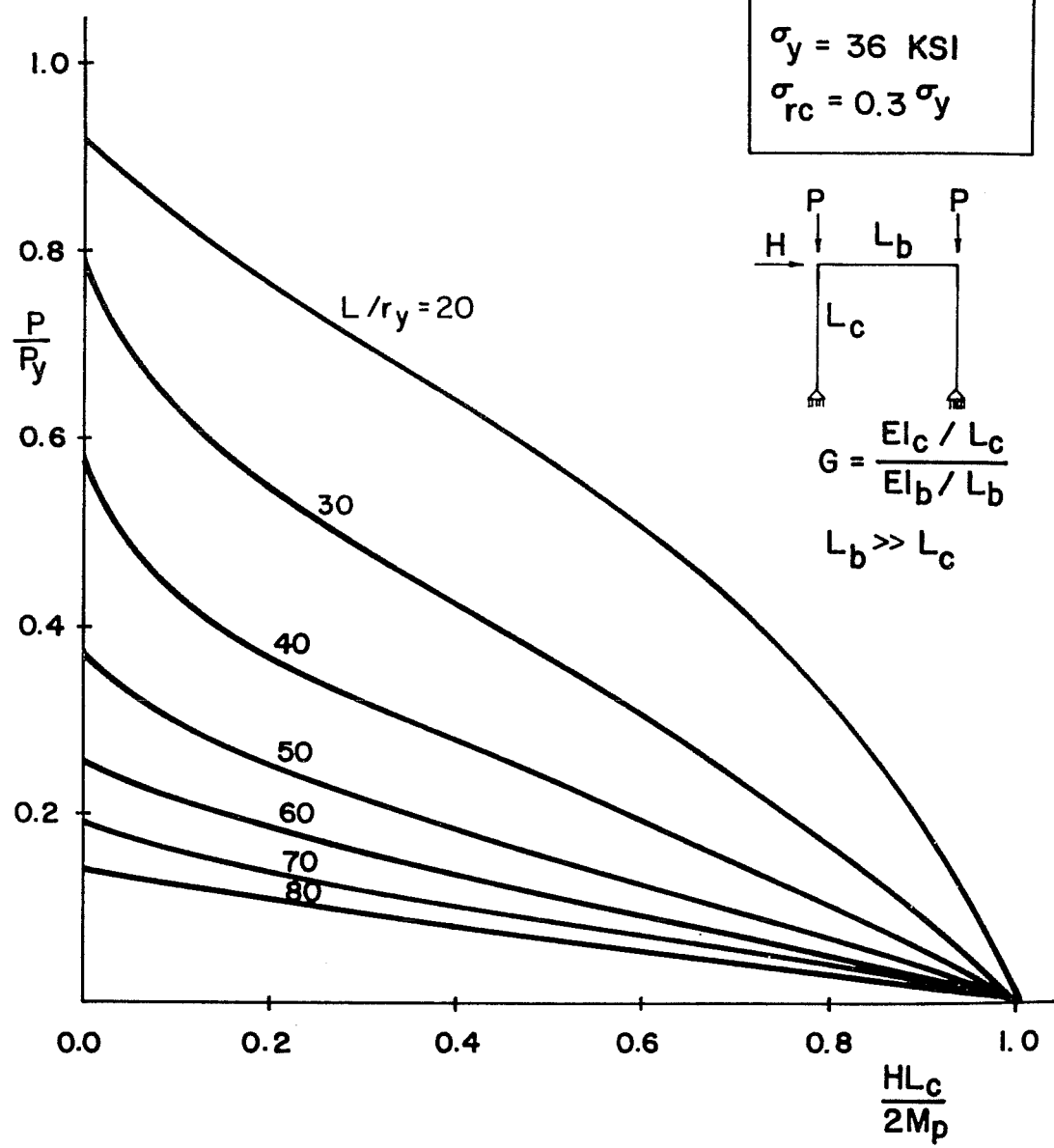


Fig. 2.16b Maximum strength of beam-column in portal frames
 ($G = 3$, weak axis bending)

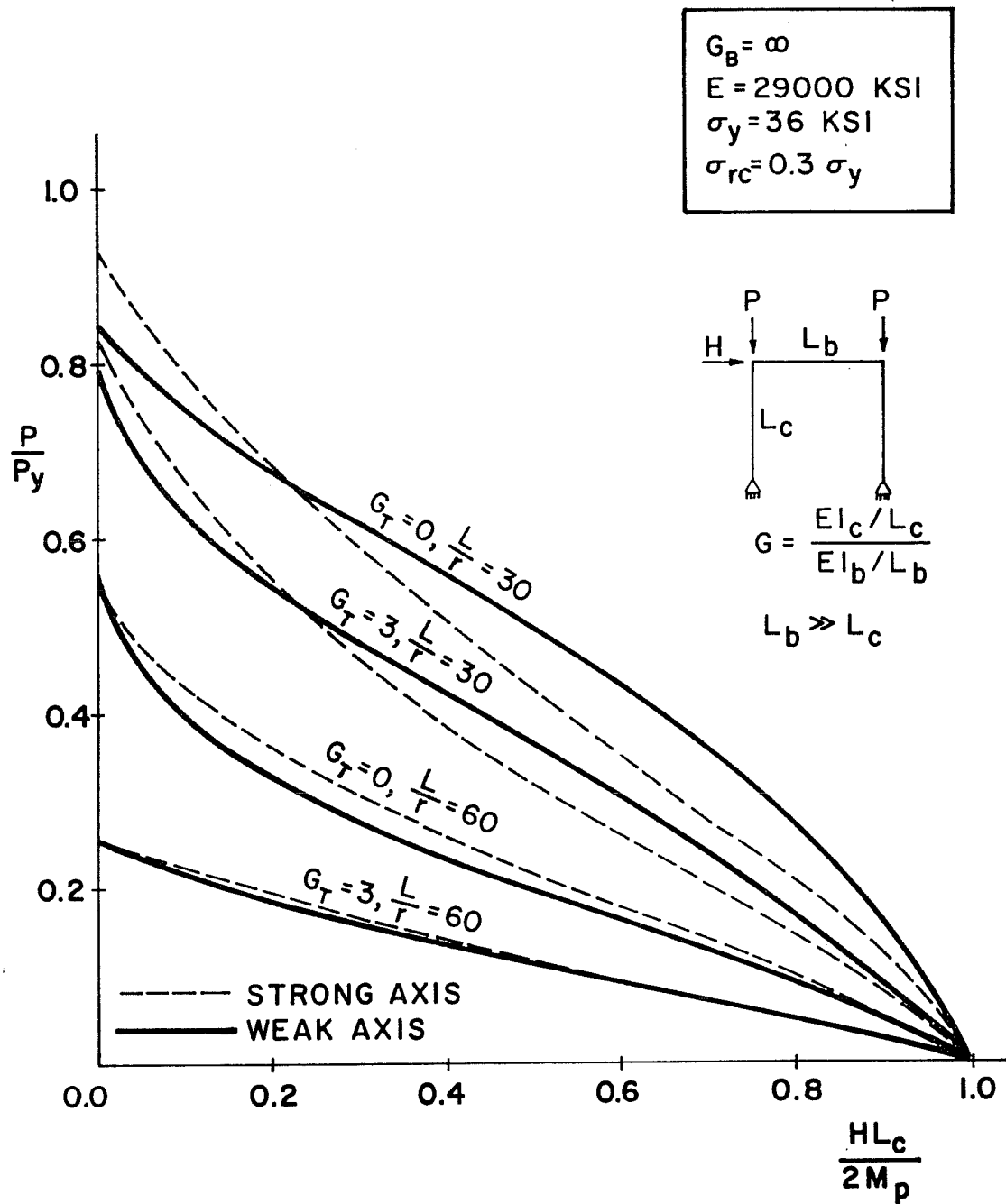


Fig. 2.17 Effect of axis of bending

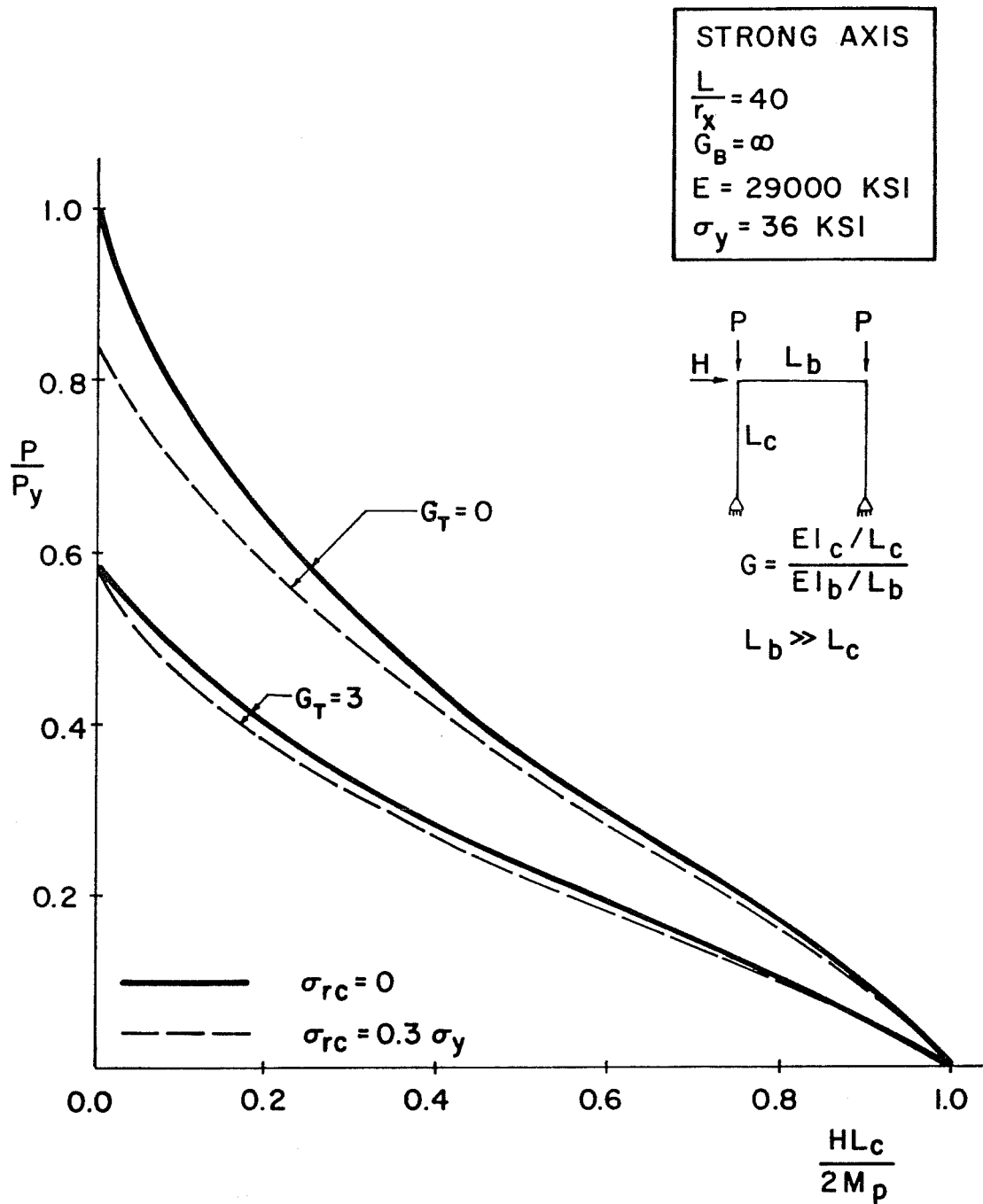


Fig. 2.18a Effect of residual stress ($L_c/r = 40$, strong axis bending)

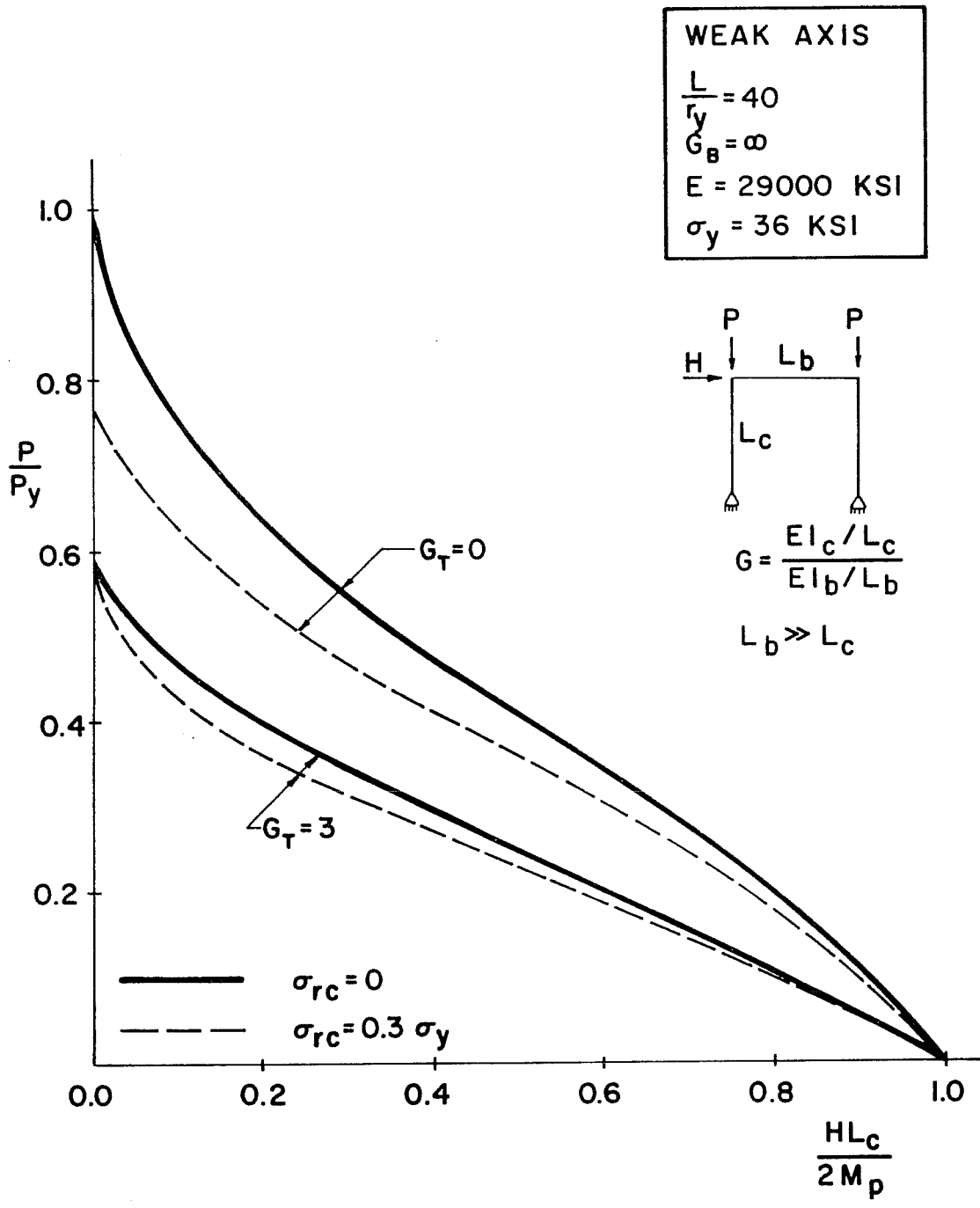


Fig. 2.18b Effect of residual stress ($L_c/r = 40$, weak axis bending)

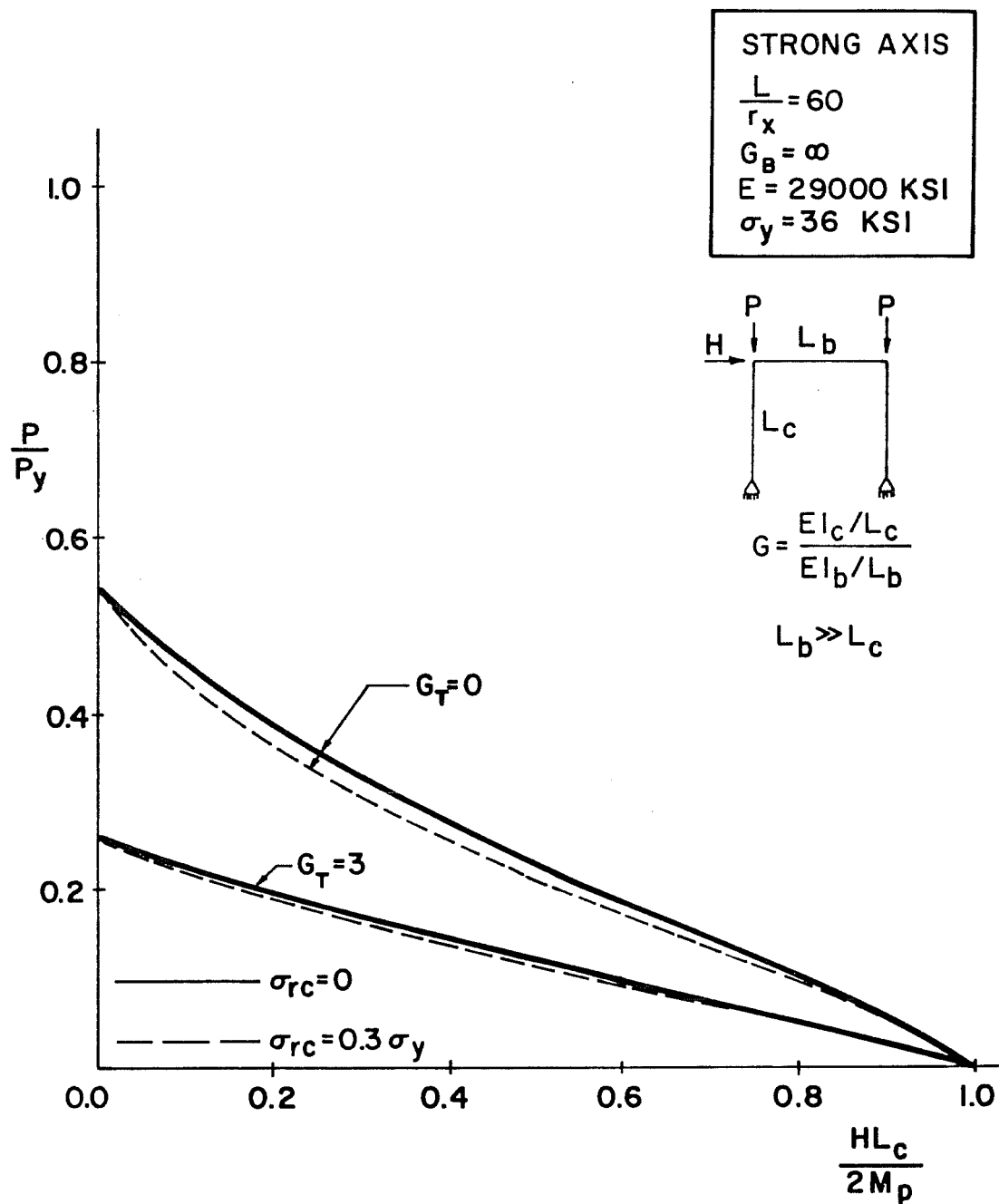


Fig. 2.19a Effect of residual stress ($L_c/r = 60$, strong axis bending)

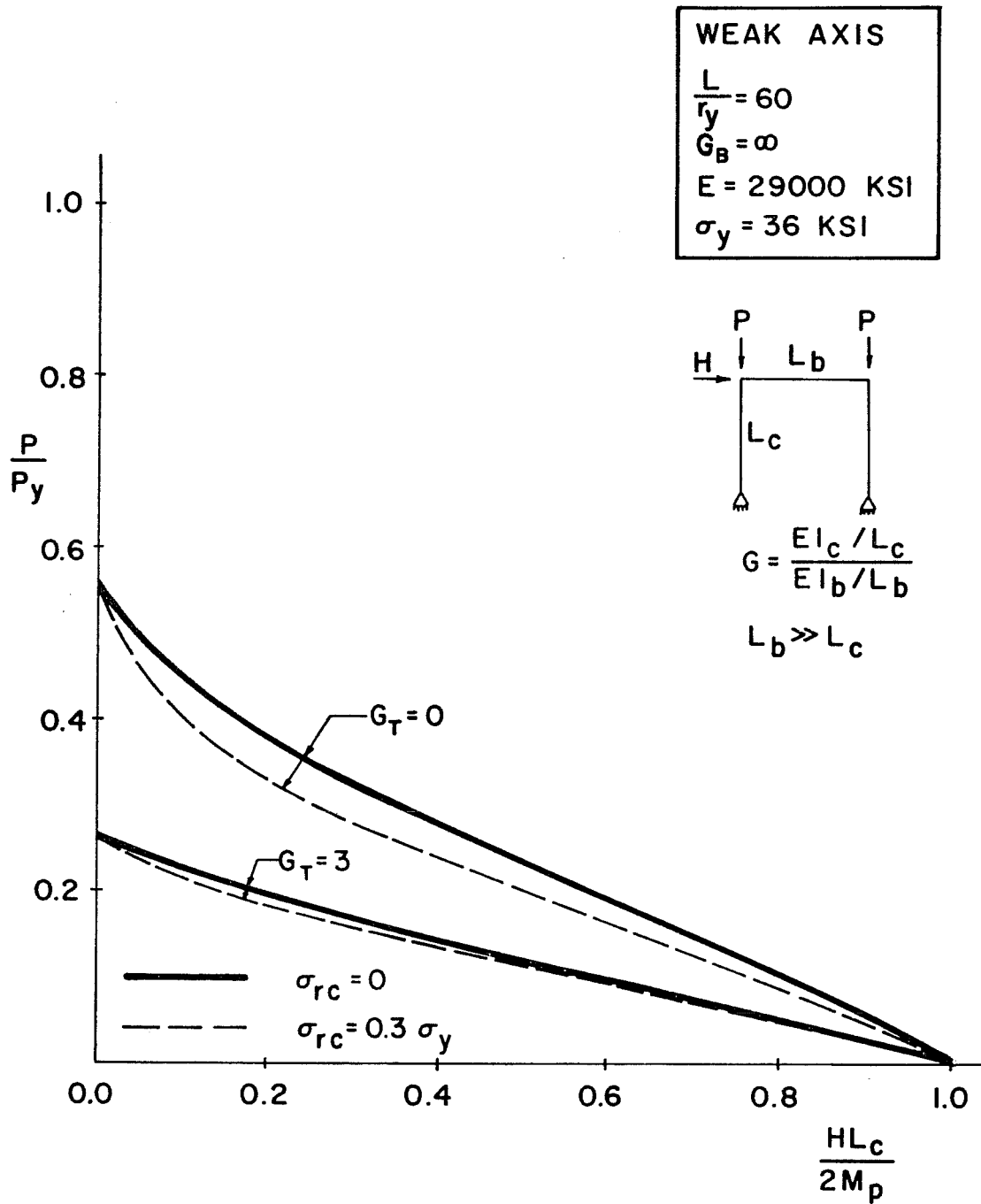


Fig. 2.19b Effect of residual stress ($L_c/r = 60$, weak axis bending)

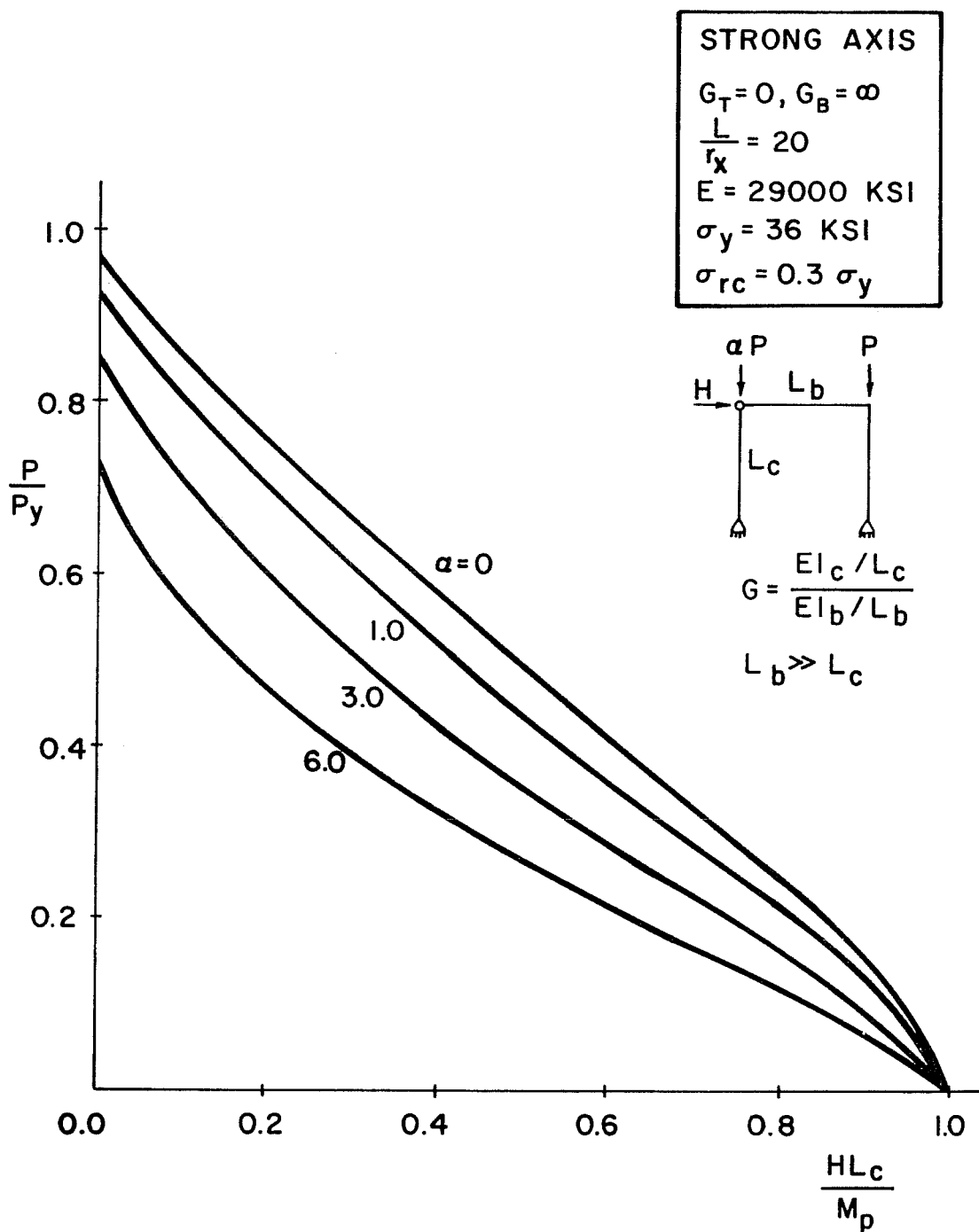


Fig. 2.20a Maximum strength of beam-columns in leaned frames ($G = 0, L_c/r = 20$, strong axis bending)

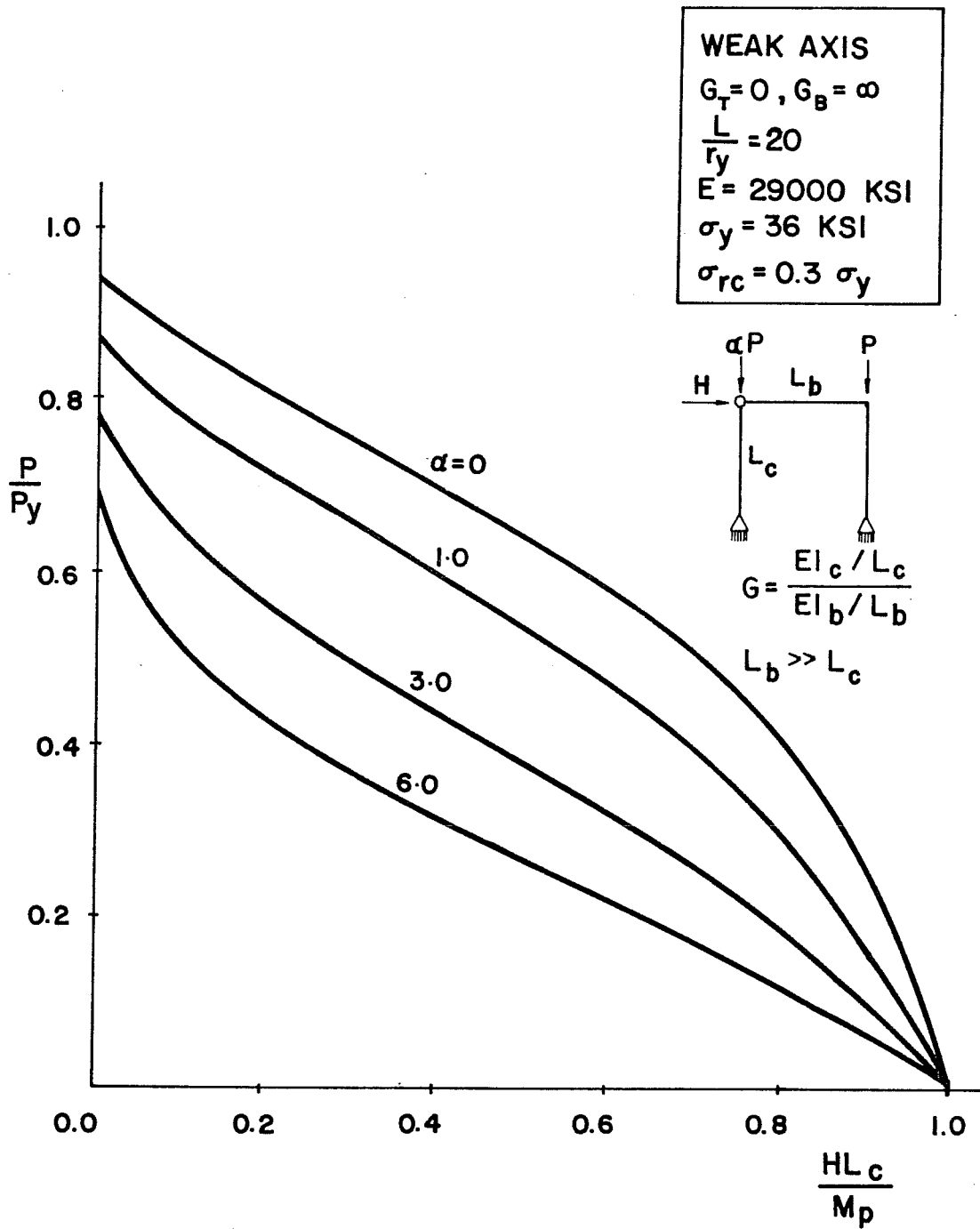


Fig. 2.20b Maximum strength of beam-columns in leaned frames
 ($G = 0, L_c/r = 20$, weak axis bending)

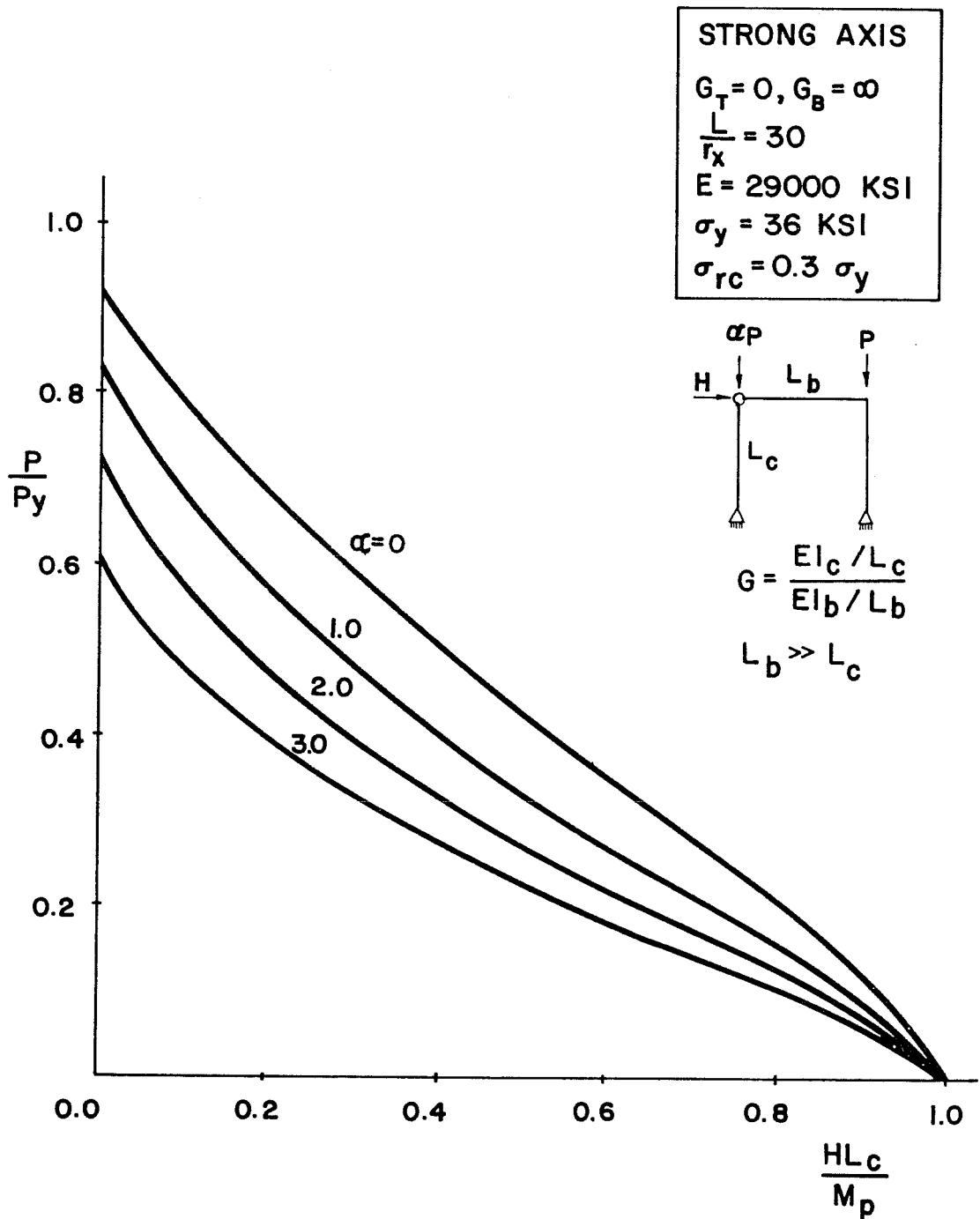


Fig. 2.21a Maximum strength of beam-columns in leaned frames
 ($G = 0, L_c/r = 30, \text{strong axis bending}$)

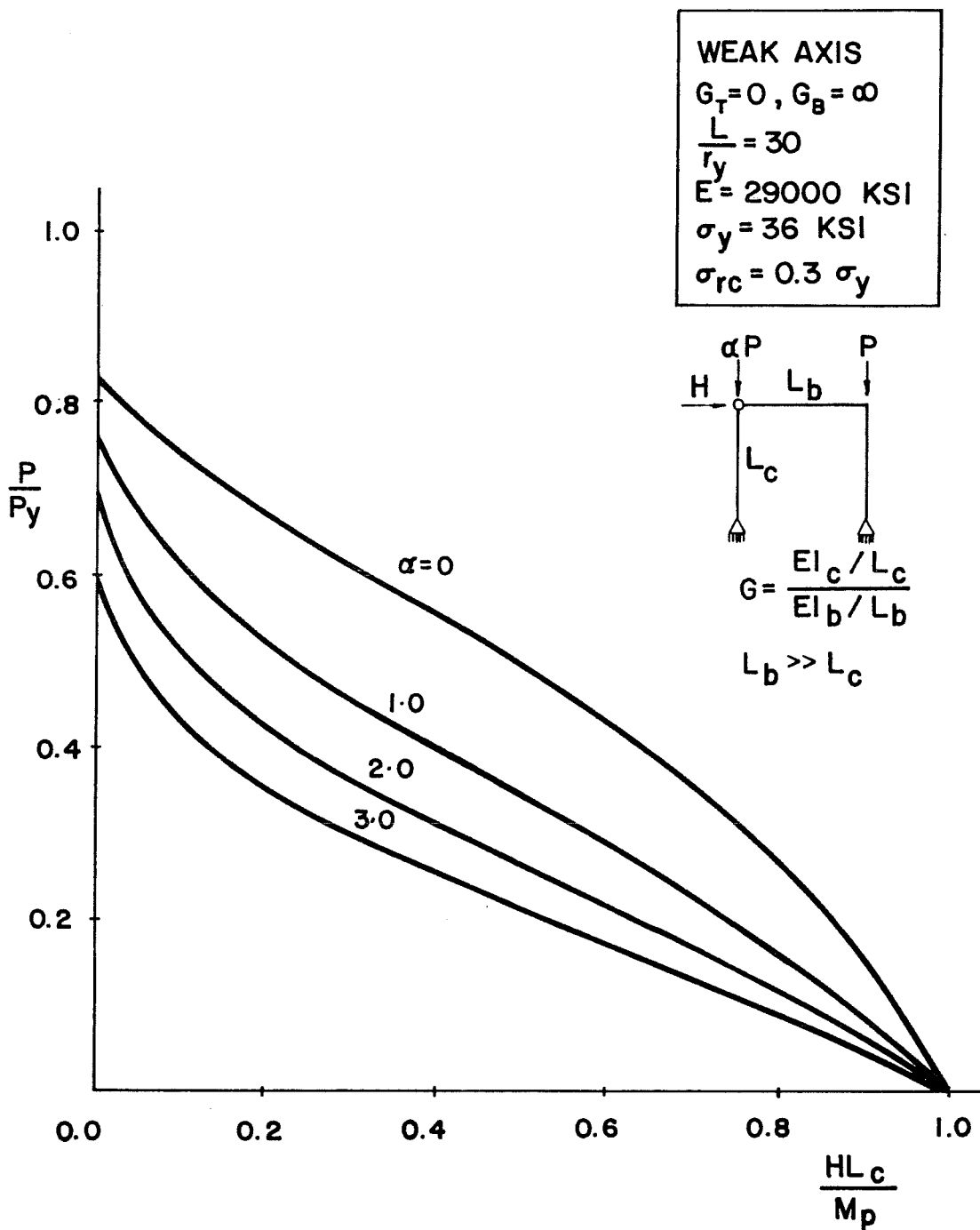


Fig. 2.21b Maximum strength of beam-columns in leaned frames
 ($G = 0, L_c/r = 30$, weak axis bending)

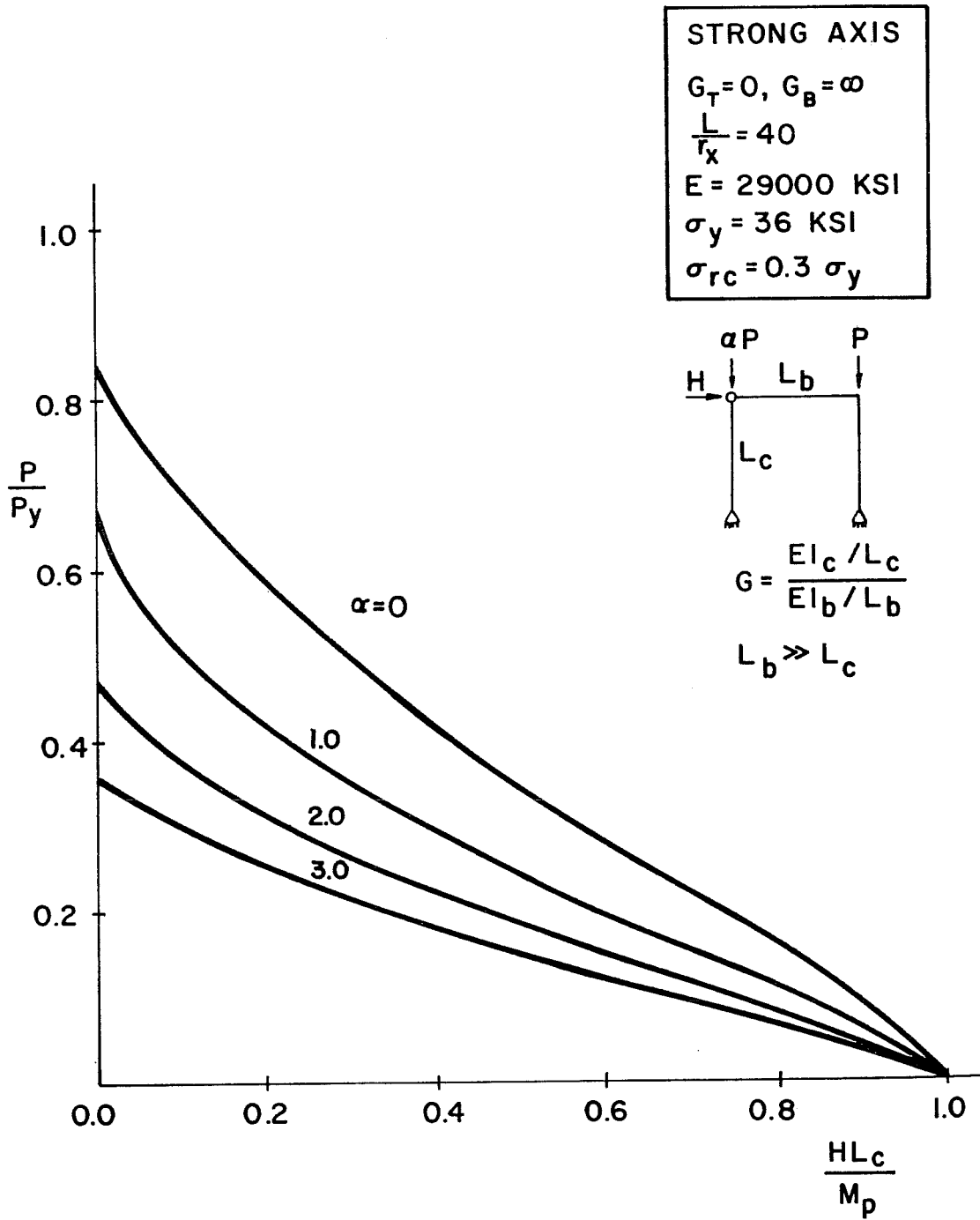


Fig. 2.22a Maximum strength of beam-columns in leaned frames
 ($G = 0, L_c/r = 40, \text{ strong axis bending}$)

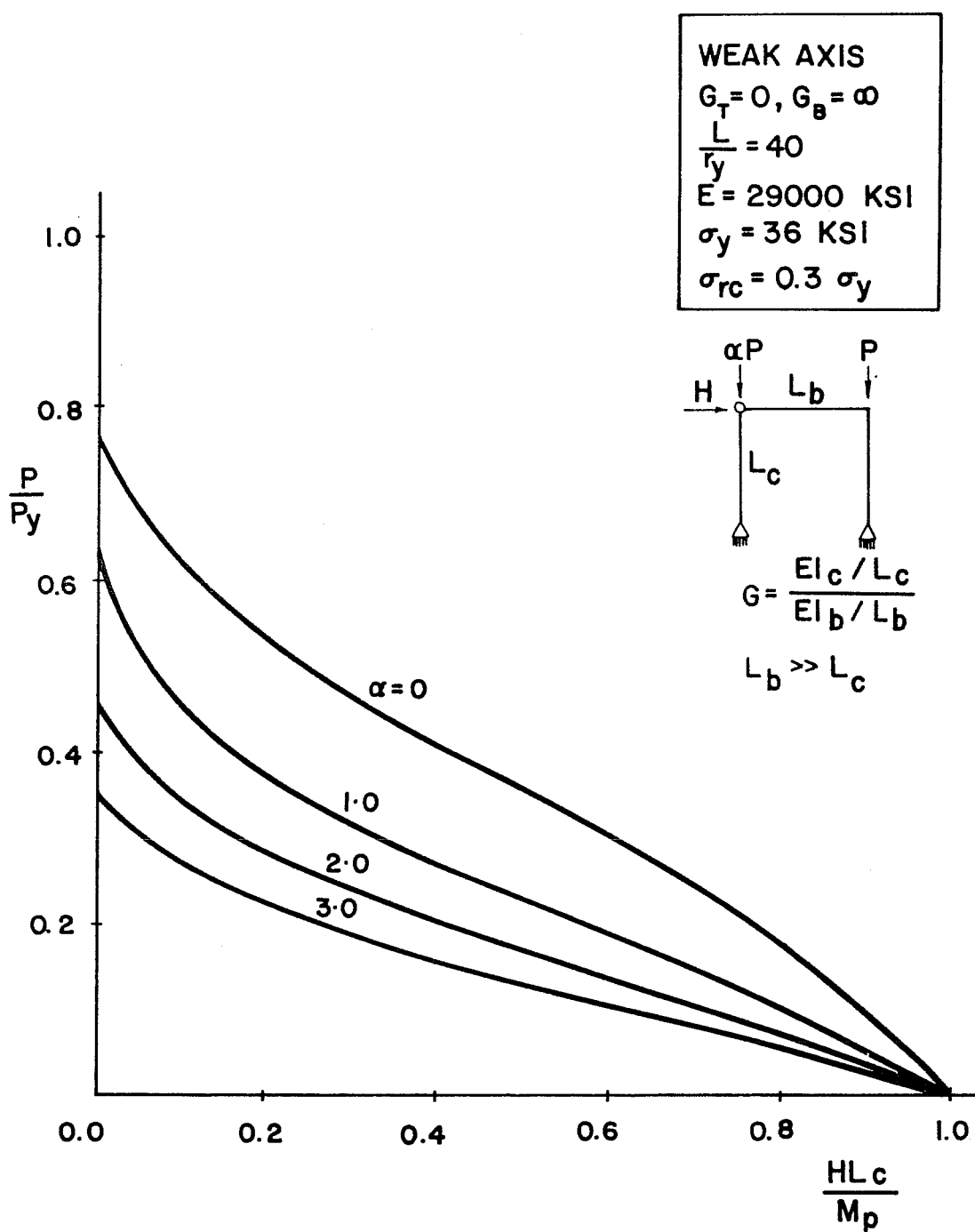


Fig. 2.22b Maximum strength of beam-columns in leaned frames
 ($G = 0, L_c/r = 40$, weak axis bending)

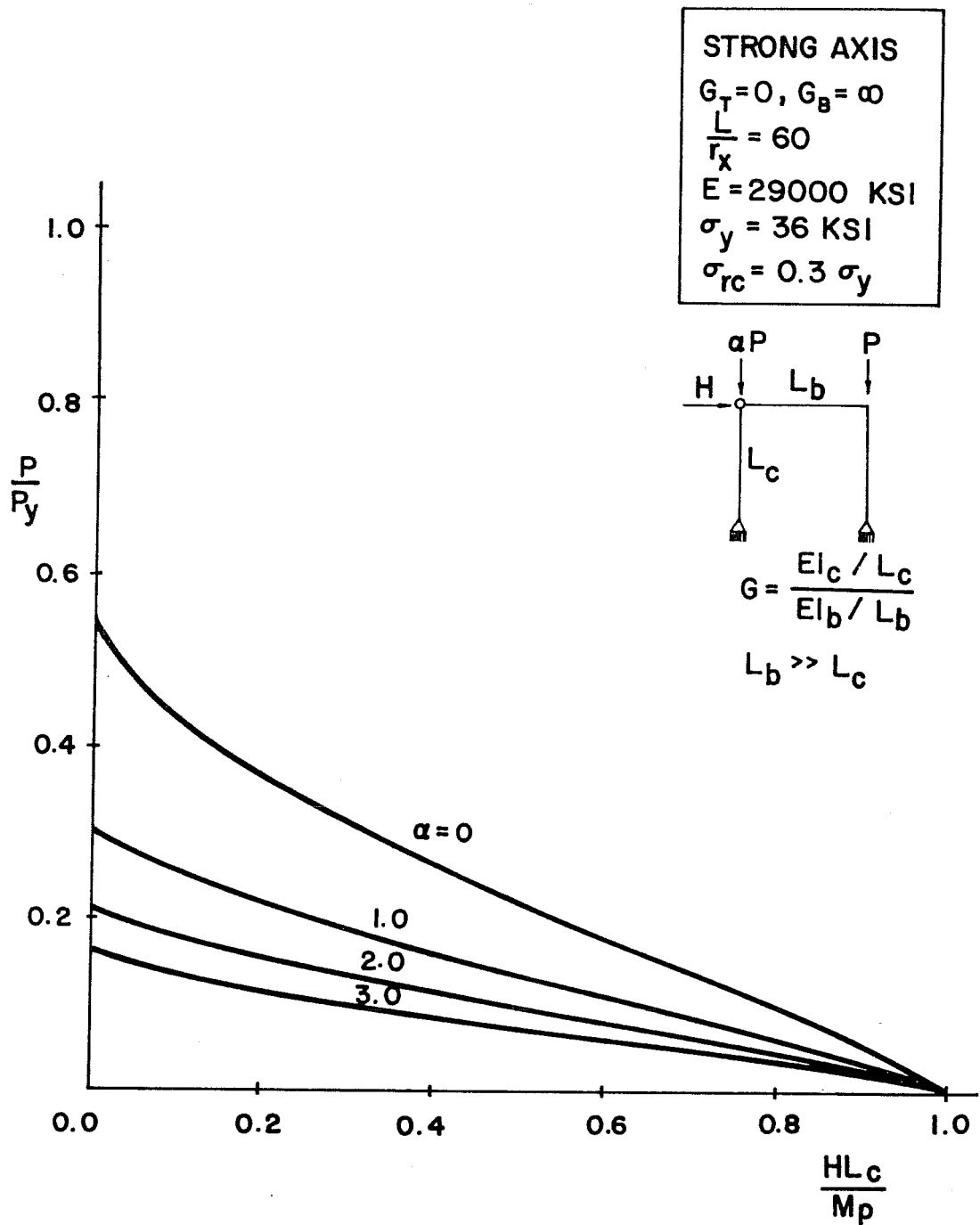


Fig. 2.23a Maximum strength of beam-columns in leaned frames
($G = 0, L_c/r = 60$, strong axis bending)

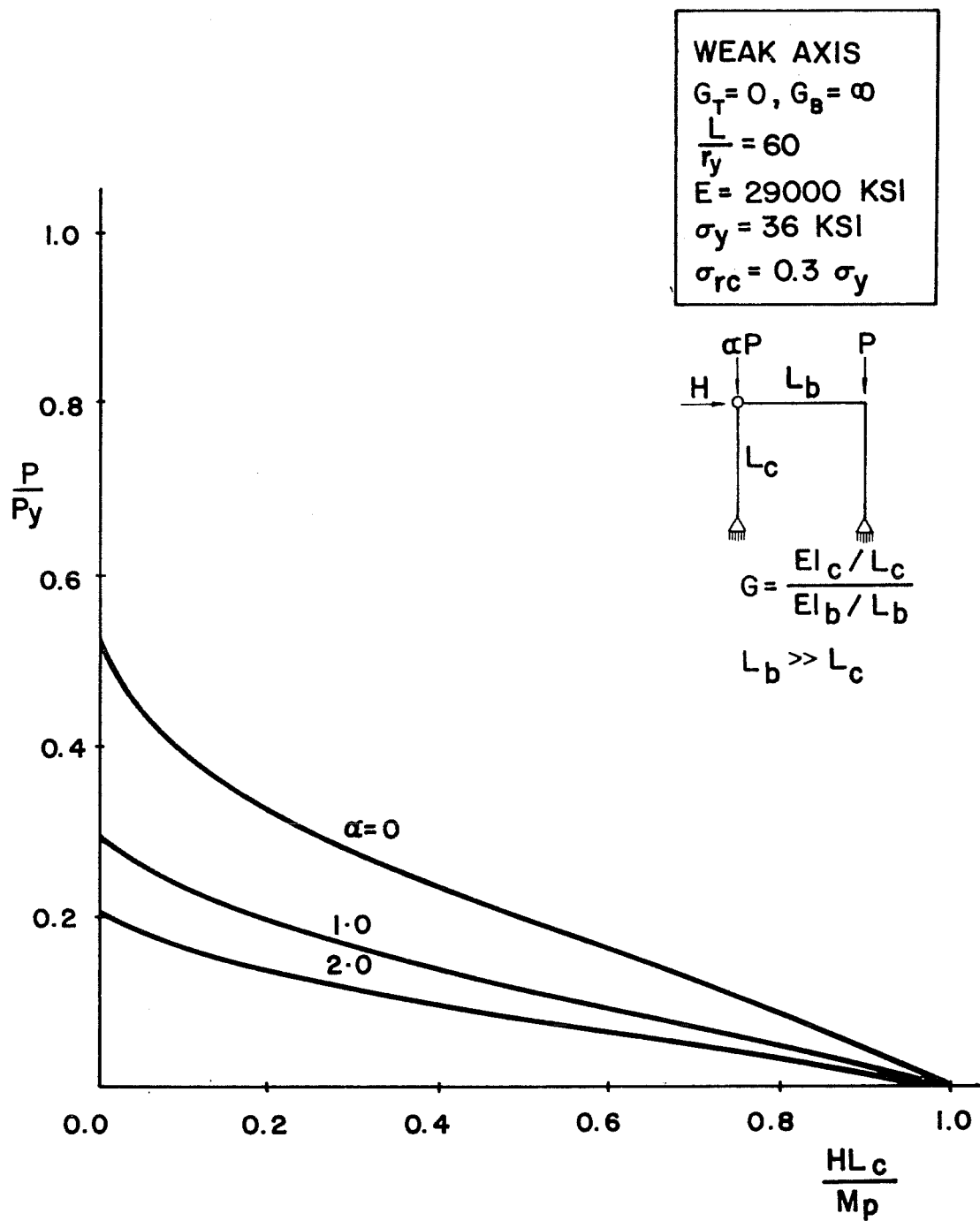


Fig. 2.23b Maximum strength of beam-columns in leaned frames
 ($G = 0, L_c/r = 60$, weak axis bending)

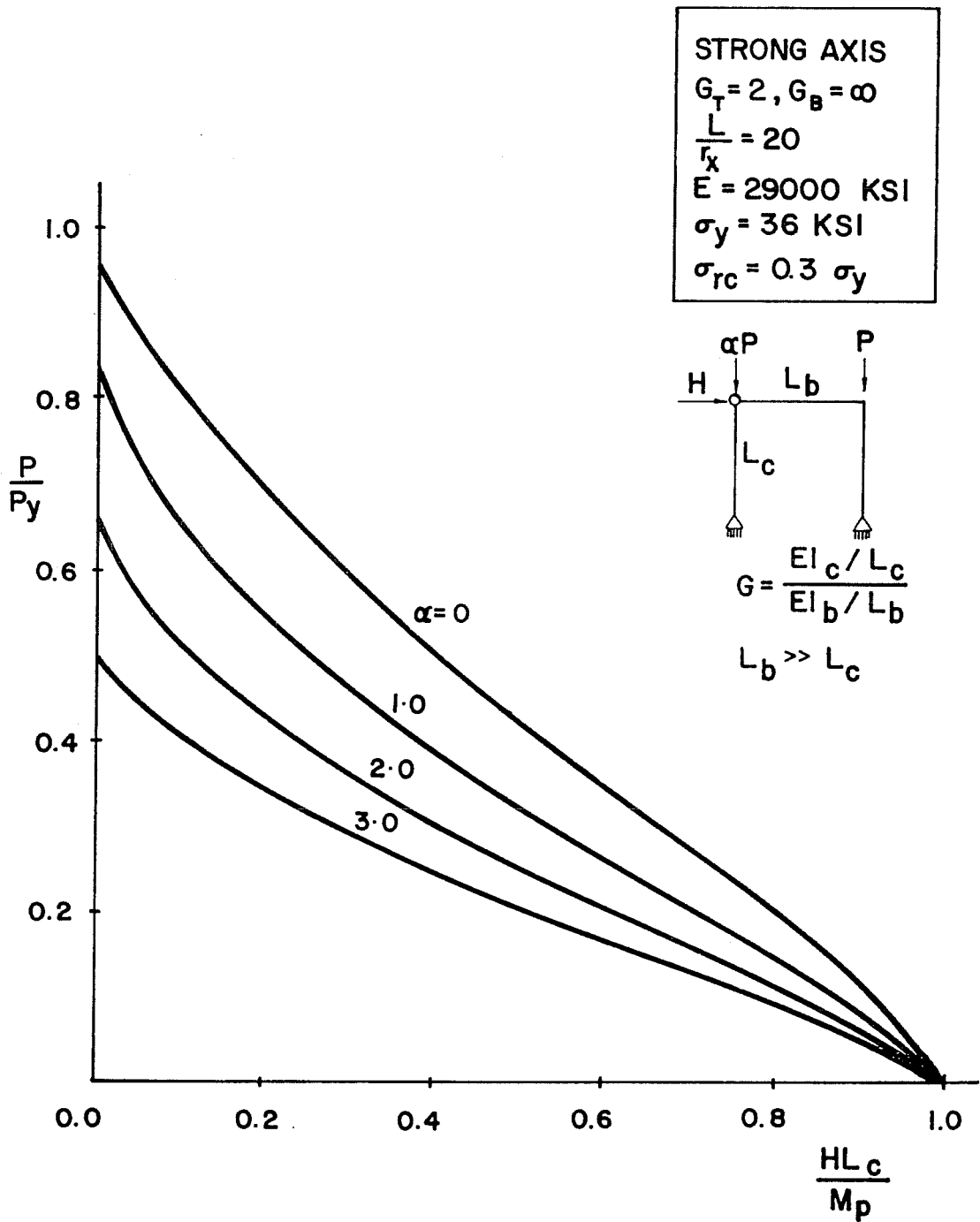


Fig. 2.24a Maximum strength of beam-columns in leaned frames
 ($G = 2, L_c/r = 20$, strong axis bending)

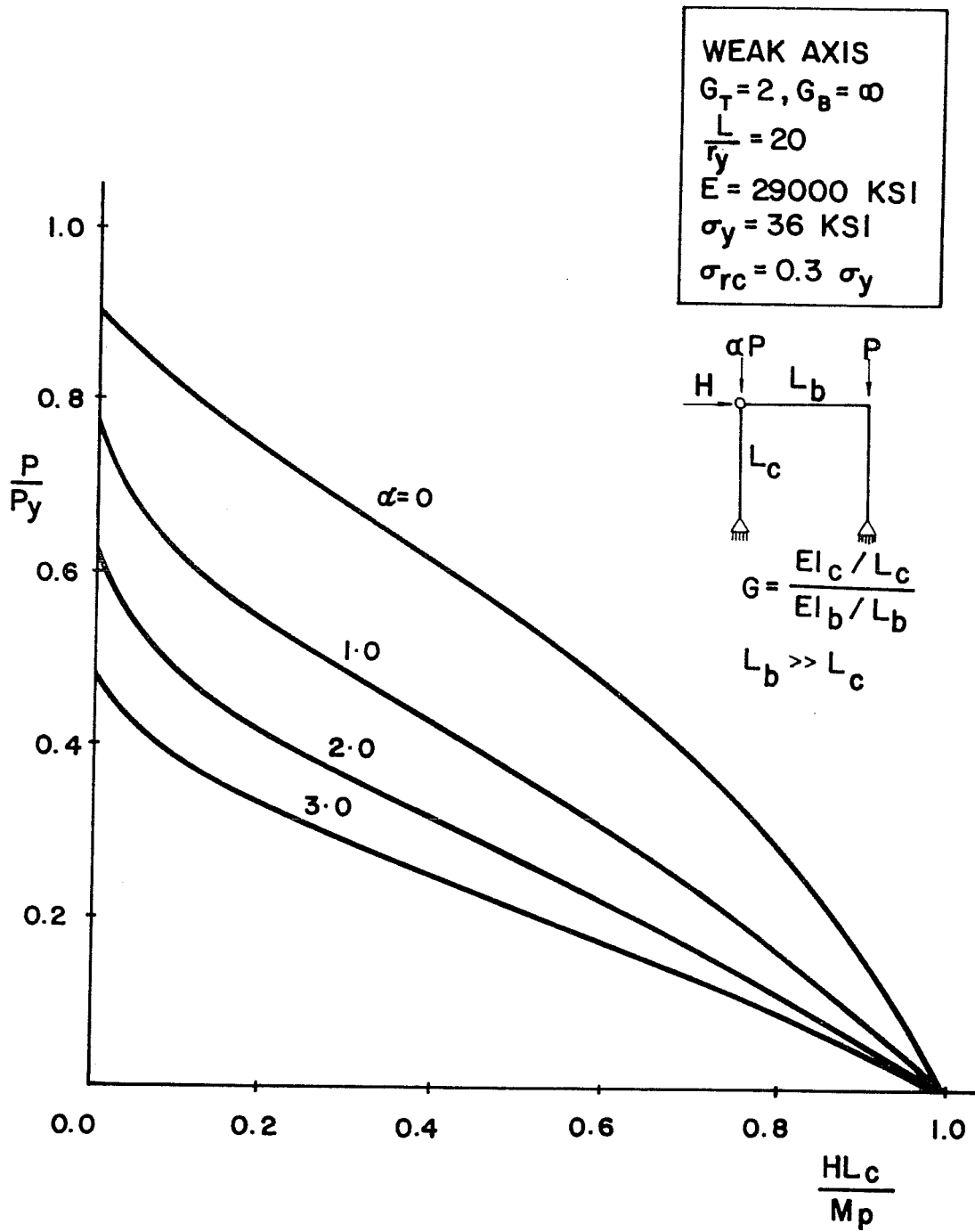


Fig. 2.24b Maximum strength of beam-columns in leaned frames
 ($G = 2, L_c/r = 20$, weak axis bending)

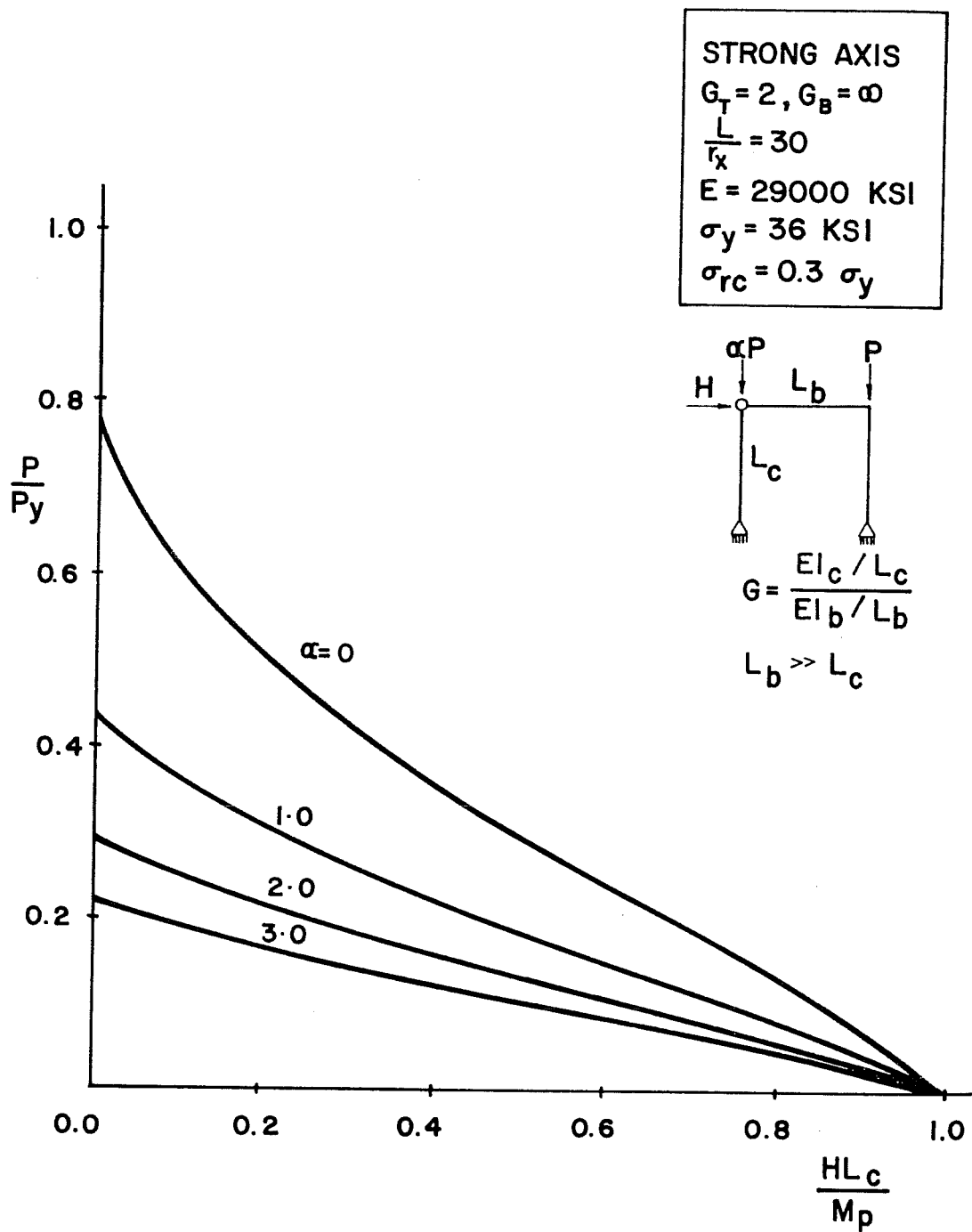


Fig. 2.25a Maximum strength of beam-columns in leaned frames
 ($G = 2, L_c/r = 30$, strong axis bending)

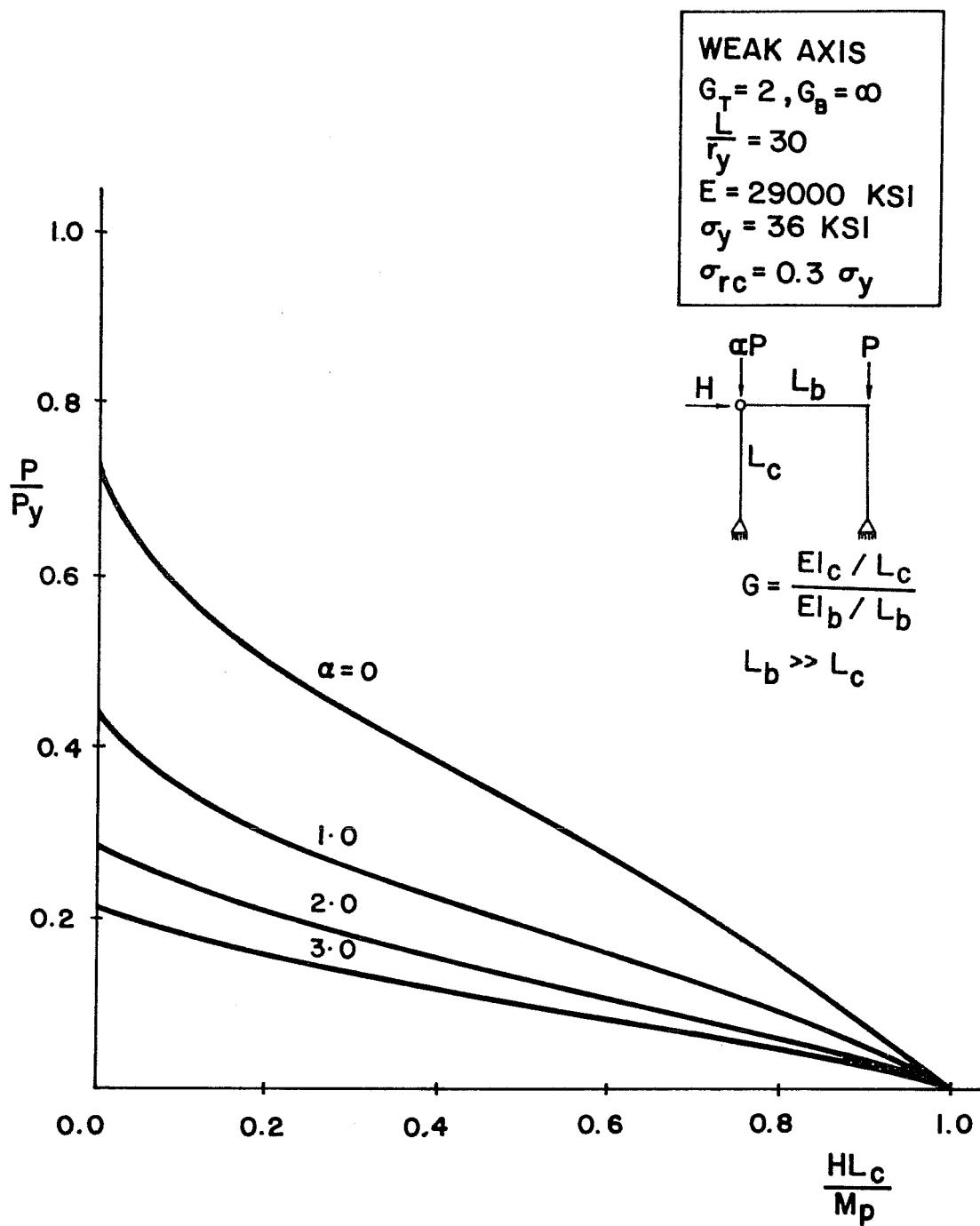


Fig. 2.25b Maximum strength of beam-columns in leaned frames
 ($G = 2, L_c/r = 30$, weak axis bending)

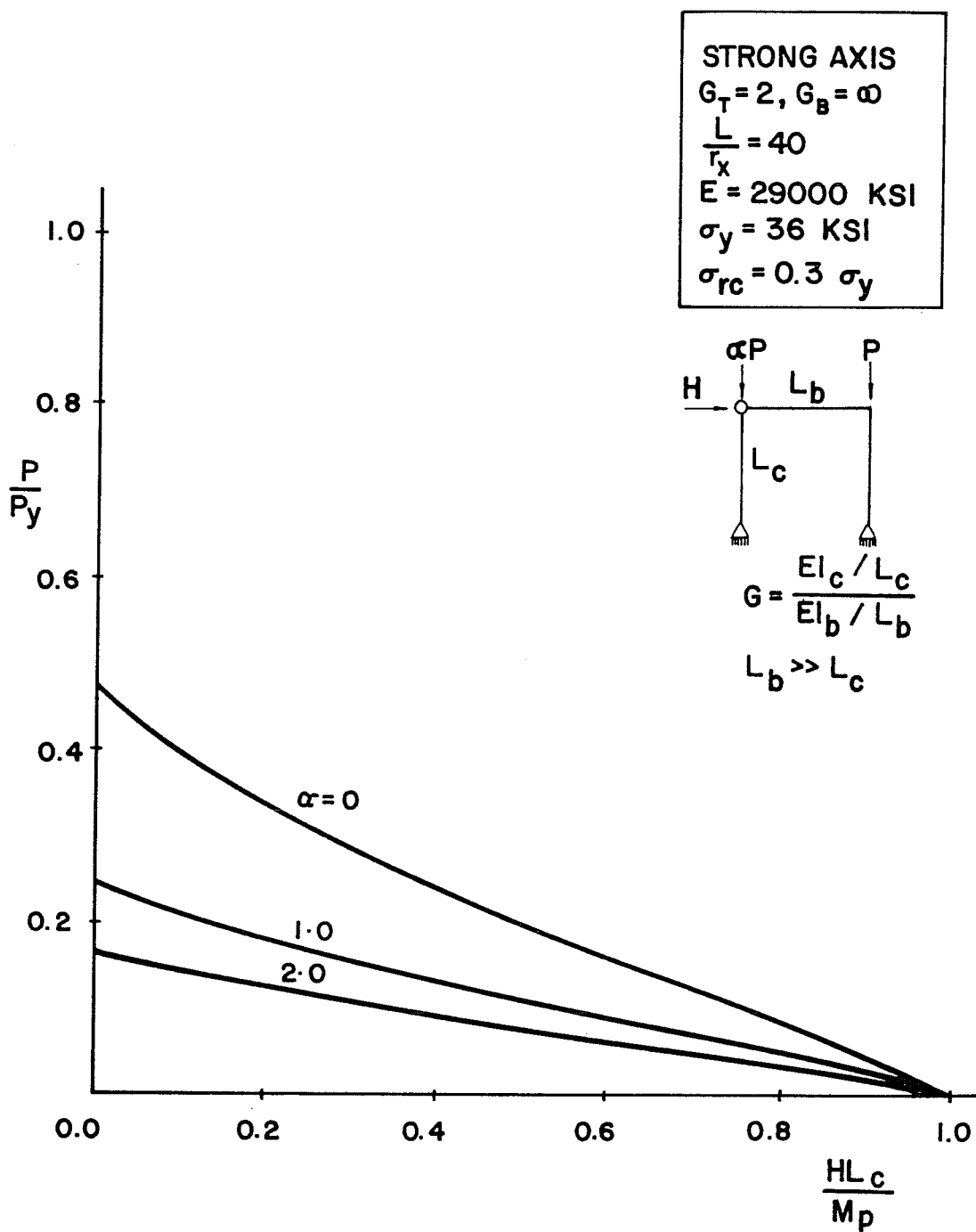


Fig. 2.26a Maximum strength of beam-columns in leaned frames
 ($G = 2, L_c/r = 40$, strong axis bending)

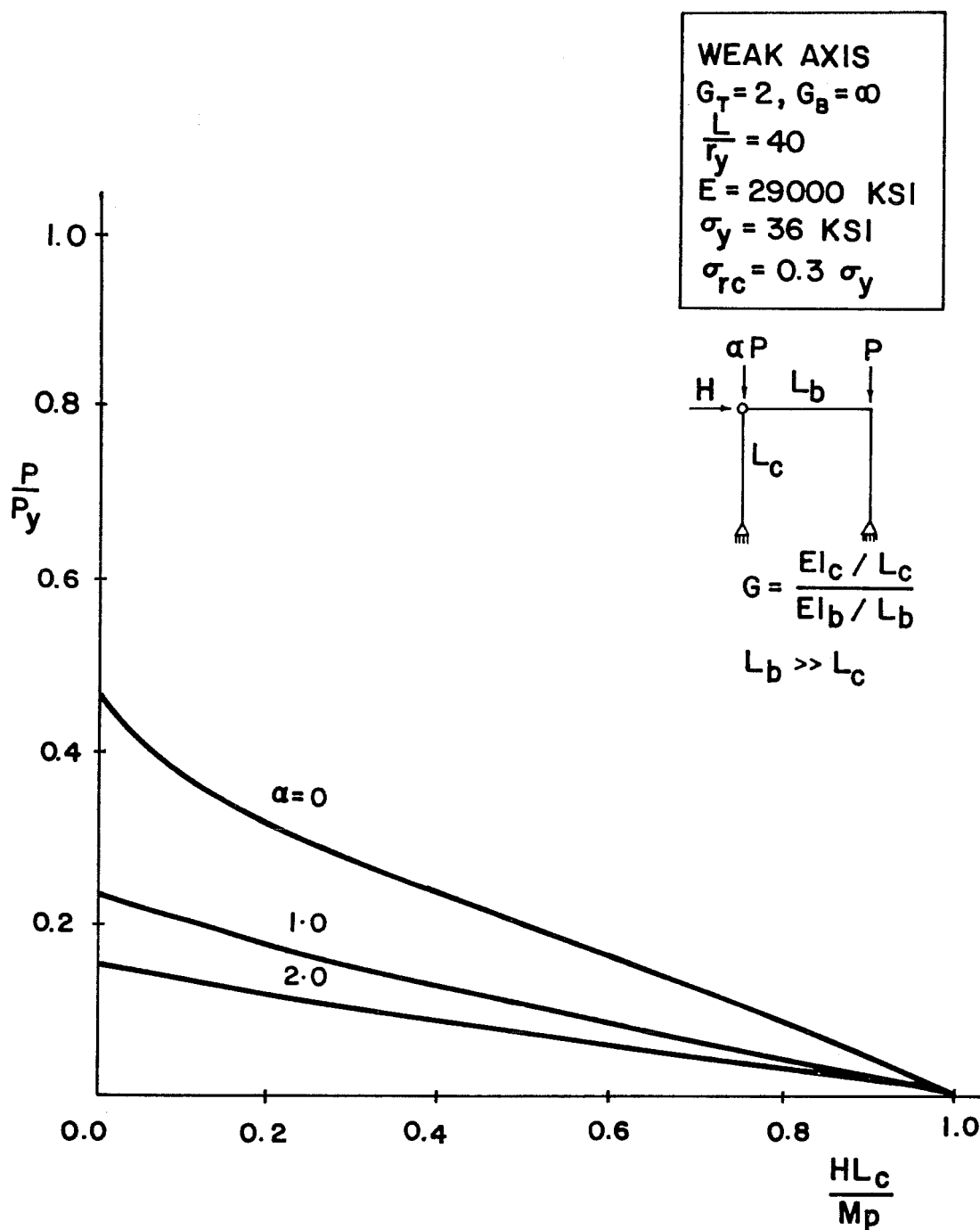


Fig. 2.26b Maximum strength of beam-columns in leaned frames
 ($G = 2, L_c/r = 40$, weak axis bending)

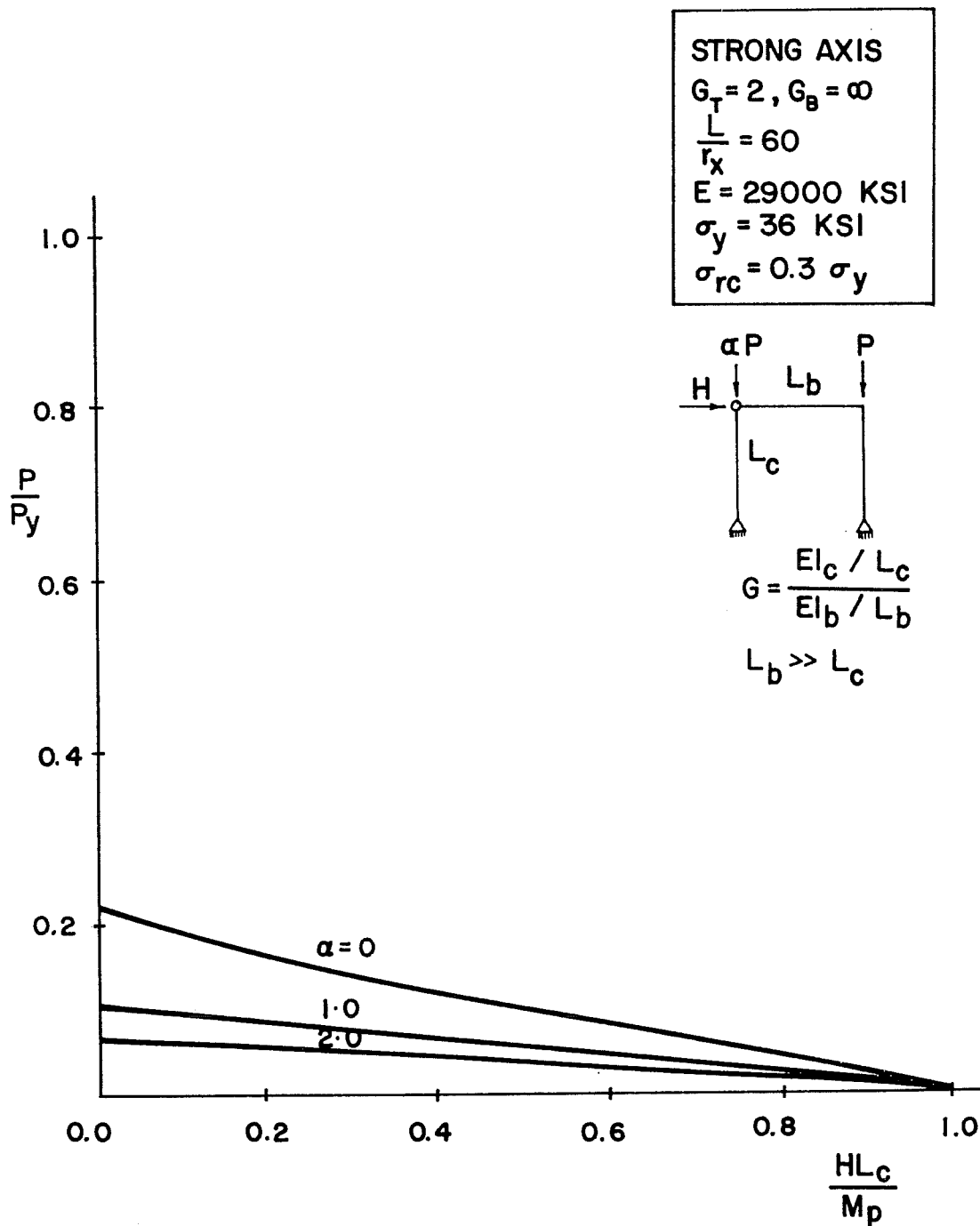


Fig. 2.27a Maximum strength of beam-columns in leaned frames
 ($G = 2, L_c/r = 60$, strong axis bending)

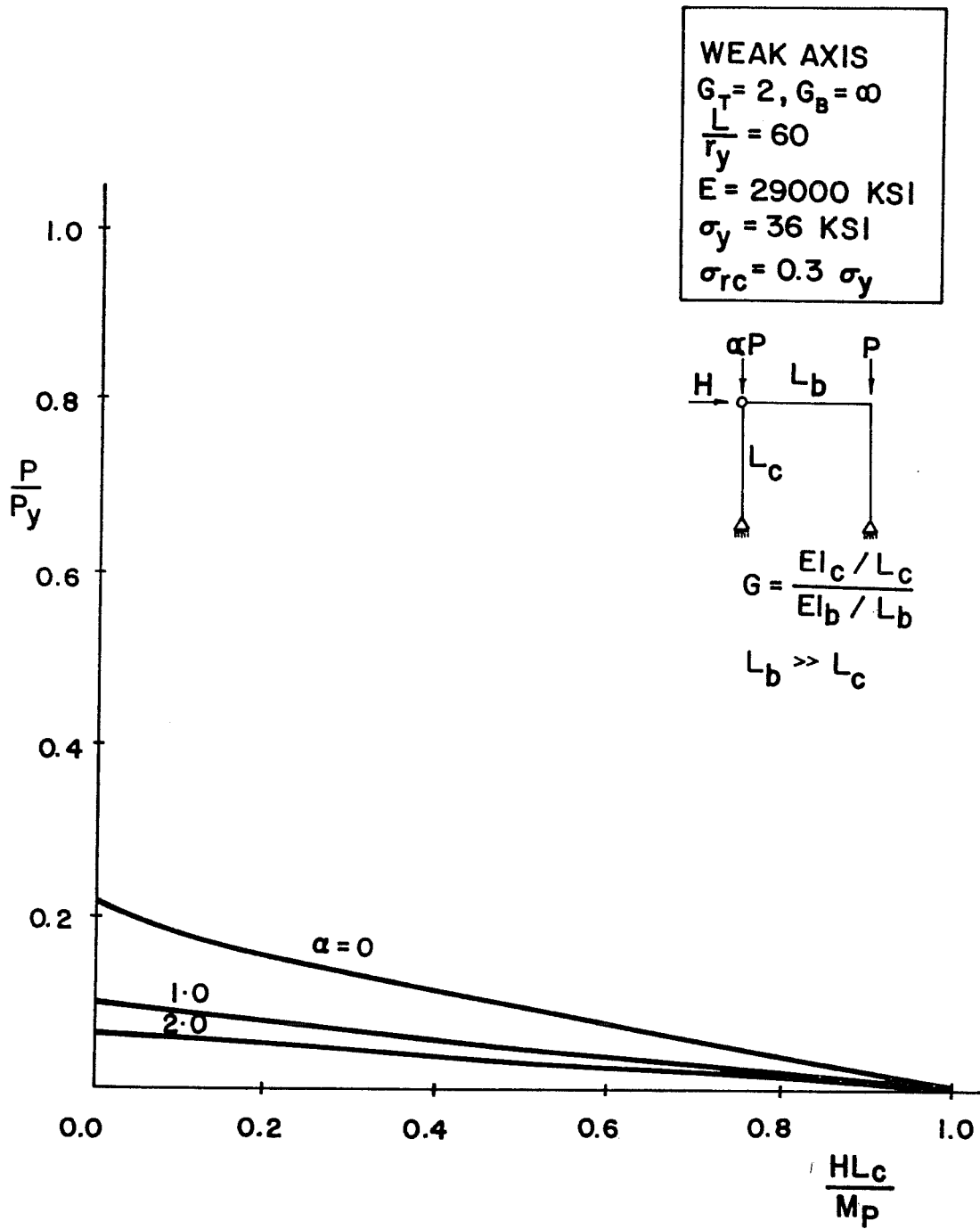


Fig. 2.27b Maximum strength of beam-columns in leaned frames
 ($G = 2, L_c/r = 60$, weak axis bending)

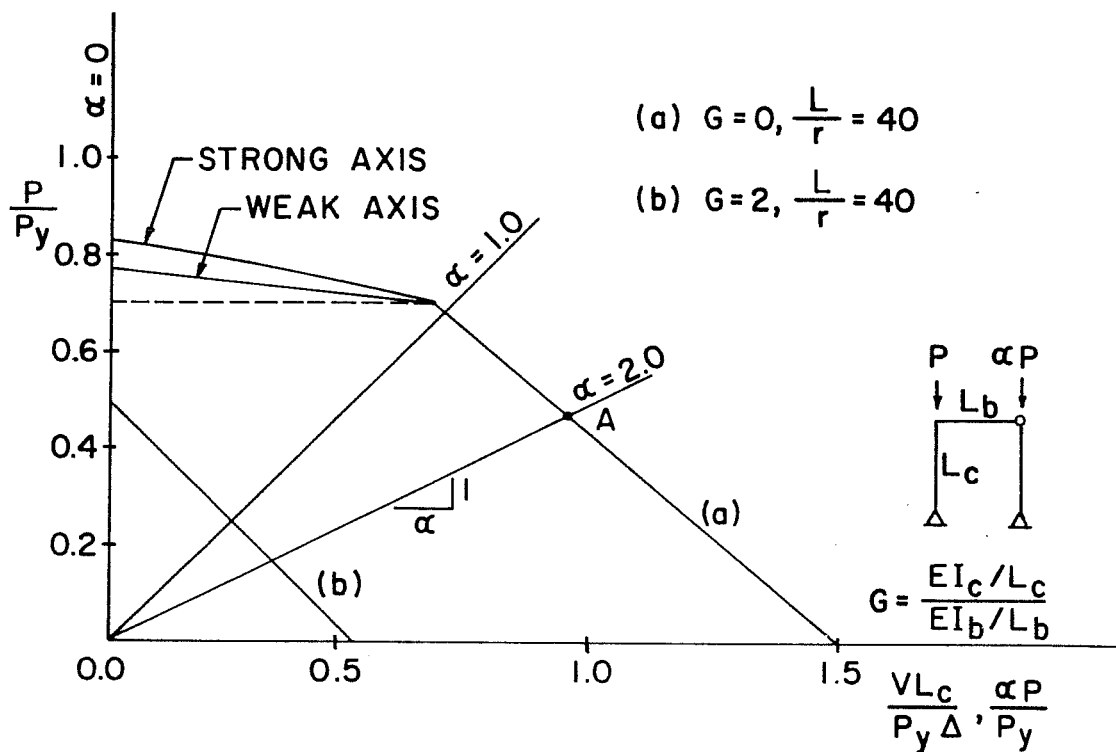


Fig. 2.28 Axial load-shear stiffness relationship

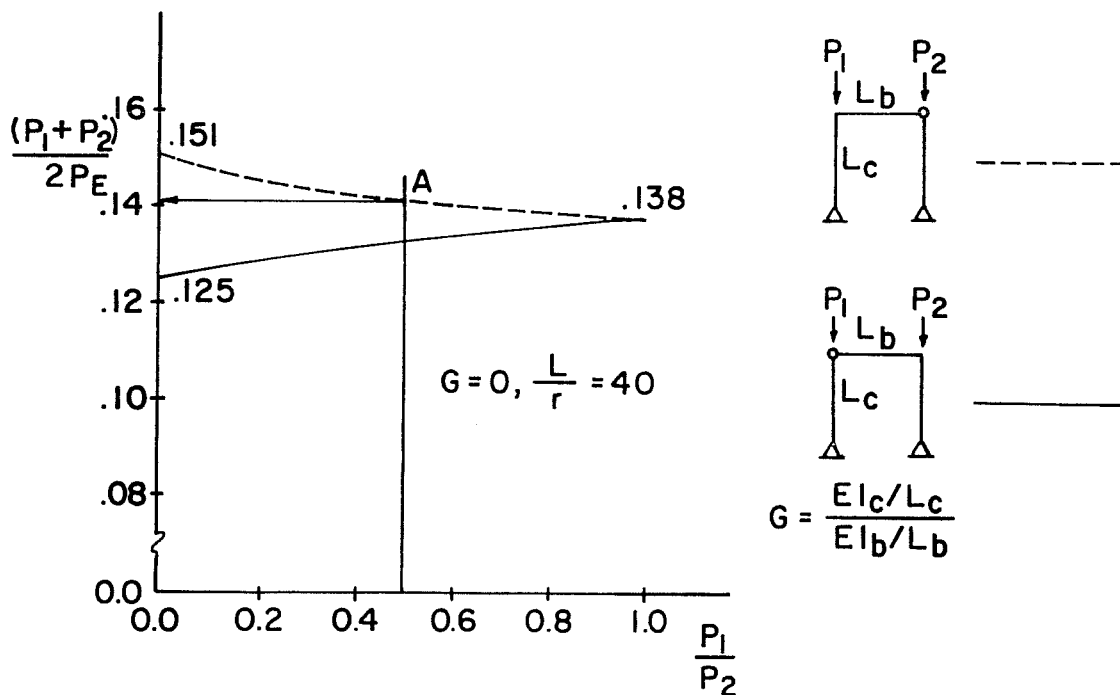


Fig. 2.29 Salem's solutions for elastic stability of leaned frames

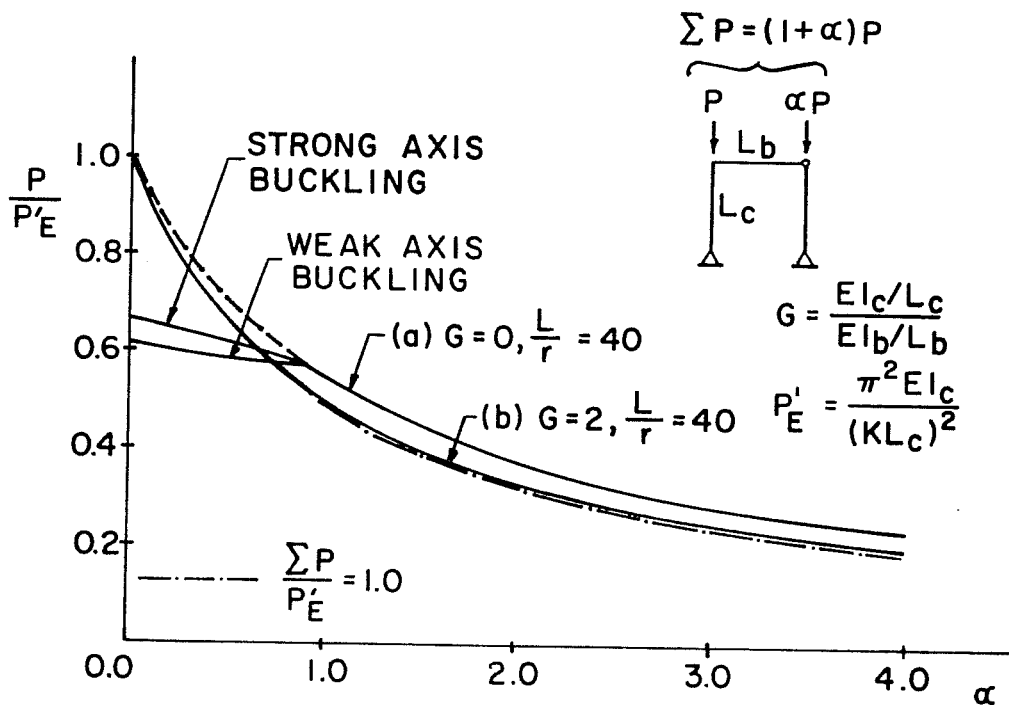


Fig. 2.30 Effect of G on the stability of leaned frames

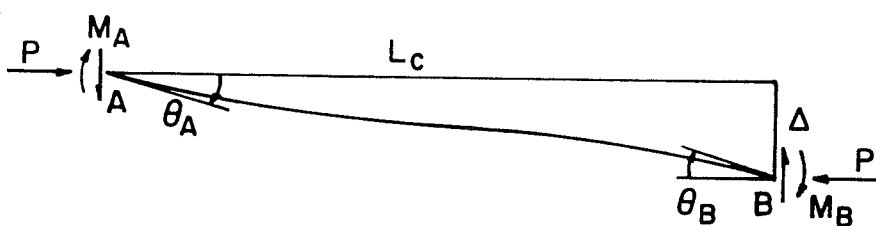


Fig. 2.31 Equilibrium of beam-column as a free body

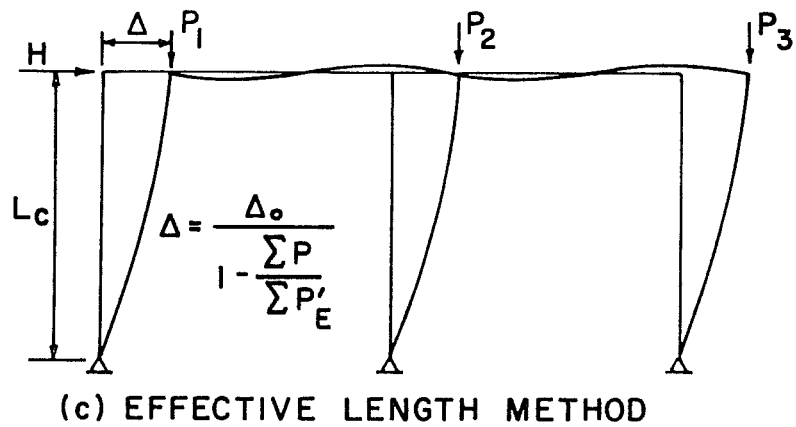
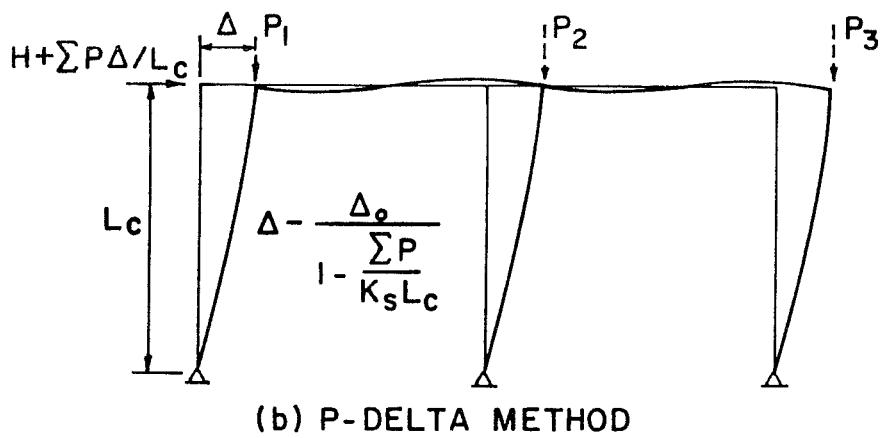
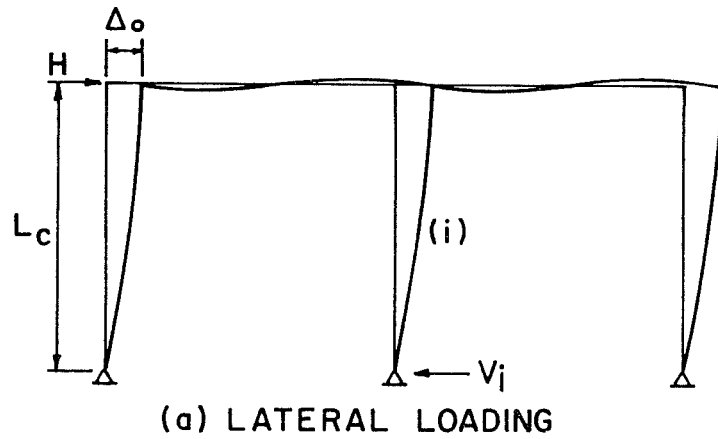


Fig. 2.32 Methods for determining second order moments

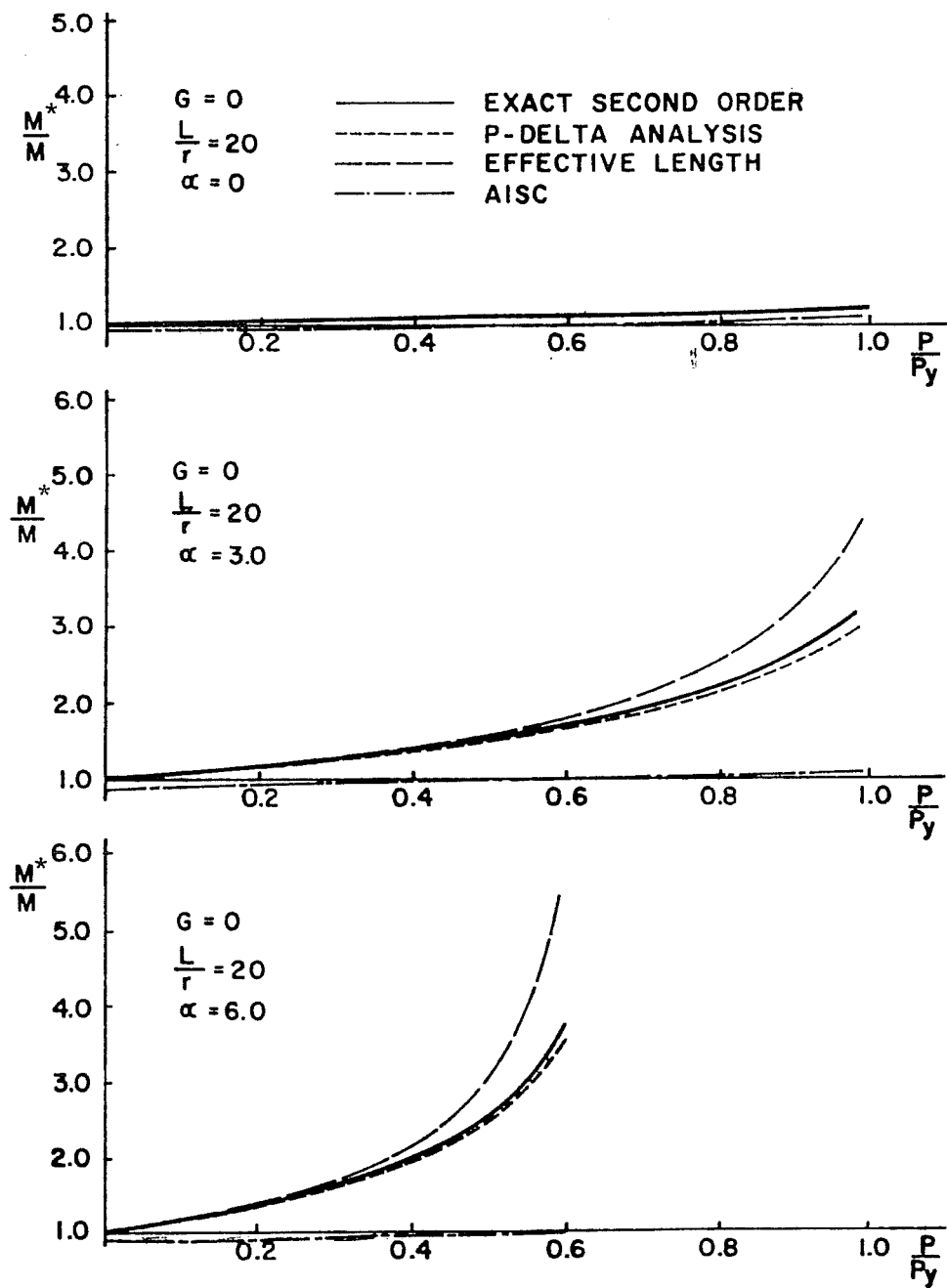


Fig. 2.33 Comparison of second order moments
($G = 0$, $L_c/r = 20$)

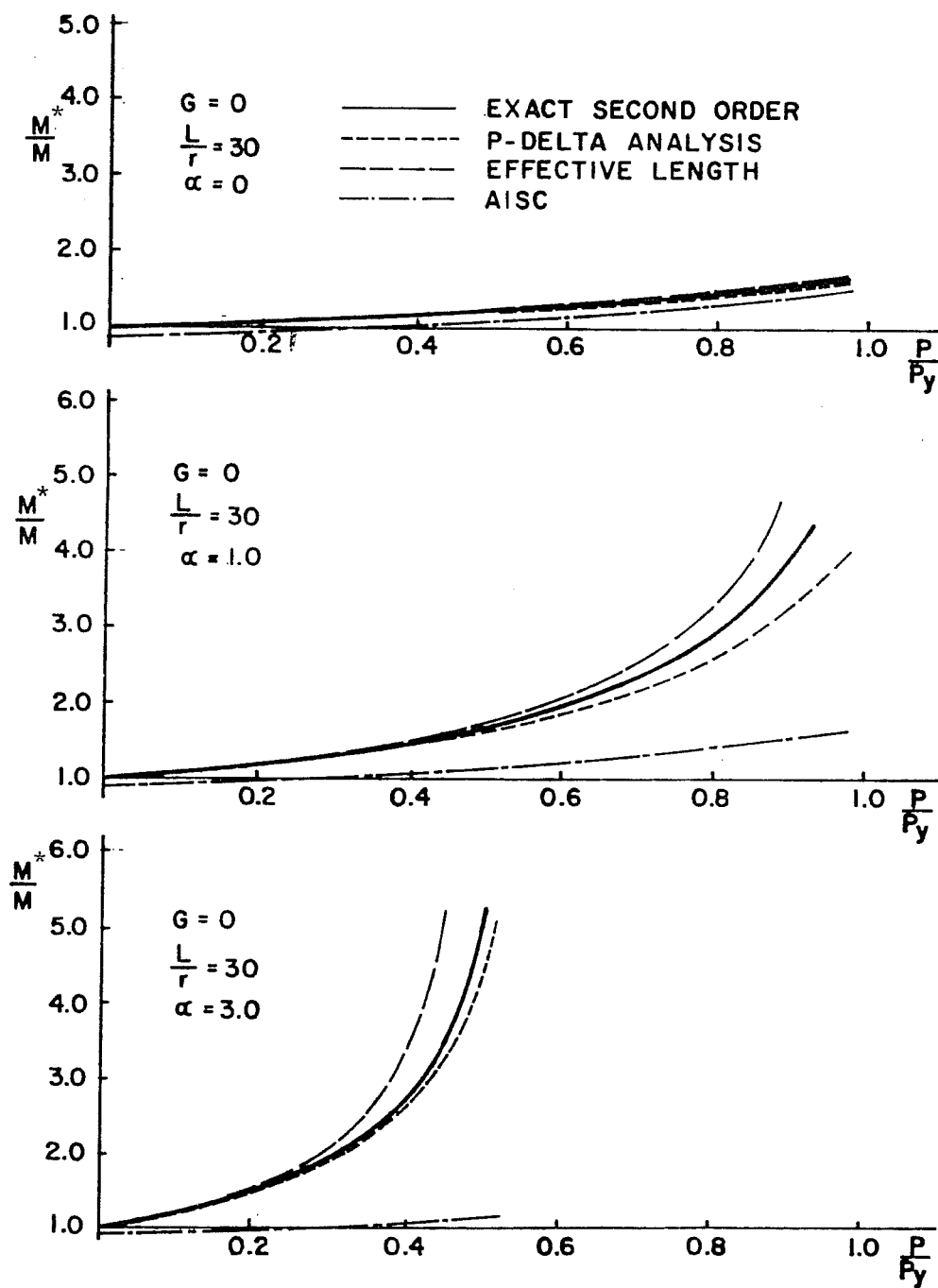


Fig. 2.34 Comparison of second order moments
($G = 0$, $L_c/r = 30$)

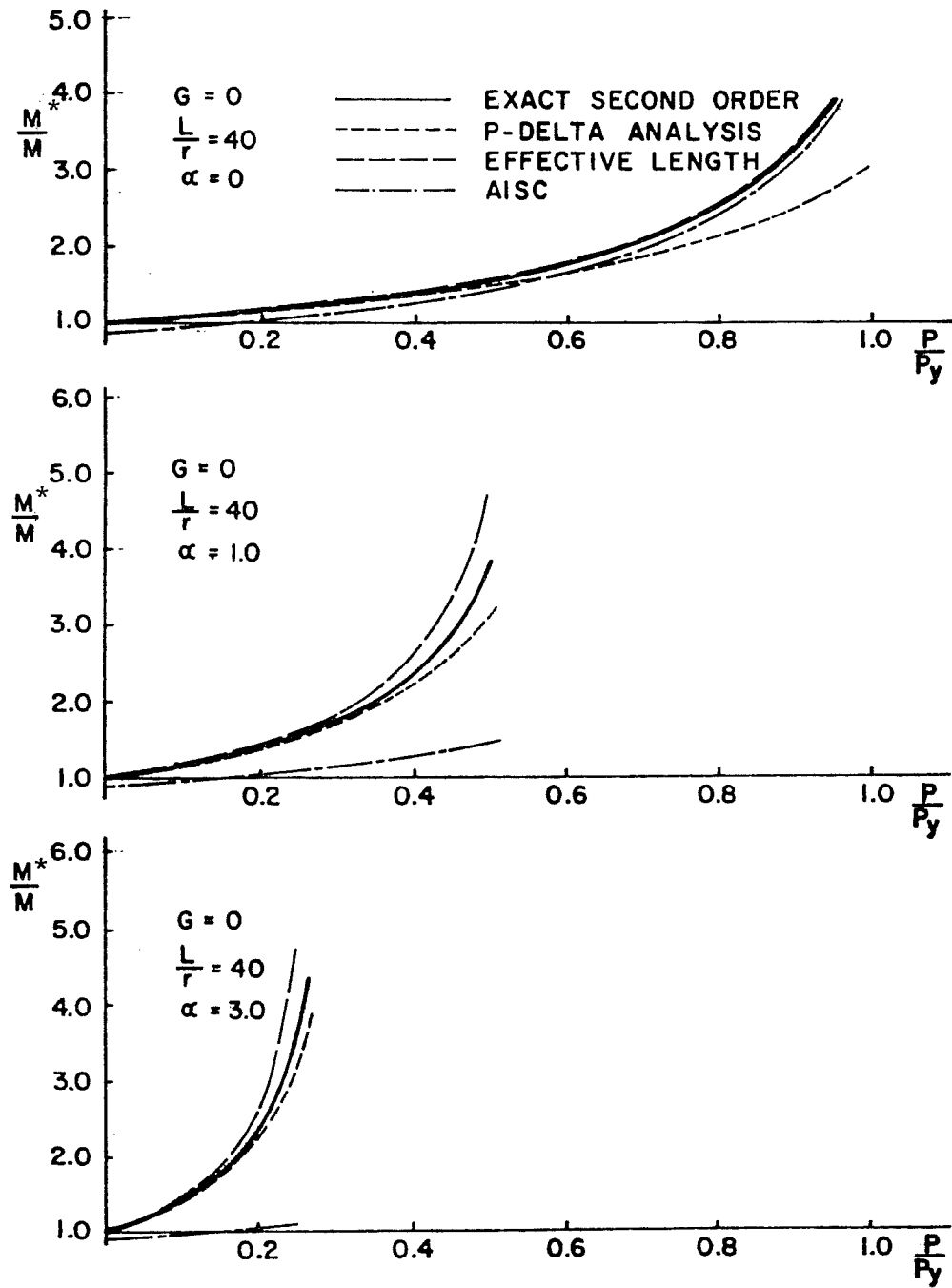


Fig. 2.35 Comparison of second order moments
($G = 0$, $L_c/r = 40$)

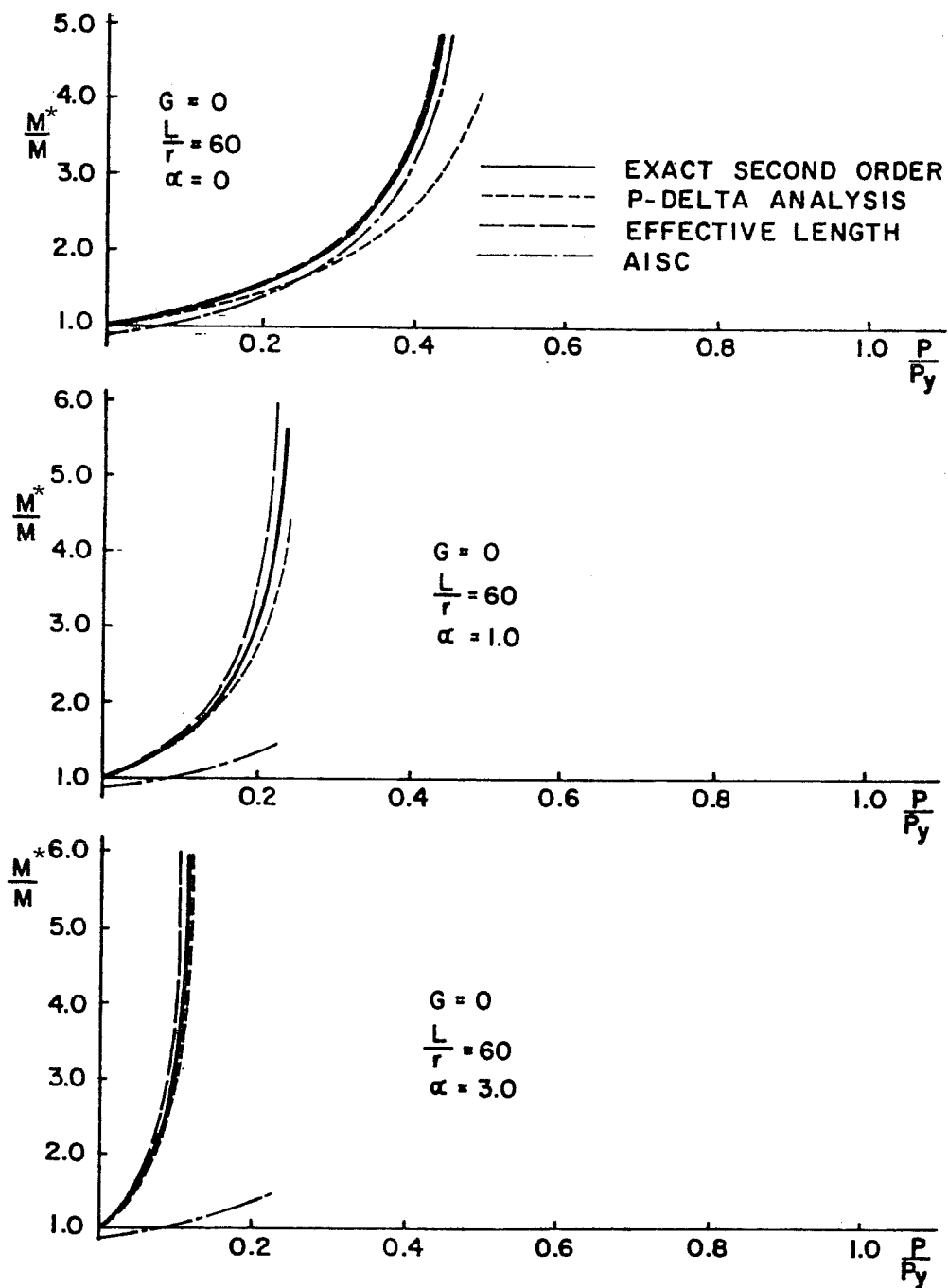


Fig. 2.36 Comparison of second order moments
($G = 0$, $L_c/r = 60$)

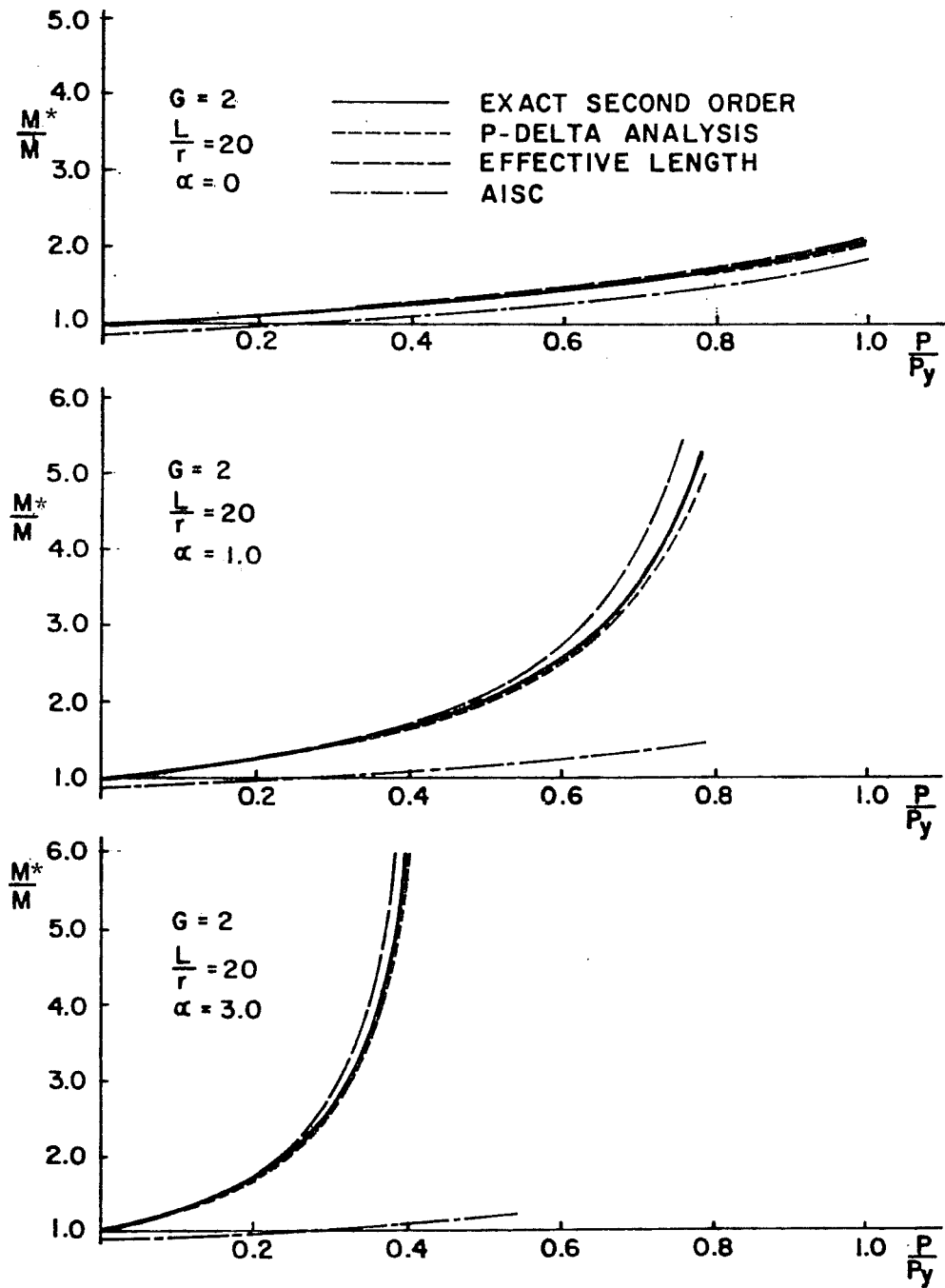


Fig. 2.37 Comparison of second order moments
($G = 2$, $L_c/r = 20$)

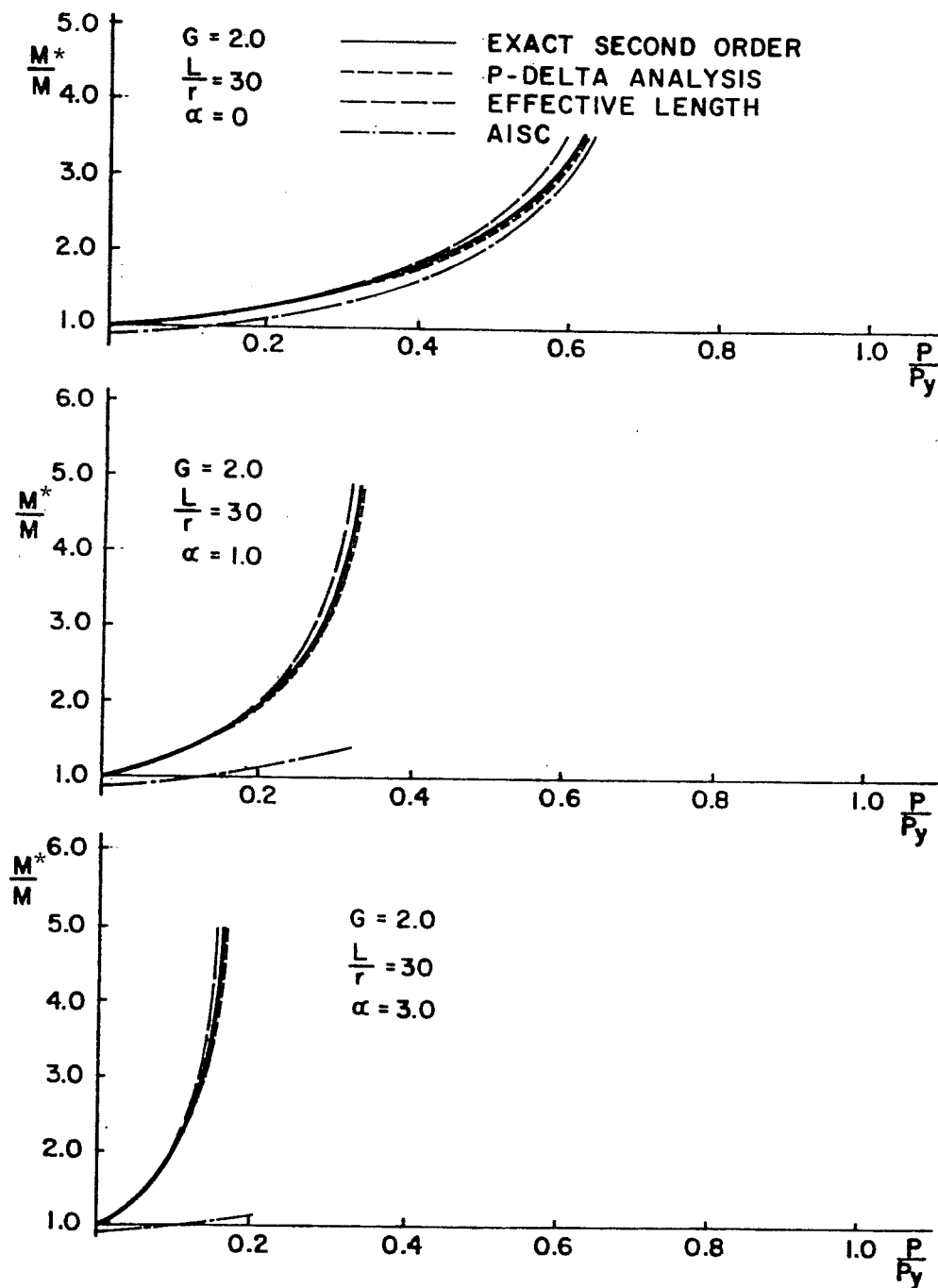


Fig. 2.38 Comparison of second order moments
($G = 2$, $L_c/r = 30$)

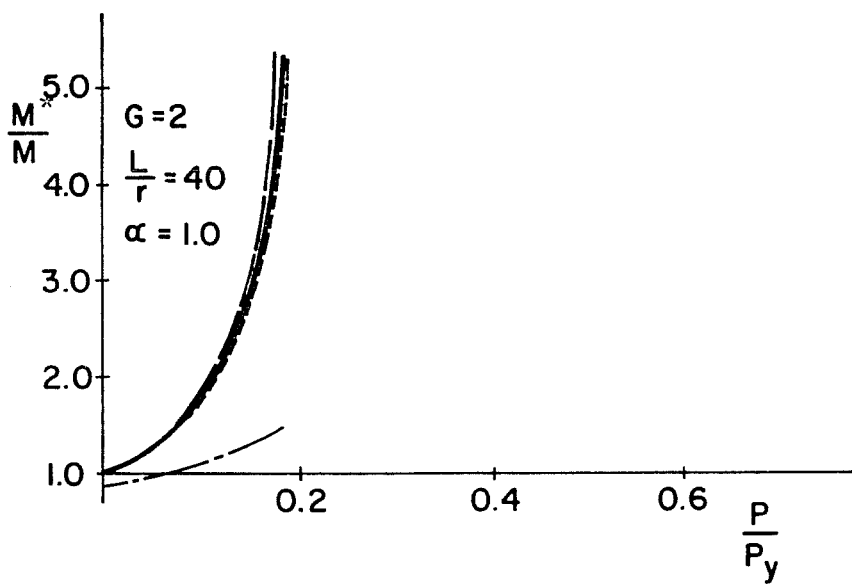
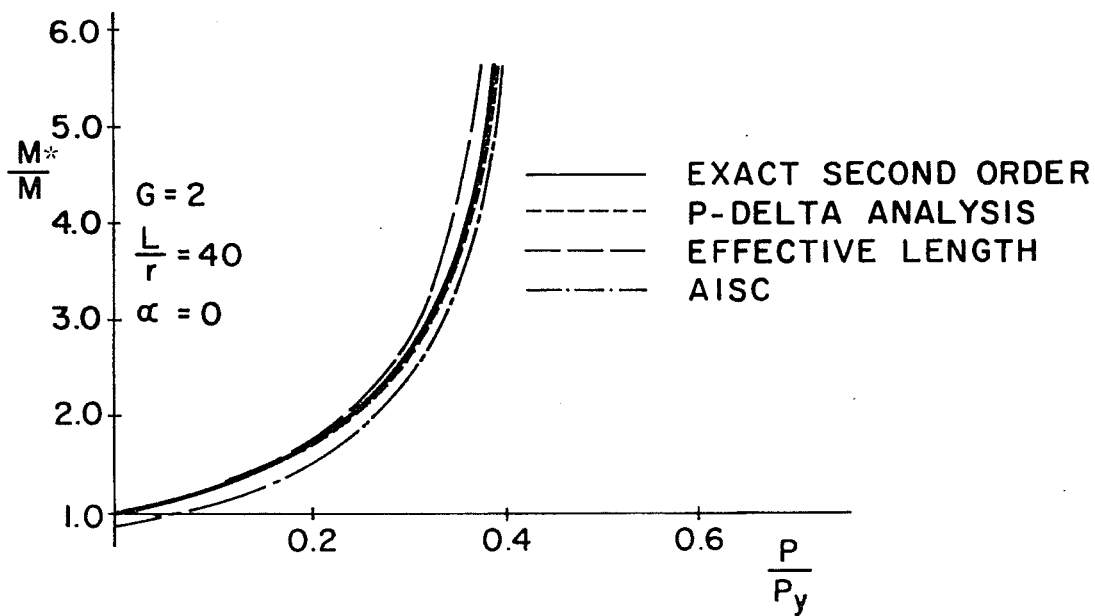


Fig. 2.39 Comparison of second order moments
 ($G = 2, L_c/r = 40$)

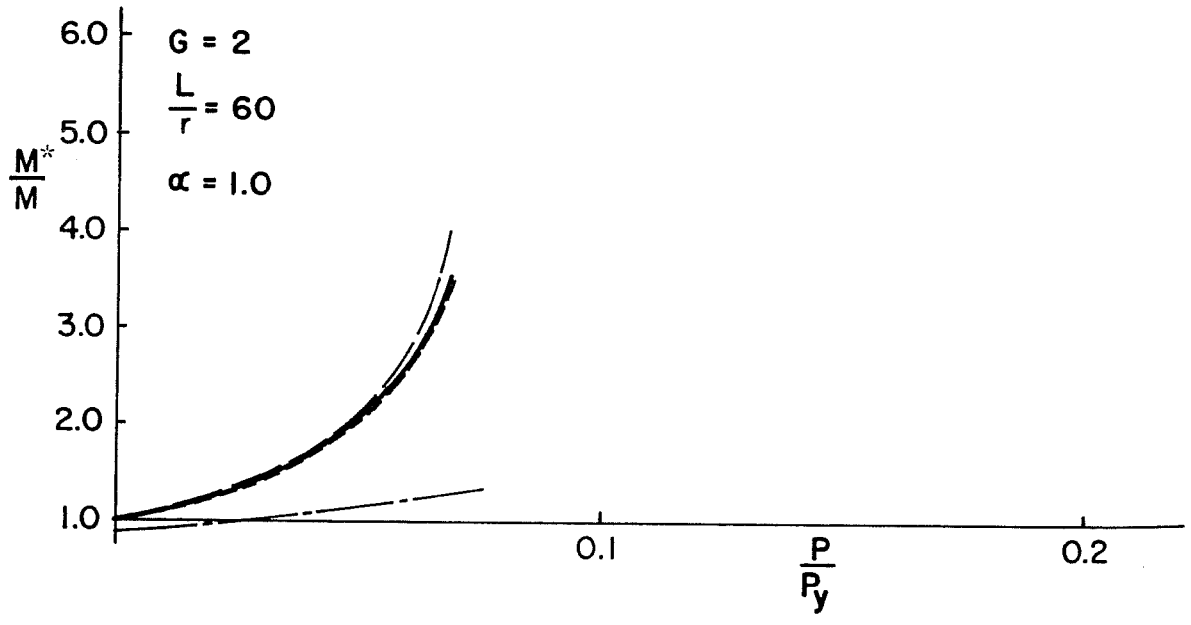
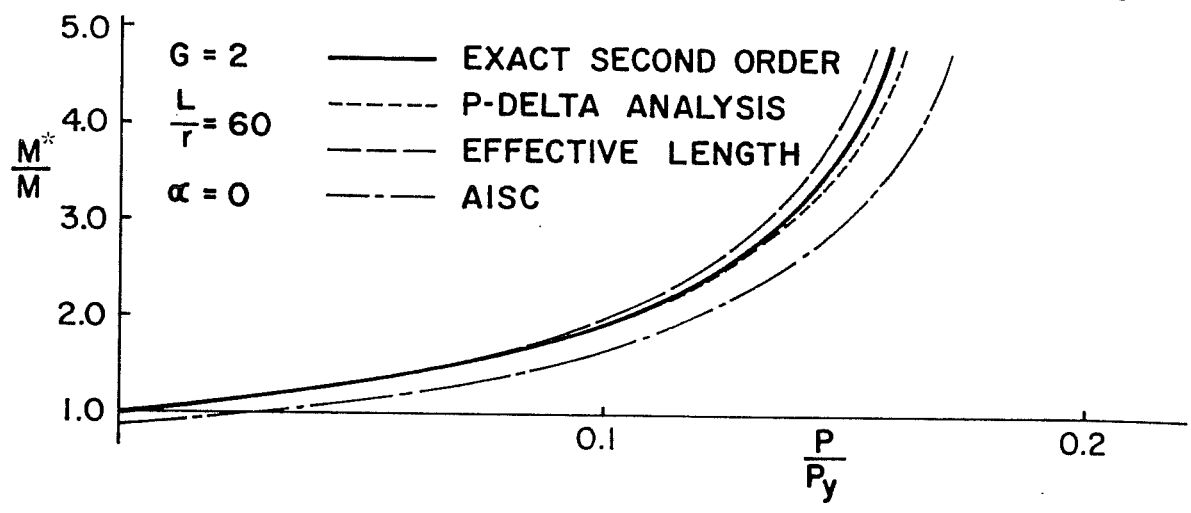


Fig. 2.40 Comparison of second order moments
($G = 2, L_c/r = 60$)

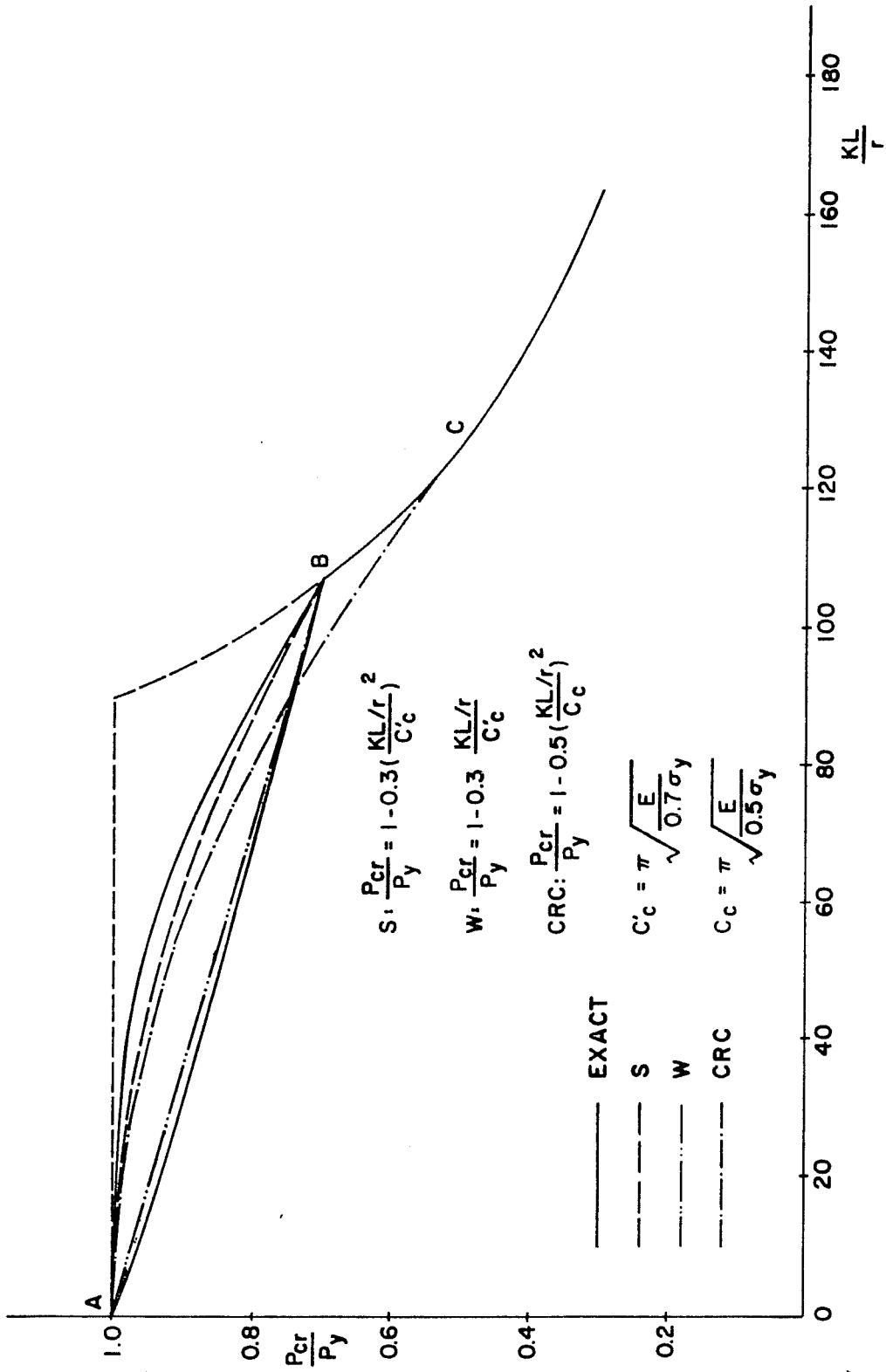


Fig. 2.41 Column curves

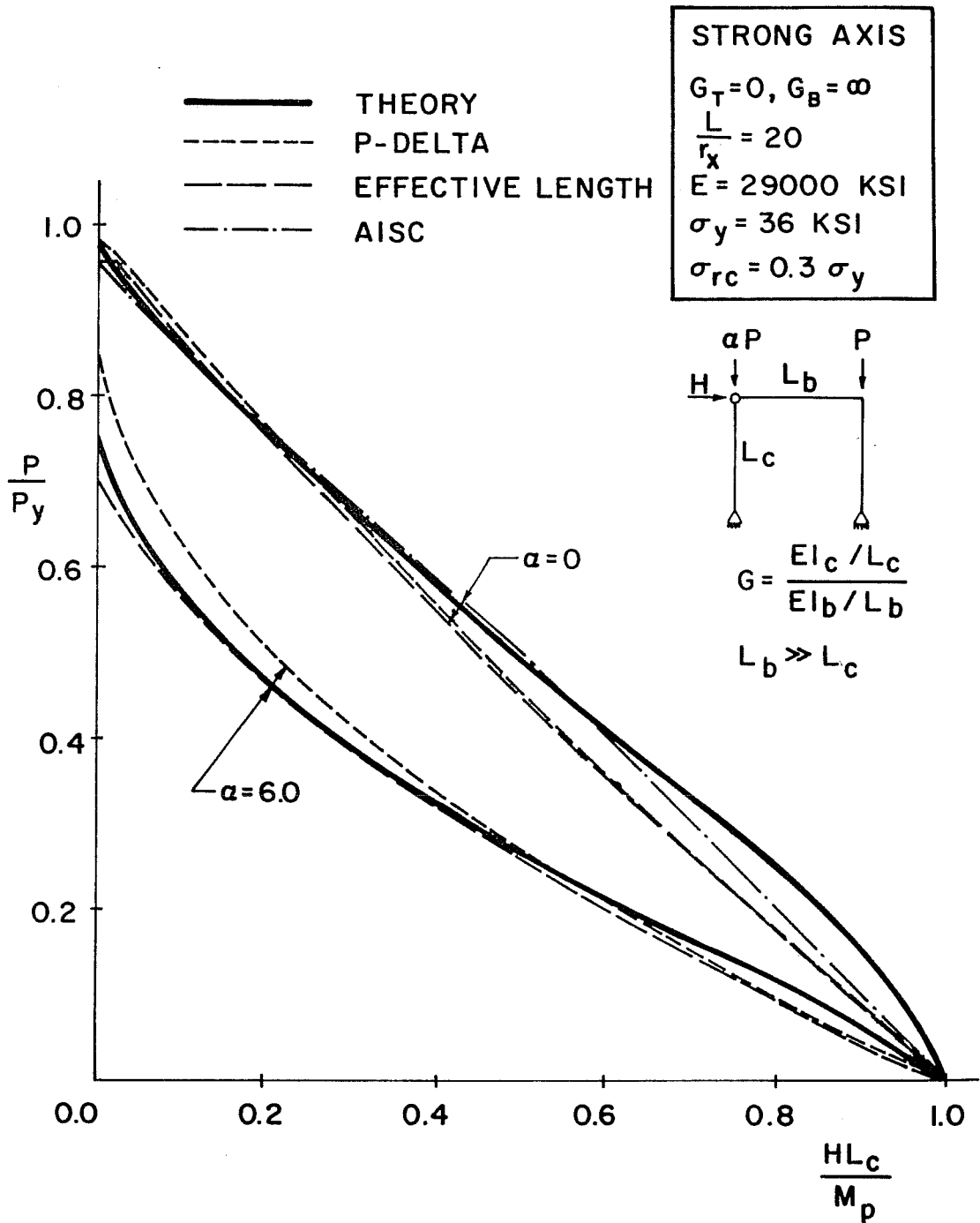


Fig. 2.42a Comparison of theoretical results with design interaction equations ($G = 0, L_c/r = 20,$ strong axis bending)

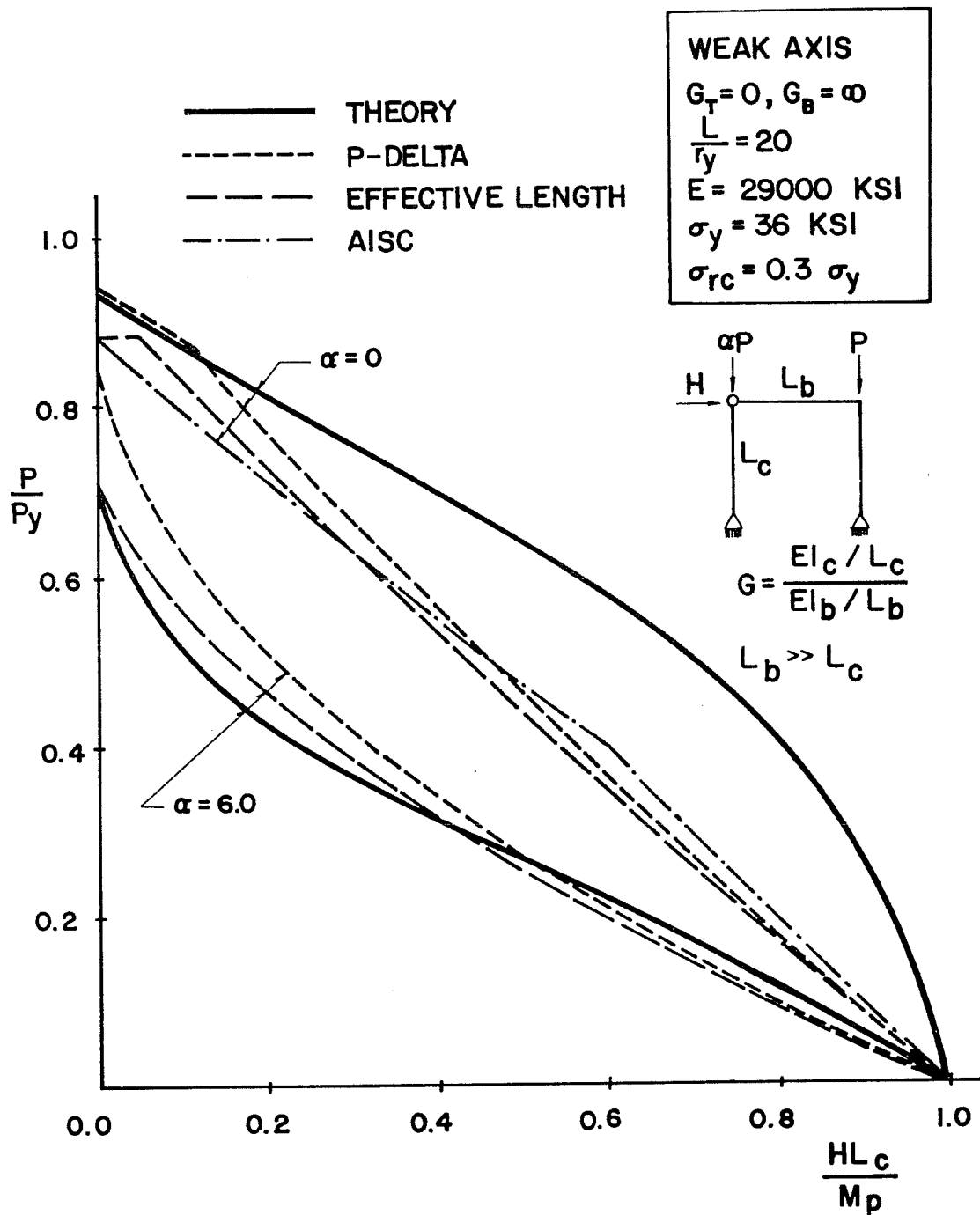


Fig. 2.42b Comparison of theoretical results with design interaction equations ($G = 0, L_c/r = 20$, weak axis bending)

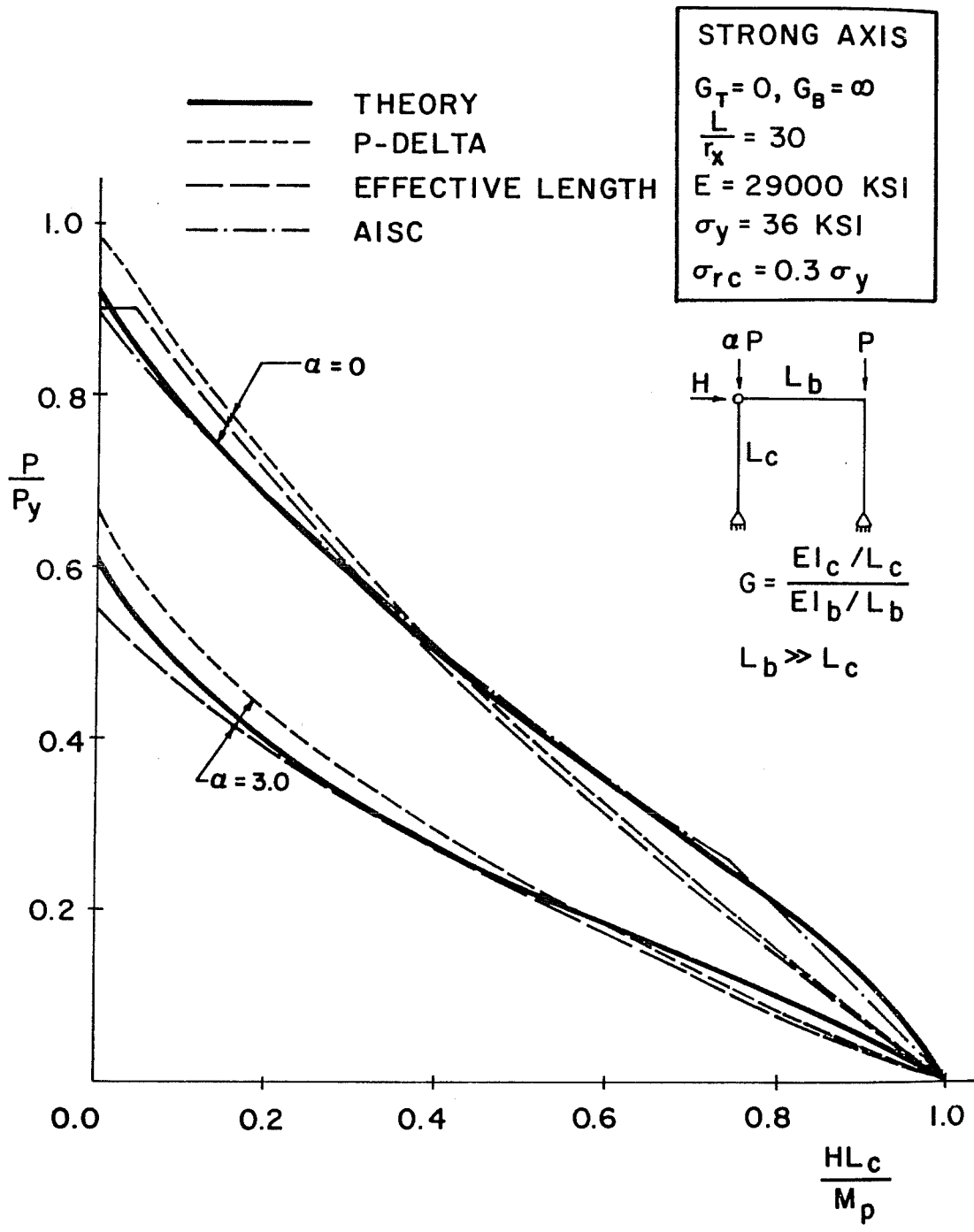


Fig. 2.43a Comparison of theoretical results with design interaction equations ($G = 0, L_c/r = 30$, strong axis bending)

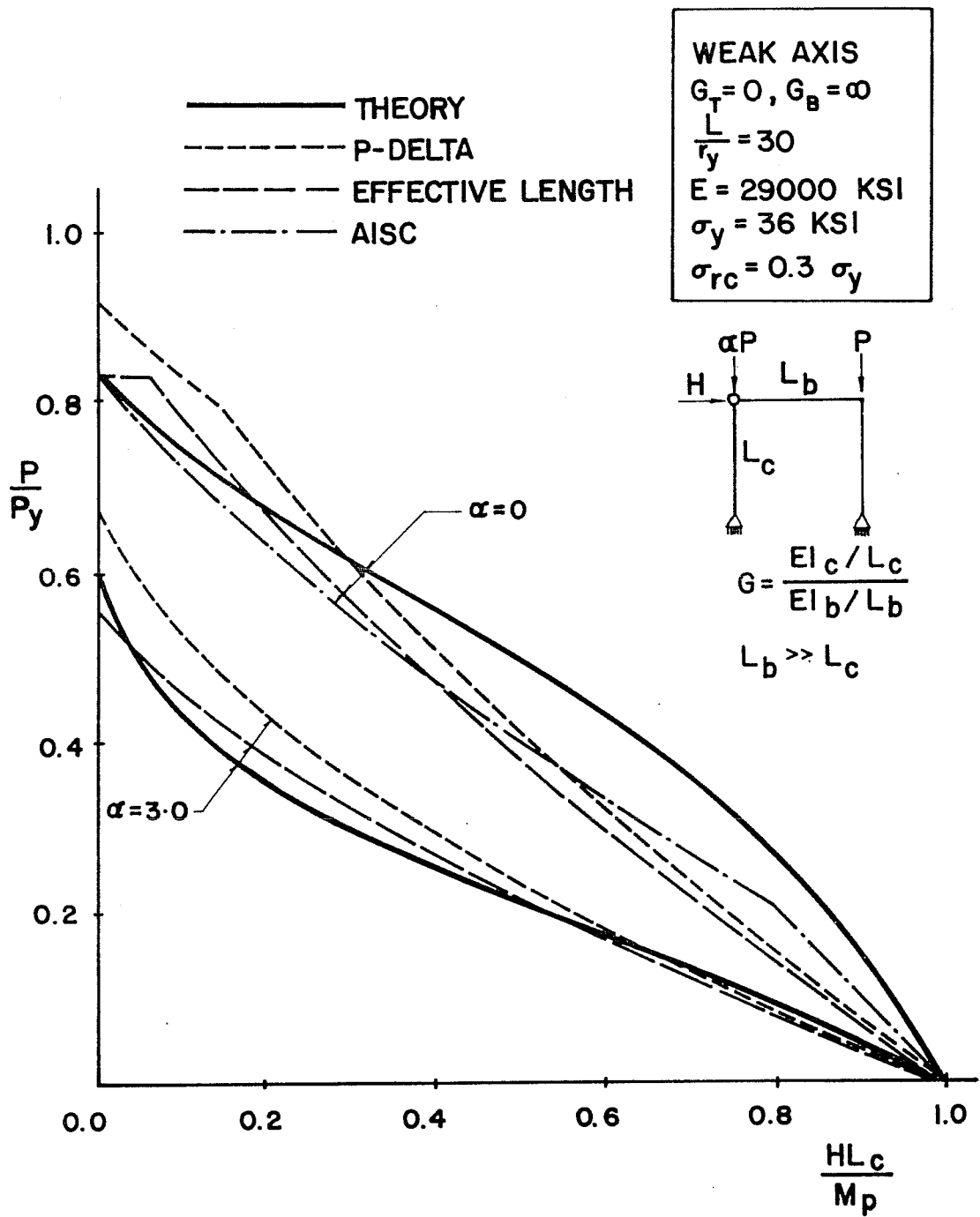


Fig. 2.43b Comparison of theoretical results with design interaction equations ($G = 0, L_c/r = 30$, weak axis bending)

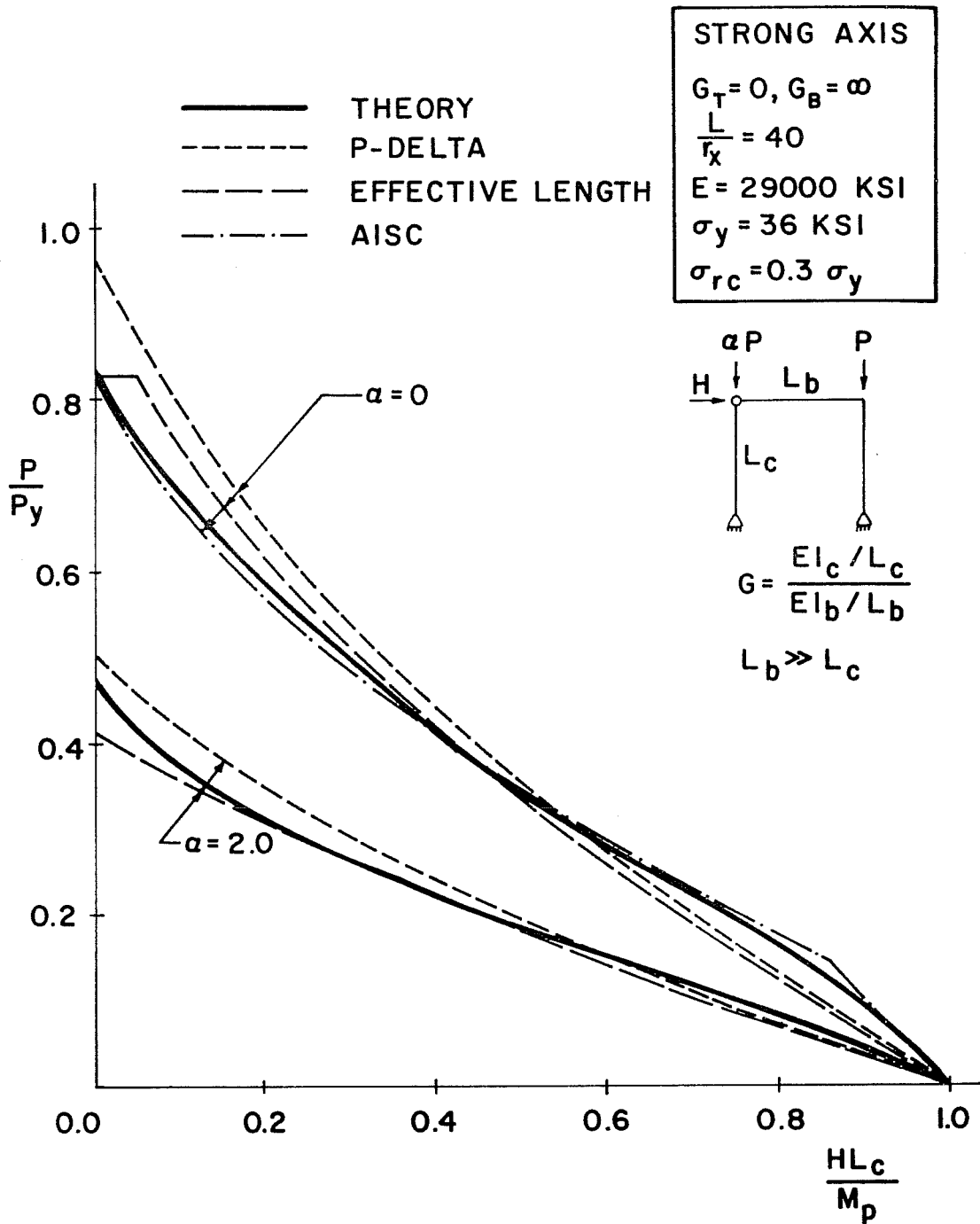


Fig. 2.44a Comparison of theoretical results with design interaction equations ($G = 0$, $L_c/r = 40$, strong axis bending)

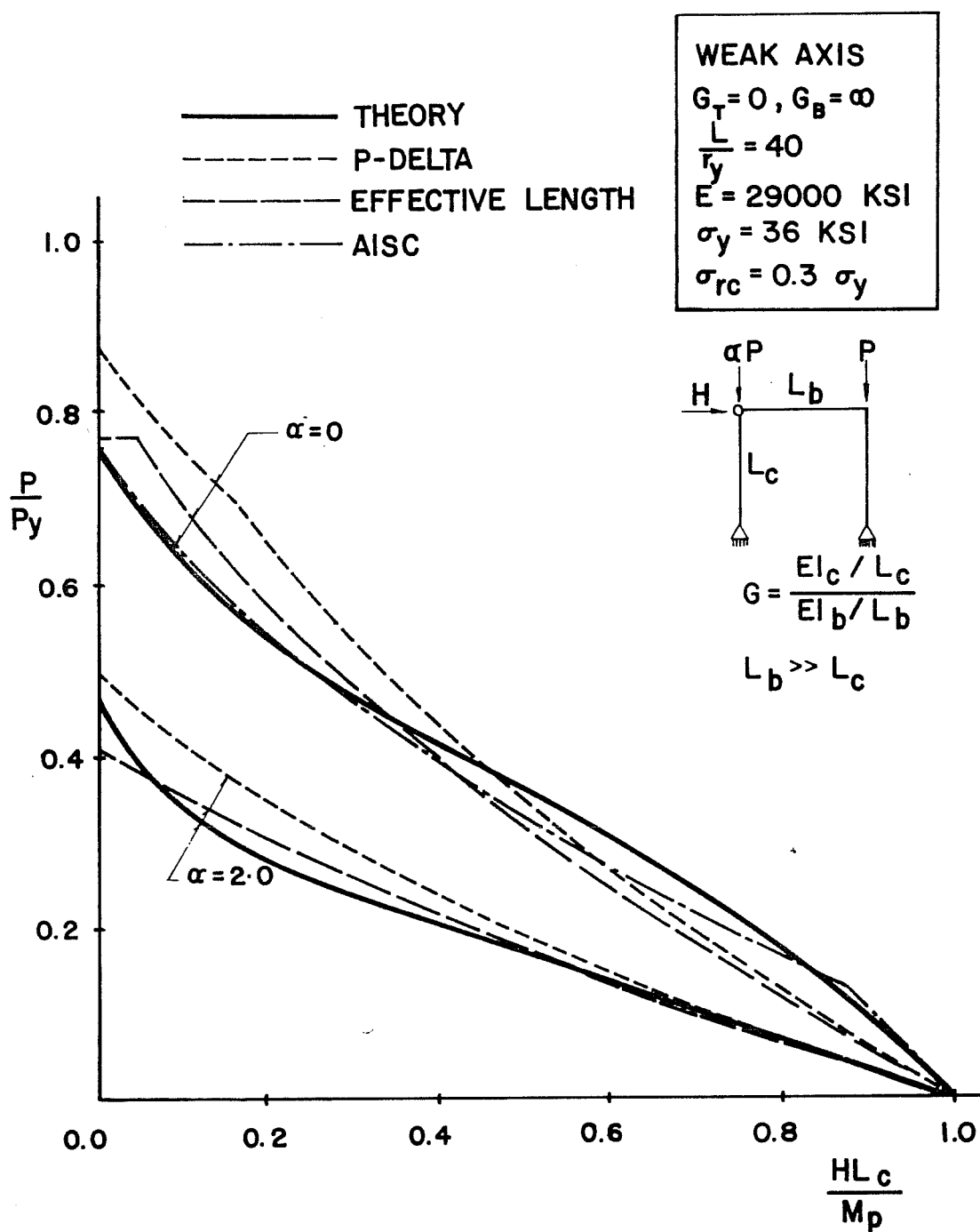


Fig. 2.44b Comparison of theoretical results with design interaction equations ($G = 0, L_c/r = 40$, weak axis bending)

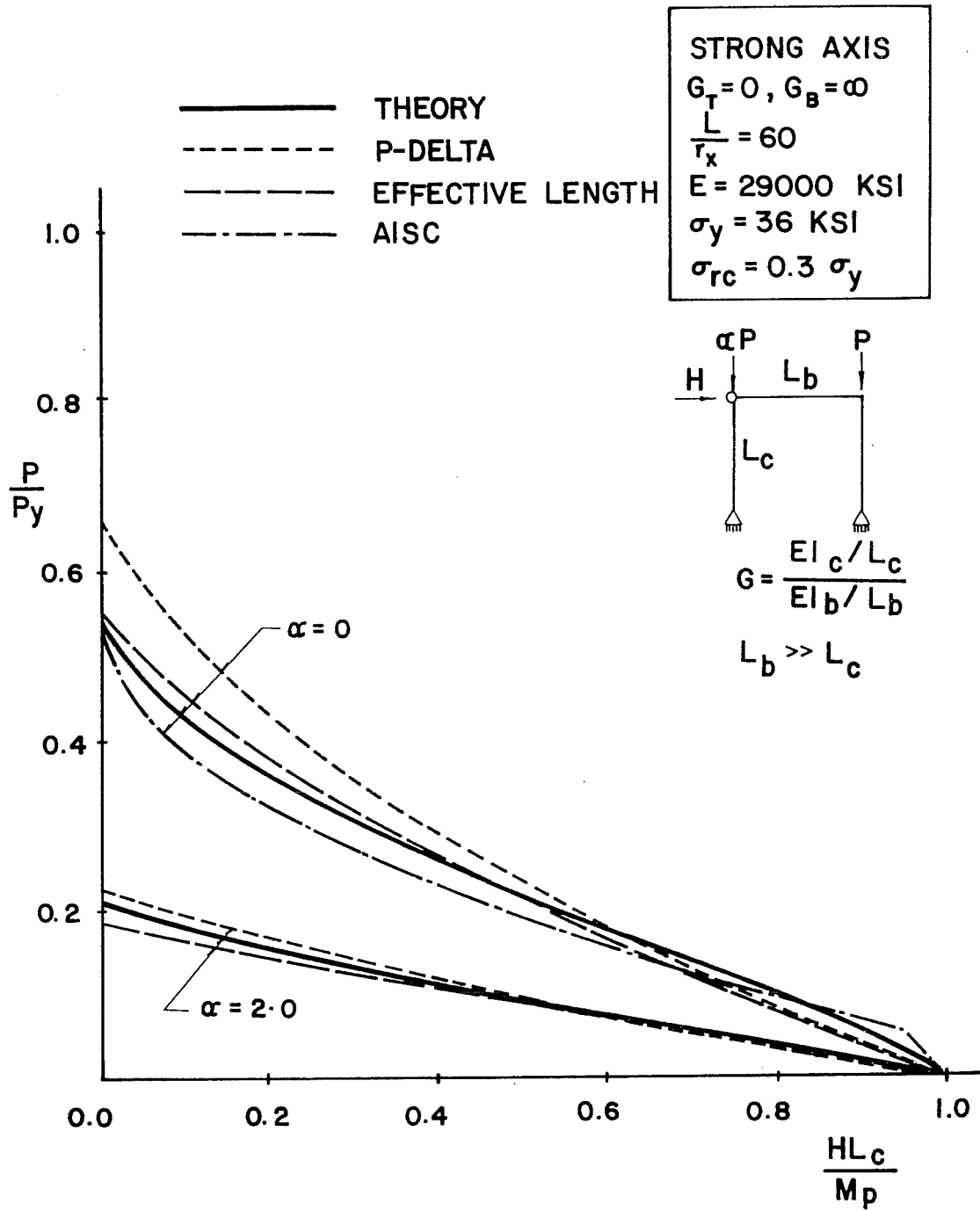


Fig. 2.45a Comparison of theoretical results with design interaction equations ($G = 0, L_c/r = 60$, strong axis bending)

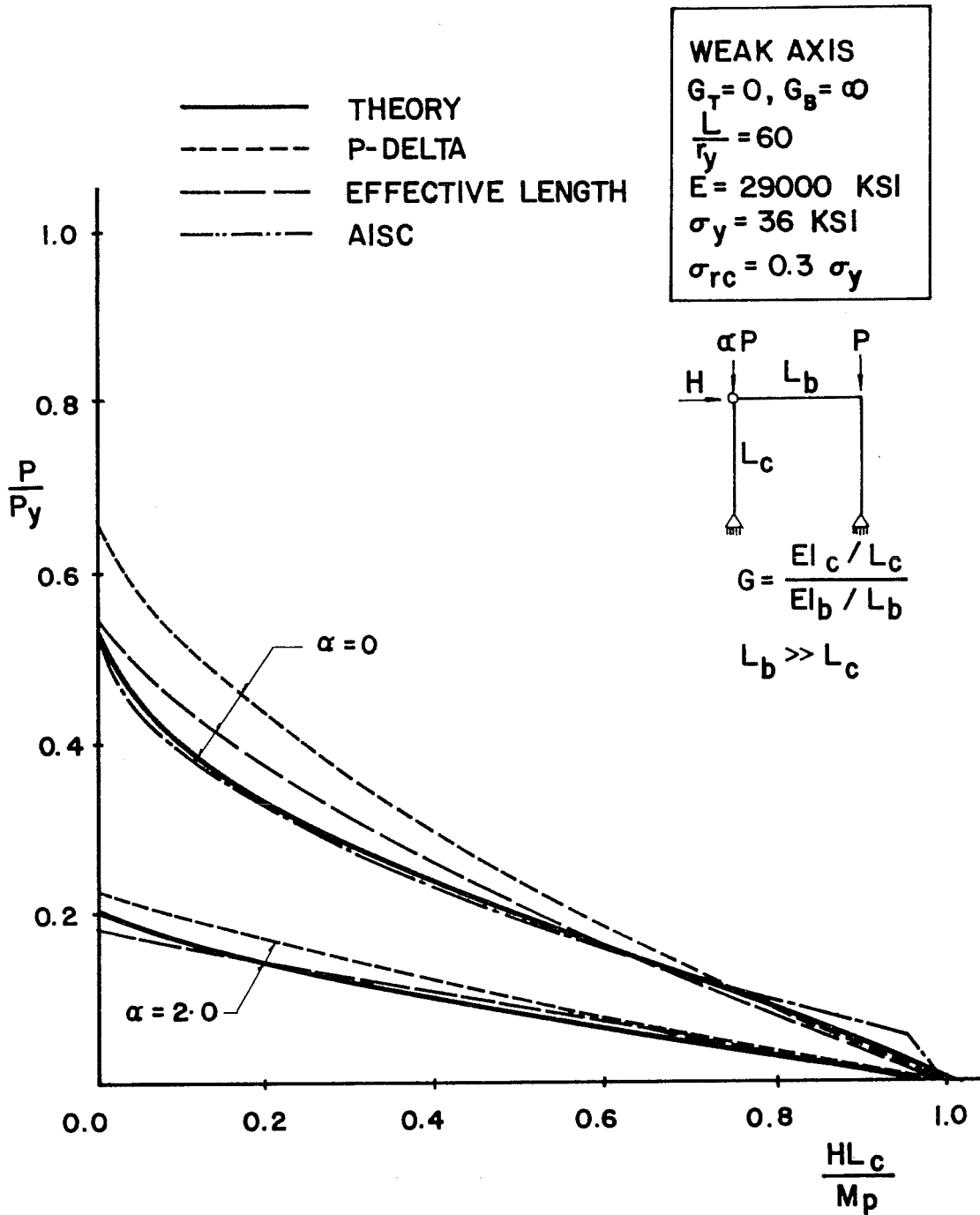


Fig. 2.45b Comparison of theoretical results with design interaction equations ($G = 0, L_c/r = 60$, weak axis bending)

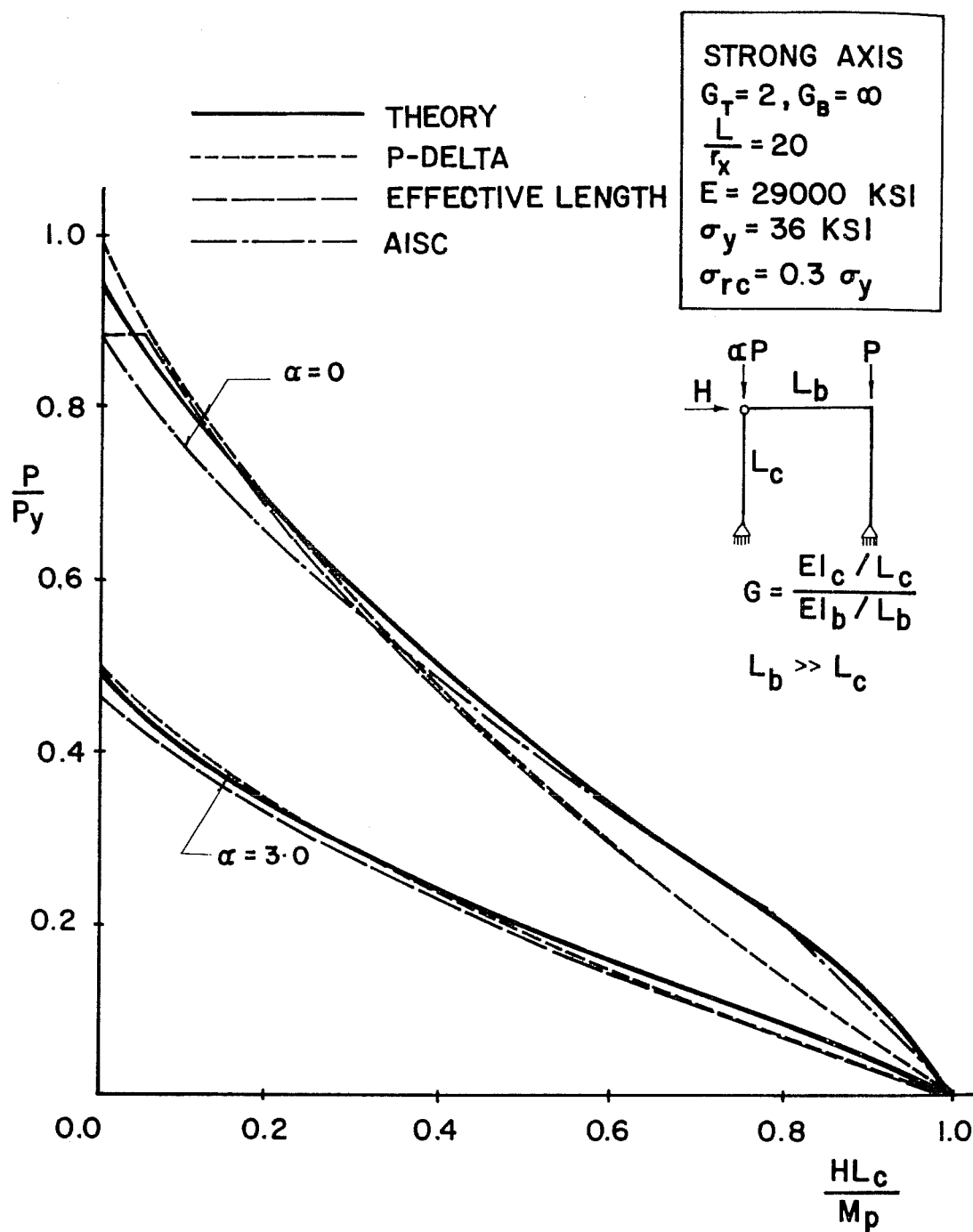


Fig. 2.46a Comparison of theoretical results with design interaction equations ($G = 2, L_c/r = 20$, strong axis bending)

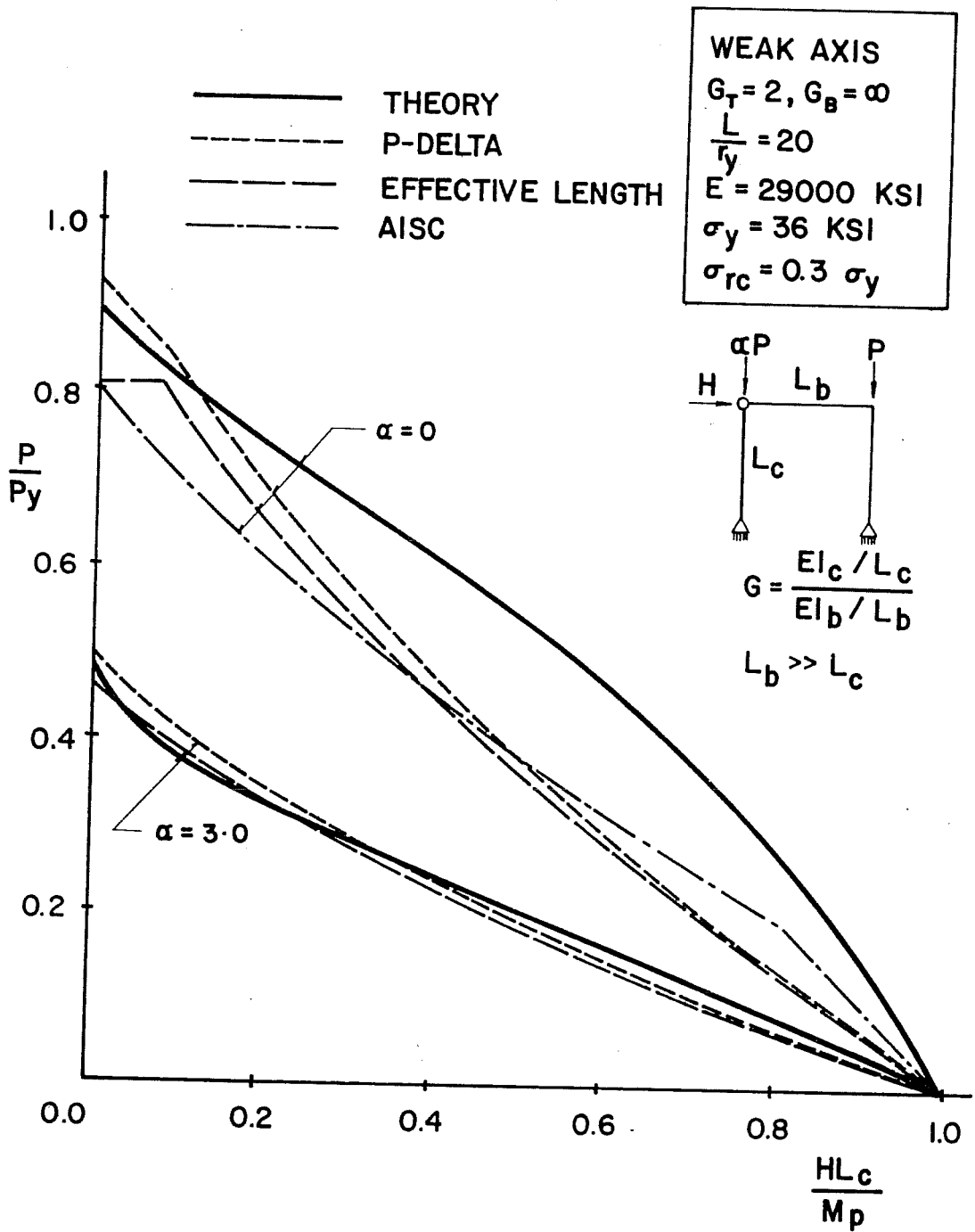


Fig. 2.46b Comparison of theoretical results with design interaction equations ($G = 2, L_c/r = 20$, weak axis bending)

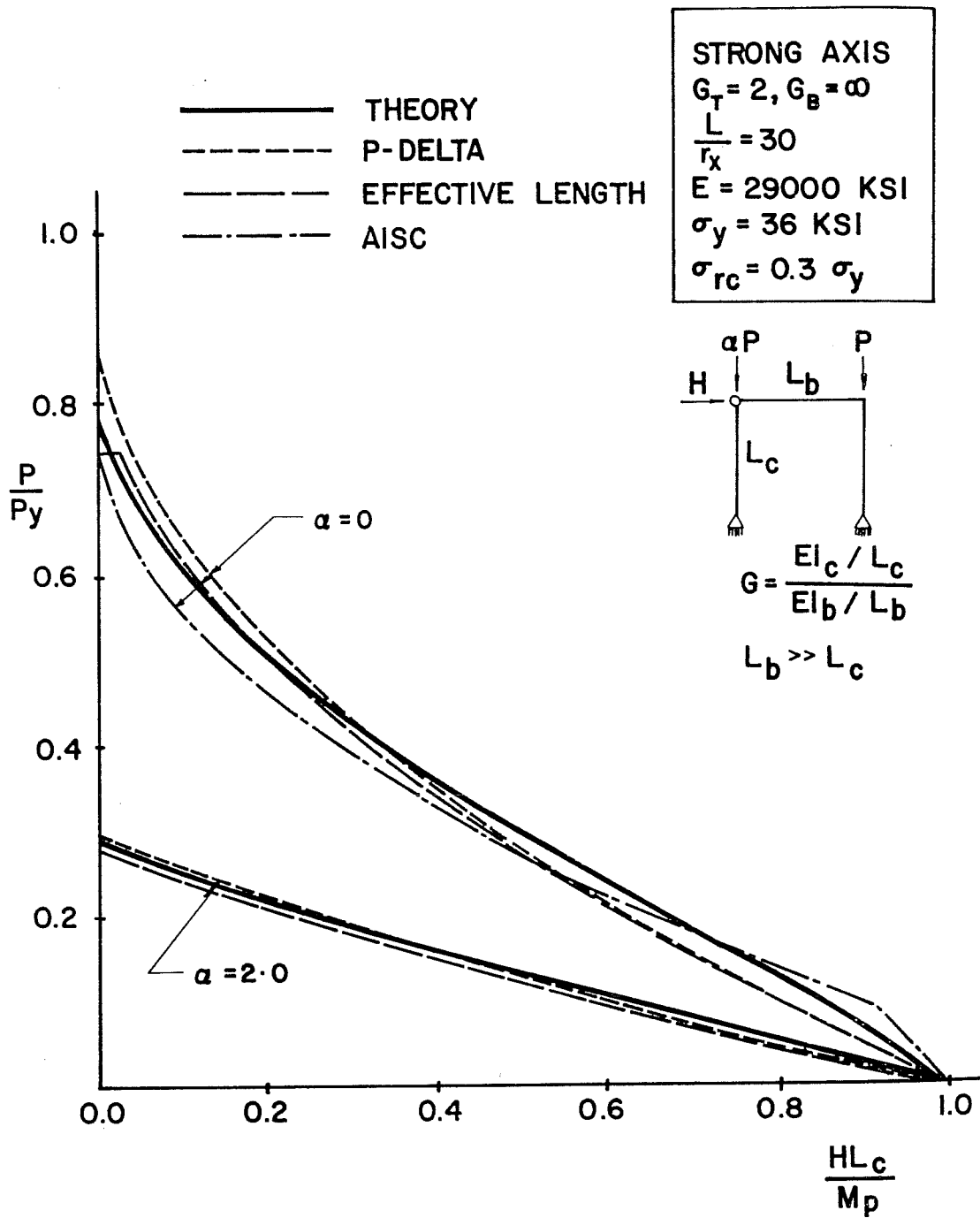


Fig. 2.47a Comparison of theoretical results with design interaction equations ($G = 2, L_c/r = 30$, strong axis bending)

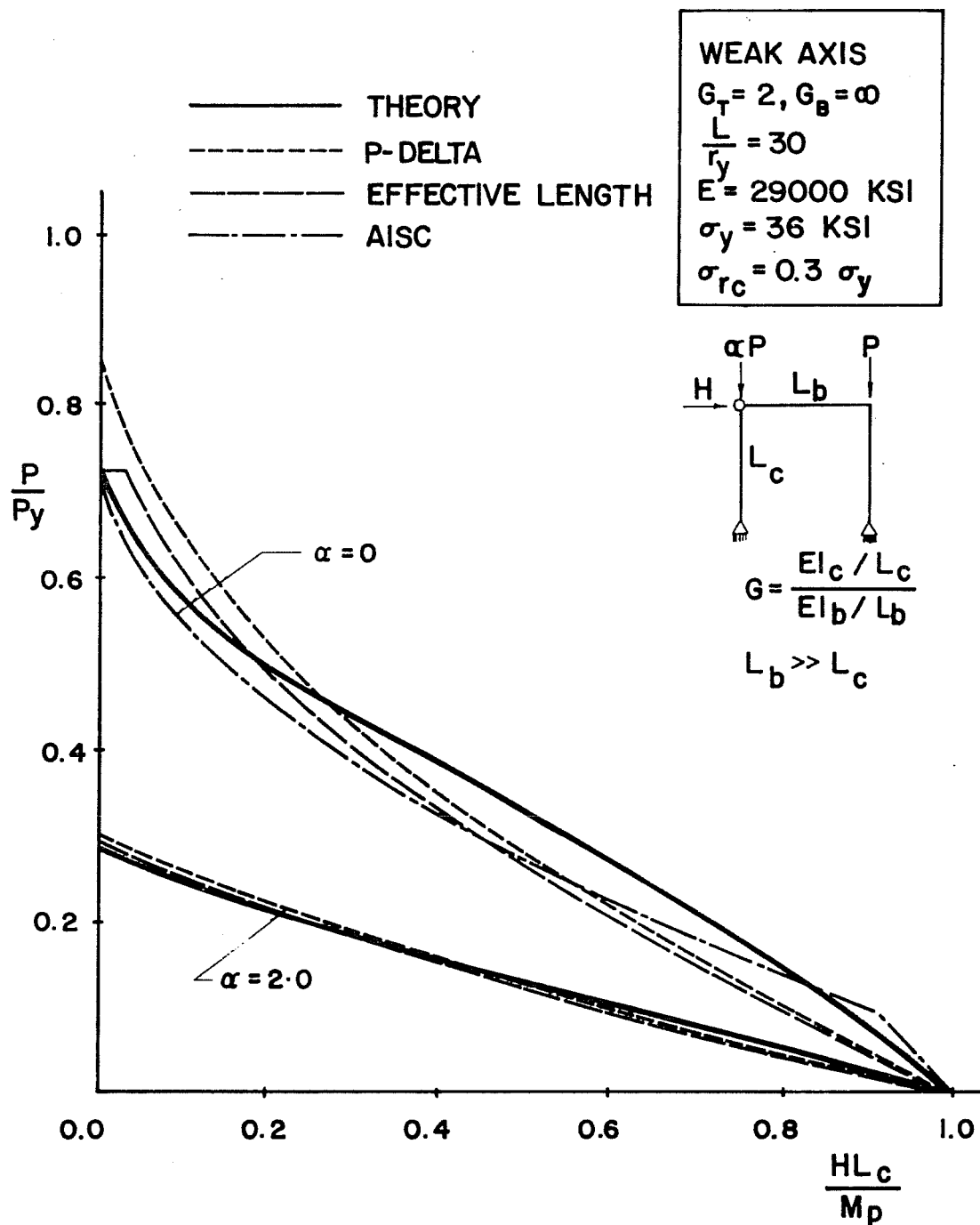


Fig. 2.47b Comparison of theoretical results with design interaction equations ($G = 2$, $L_c/r = 30$, weak axis bending)

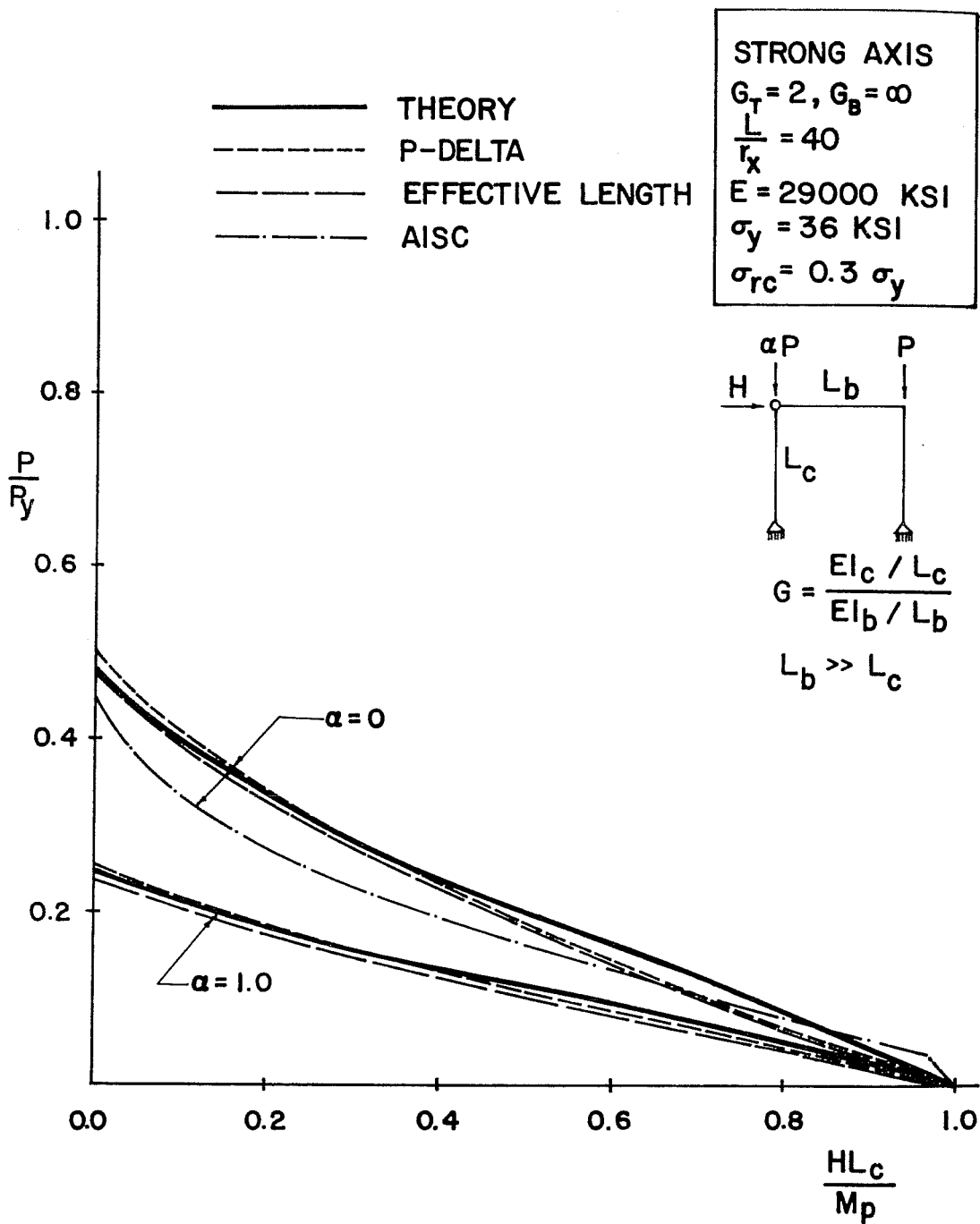


Fig. 2.48a Comparison of theoretical results with design interaction equations ($G = 2, L_c/r = 40$, strong axis bending)

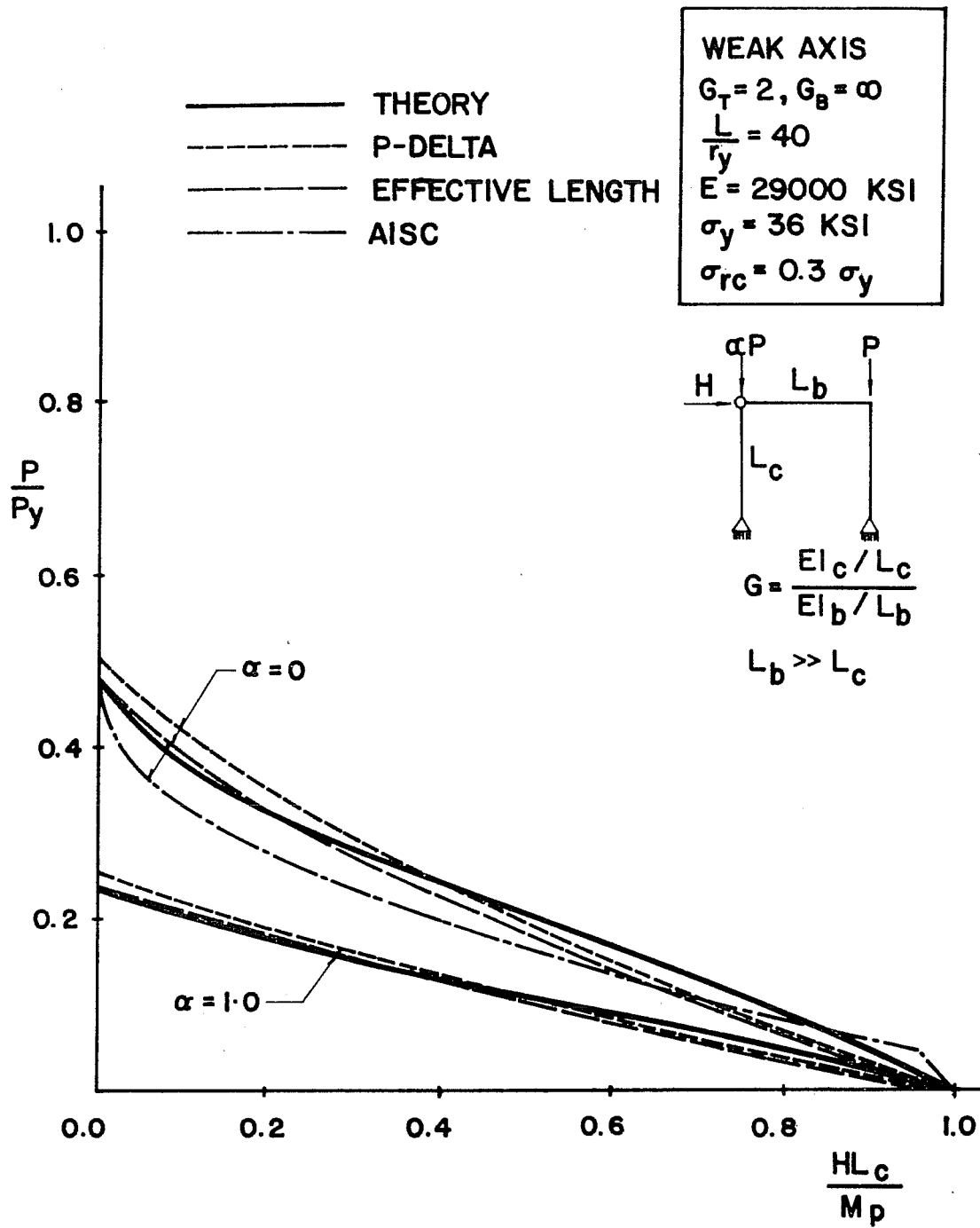


Fig. 2.48b Comparison of theoretical results with design interaction equations ($G = 2, L_c/r = 40$, weak axis bending)

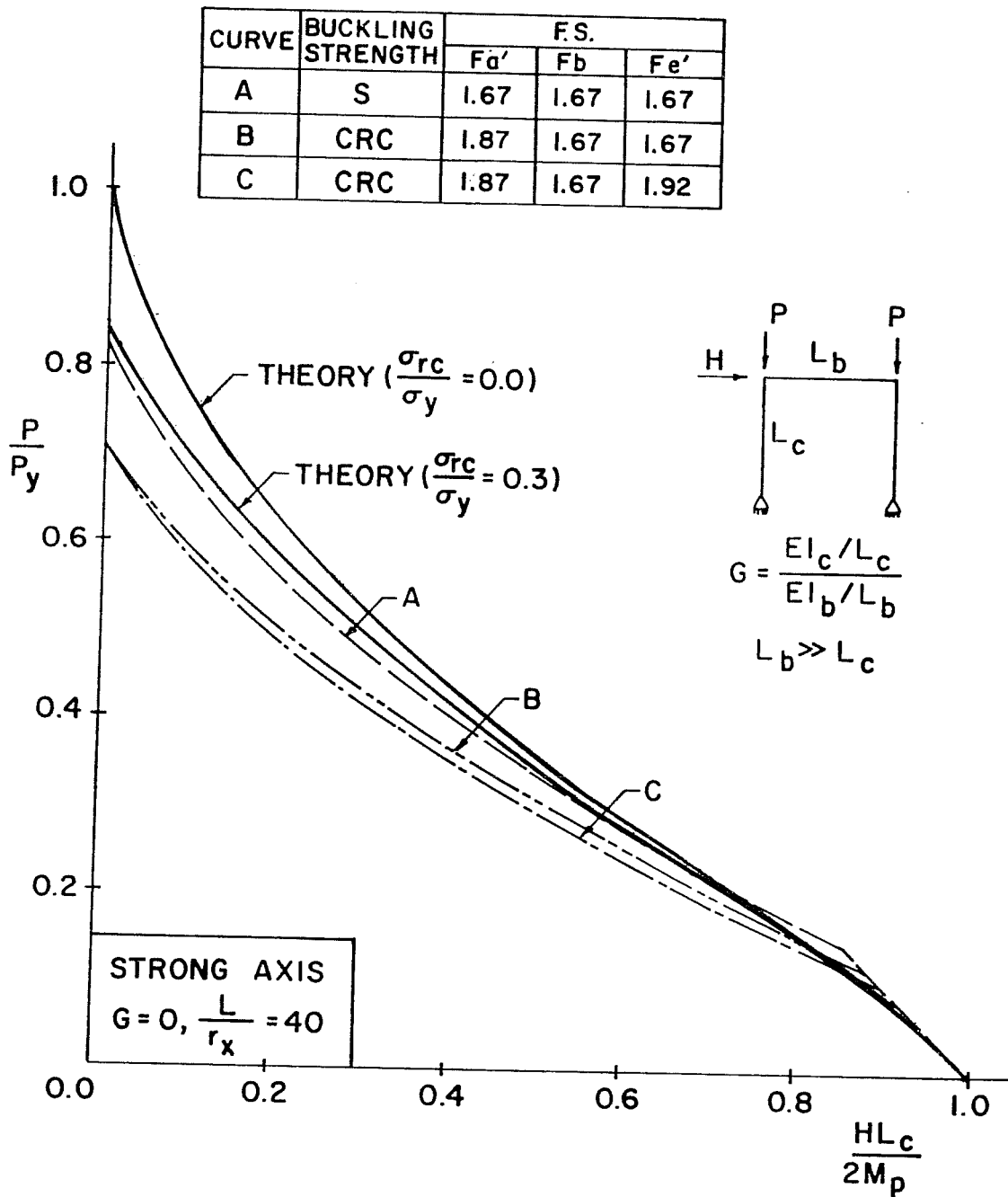


Fig. 2.49a Effect of variable factors of safety, AISC method ($G = 0, L_c/r = 40$, strong axis bending)

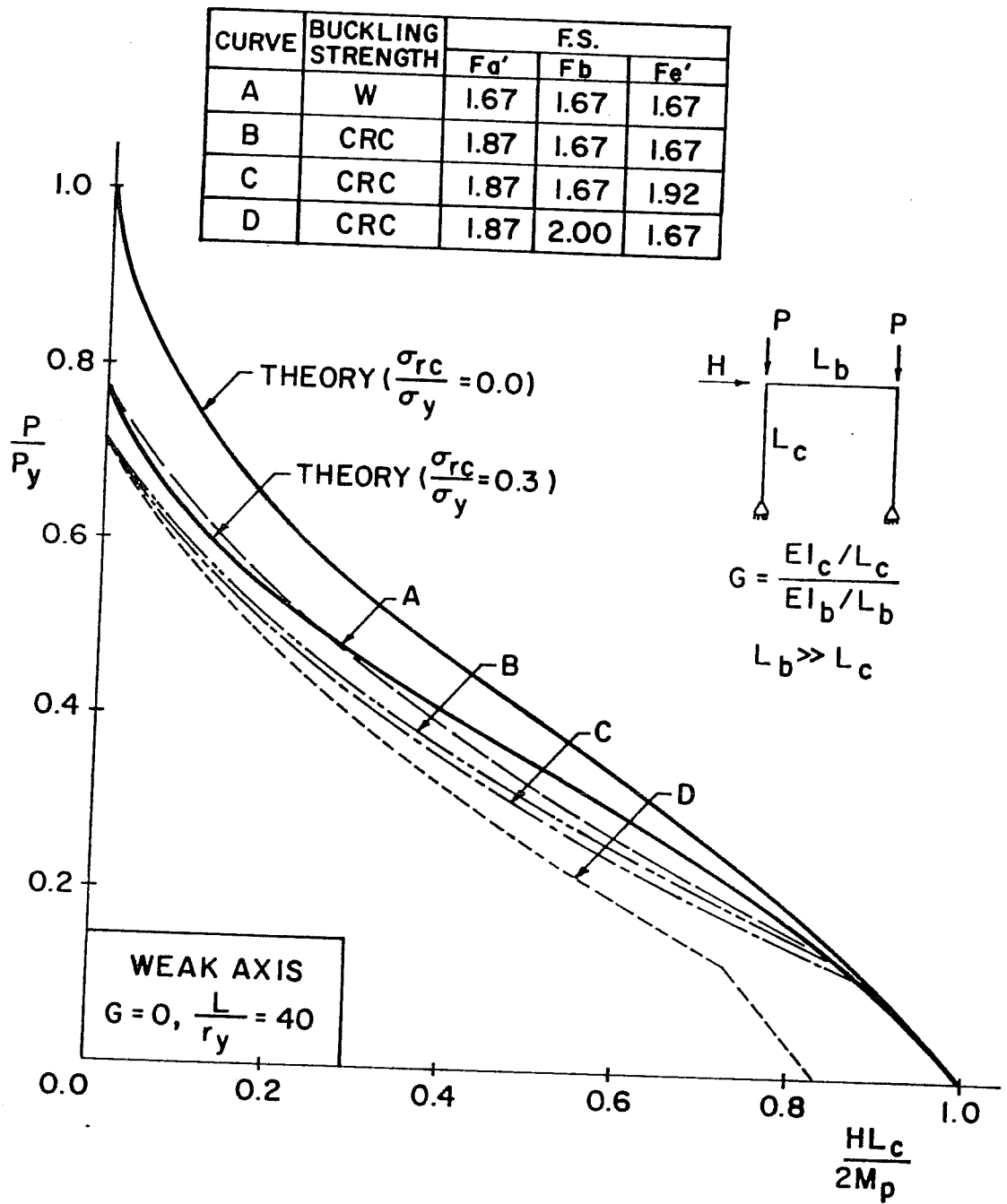


Fig. 2.49b Effect of variable factors of safety, AISC method
 ($G = 0, L_c/r = 40$, weak axis bending)

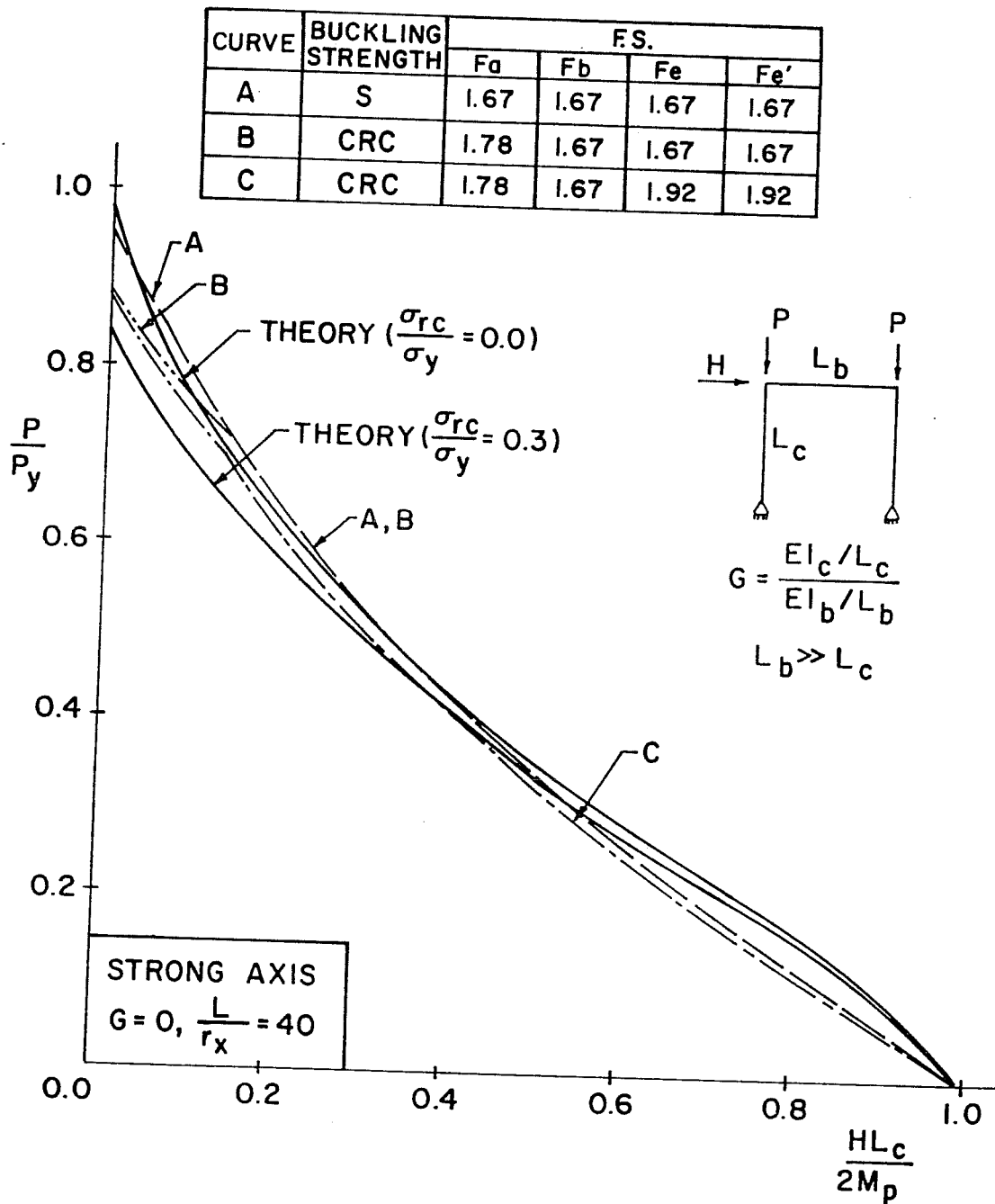


Fig. 2.50a Effect of variable factors of safety, P-delta method ($G = 0, L_c/r = 40$, strong axis bending)

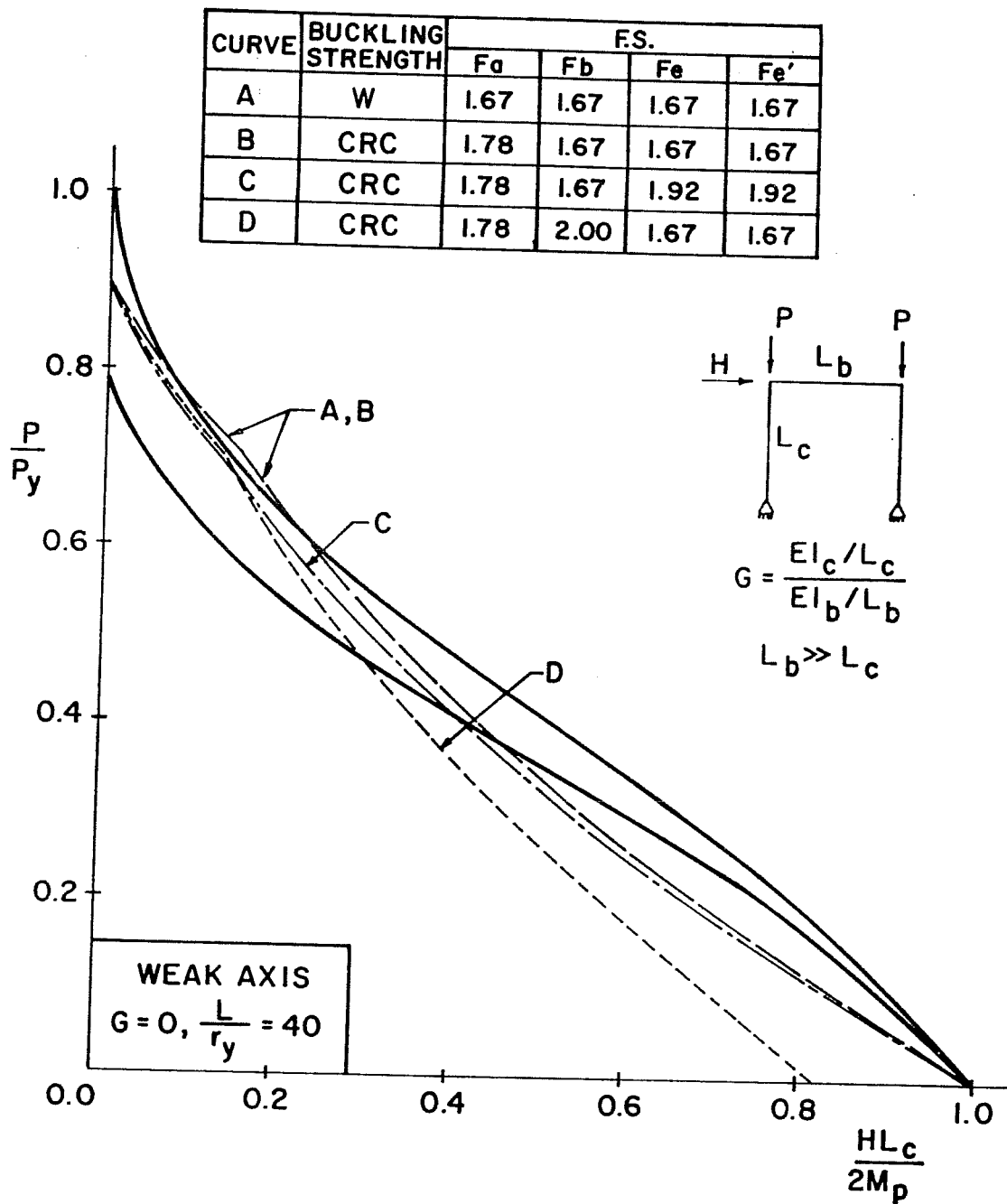


Fig. 2.50b Effect of variable factors of safety, P-delta method ($G = 0, L_c/r = 40$, weak axis bending)

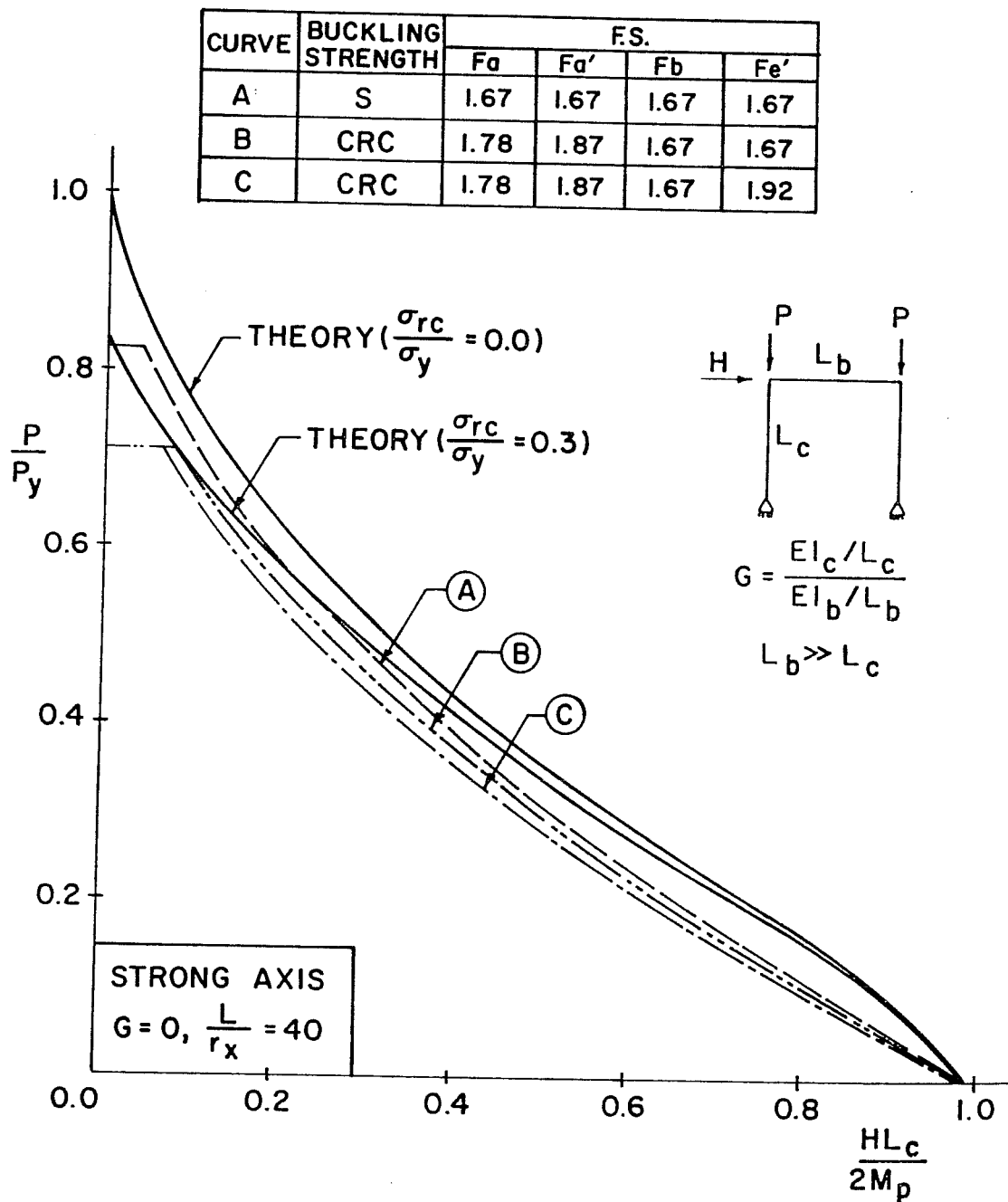


Fig. 2.51a Effect of variable factors of safety, effective length method ($G = 0, L_c/r = 40$, strong axis bending)

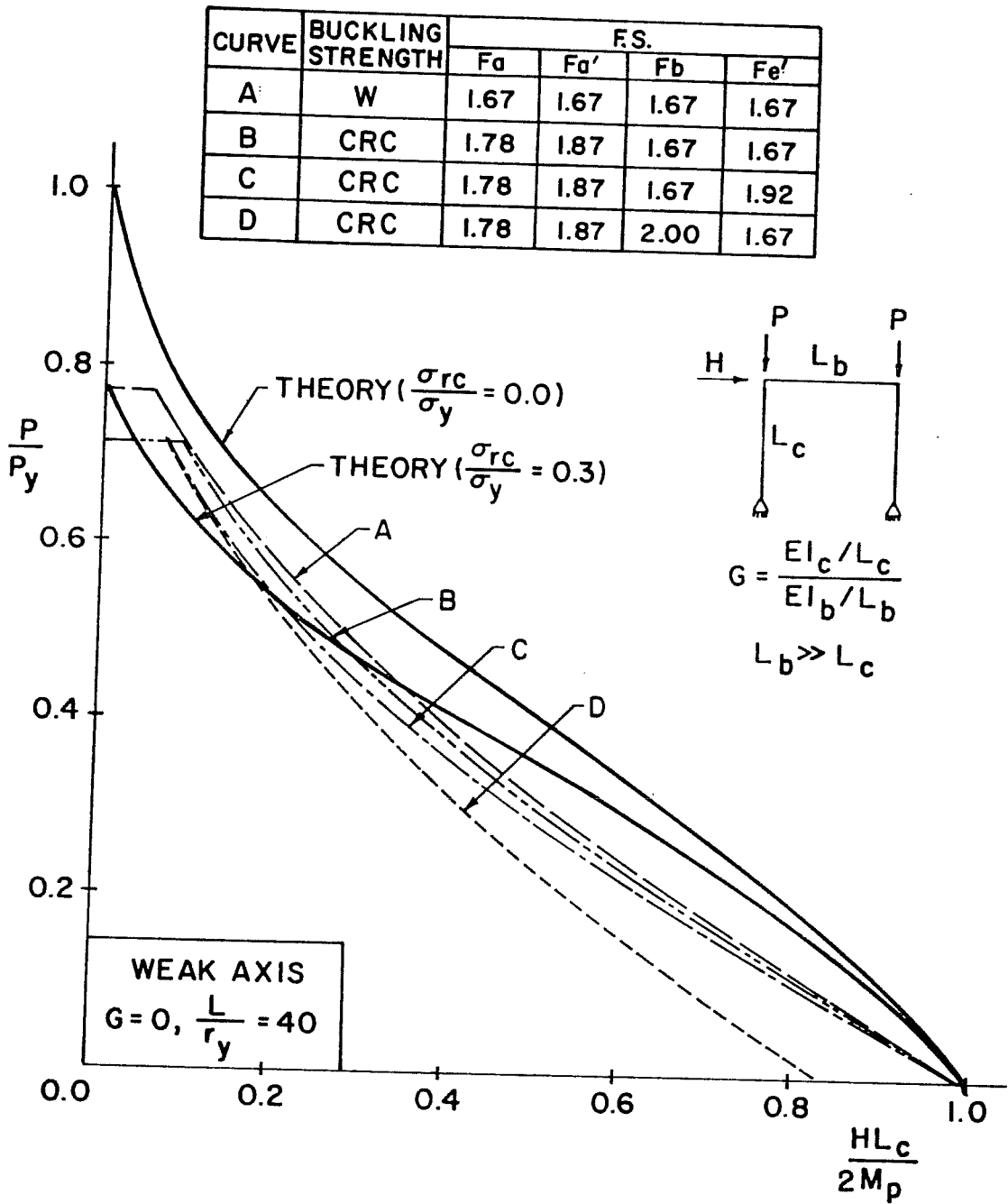


Fig. 2.51b Effect of variable factors of safety, effective length method ($G = 0, L_c/r_y = 40$, weak axis bending)

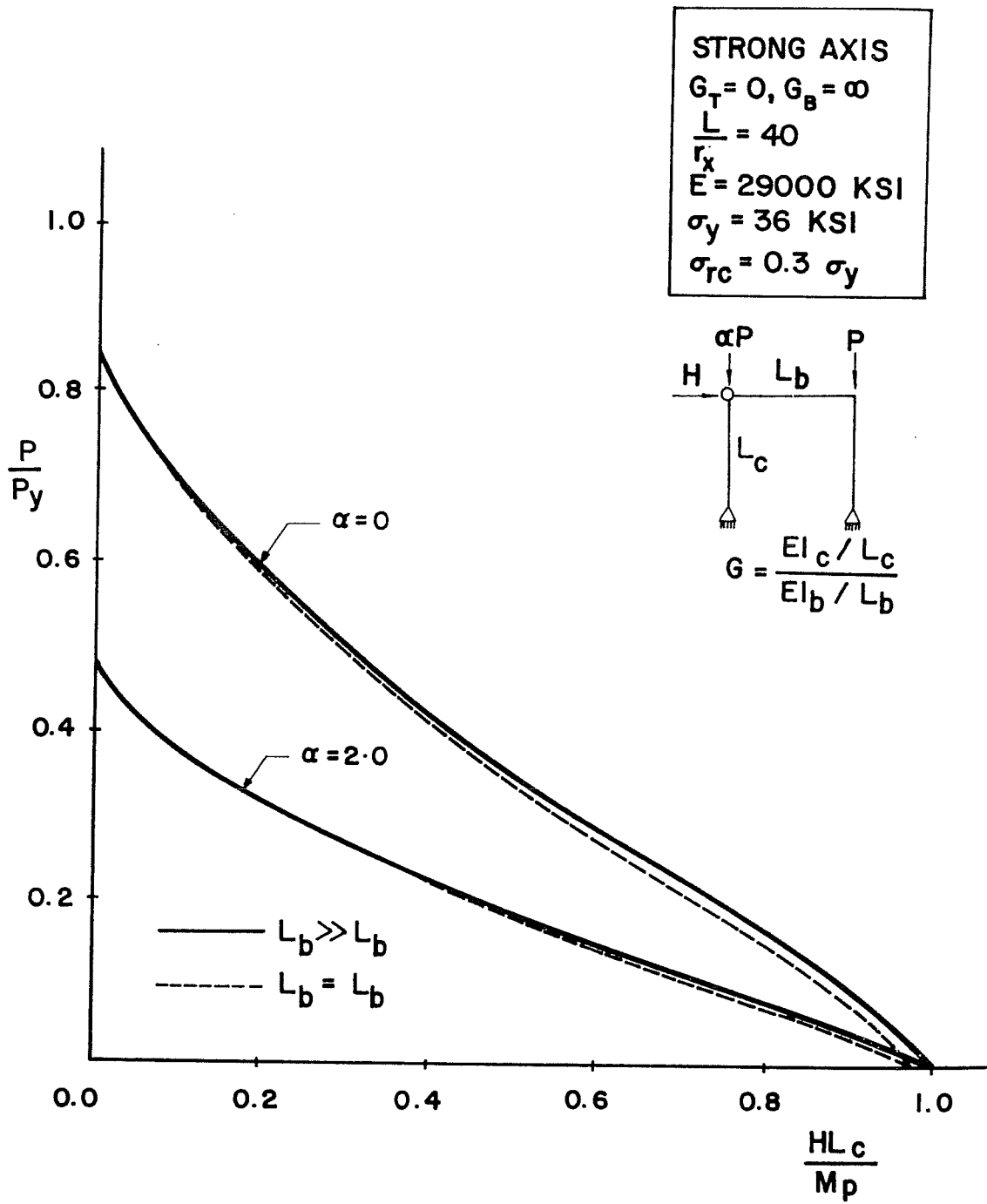


Fig. 2.52 Effect of beam length on maximum strength curves

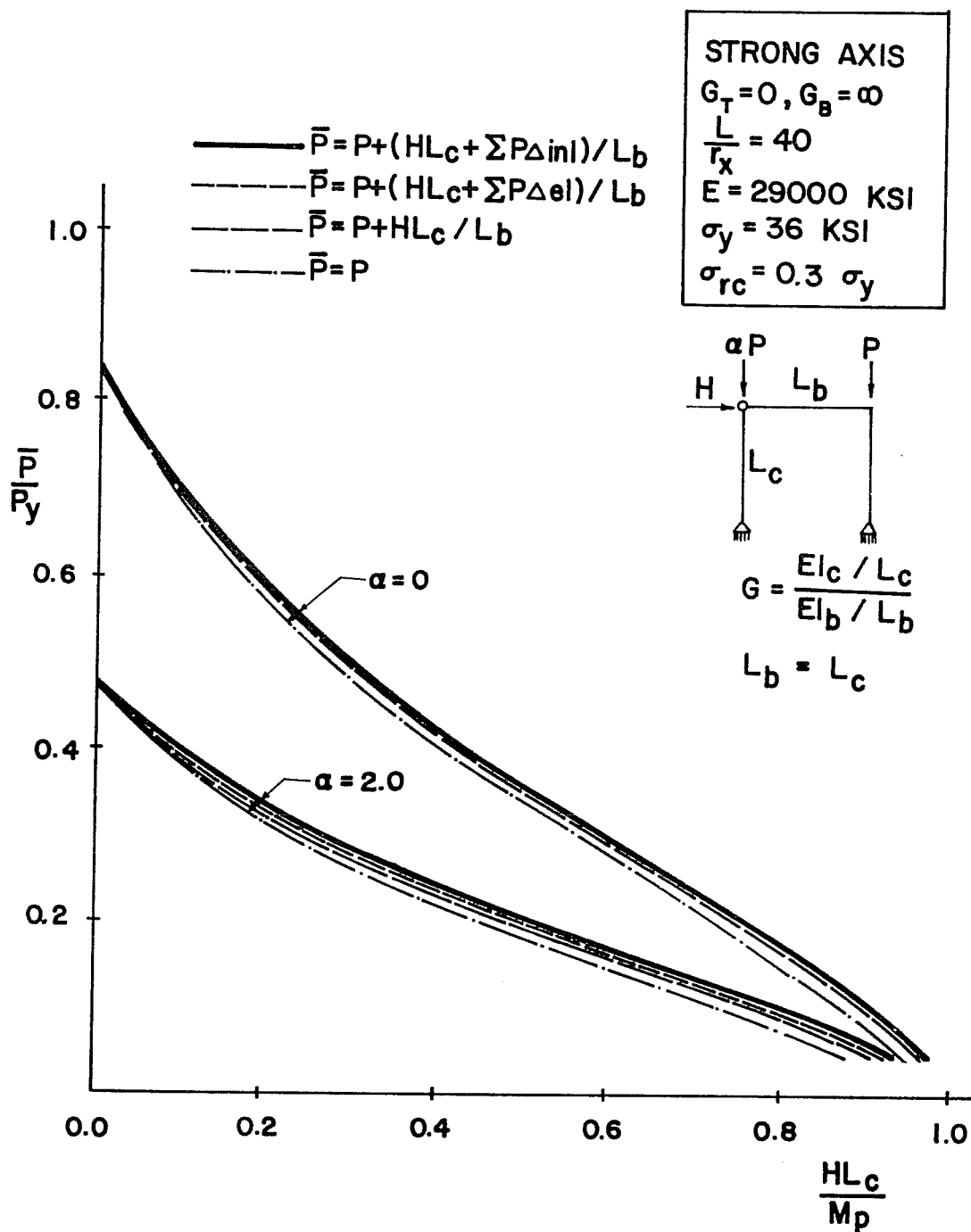


Fig. 2.53 Effect of axial load definitions on maximum strength curves

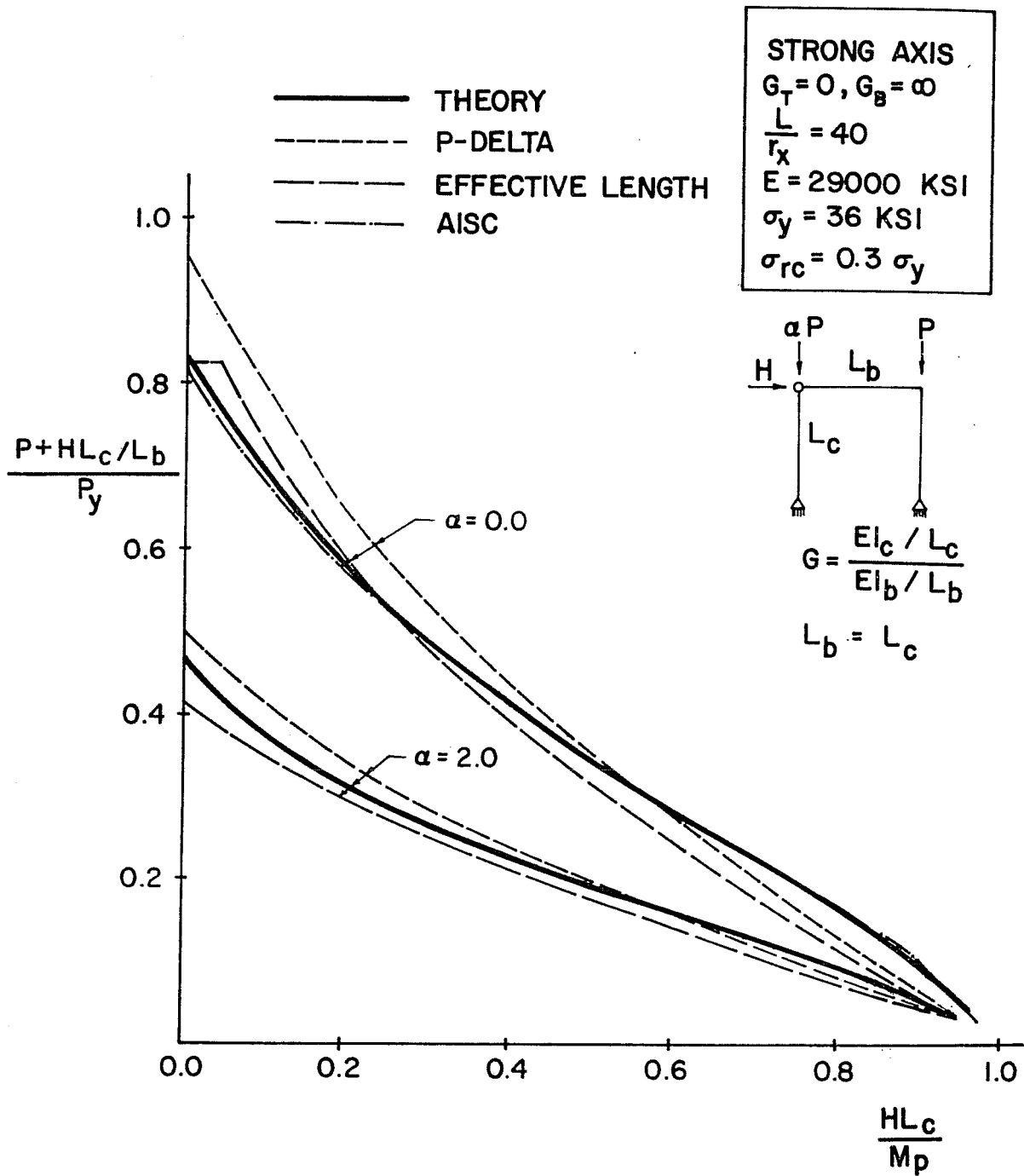
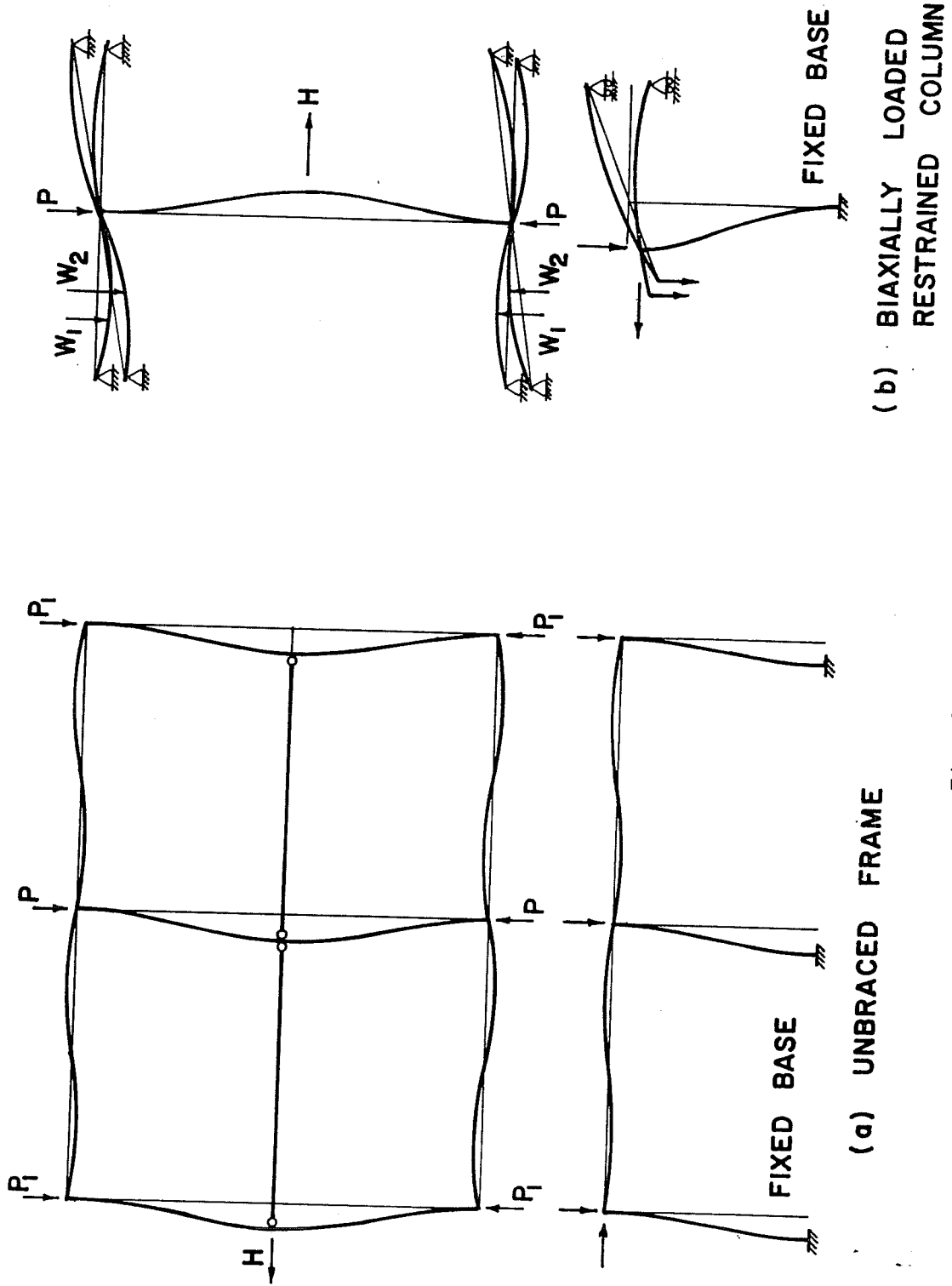


Fig. 2.54 Typical comparison of design interaction equations for beam-columns in frames with finite beam length



(a) UNBRACED FRAME

(b) BIAXIALLY LOADED RESTRAINED COLUMN

Fig. 3.1 Test arrangement

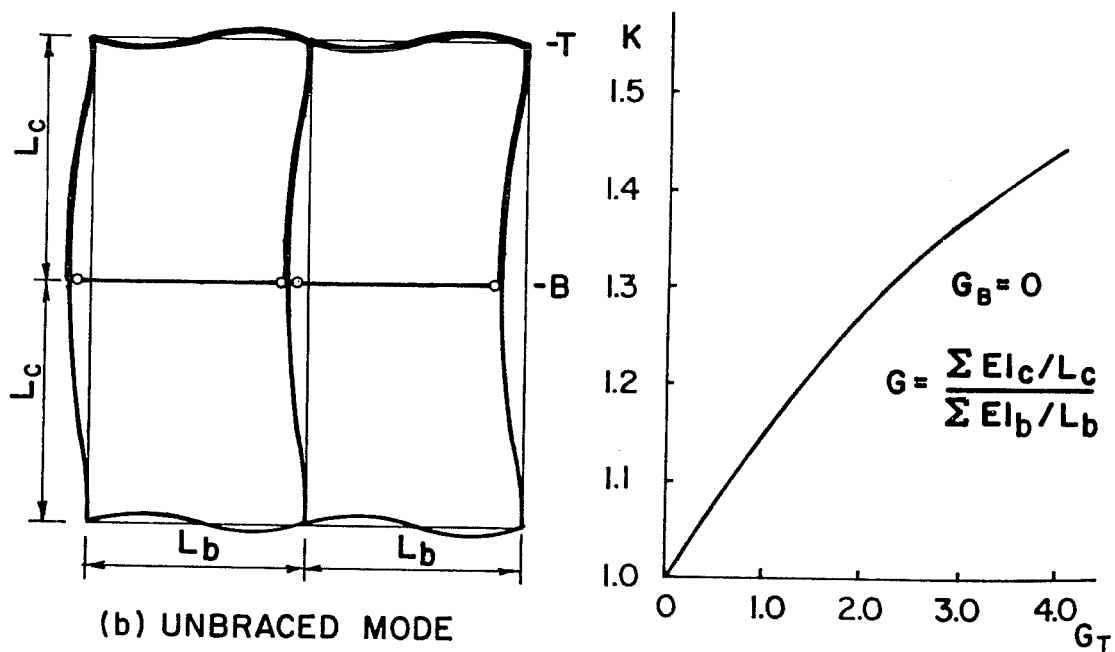
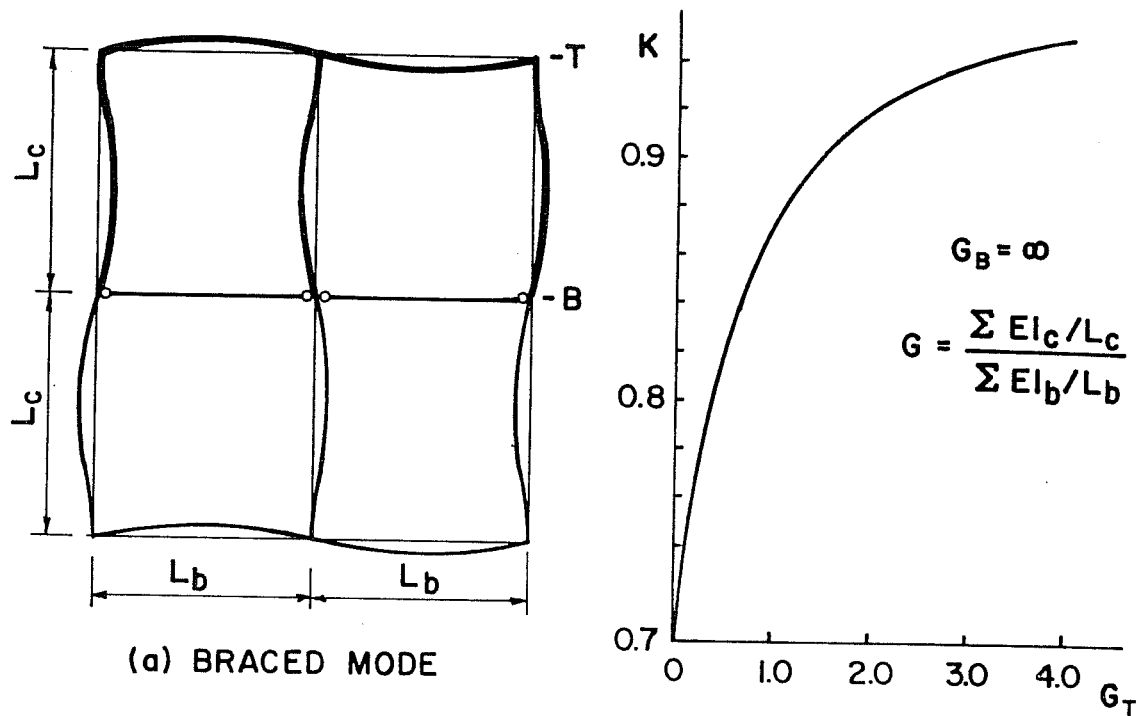


Fig. 3.2 Two-bay frame buckling in braced and unbraced modes

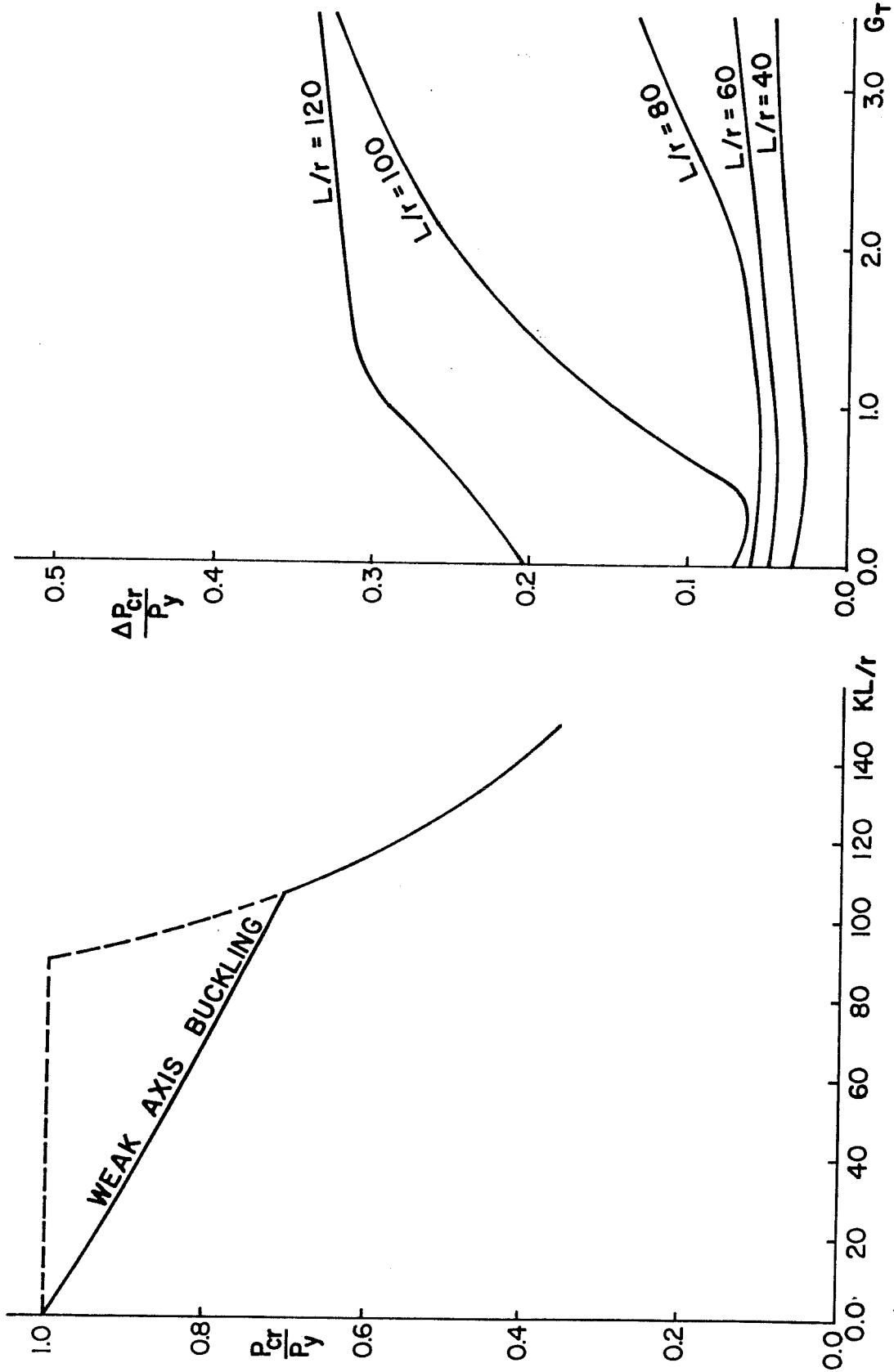


Fig. 3.3 Selection of L_c/r and G for unbraced frame specimens

ALL MEMBERS BENT ABOUT WEAK AXIS

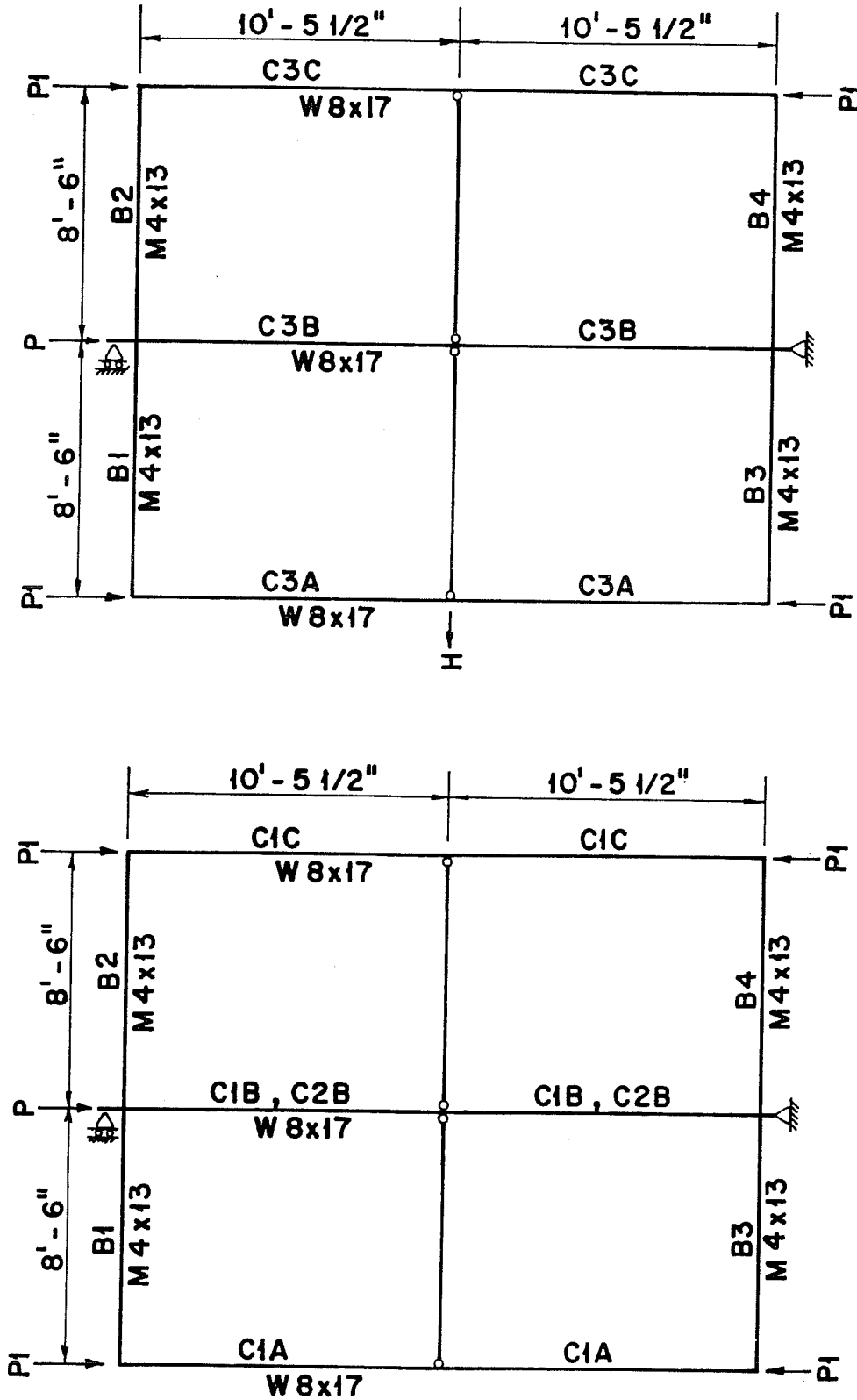


Fig. 3.4 Test program for unbraced frames

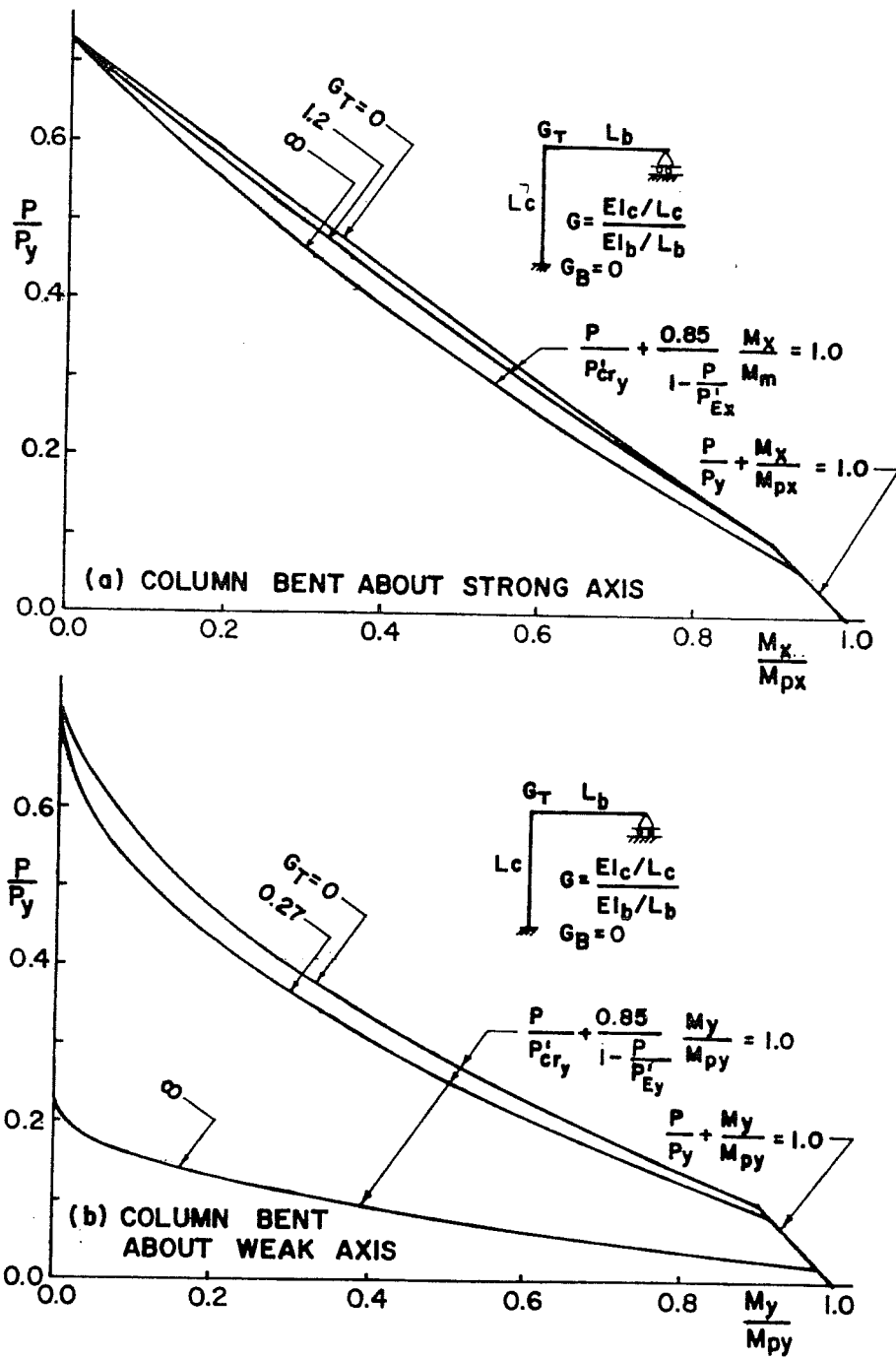


Fig. 3.5 Selection of biaxially loaded restrained beam-column specimens

BEAMS BENT ABOUT STRONG AXIS

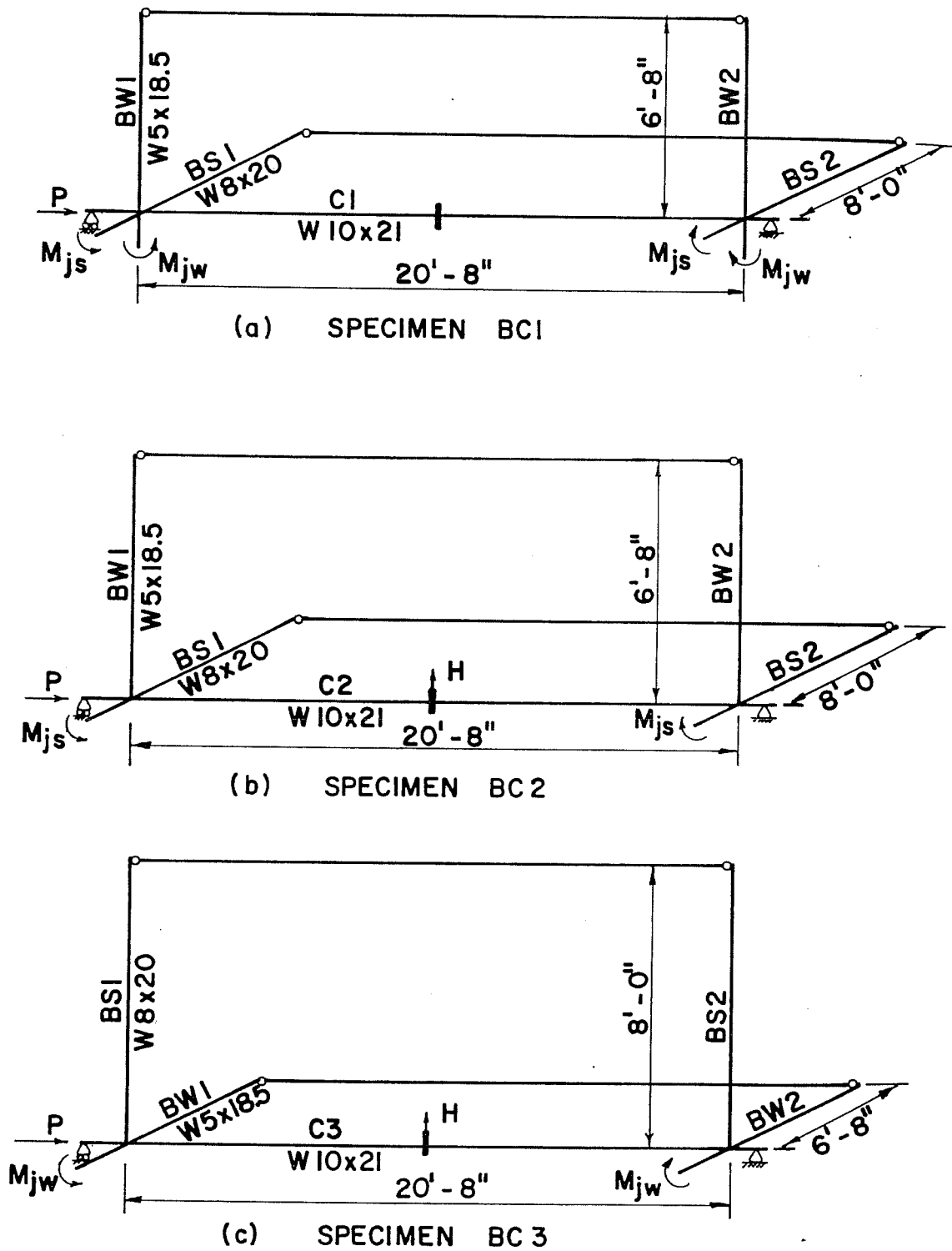


Fig. 3.6 Test program for biaxially loaded restrained beam-columns

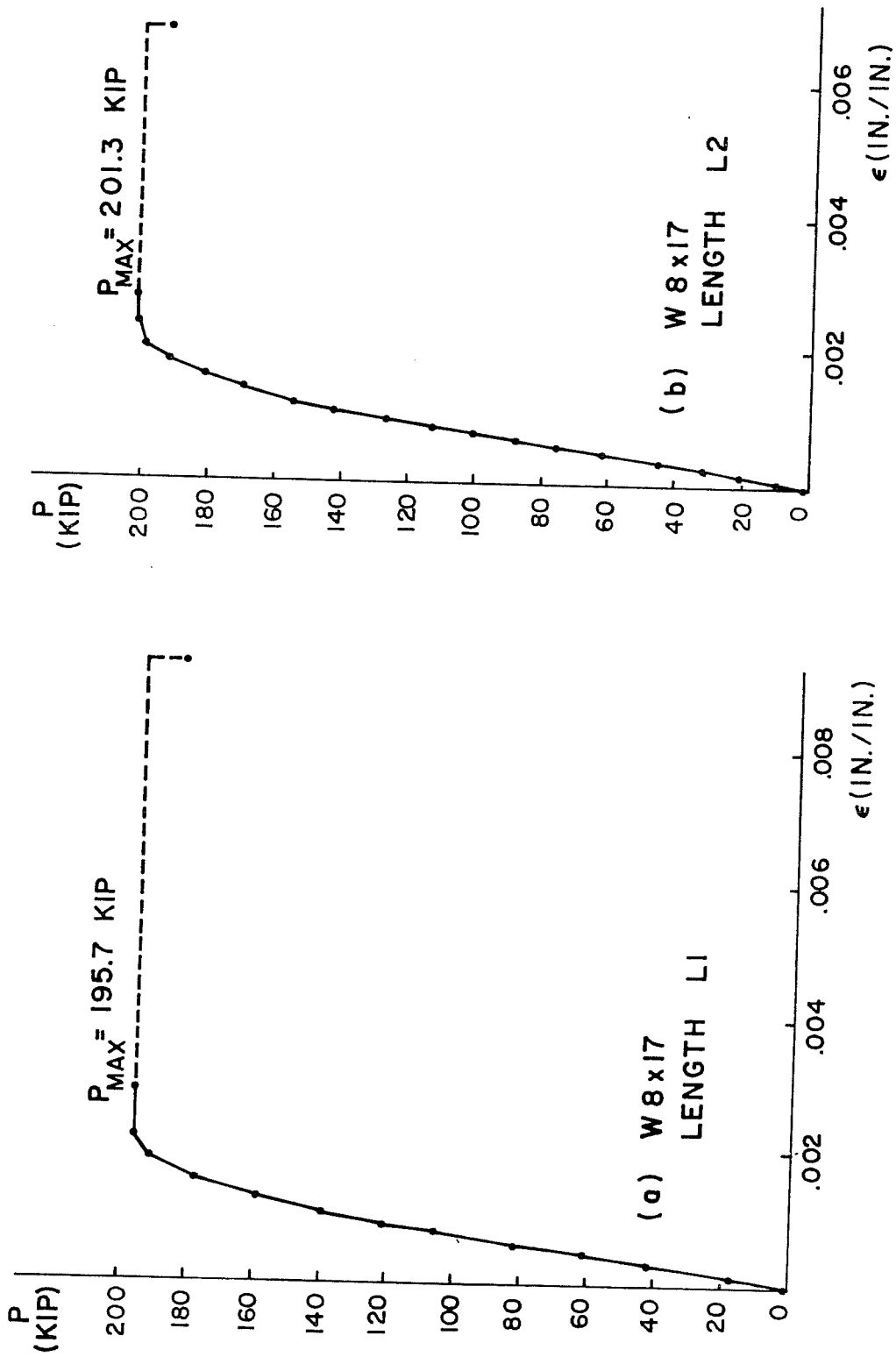


Fig. 3.7 Stub column test results

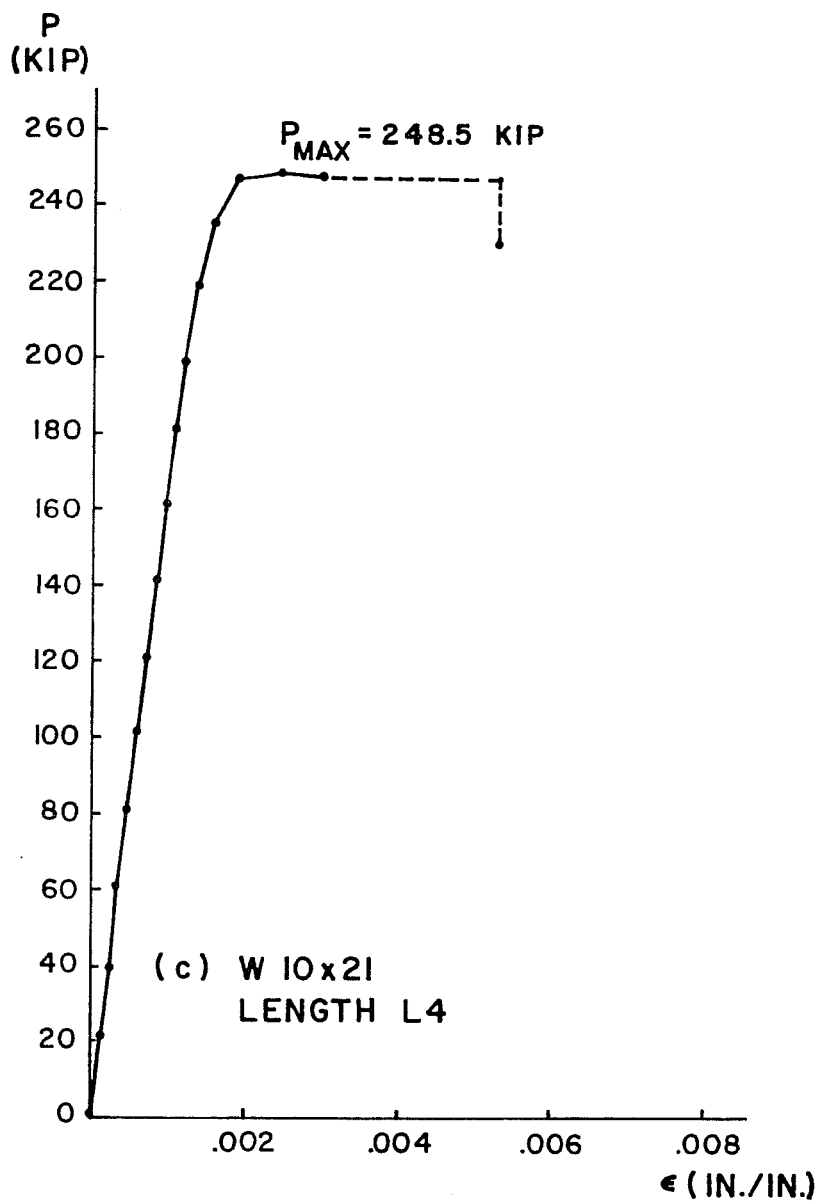
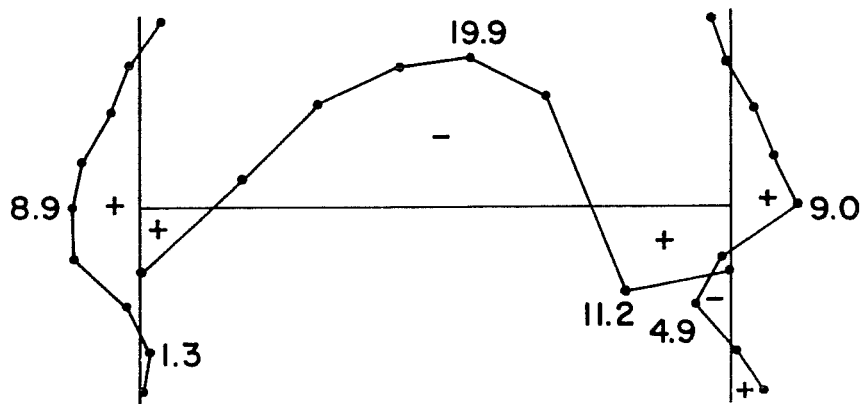
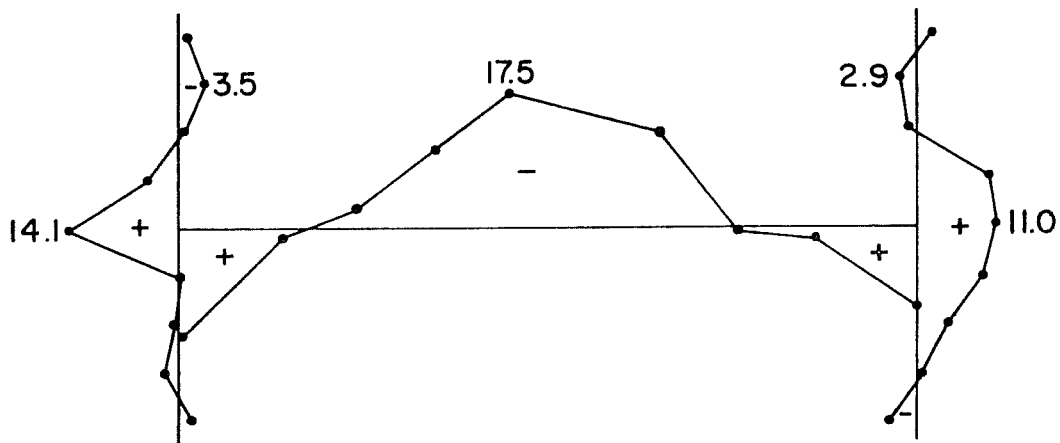


Fig. 3.7 (Continued)



W 8 x 17, LENGTH L2

-10 0 +10 (ksi)
 COMPRESSION TENSION



W 10 x 21, LENGTH L4

Fig. 3.8 Residual stress patterns

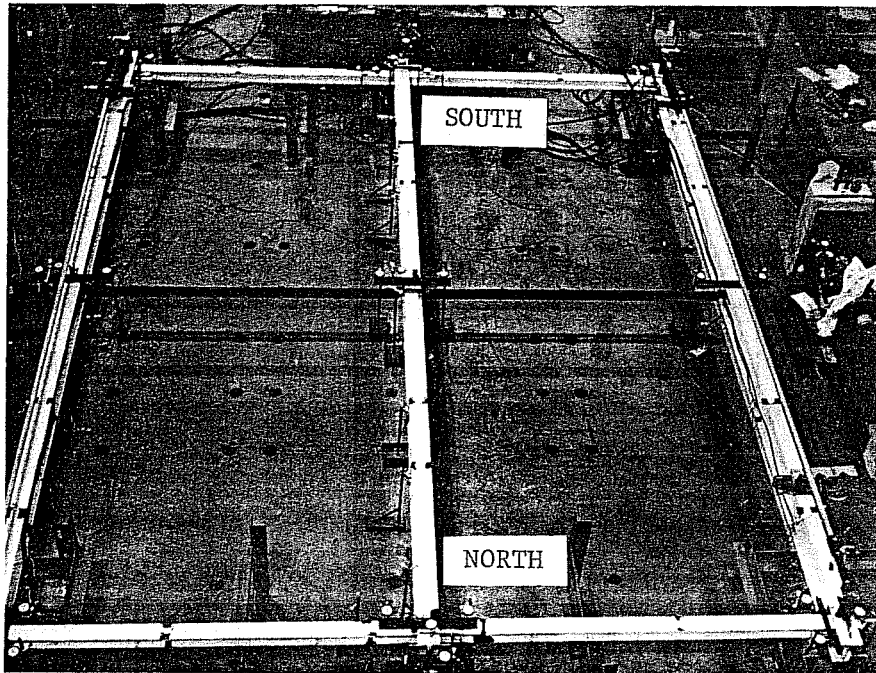


Fig. 4.1 General view of test setup

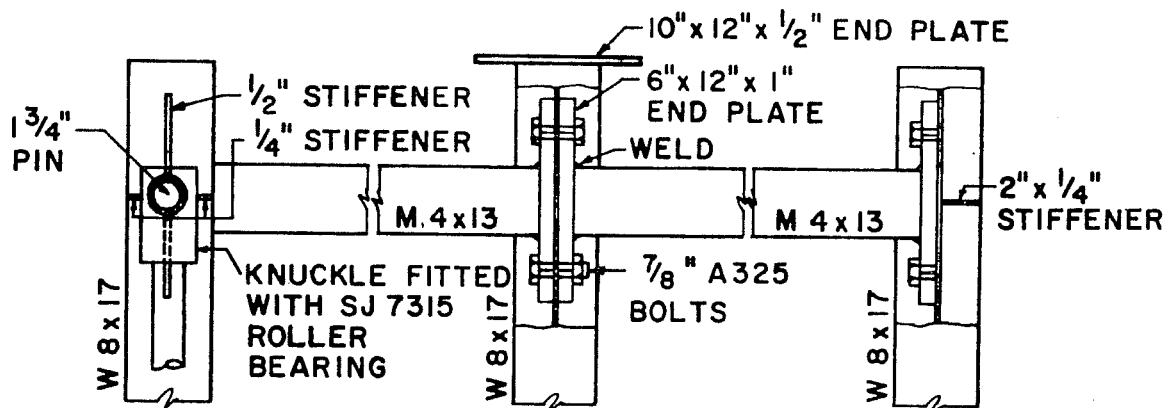


Fig. 4.2 Beam-to-column connection details

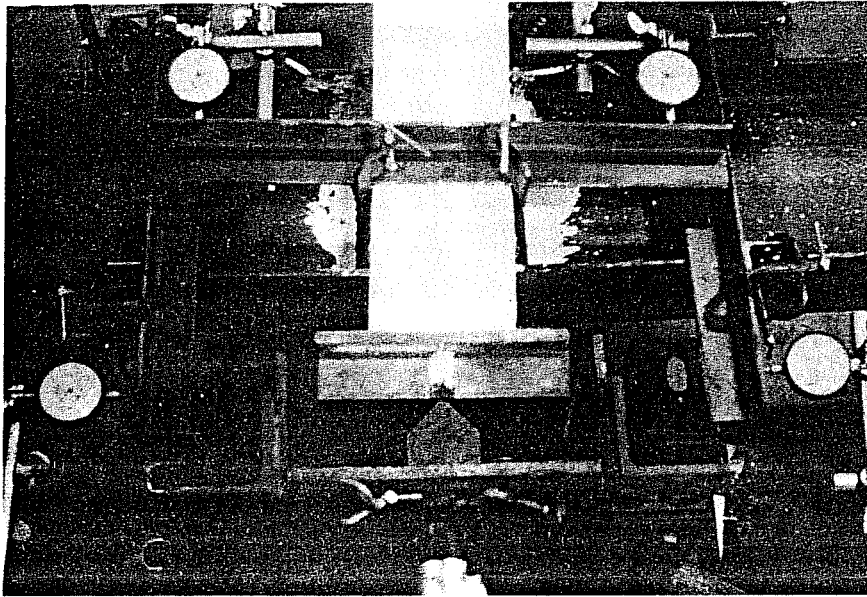


Fig. 4.3 Knife-edge support of interior column

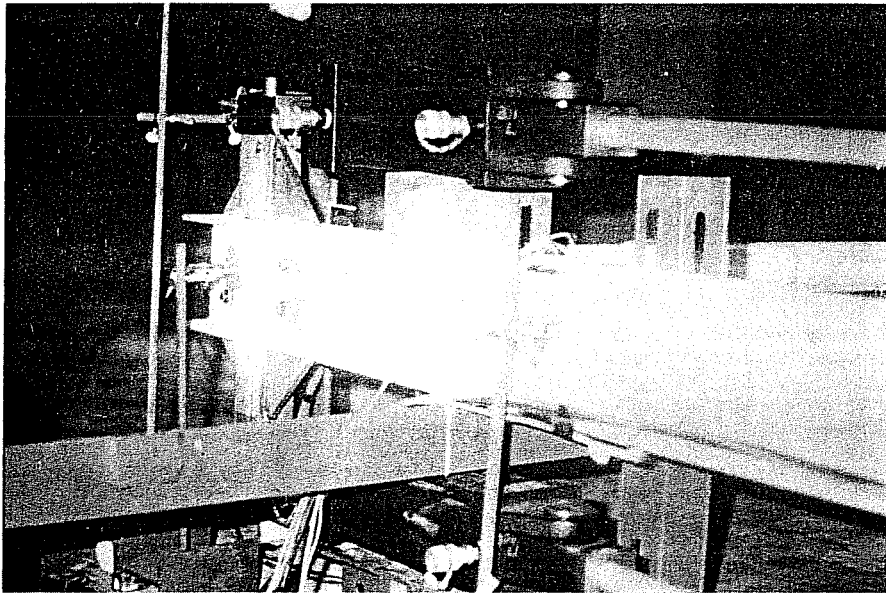


Fig. 4.4 Loading system for exterior columns

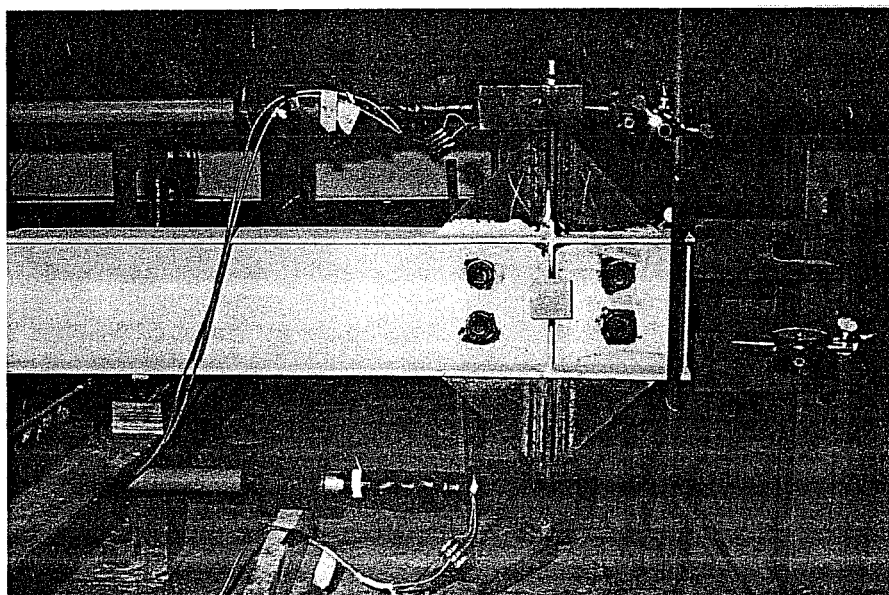


Fig. 4.5 Tension load cells for exterior columns

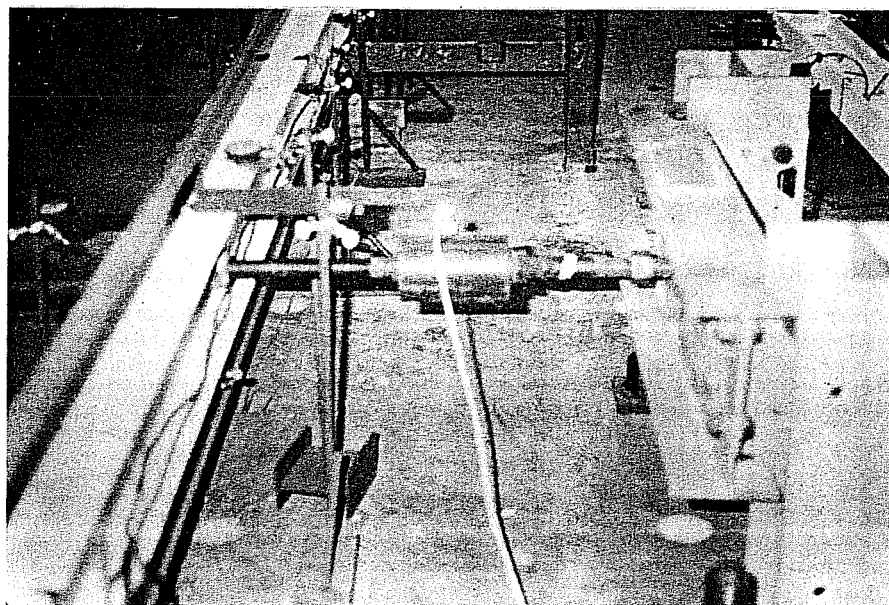
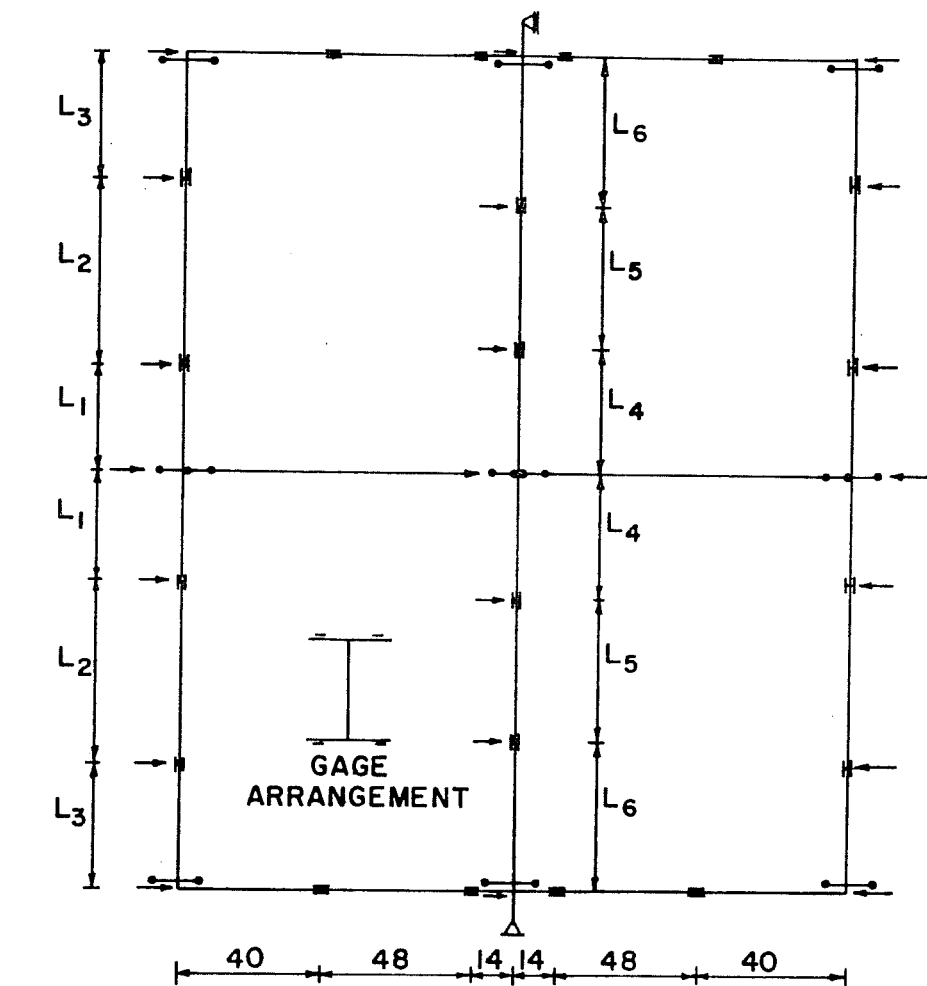


Fig. 4.6 Lateral loading system



LEGEND

- ▬ STRAIN GAGES
- DIAL GAGE
- ROTATION ARM

SPECIMEN	L ₁	L ₂	L ₃	L ₄	L ₅	L ₆
F1	30	66	29.5	42	48	35.5
F2	30	66	29.5	44	44	37.5
F3	52	40	33.5	52	24	49.5

NOTE: 1. ALL UNITS IN INCHES
2. INSTRUMENTATION ARRANGEMENT IS SYMMETRICAL.

Fig. 4.7 Instrumentation diagram

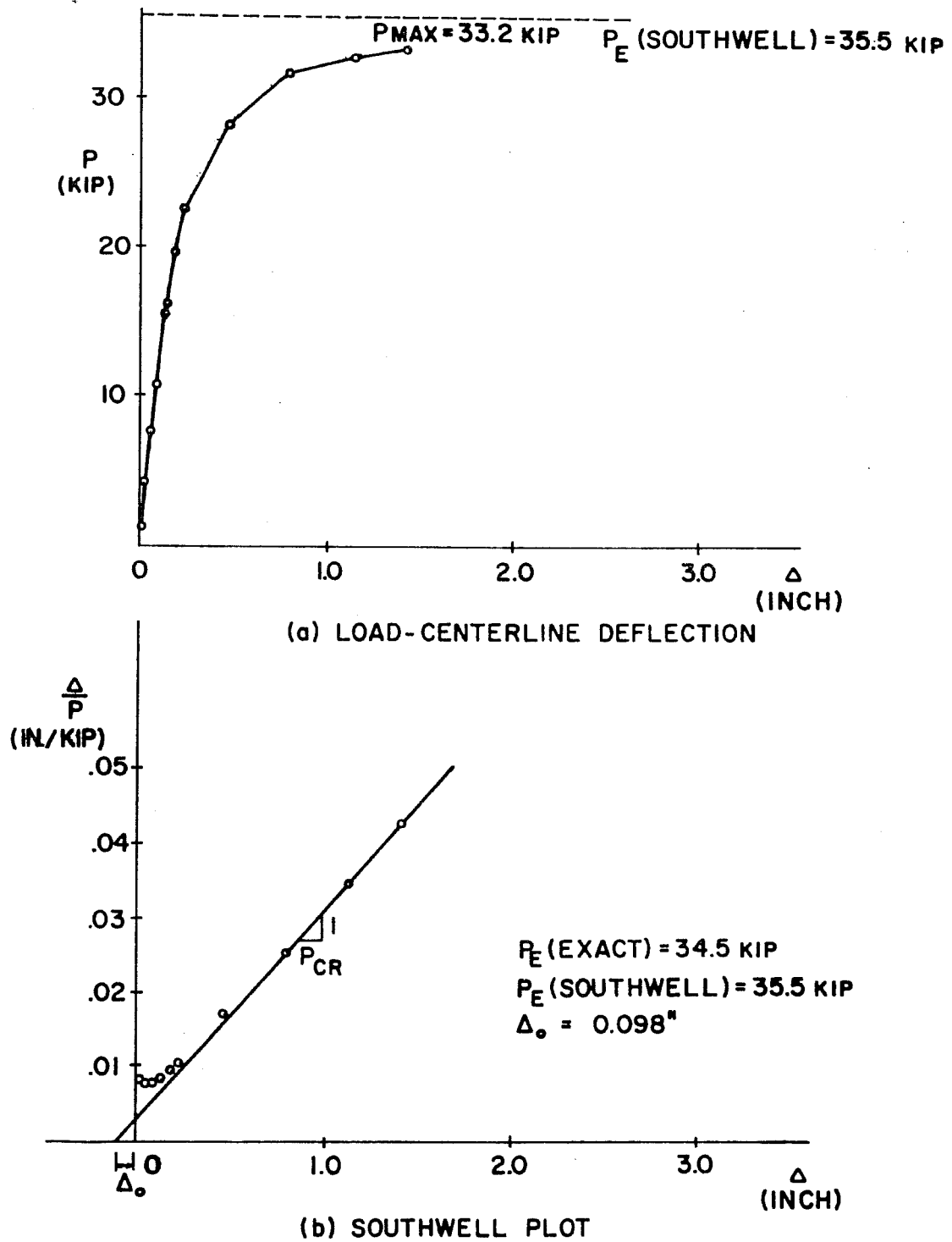


Fig. 4.8 Results of Euler test on column C1A

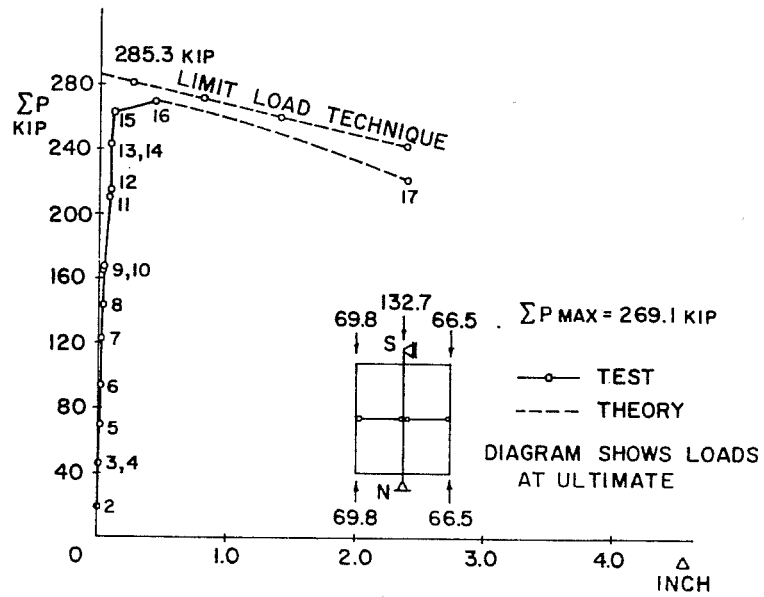


Fig. 4.9 Load-deflection relationship of Specimen F1

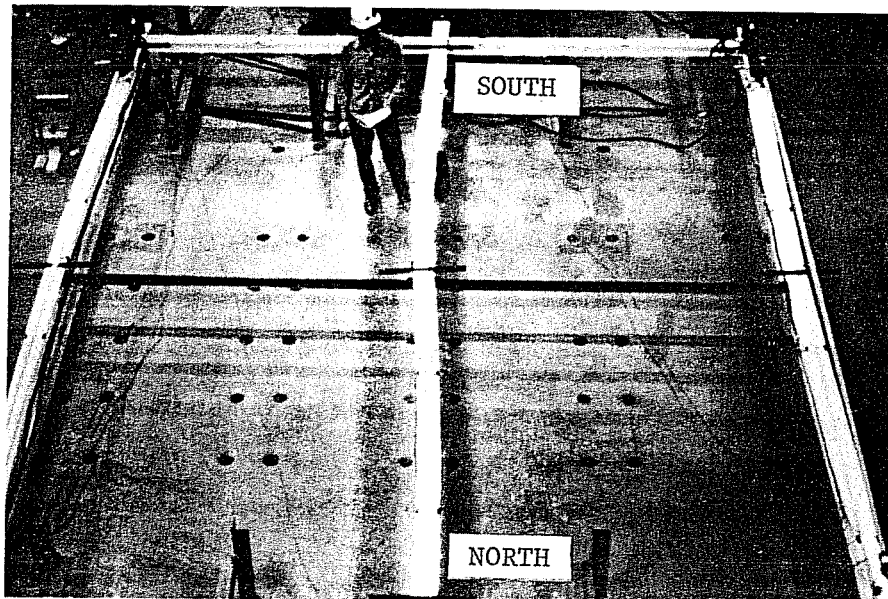


Fig. 4.10 Specimen F1 after failure

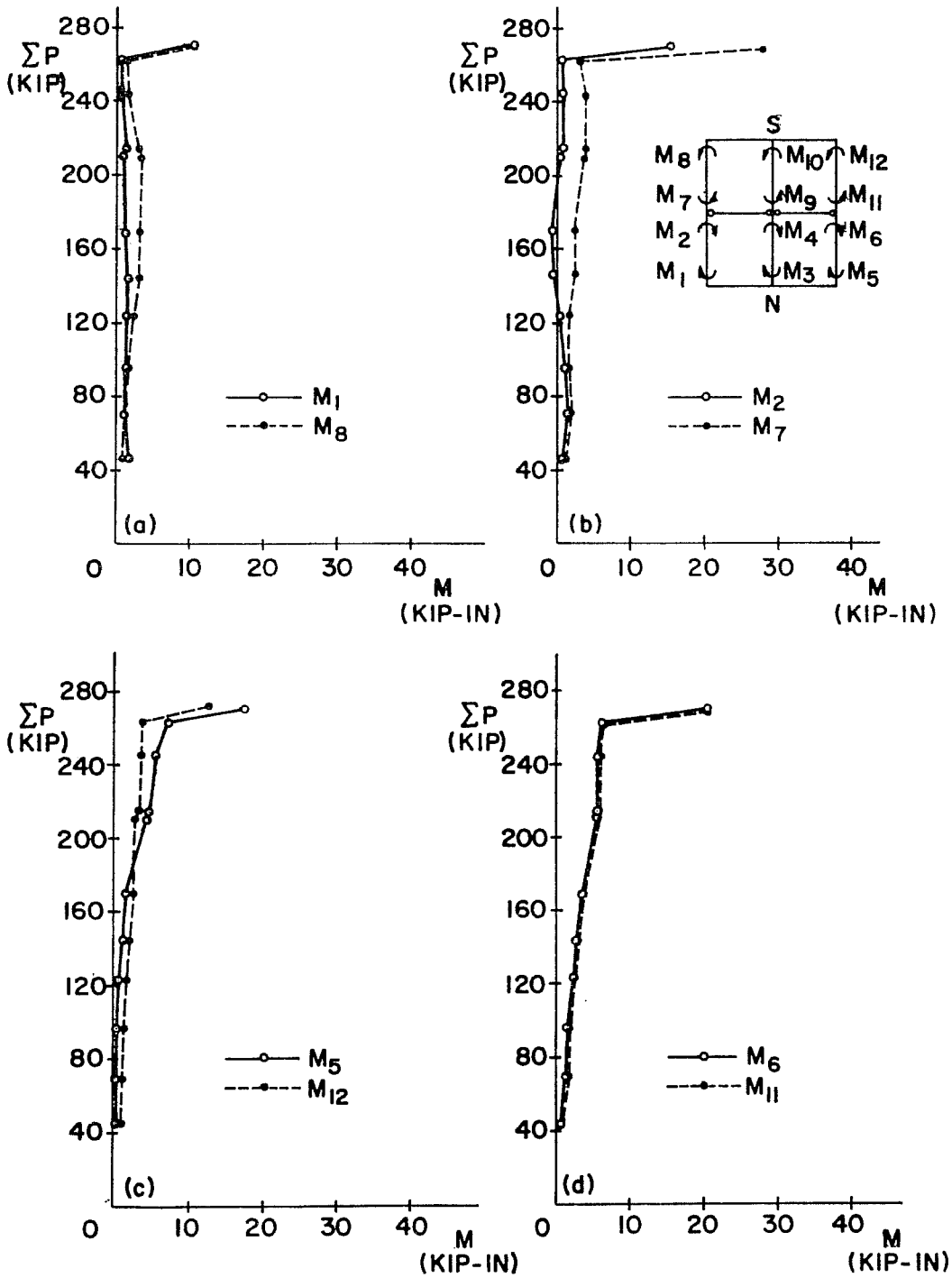


Fig. 4.11 Variation of column moments with axial loads (Specimen F1)

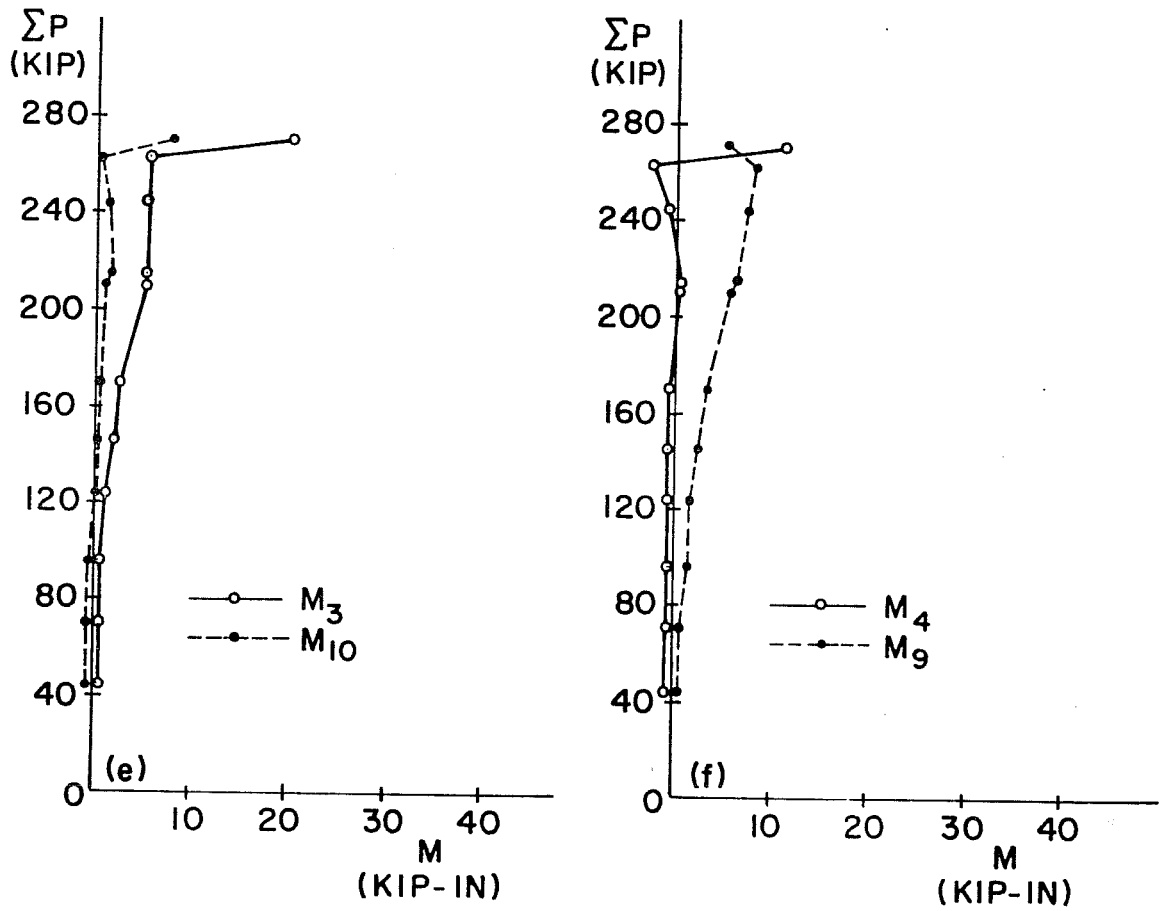


Fig. 4.11 (Continued)

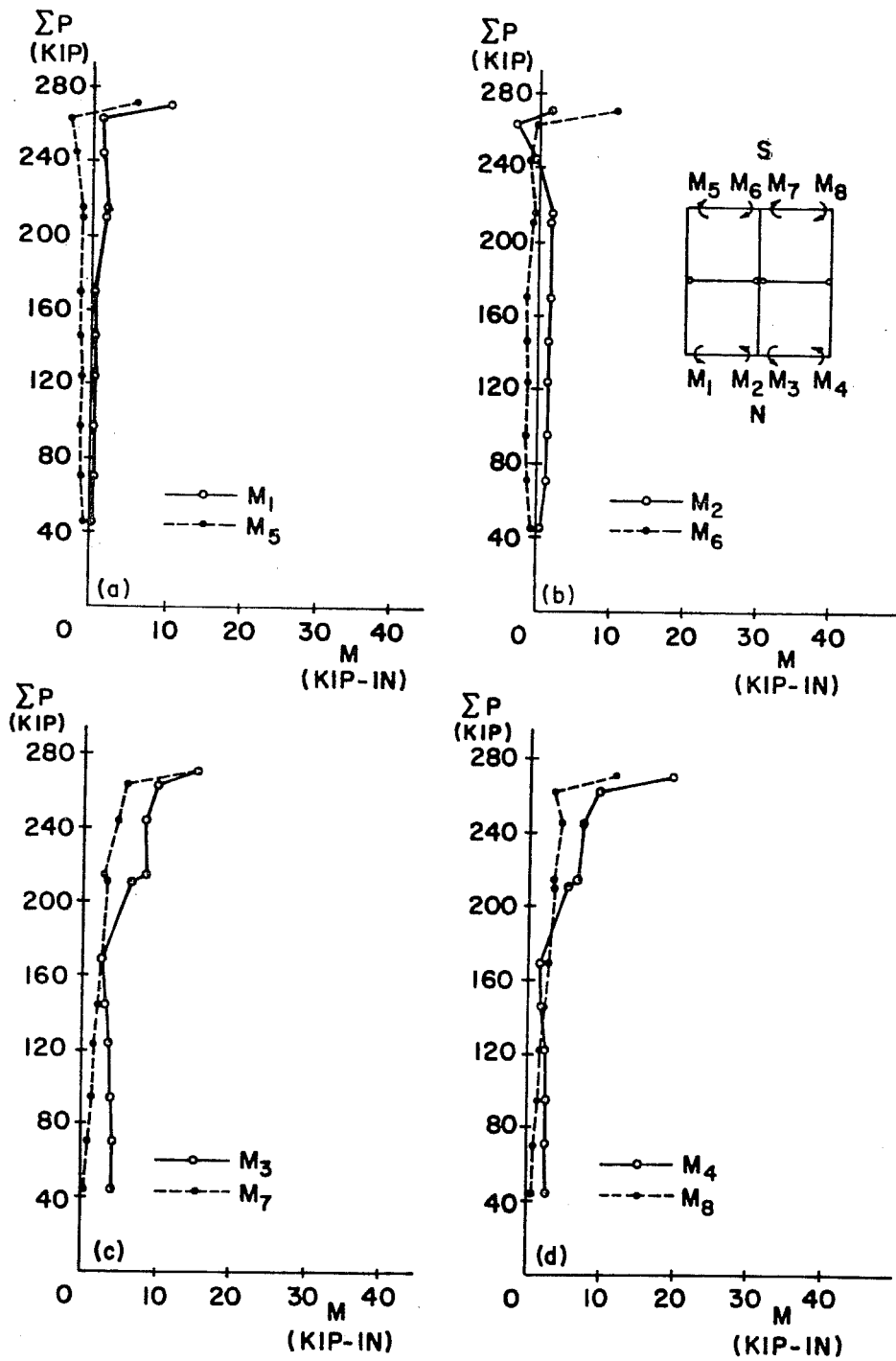


Fig. 4.12 Variation of beam moments with axial loads (Specimen F1)

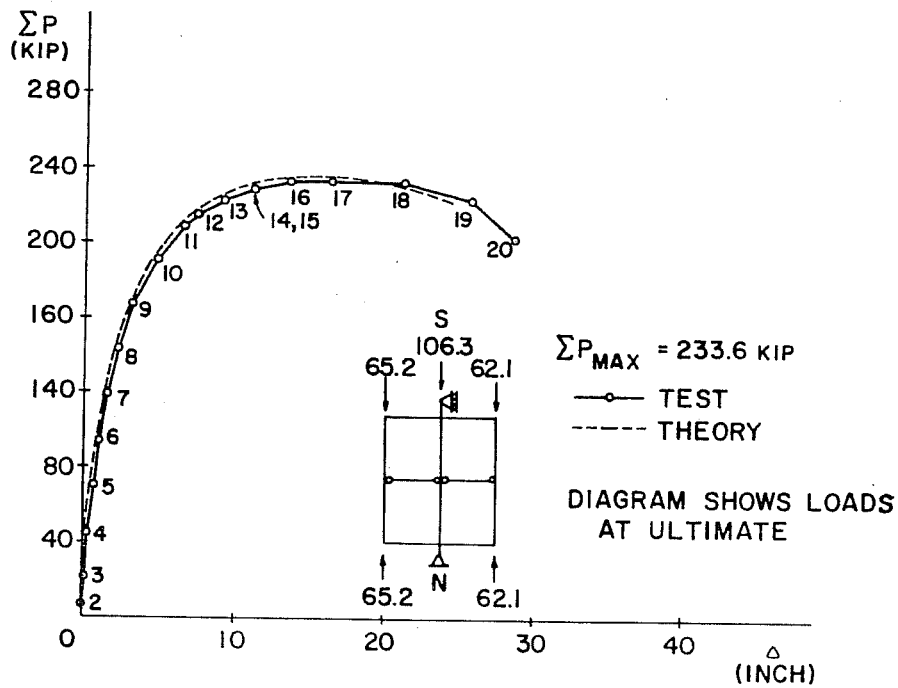


Fig. 4.13 Load-deflection relationship of Specimen F2

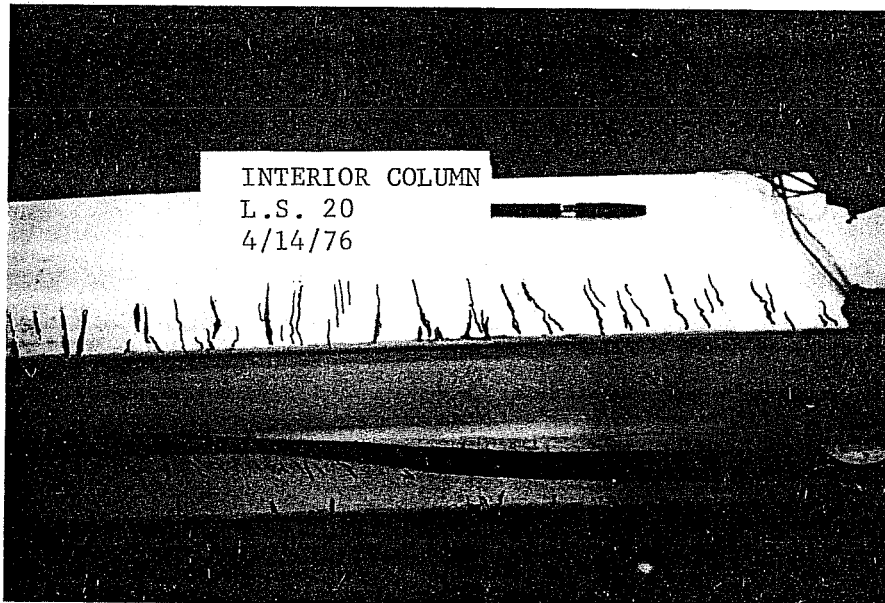


Fig. 4.14 Yielded zone at midlength region of interior column of Specimen F2

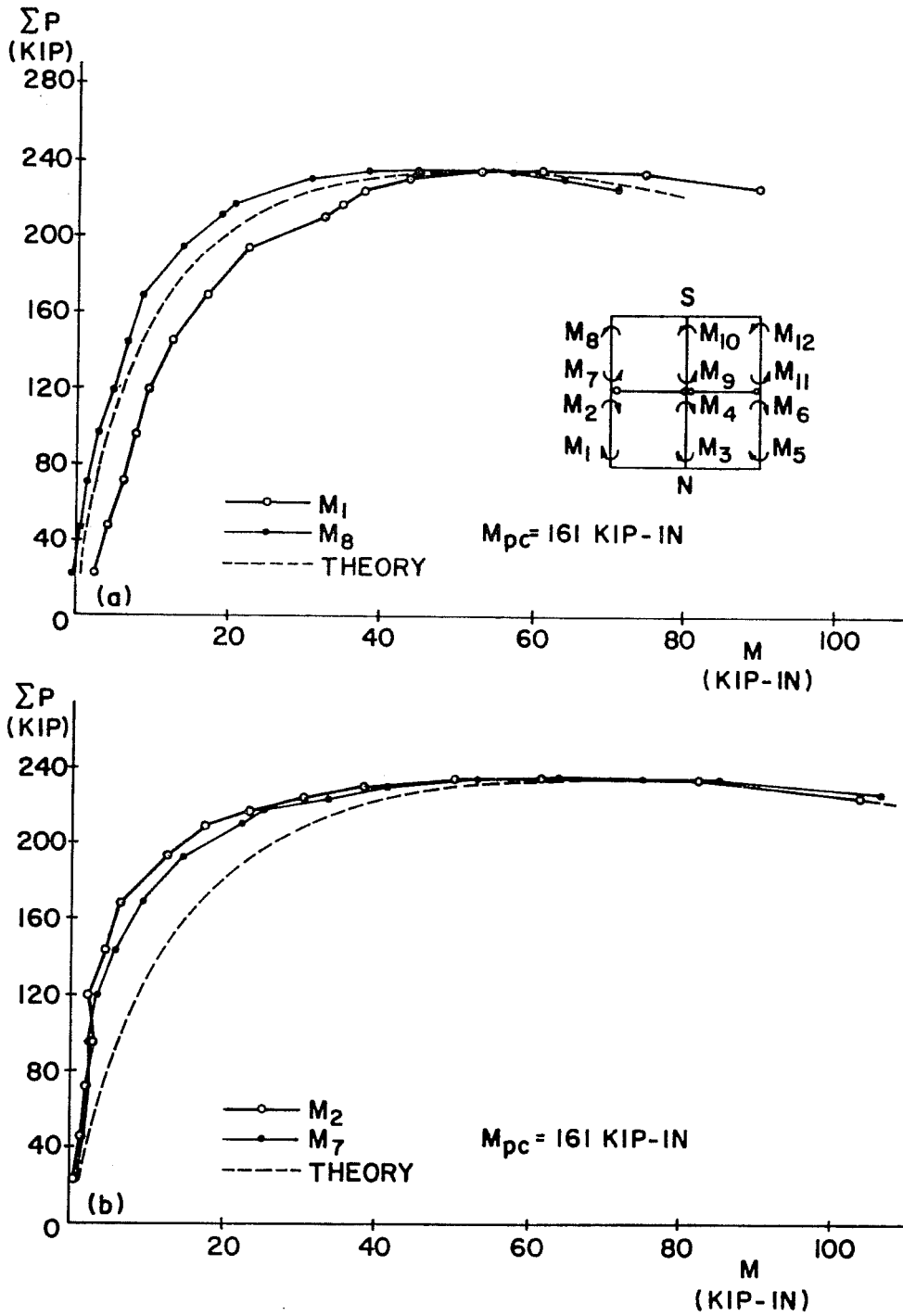


Fig. 4.15 Variation of column moments with axial loads (Specimen F2)

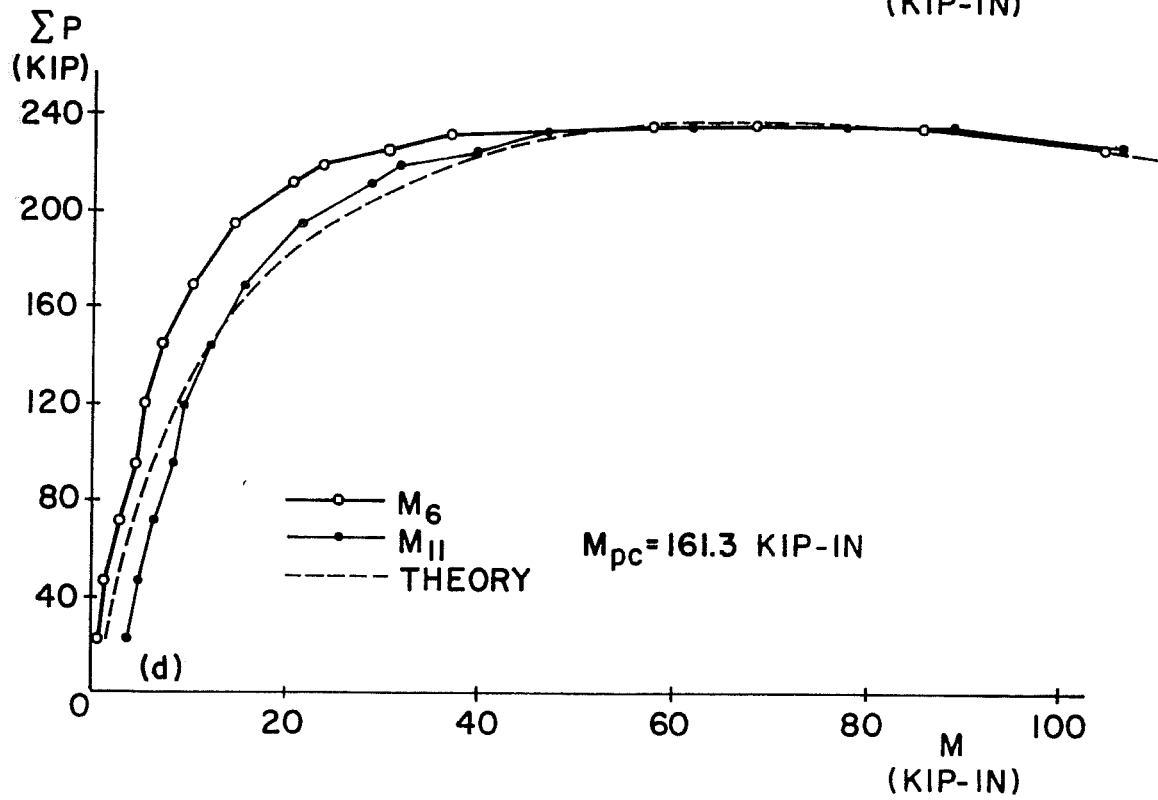
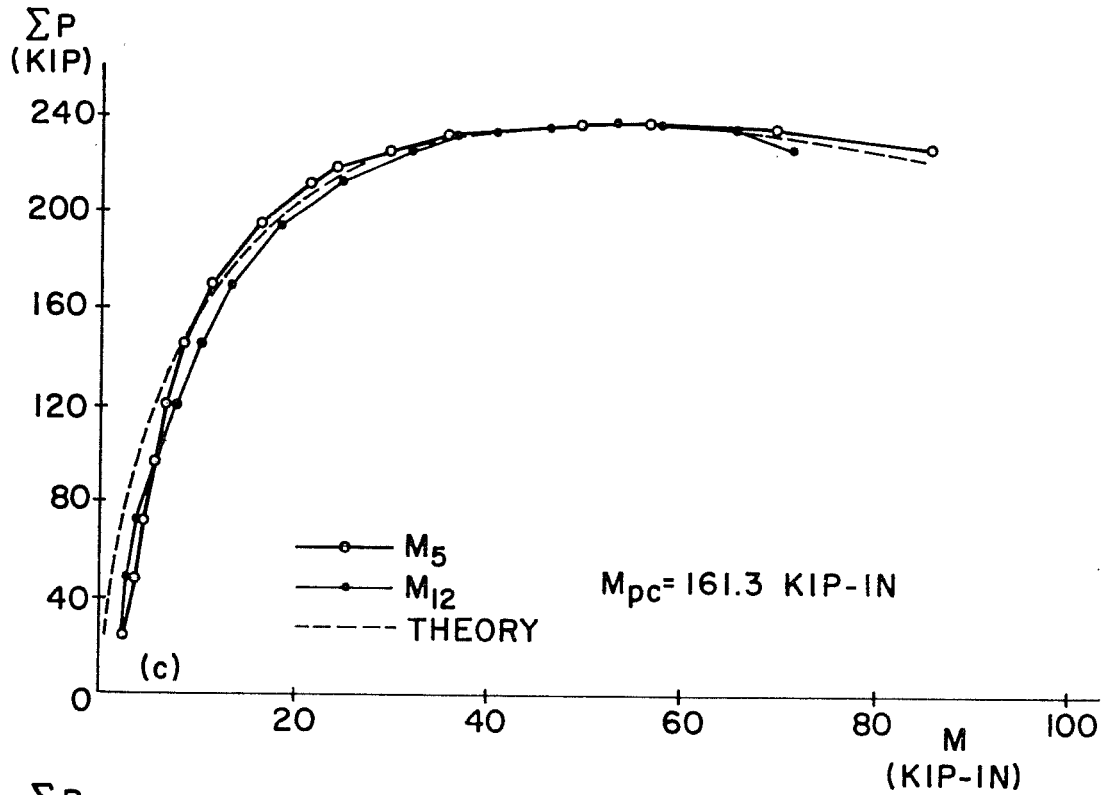


Fig. 4.15 (Continued)

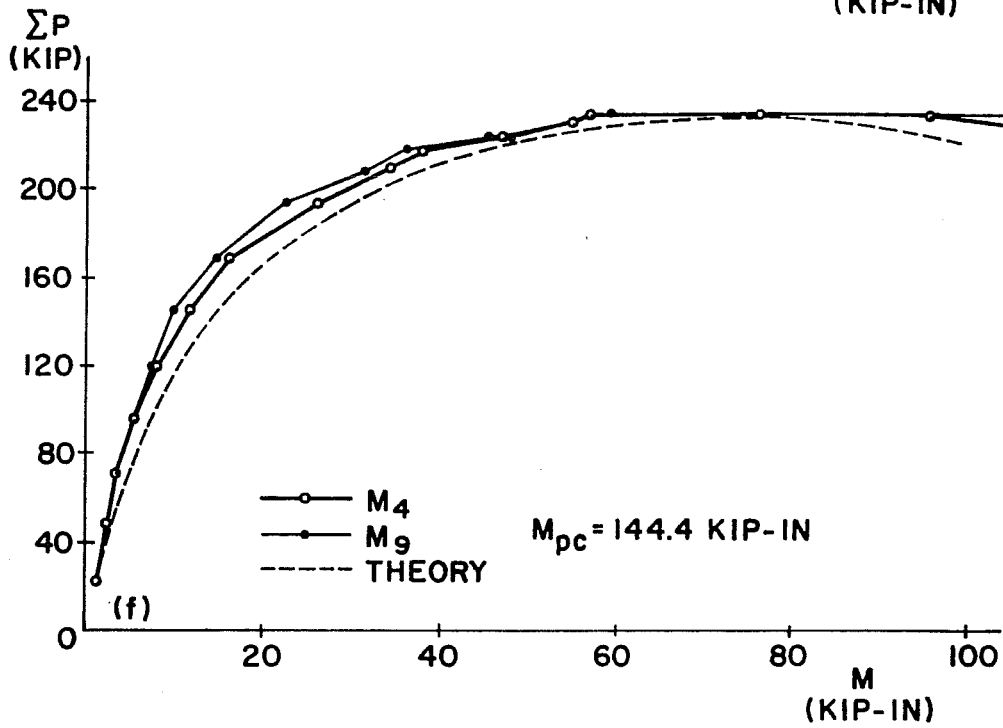
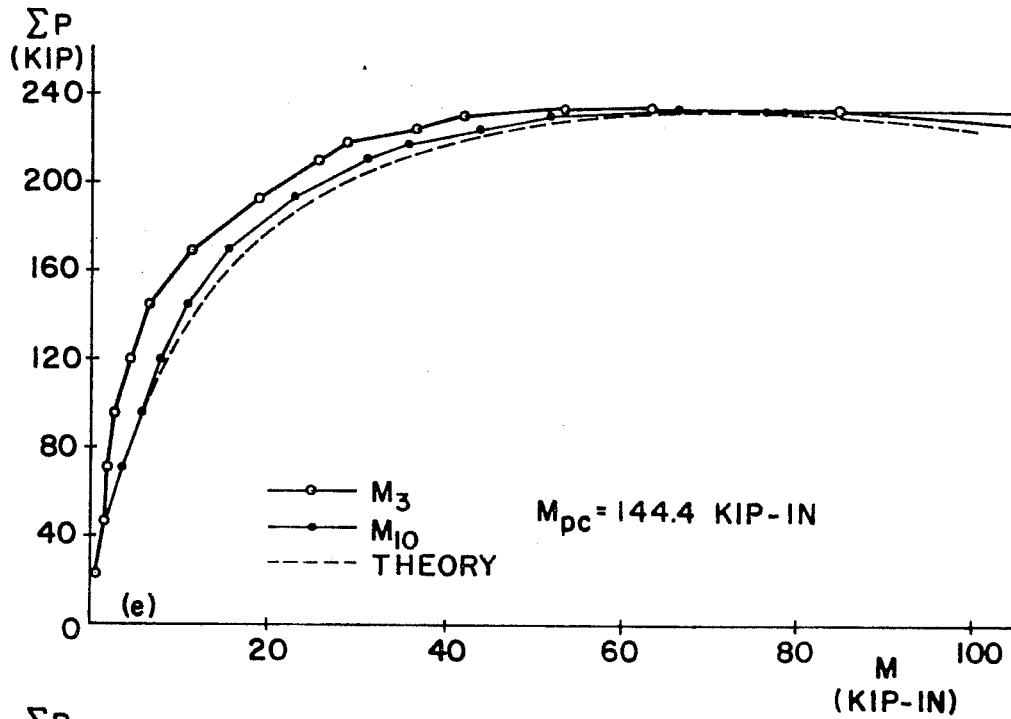


Fig. 4.15 (Continued)

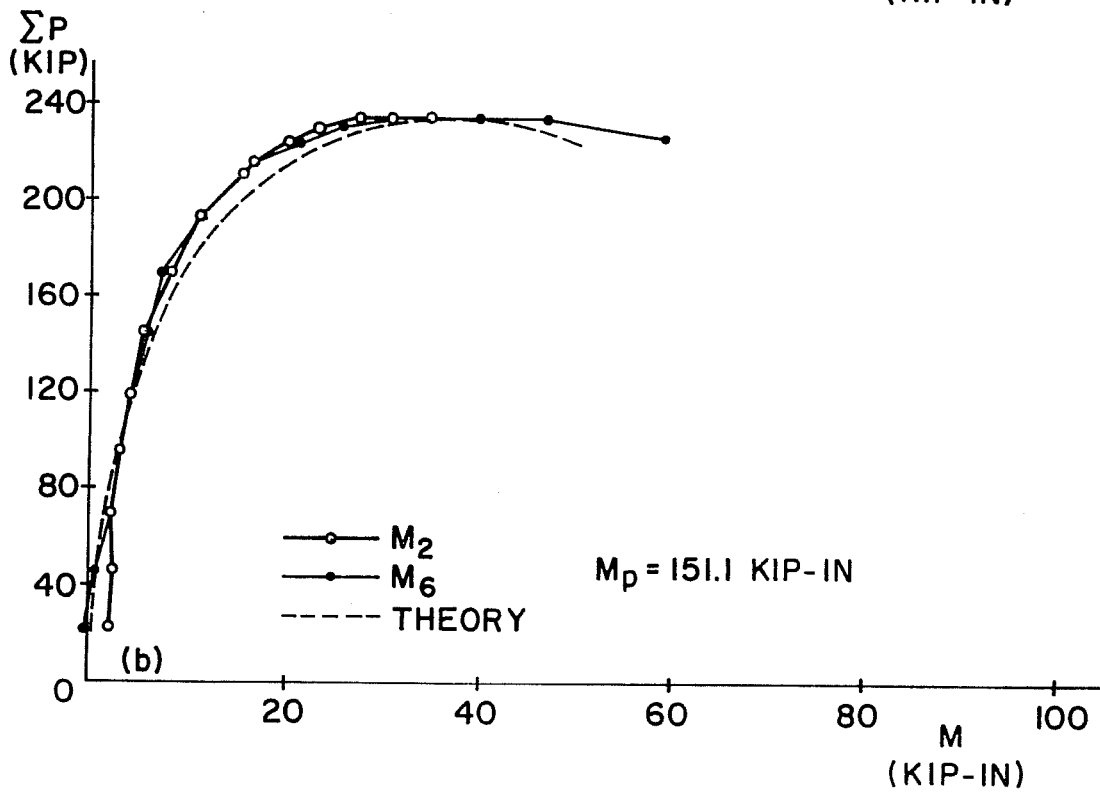
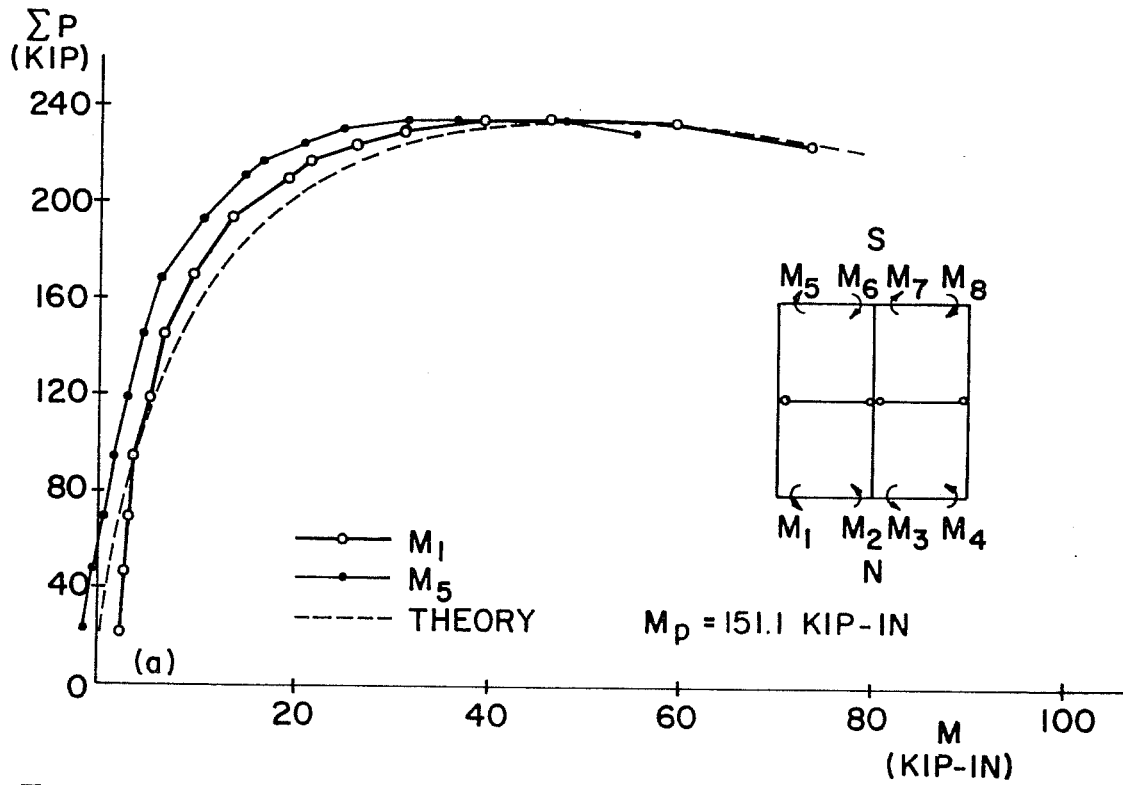


Fig. 4.16 Variation of beam moments with axial loads (Specimen F2)

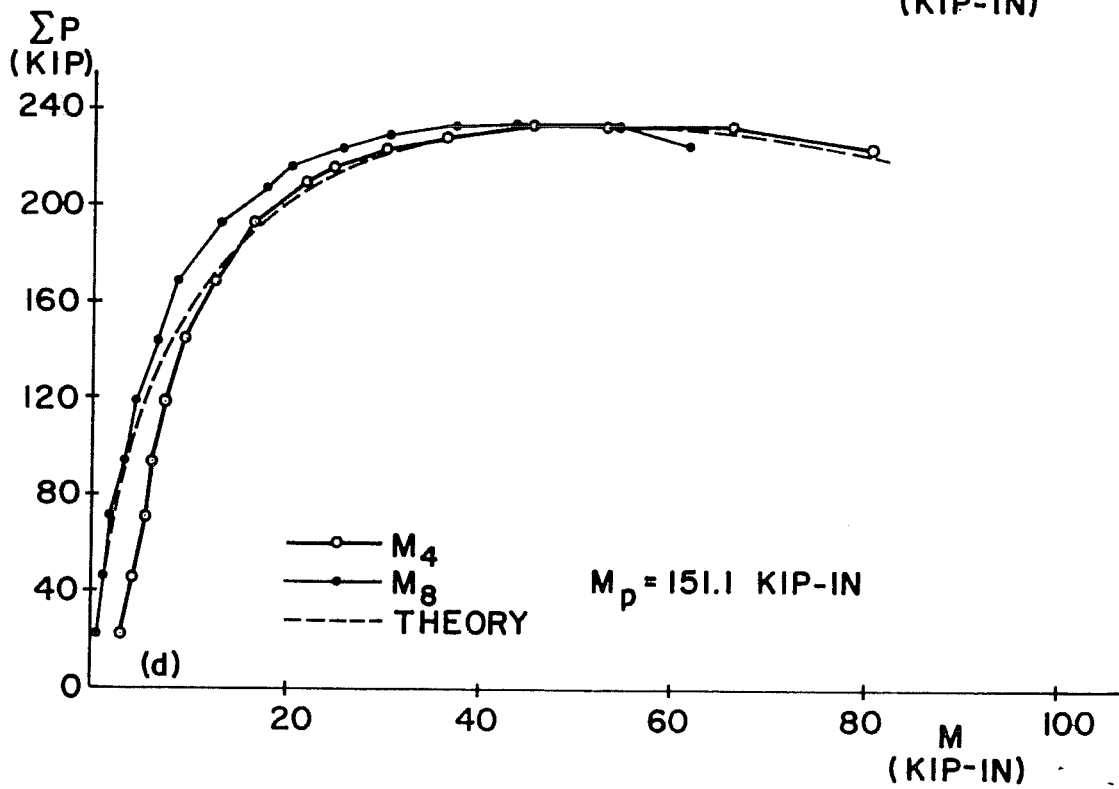
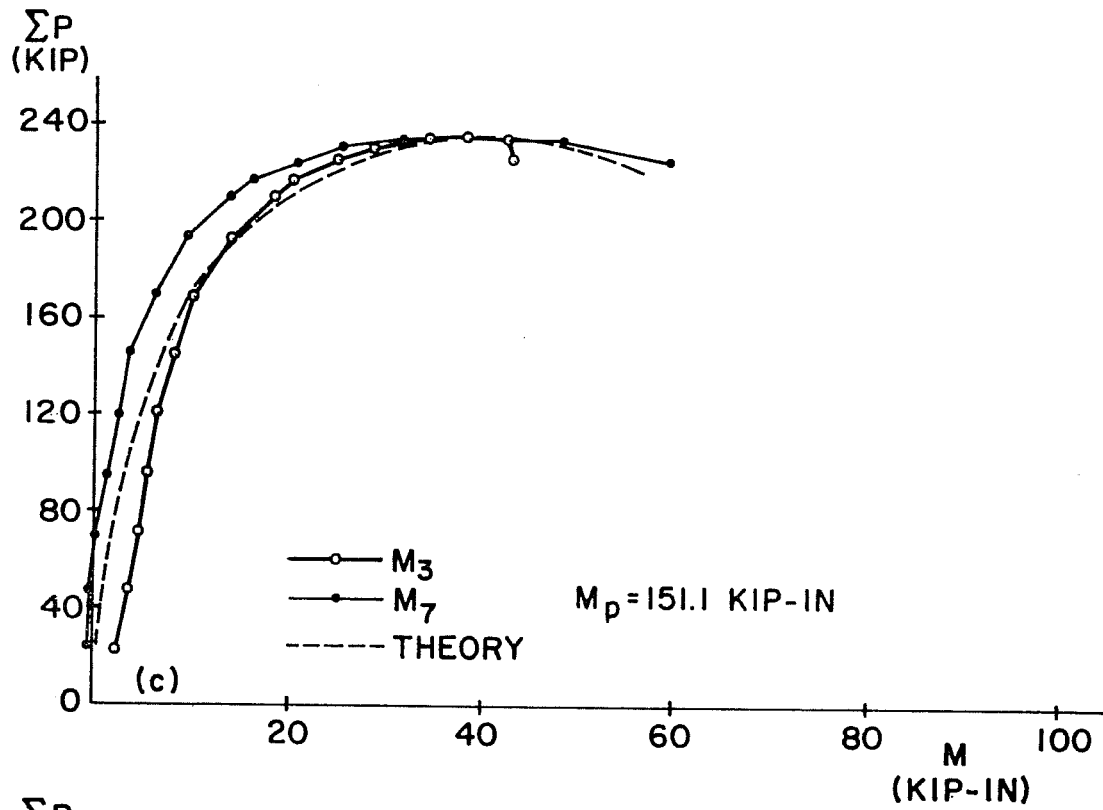


Fig. 4.16 (Continued)

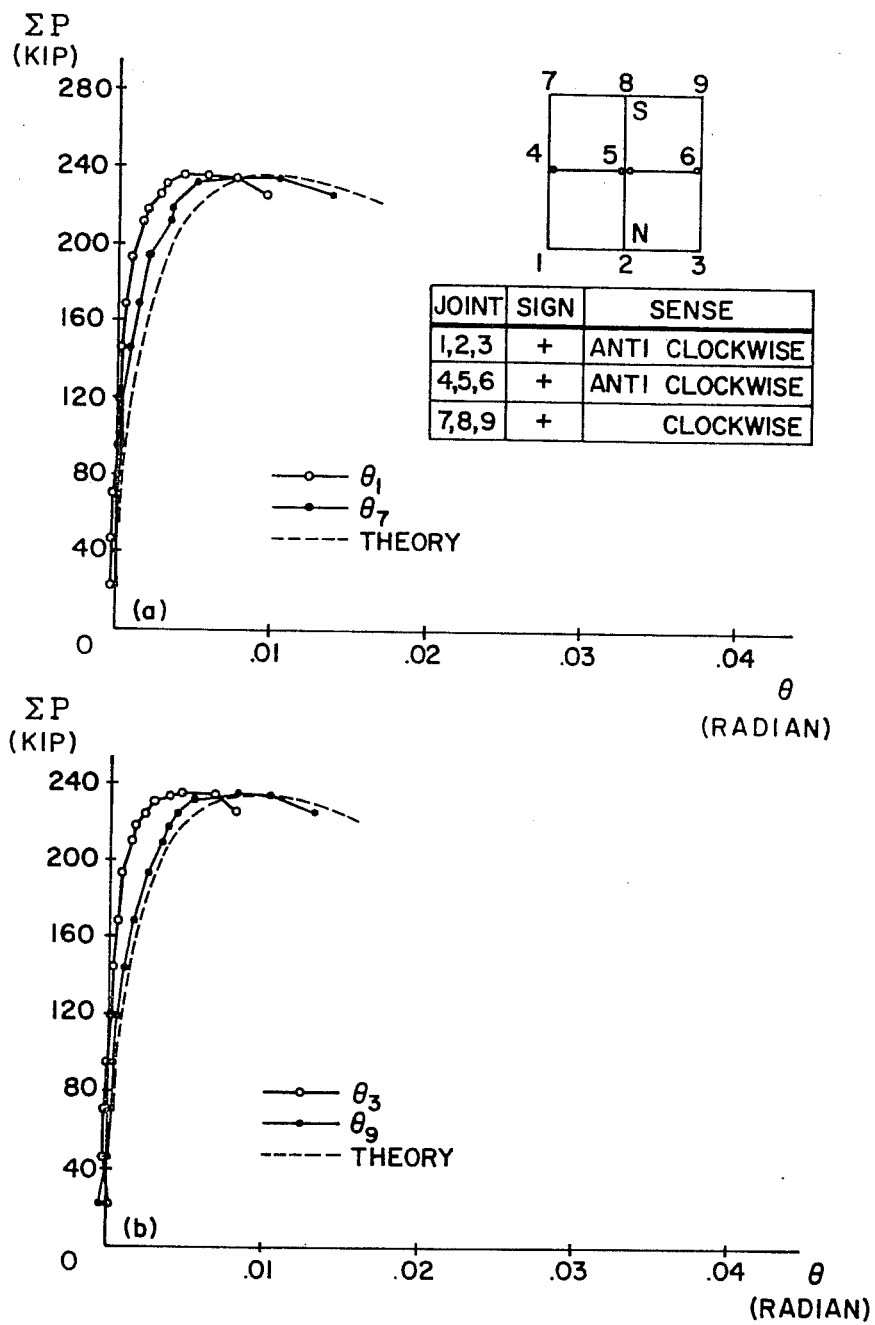


Fig. 4.17 Variation of joint rotations with axial loads (Specimen F2)

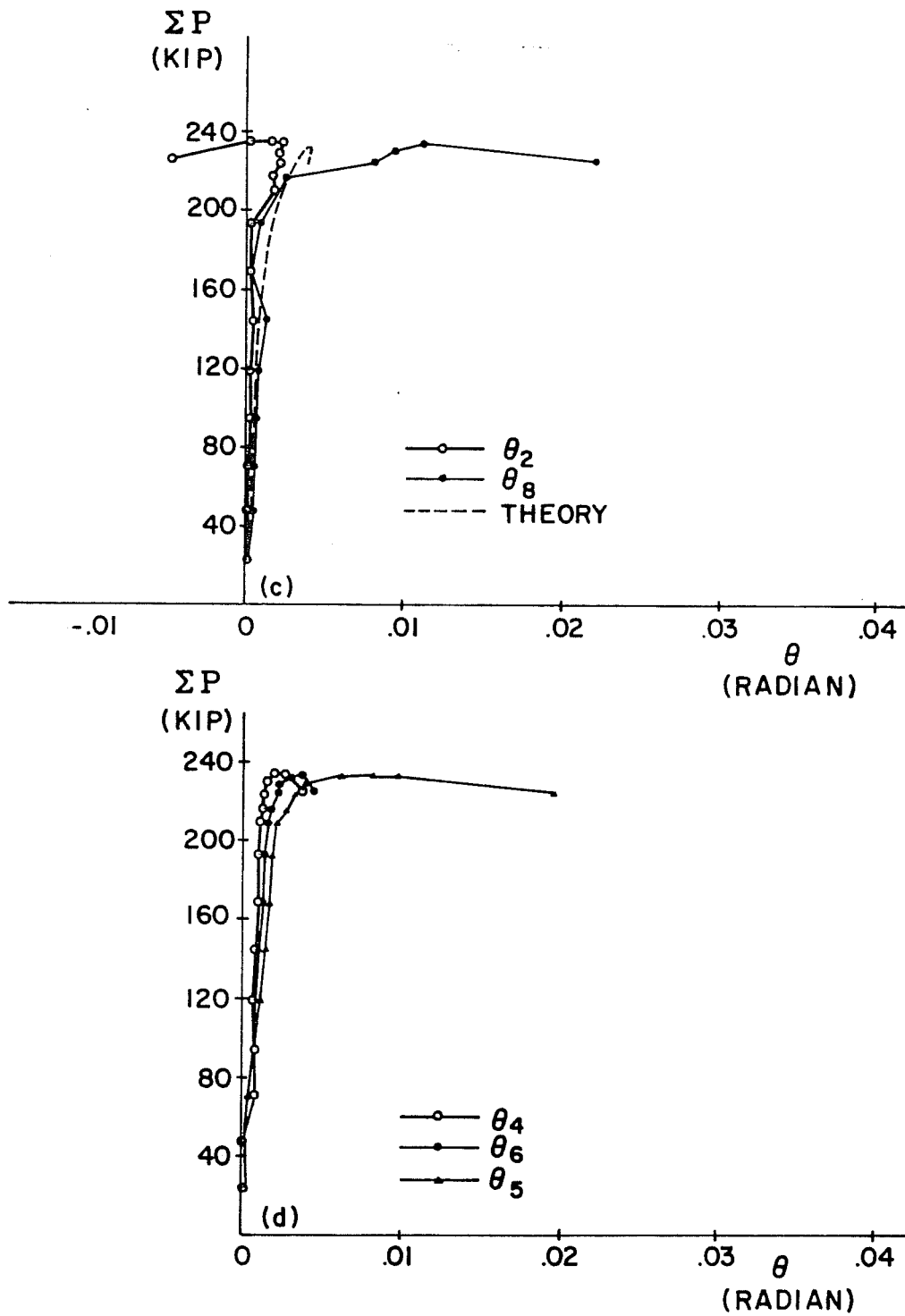


Fig. 4.17 (Continued)

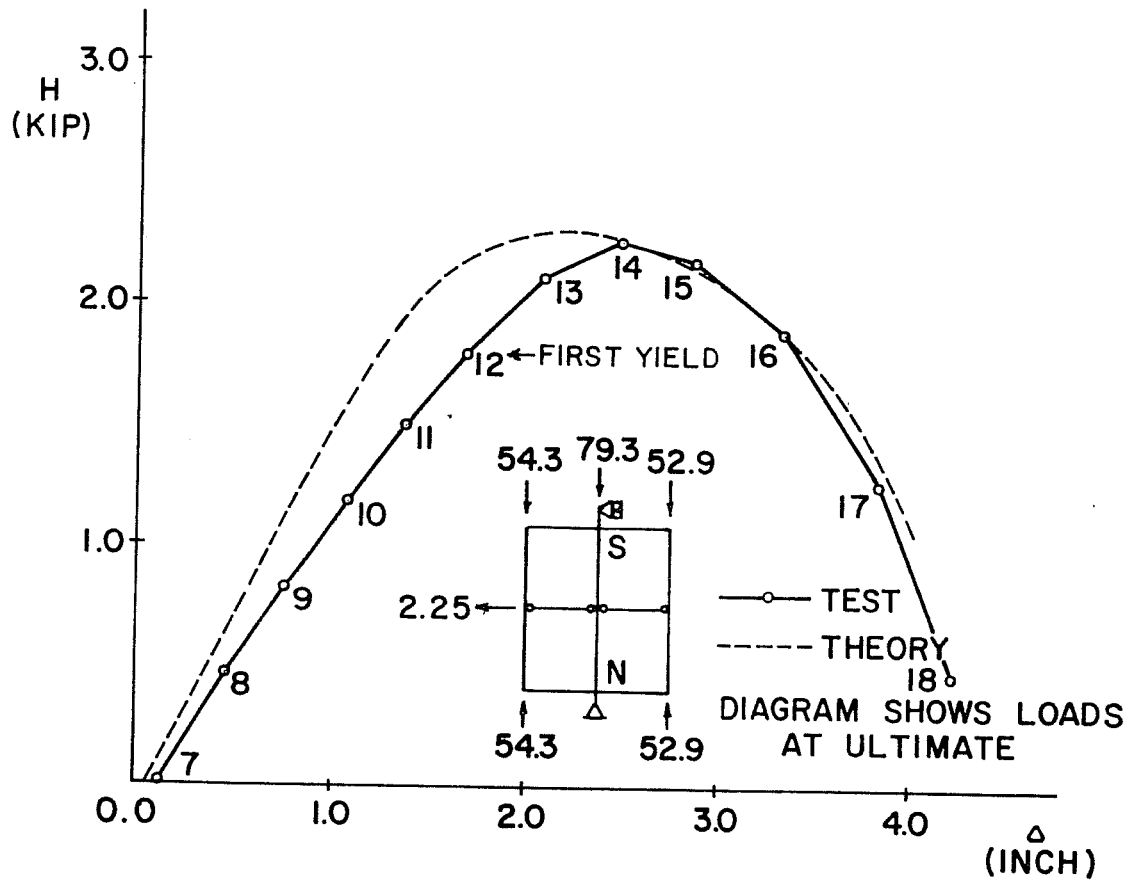


Fig. 4.18 Load-deflection relationship of Specimen F3

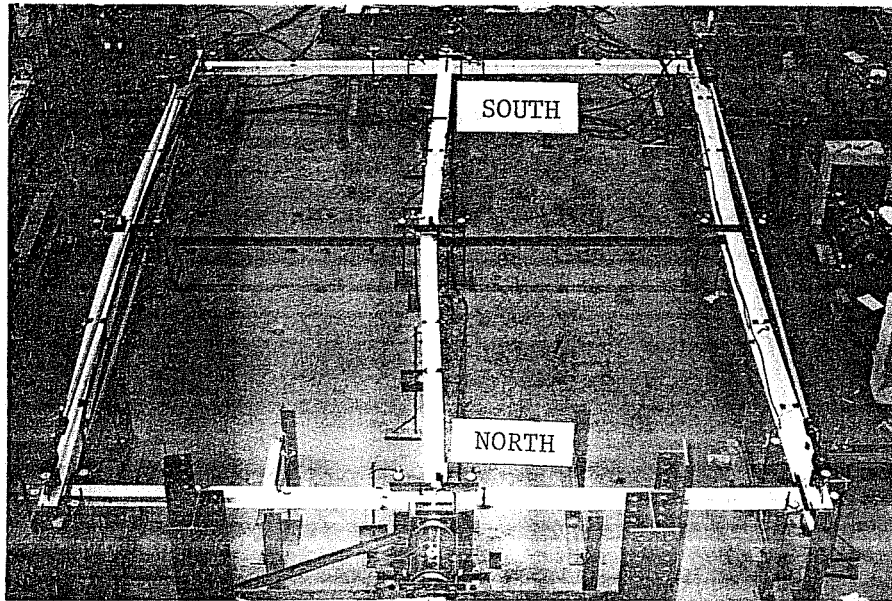


Fig. 4.19 Specimen F3 after failure

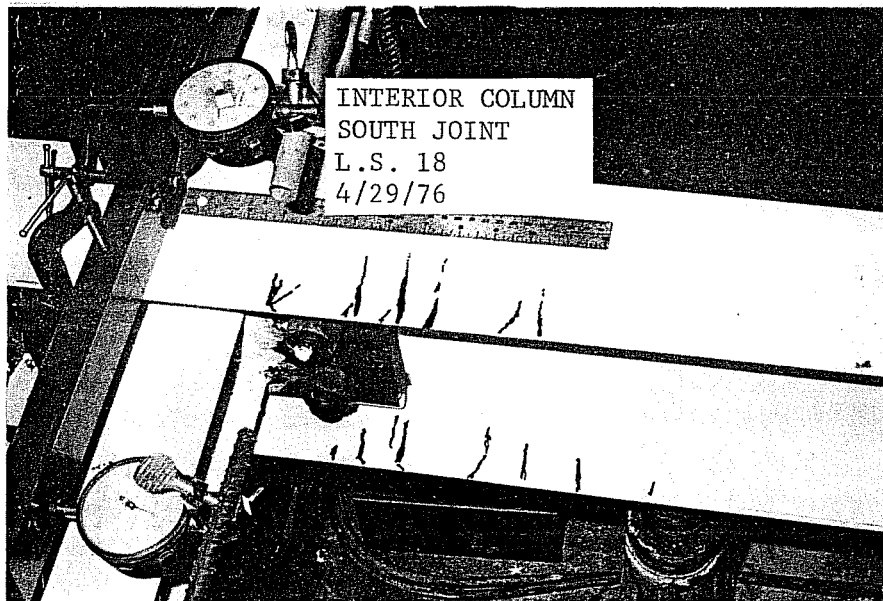


Fig. 4.20 Yielded zone at south joint of interior column of Specimen F3

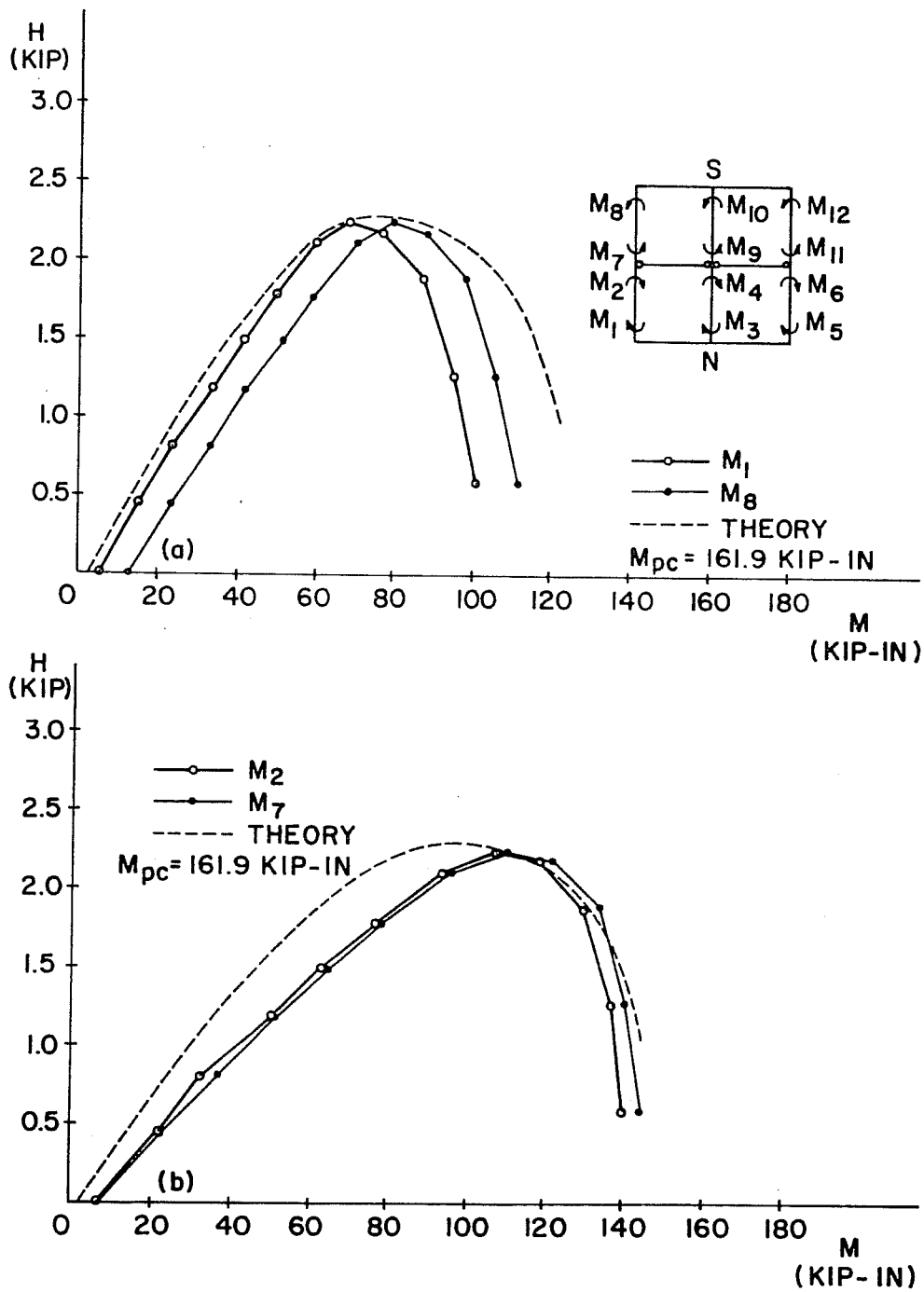


Fig. 4.21 Variation of column moments with lateral load (Specimen F3)

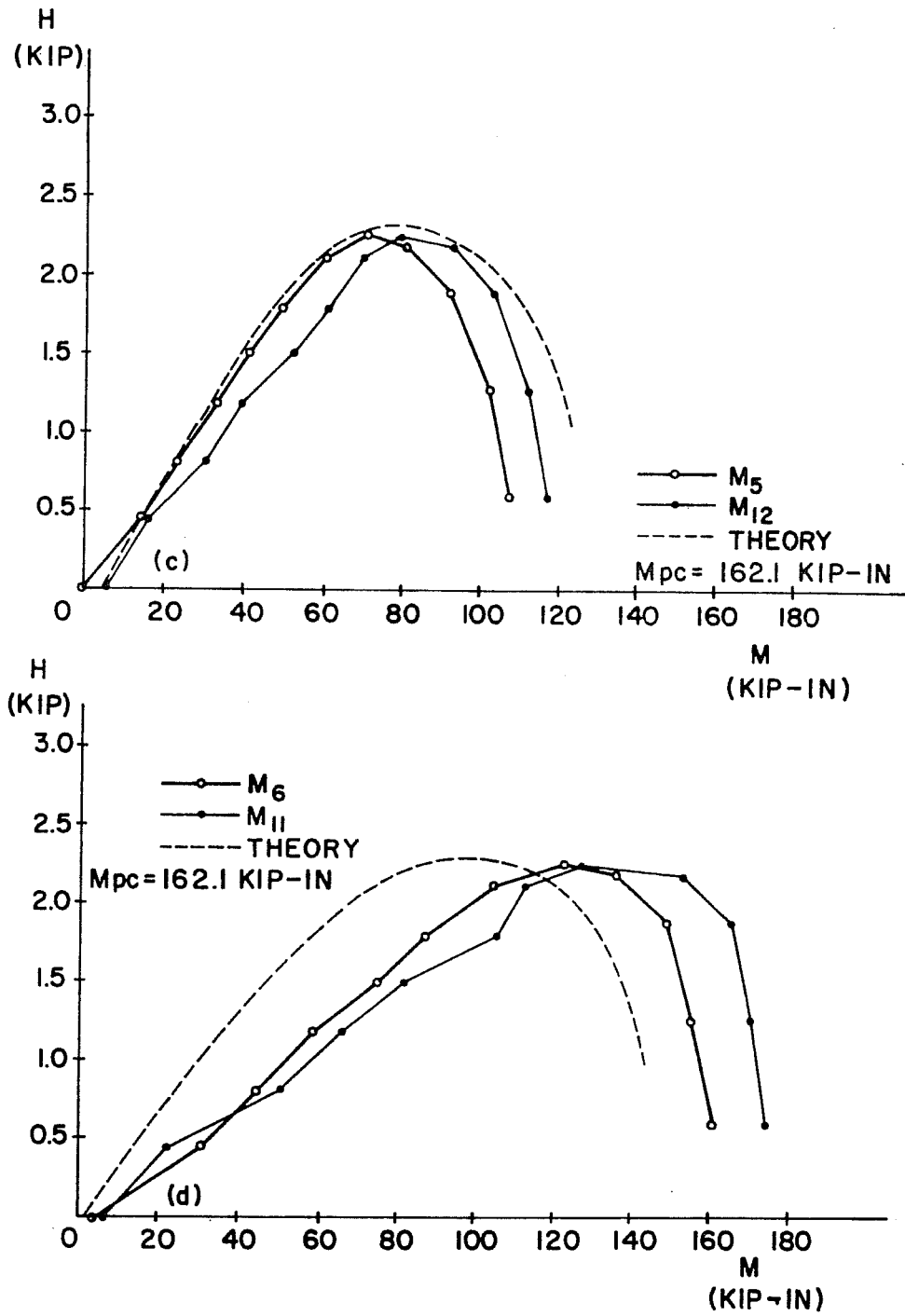


Fig. 4.21 (Continued)

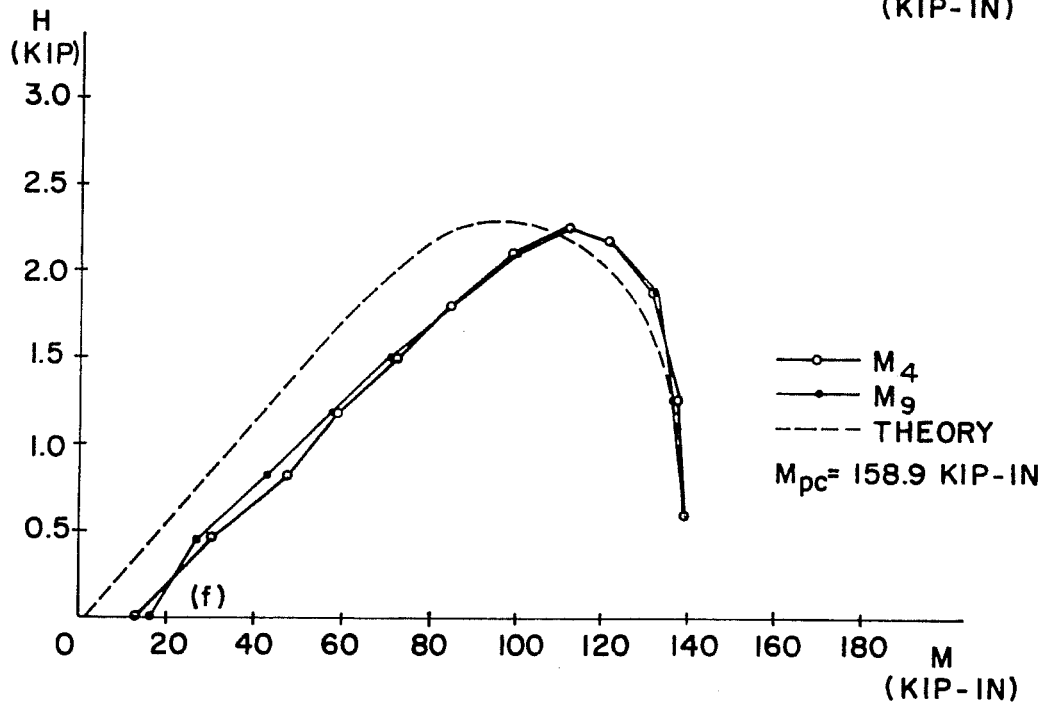
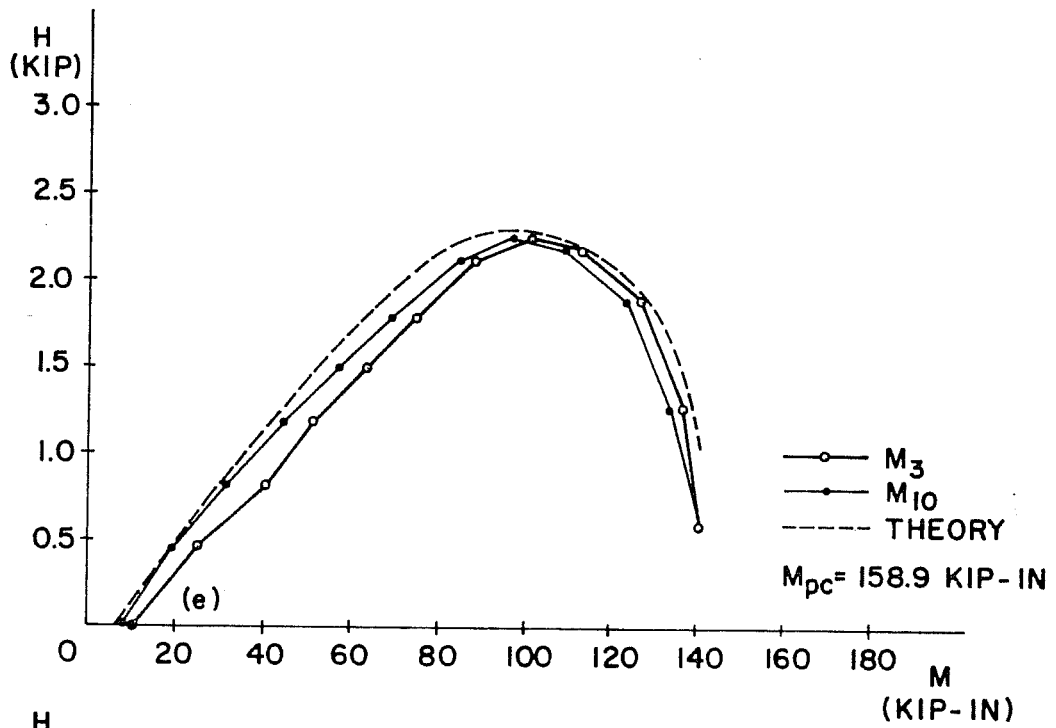


Fig. 4.21 (Continued)

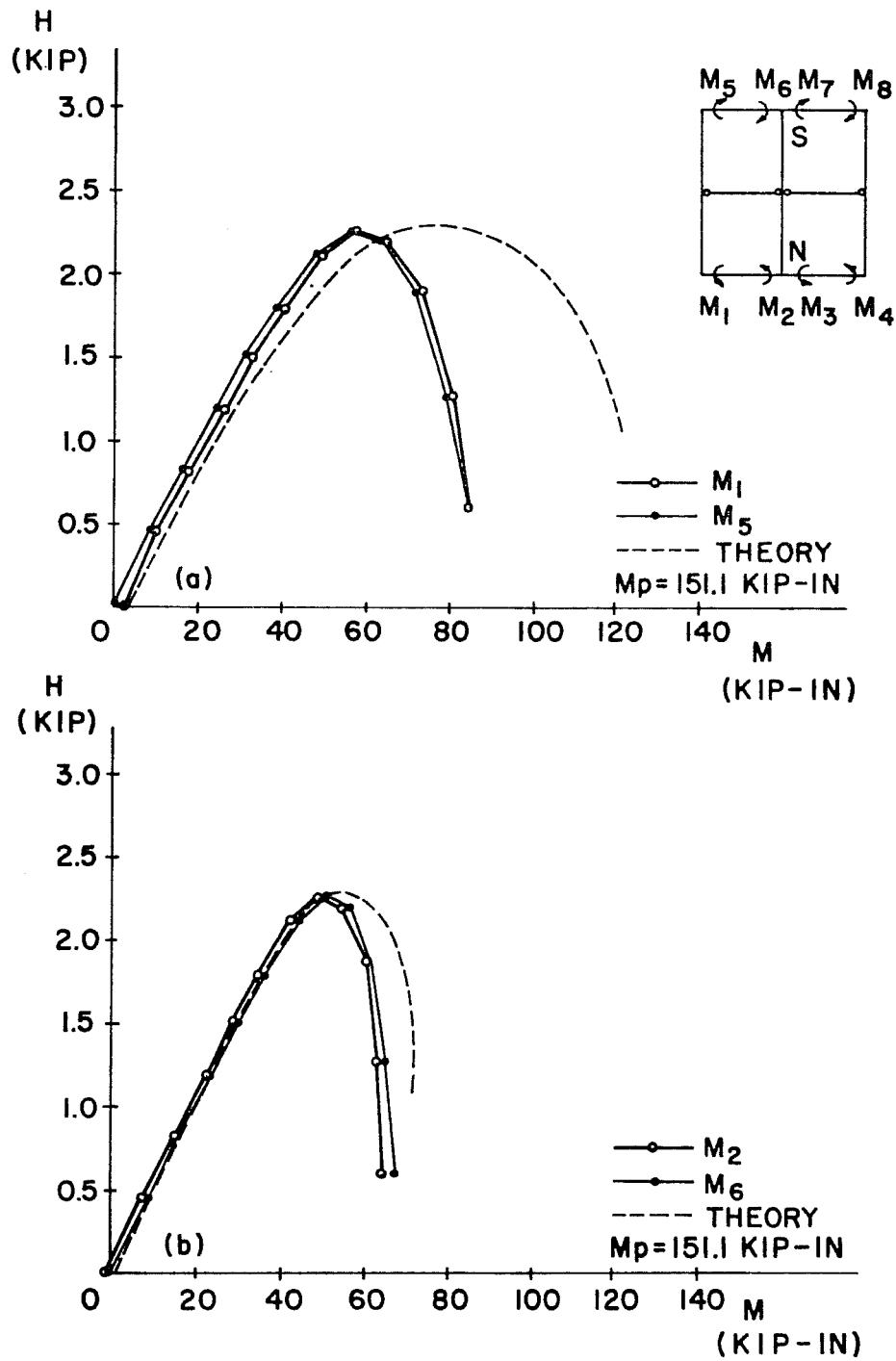


Fig. 4.22 Variation of beam moments with lateral load (Specimen F3)

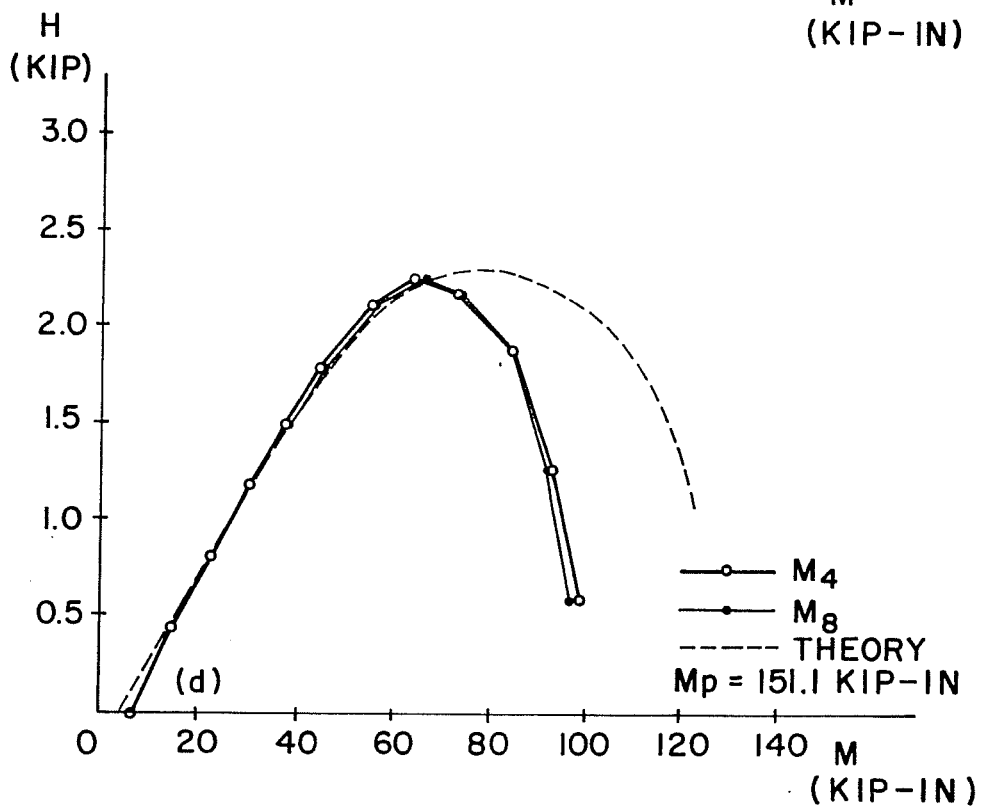
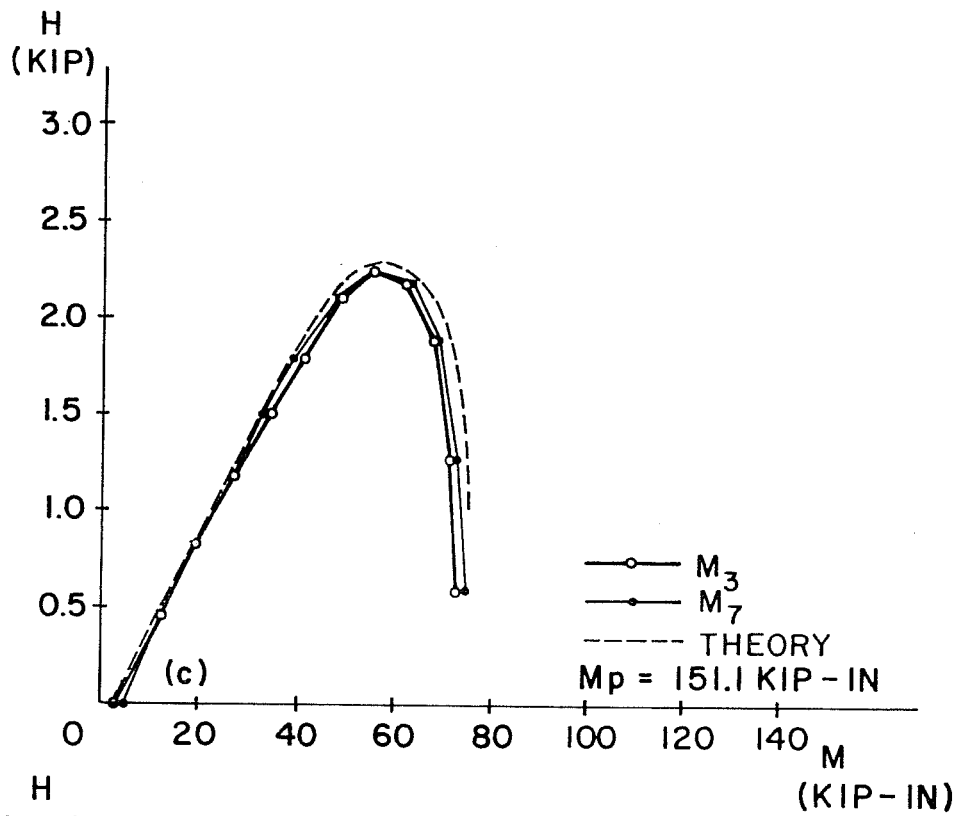
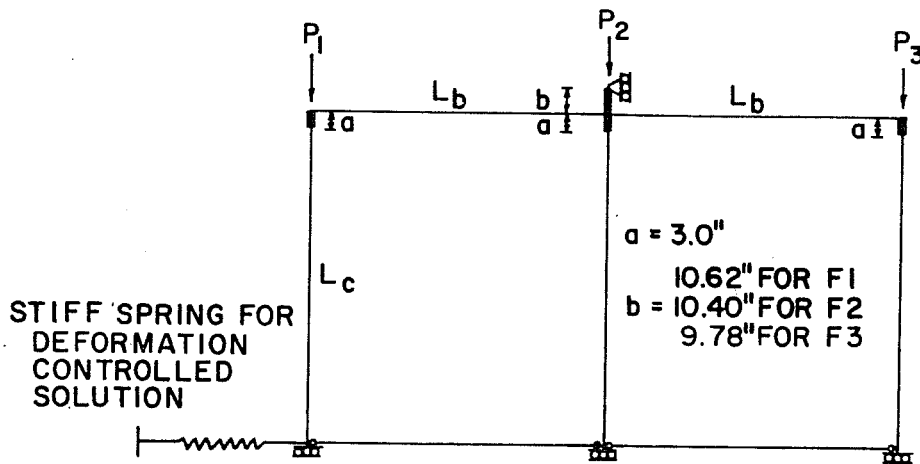
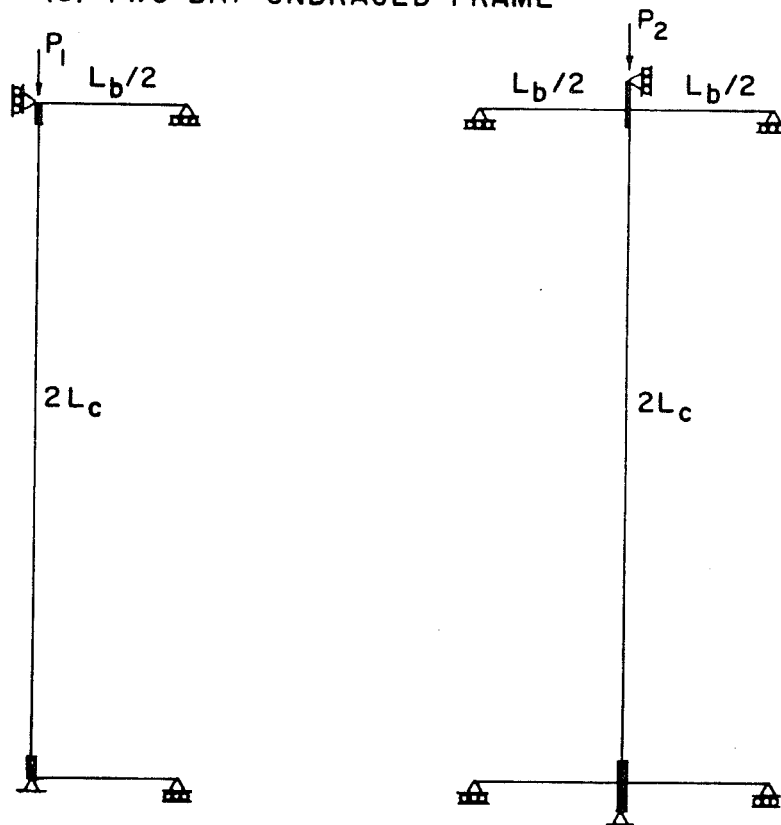


Fig. 4.22 (Continued)



(a) TWO BAY UNBRACED FRAME



(b) EXTERIOR SUBASSEMBLAGE (c) INTERIOR SUBASSEMBLAGE

Fig. 4.23 Analytical models of frame specimens

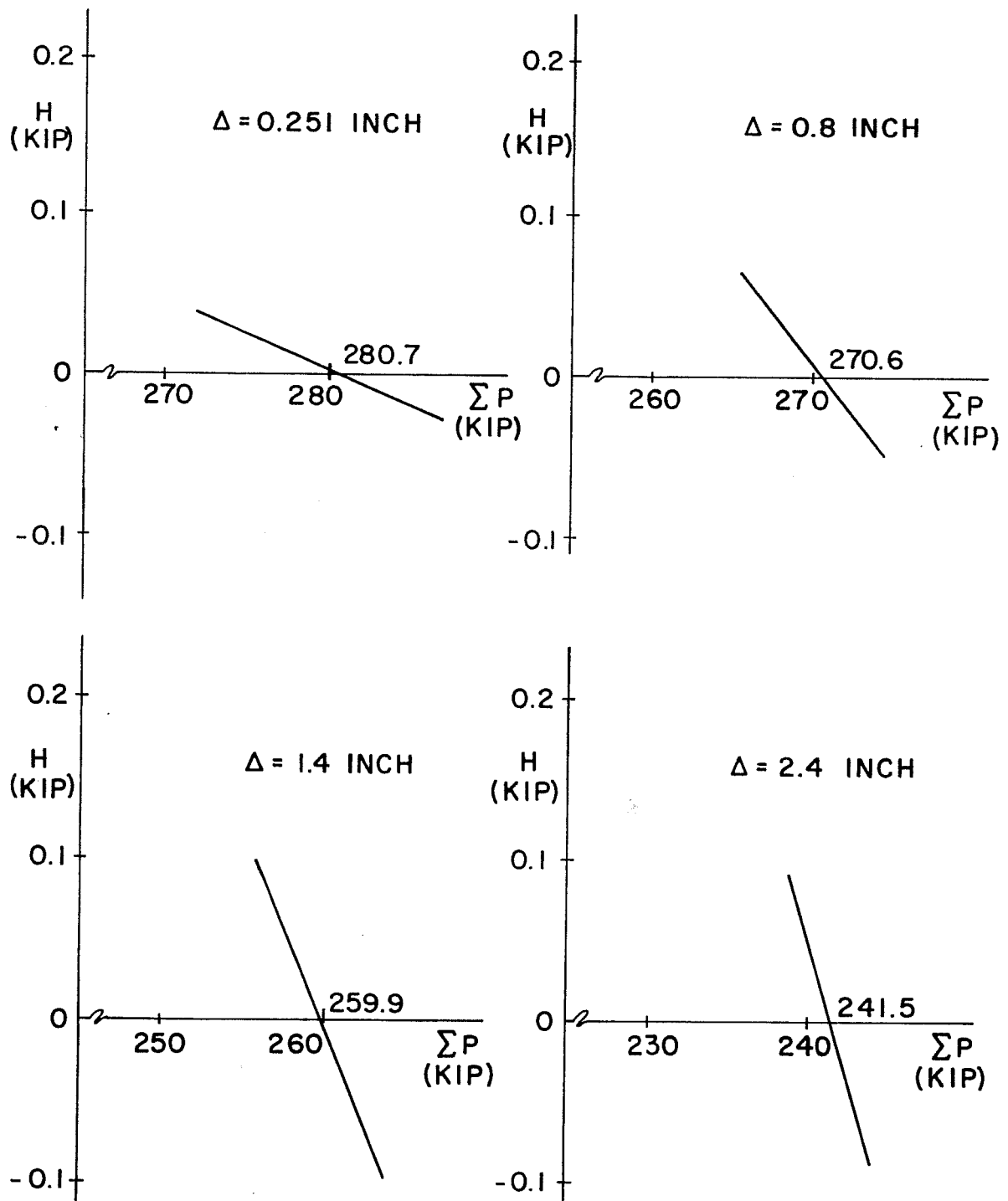


Fig. 4.24 Typical ΣP - H relationships for Specimen F1 using a limit load technique

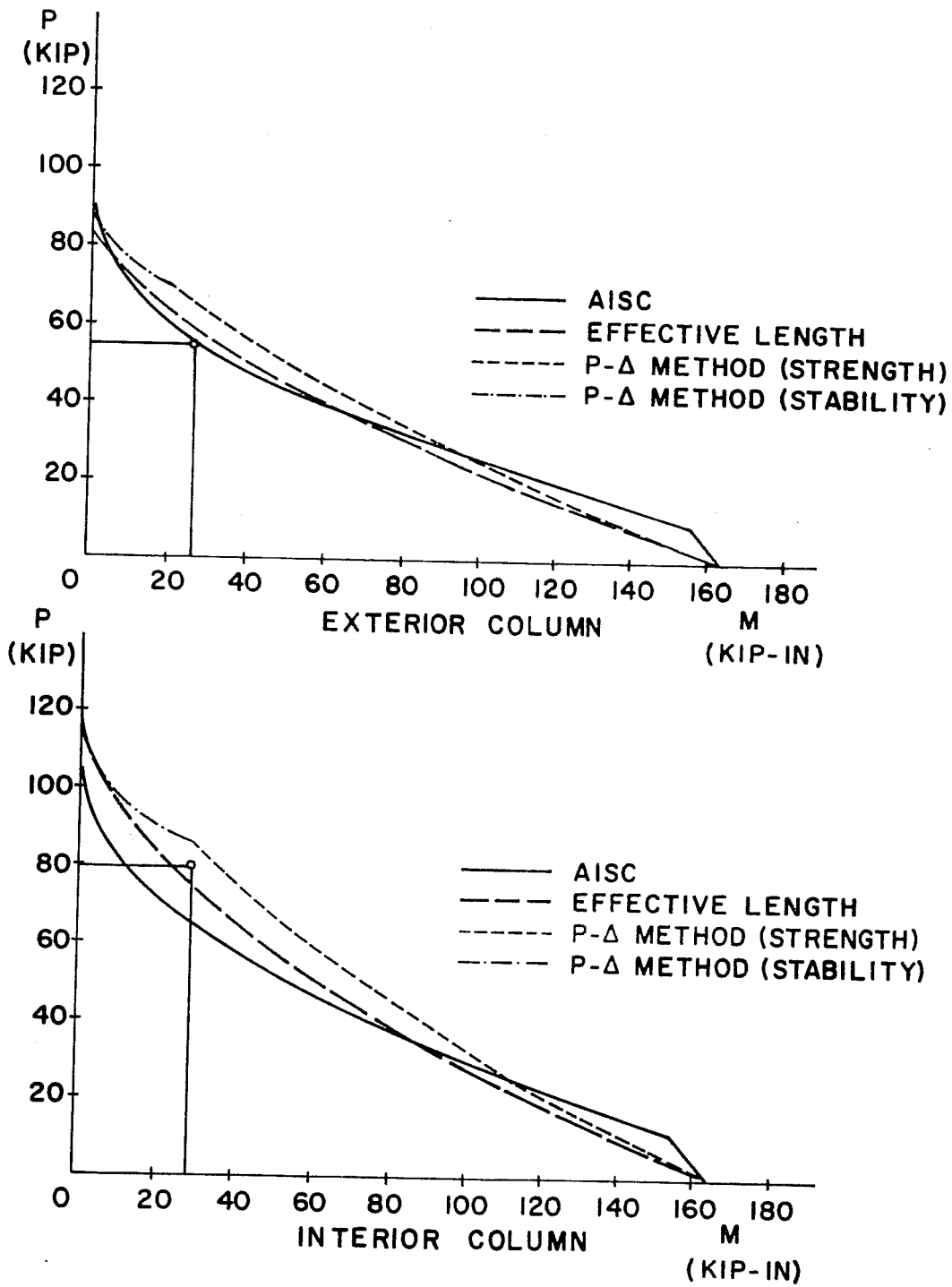


Fig. 4.25 Comparison of test and predicted results

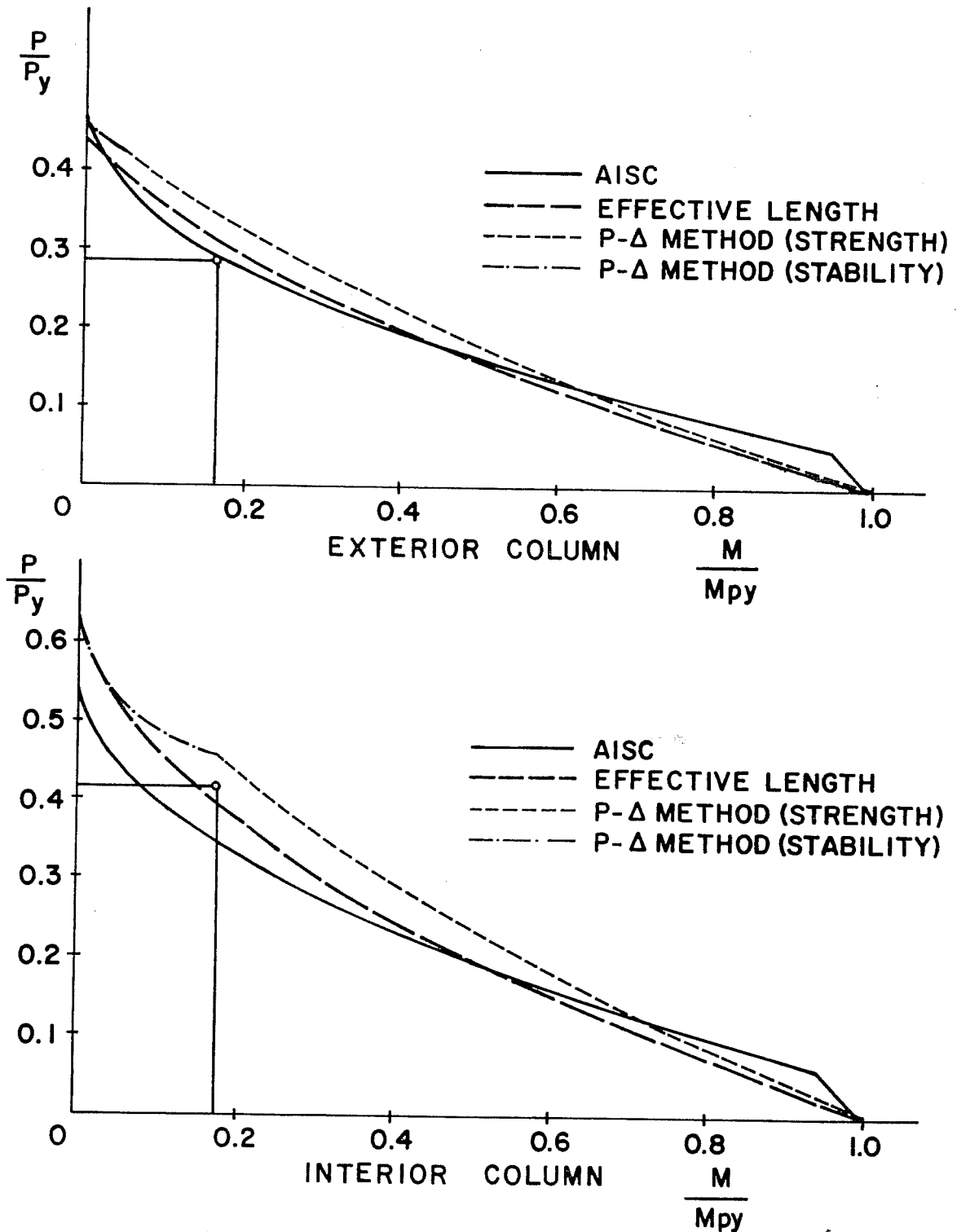


Fig. 4.26 Comparison of test and predicted results (nondimensionalized forms)

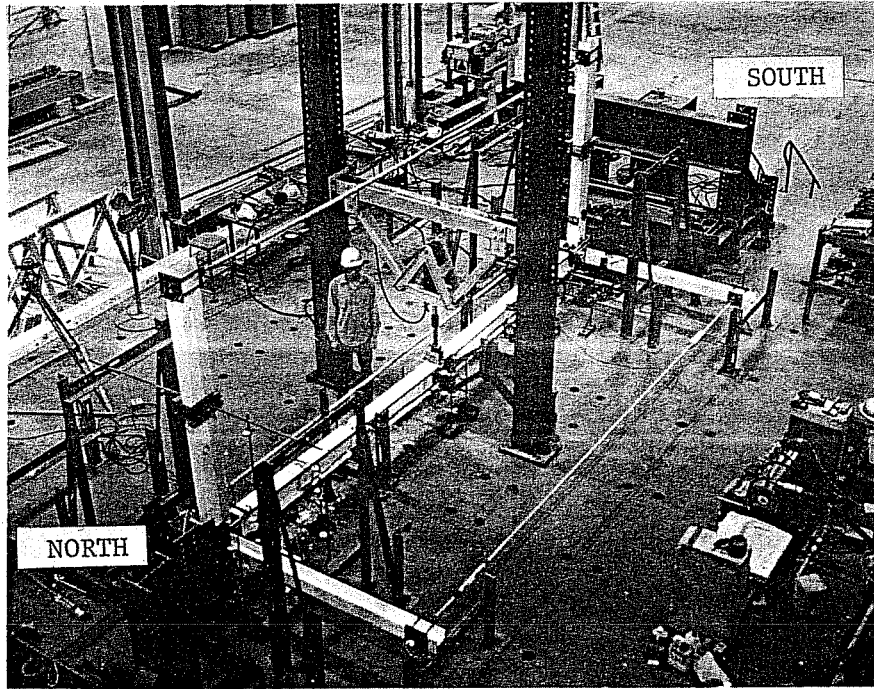


Fig. 5.1 General view of test setup

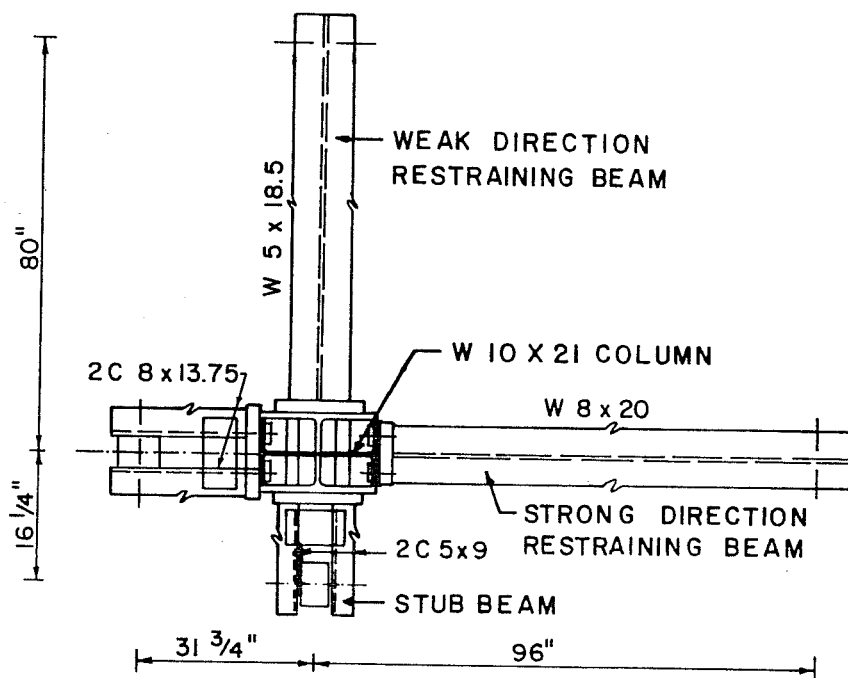


Fig. 5.2 End view of test specimens

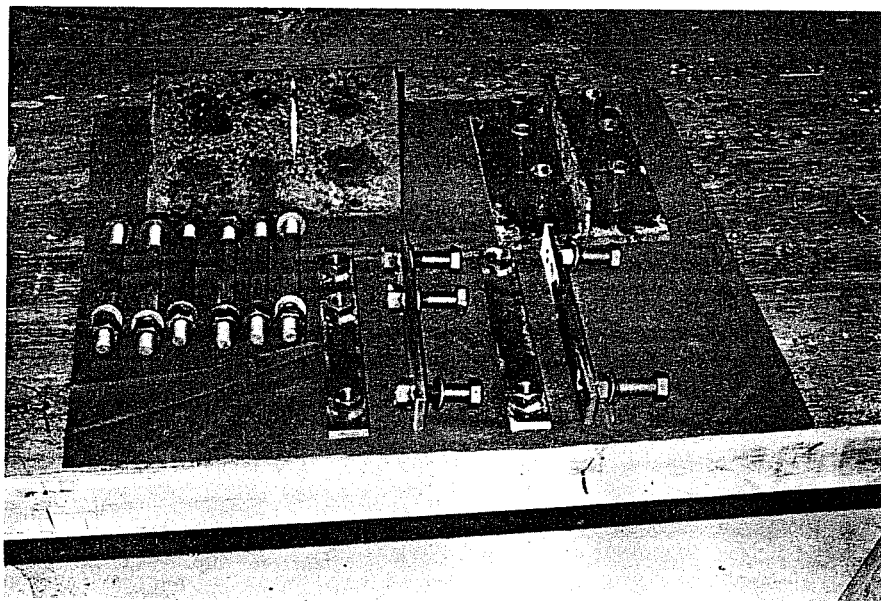


Fig. 5.3 Components for joint fabrication

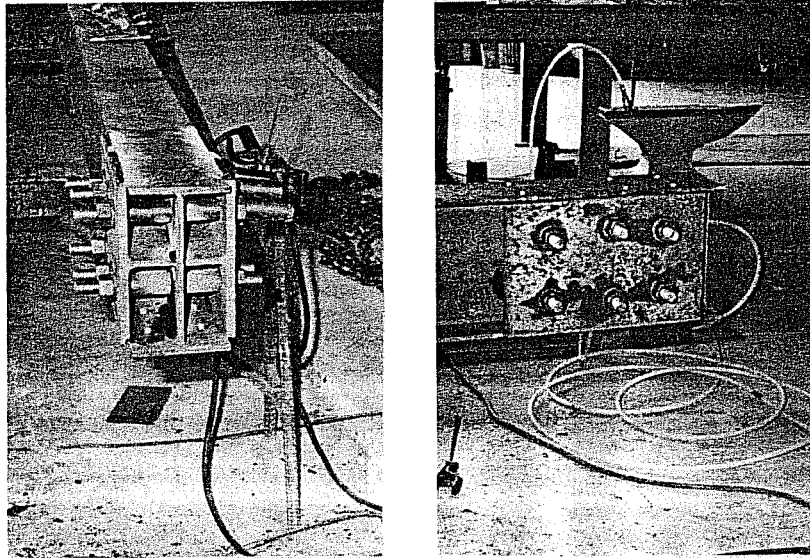


Fig. 5.4 Joint fabrication process

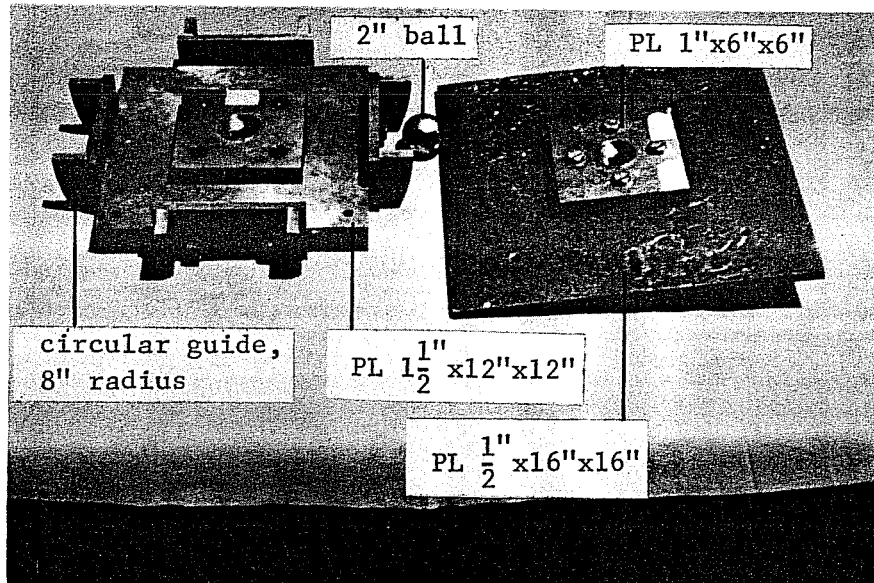


Fig. 5.5 End fixtures, exploded view

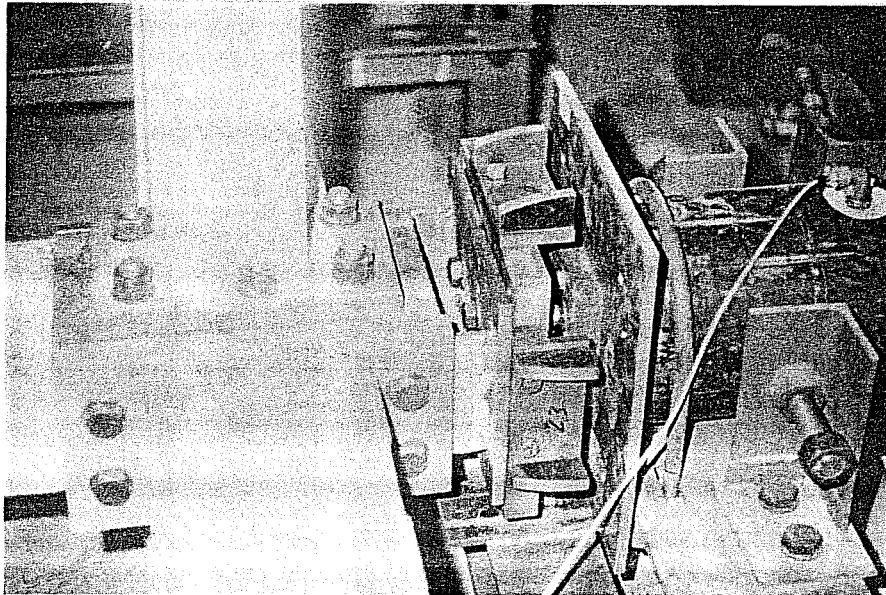


Fig. 5.6 Column end showing end fixture assembly

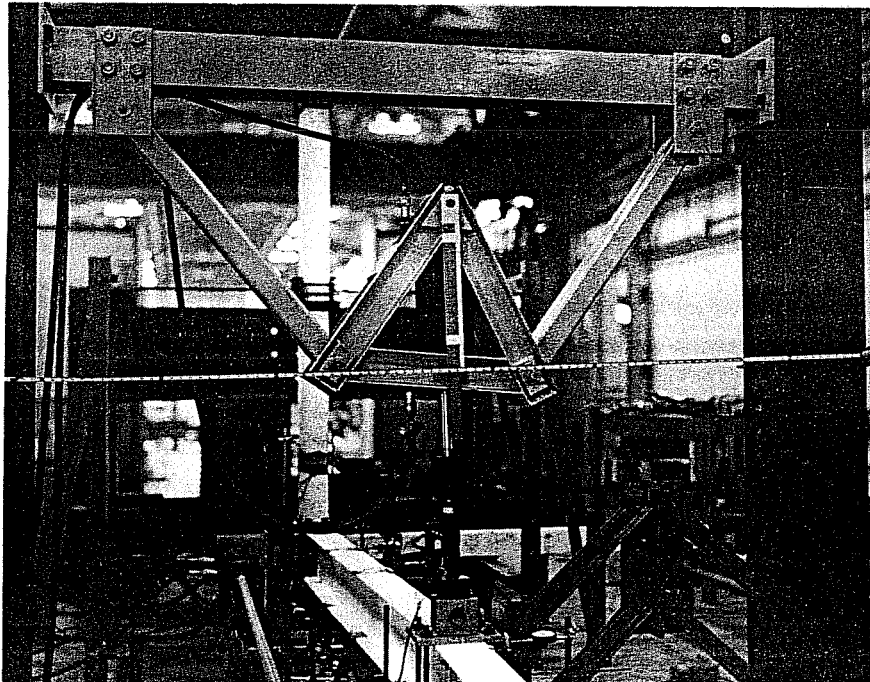


Fig. 5.7 Gravity load simulator

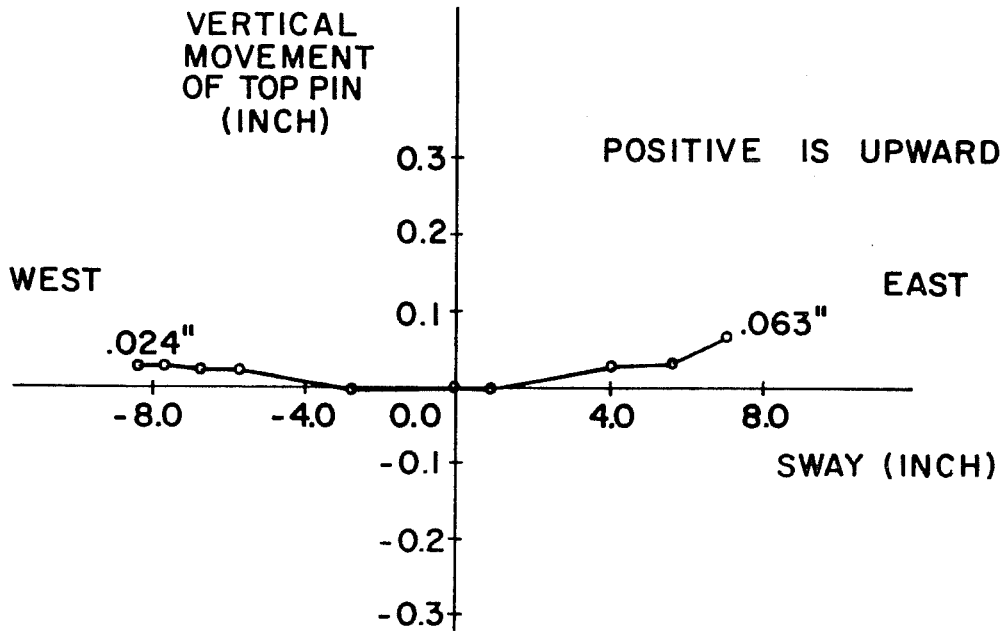


Fig. 5.8 Movement of top pin of simulator during sway

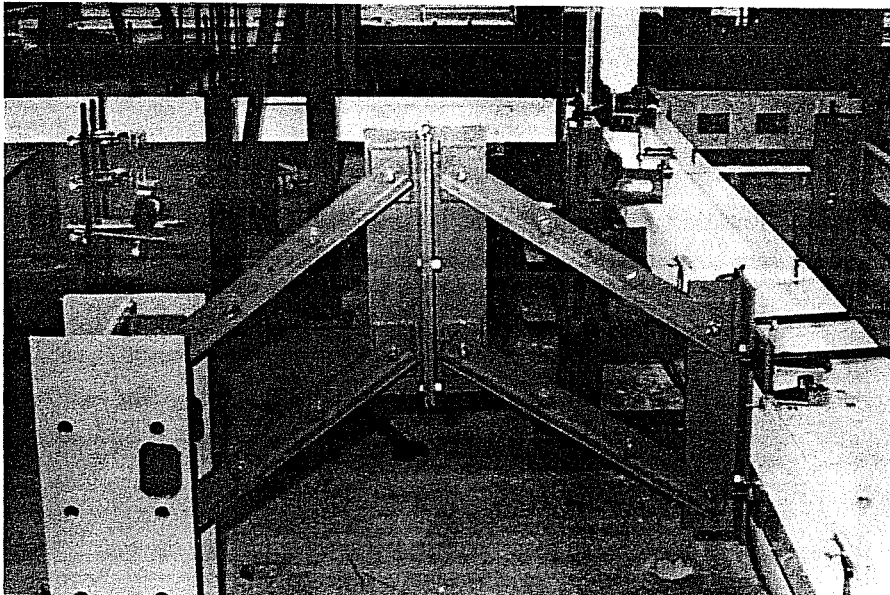


Fig. 5.9 Mechanism for preventing twist at the midlength section

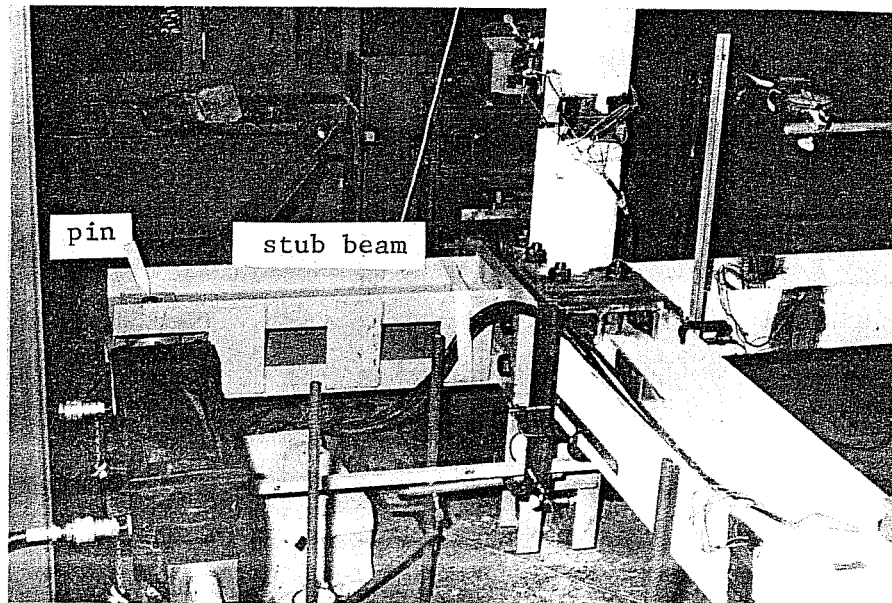


Fig. 5.10 Joint loading apparatus

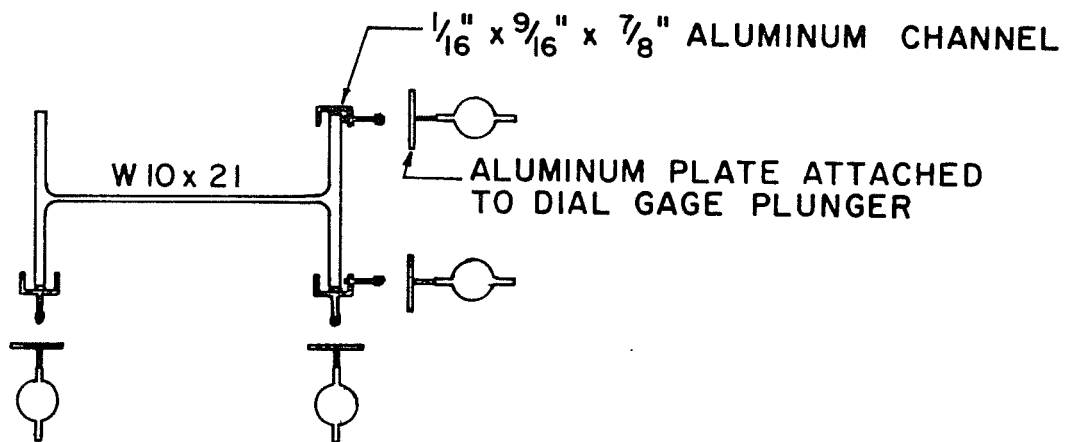
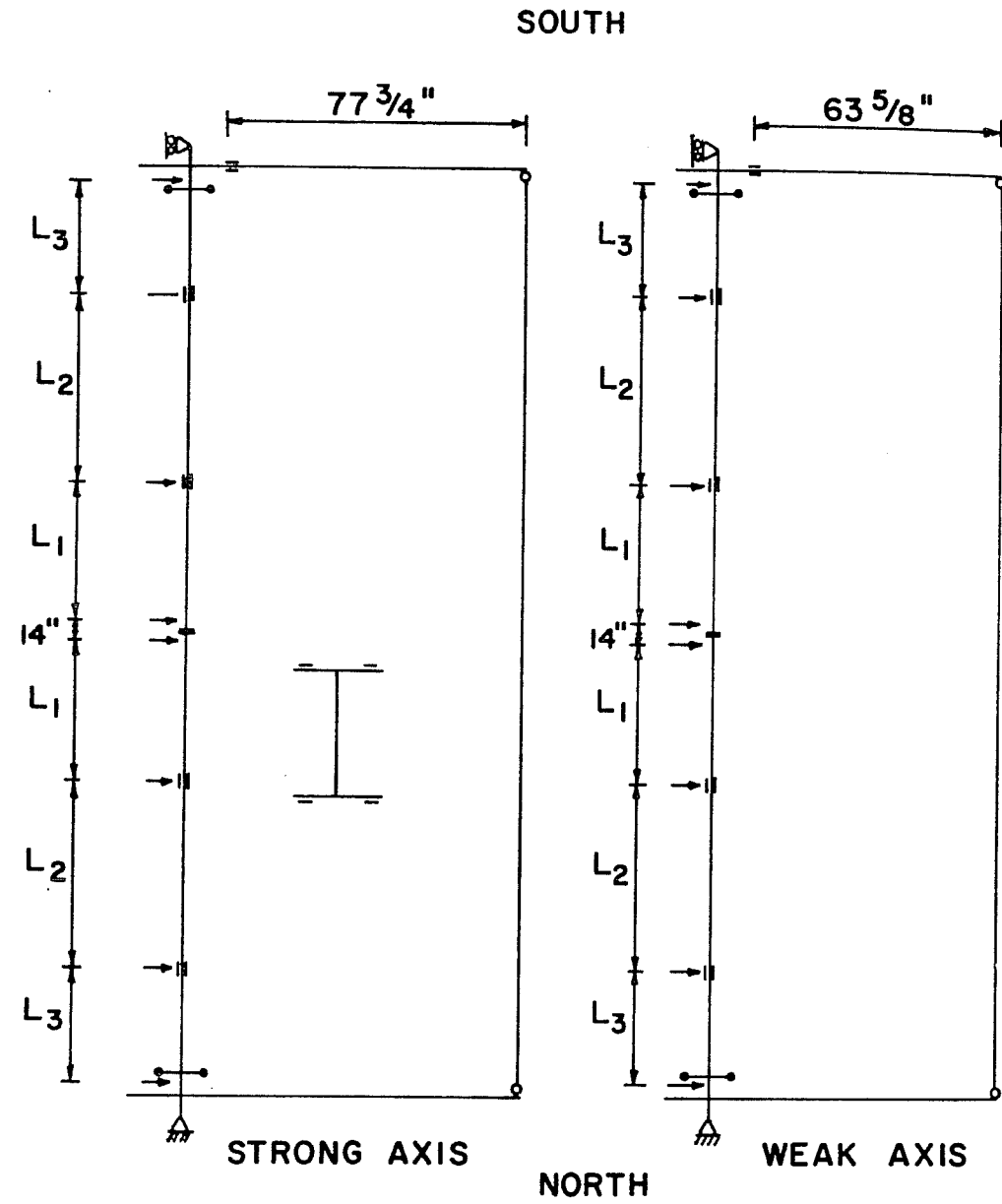


Fig. 5.11 Dial gage arrangement for measuring displacements



LEGEND

- STRAIN GAGE
- DIAL GAGE
- ROTATION ARM

SPECIMEN	L ₁	L ₂	L ₃
BC-1	28	55	32
BC-2	54	28	33
BC-3	54	28	33

NOTE: ALL UNITS IN INCHES

Fig. 5.12 Instrumentation diagram

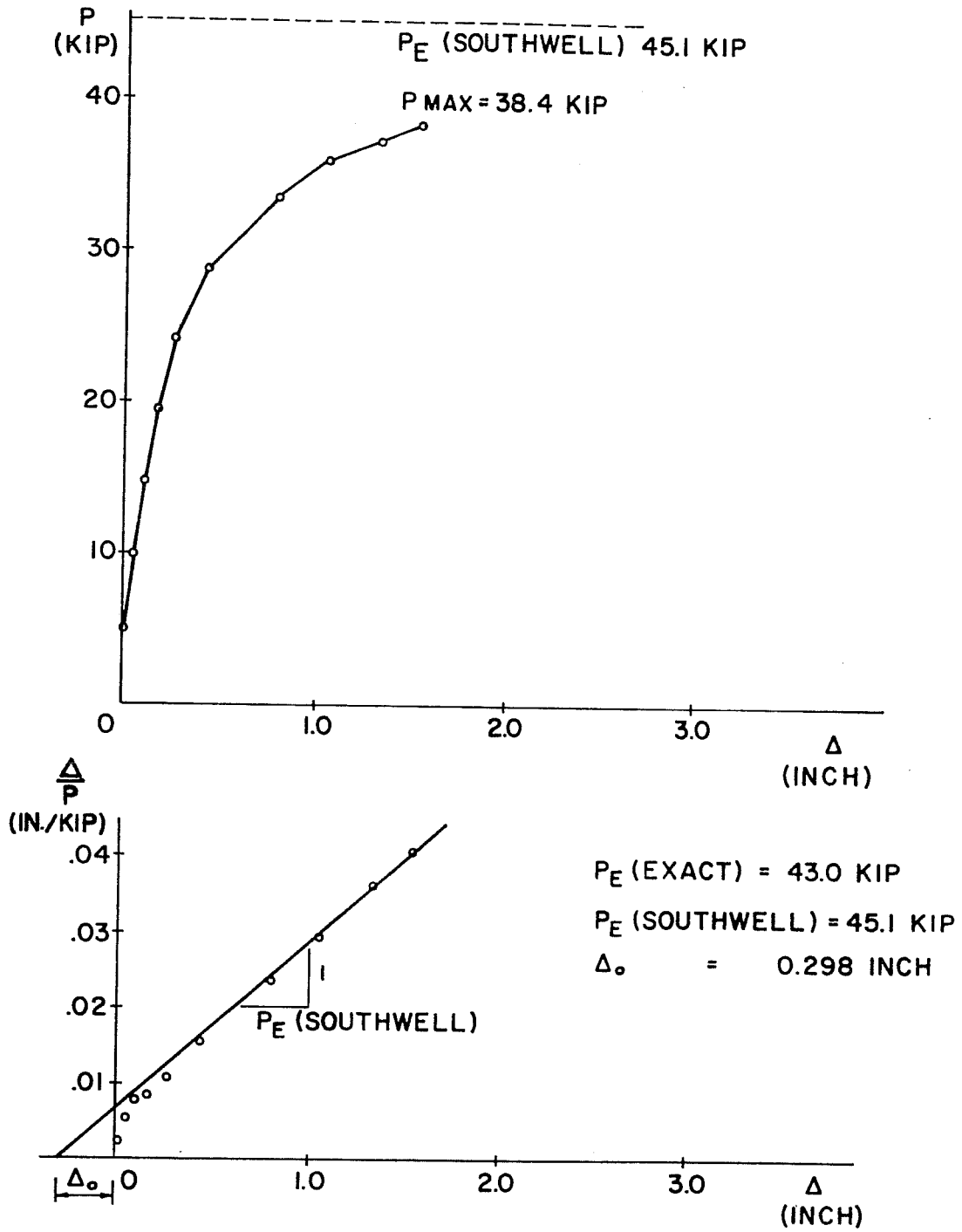


Fig. 5.13 Results of Euler test on Specimen BC-1

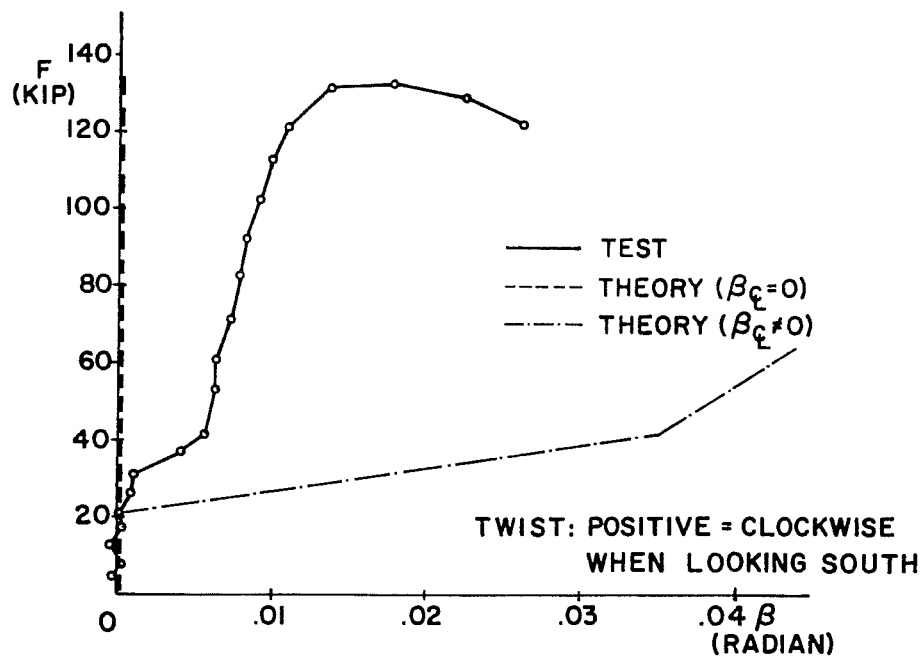
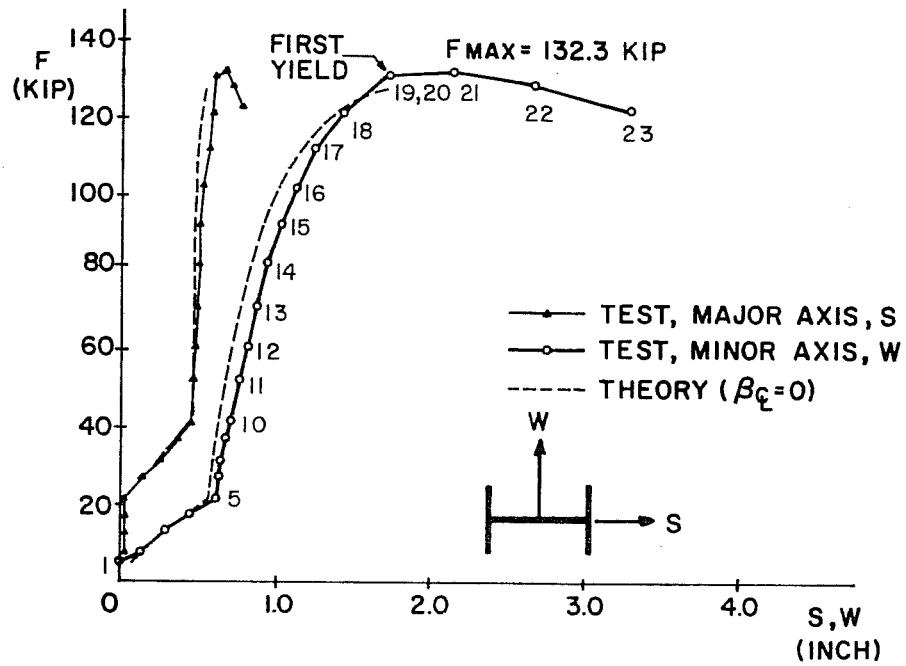


Fig. 5.14 Load-displacement relationship at the midlength (Specimen BC-1)

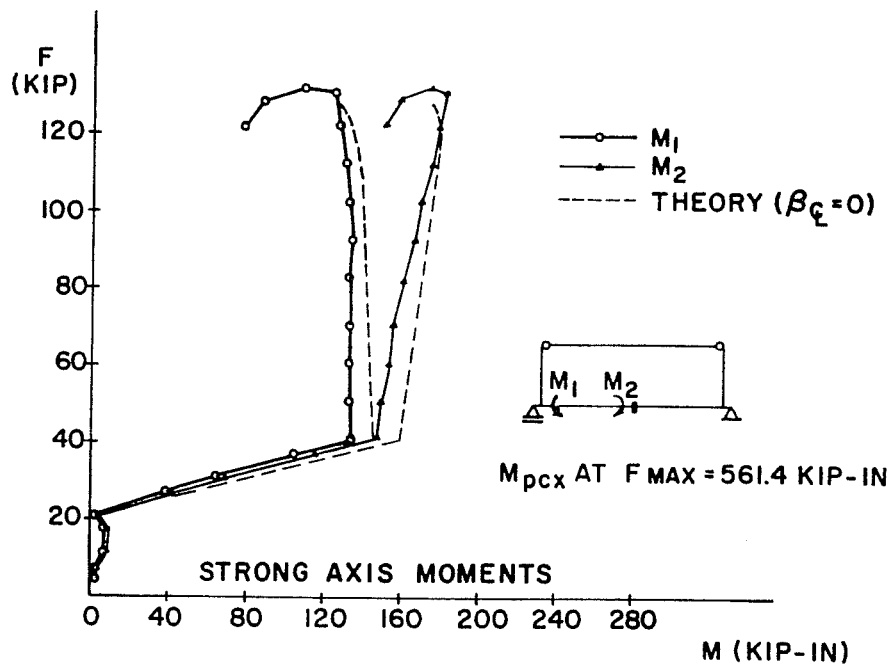
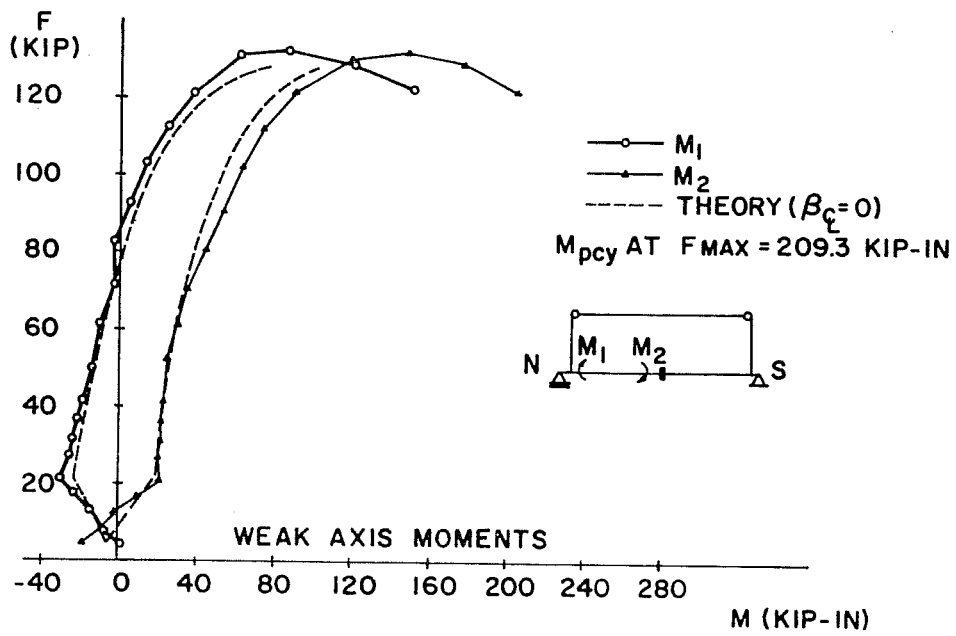


Fig. 5.15 Variation of column moments with axial force (Specimen BC-1)

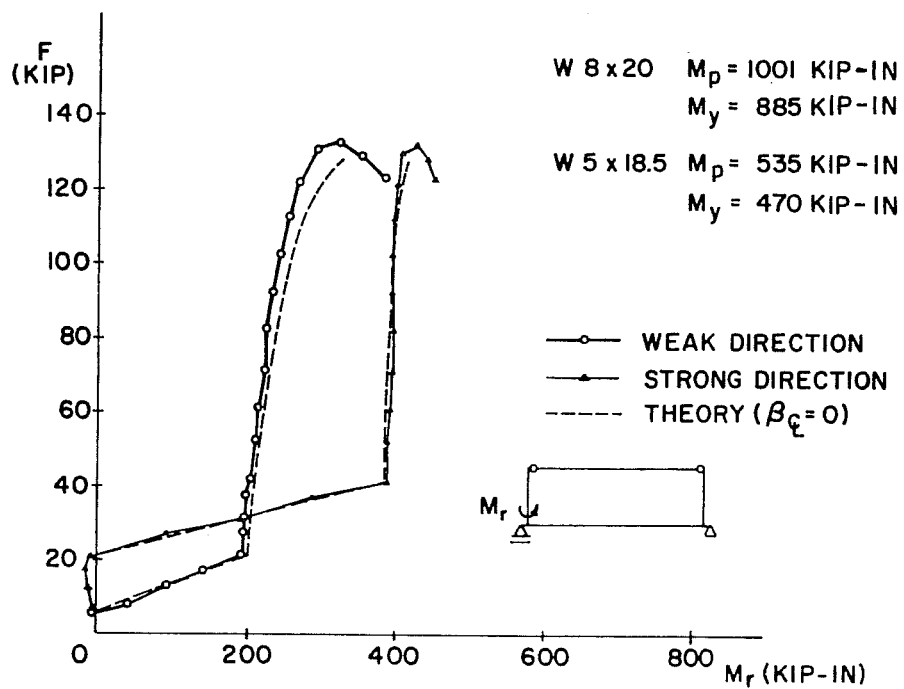


Fig. 5.16 Variation of restraining moments with axial force (Specimen BC-1)

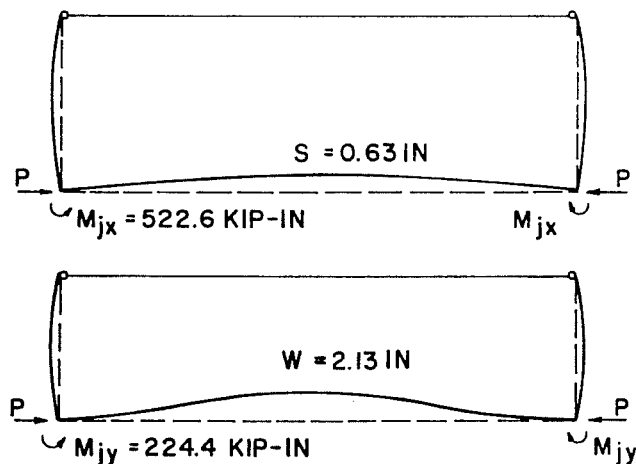


Fig. 5.17 Deflected shapes of Specimen BC-1 at the maximum load

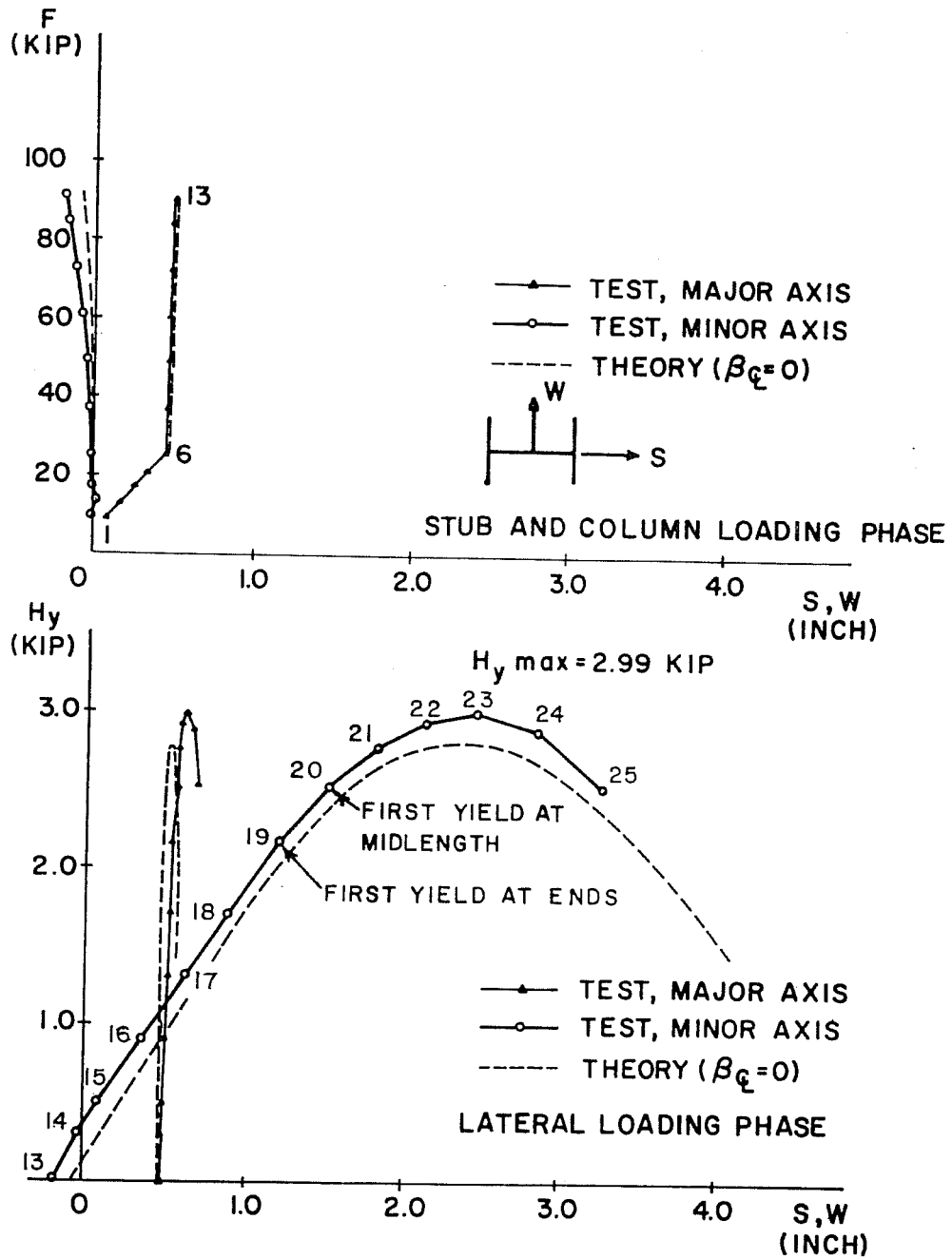


Fig. 5.18 Load-displacement relationship at the midlength (Specimen BC-2)

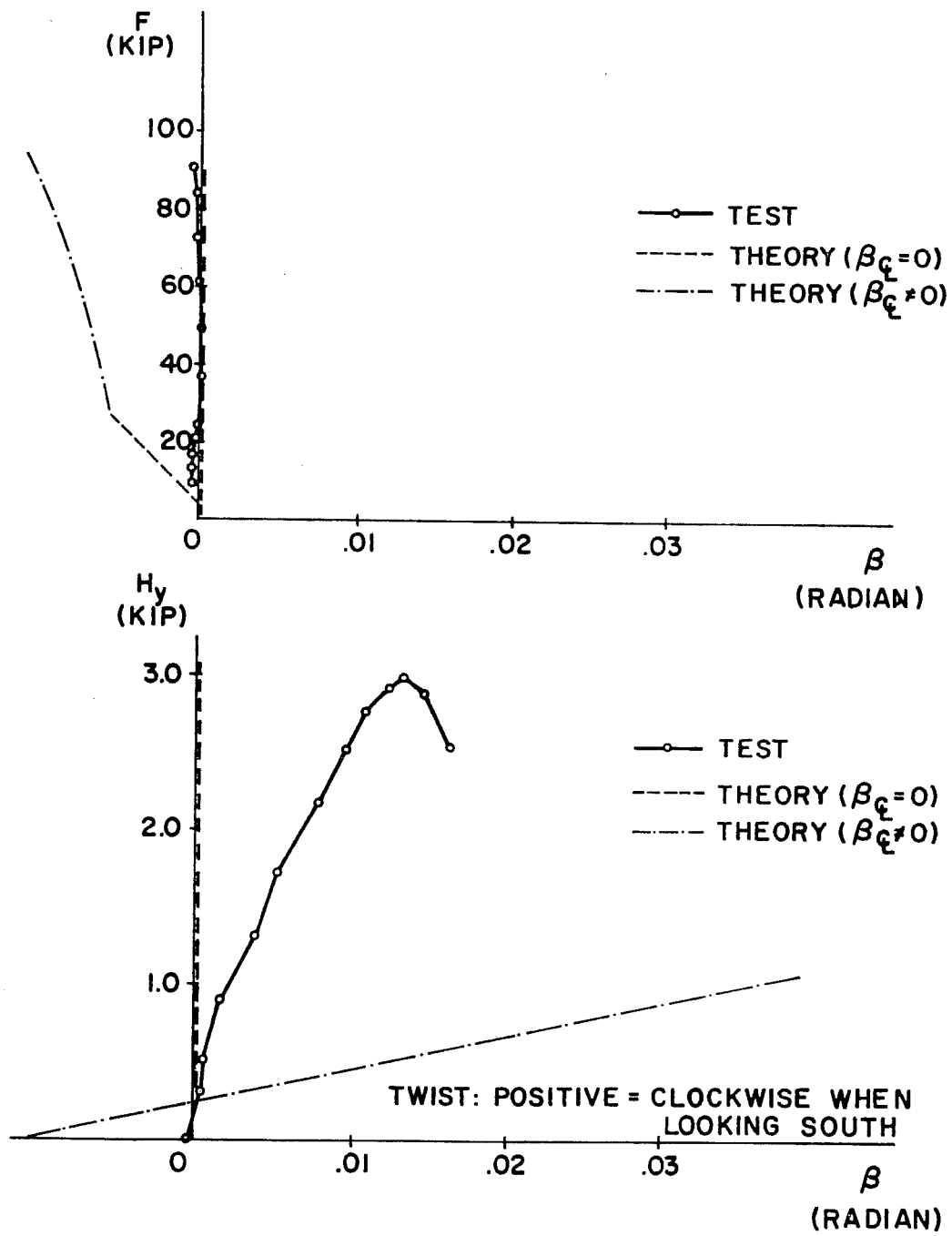


Fig. 5.18 (Continued)

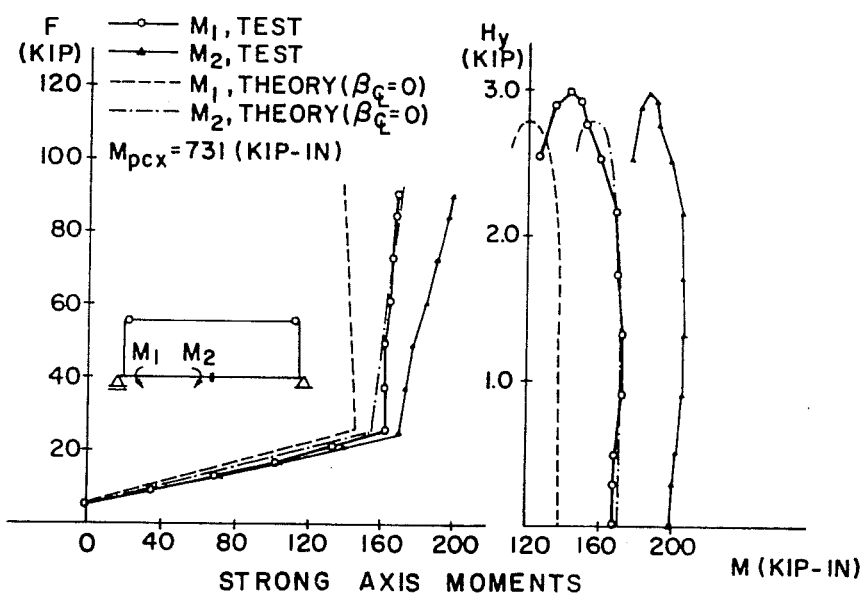
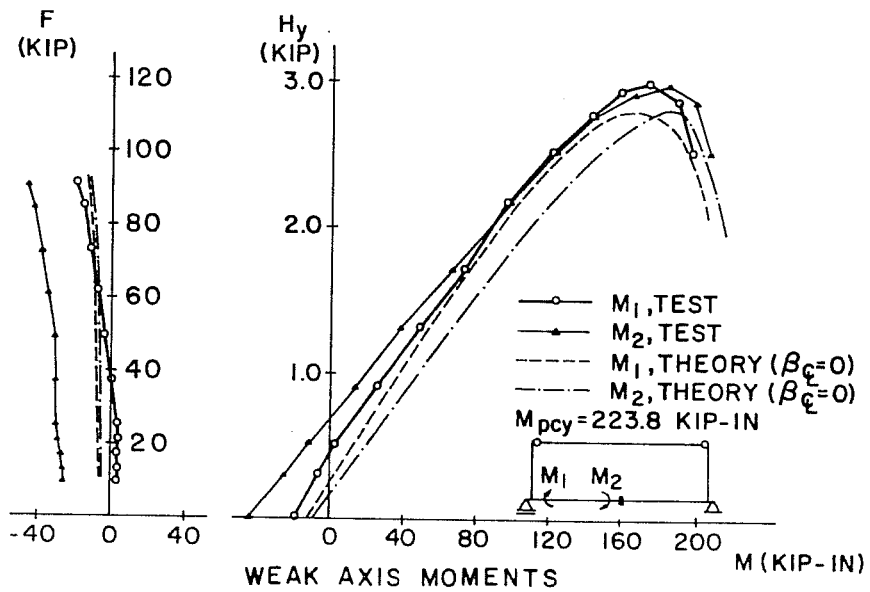


Fig. 5.19 Variation of column moments with loads (Specimen BC-2)

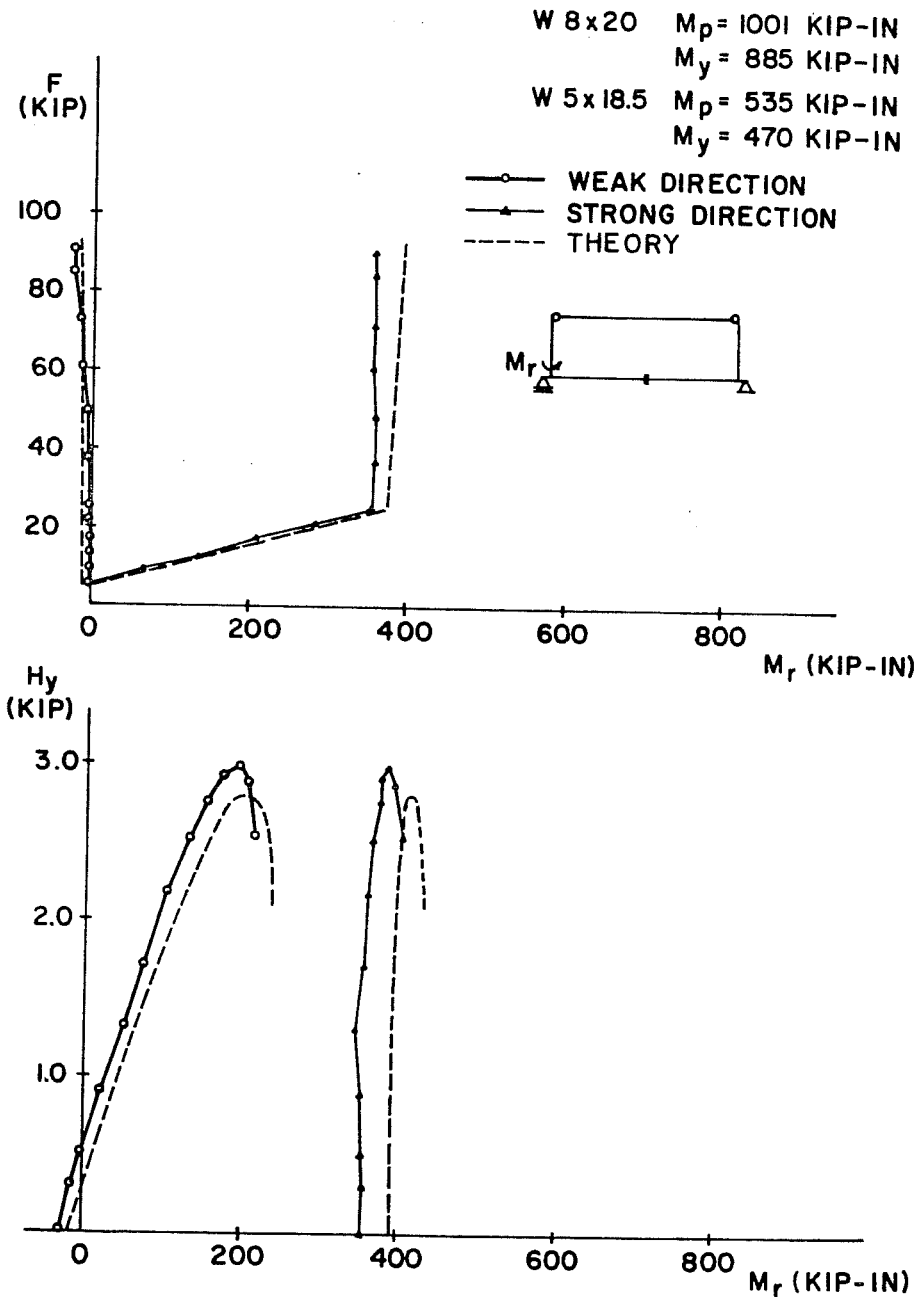


Fig. 5.20 Variation of restraining moments with loads (Specimen BC-2)

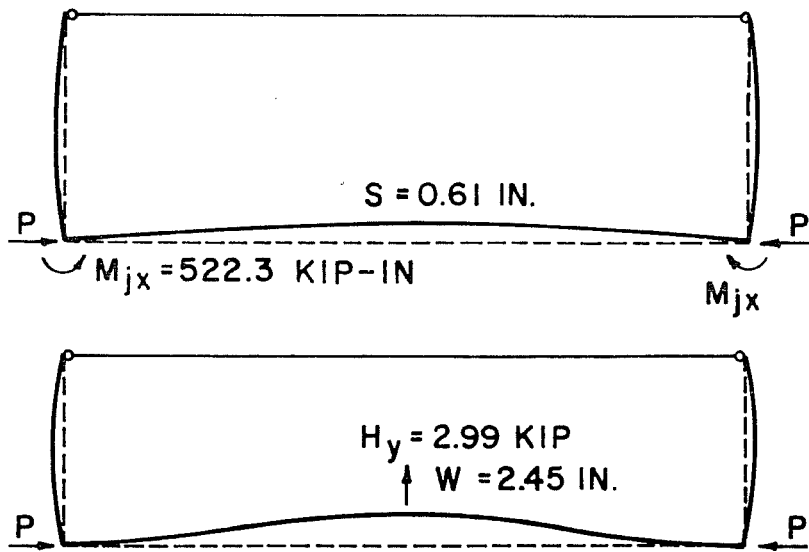


Fig. 5.21 Deflected shapes of Specimen BC-2 at the maximum load

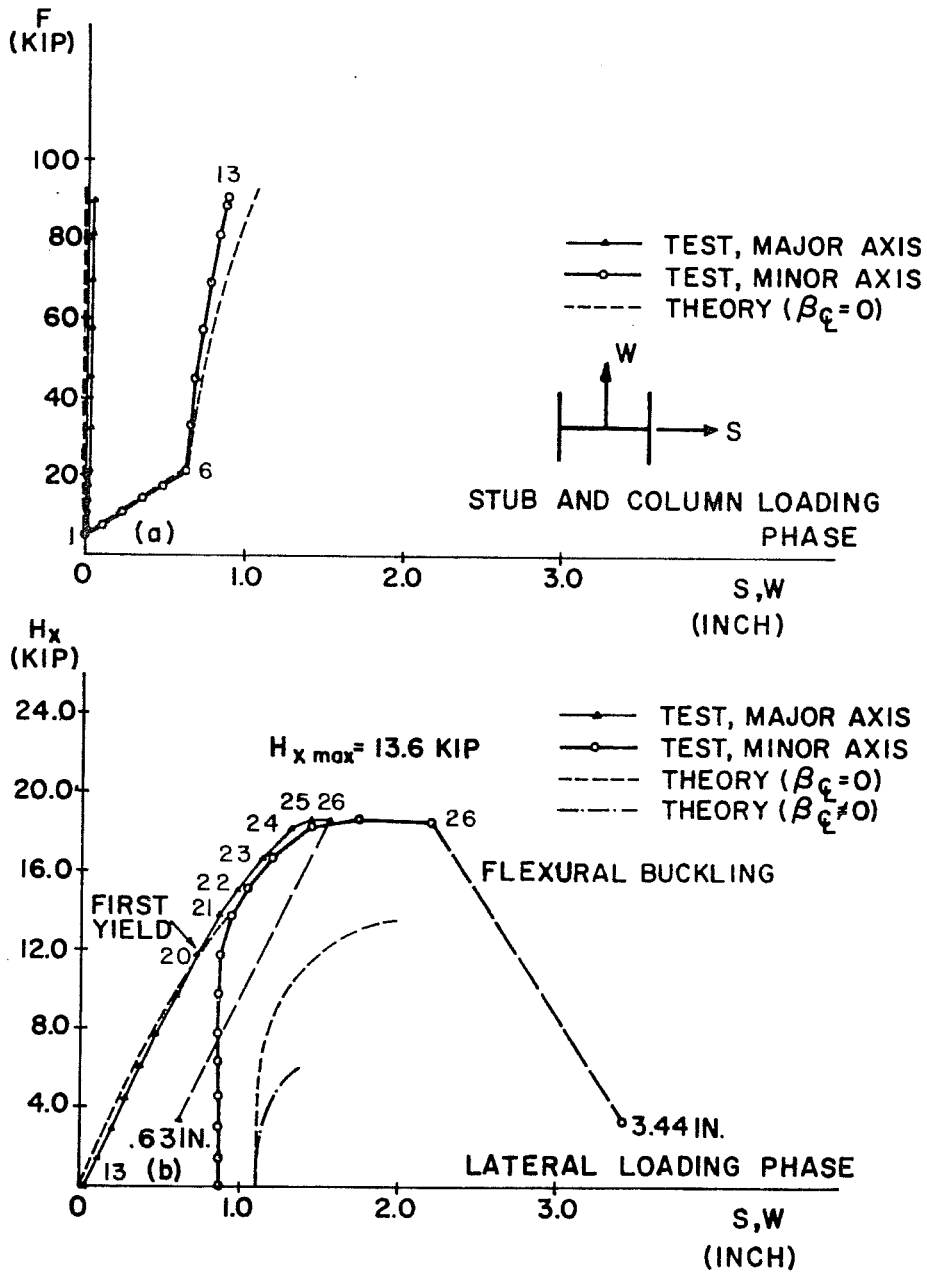


Fig. 5.22 Load-displacement relationship at the midlength (Specimen BC-3)

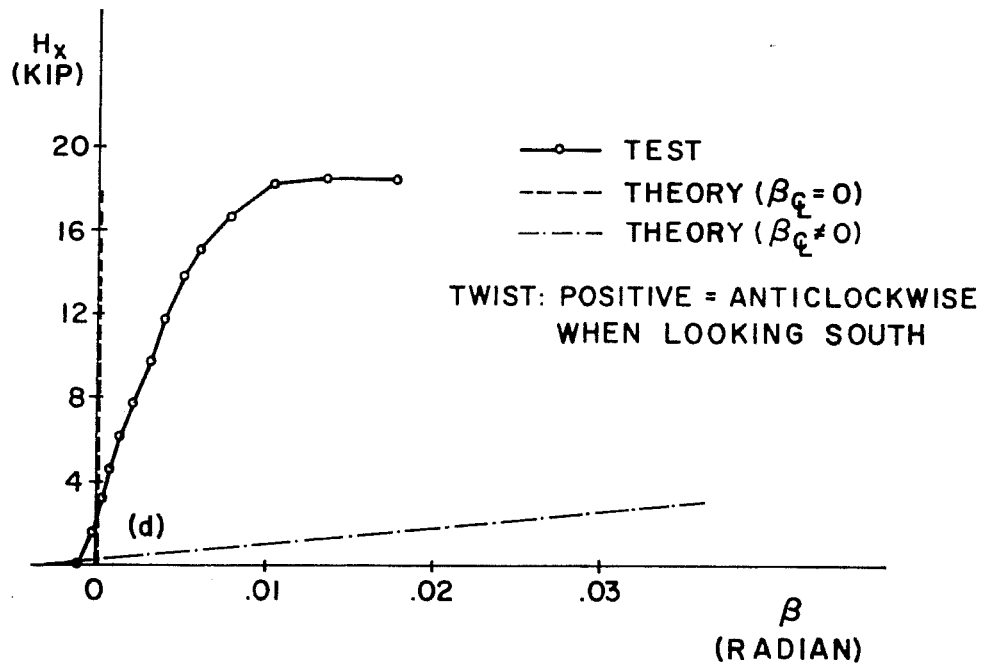
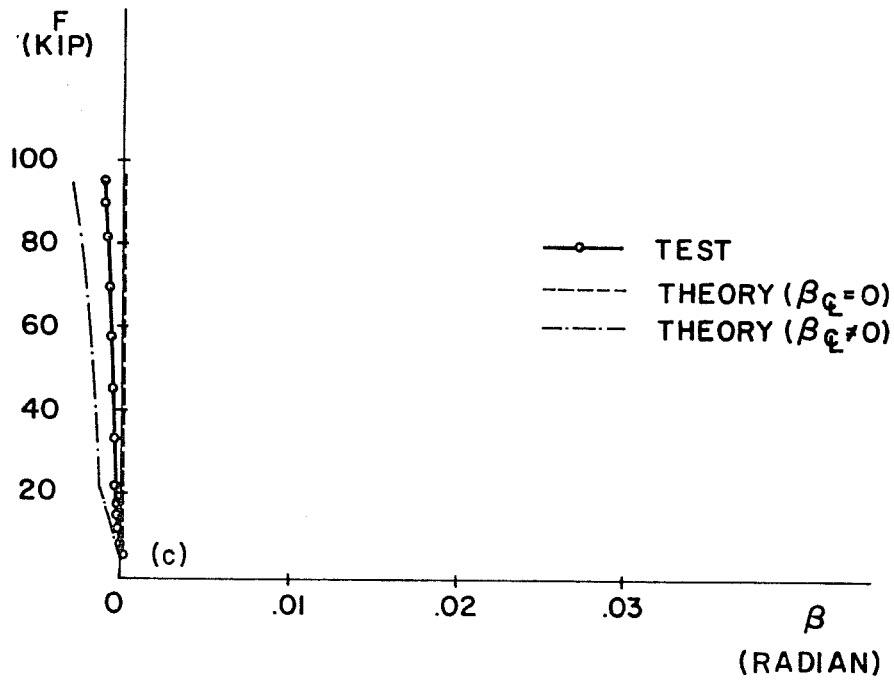


Fig. 5.22 (Continued)

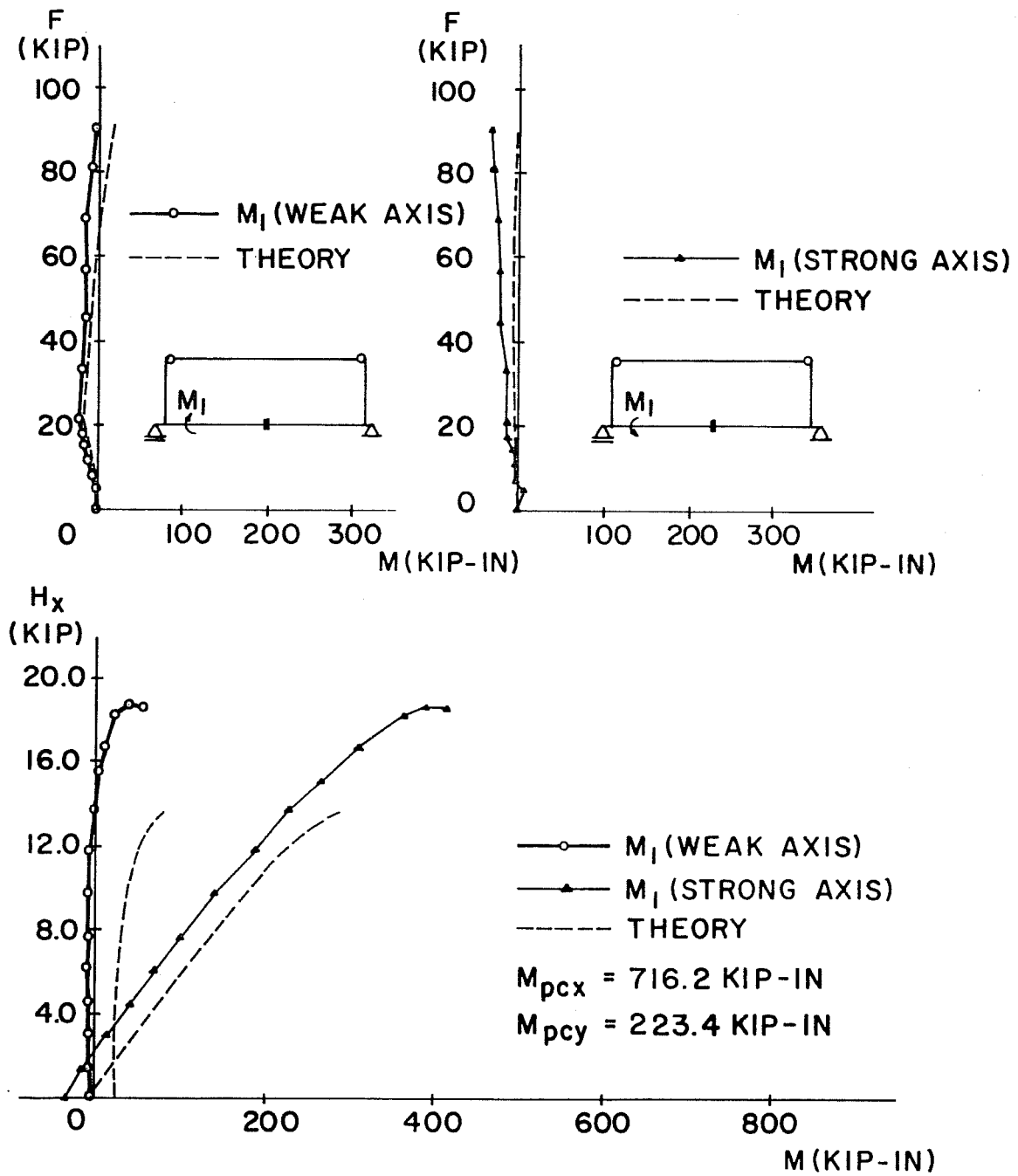


Fig. 5.23 Variation of column moments with loads (Specimen BC-3)

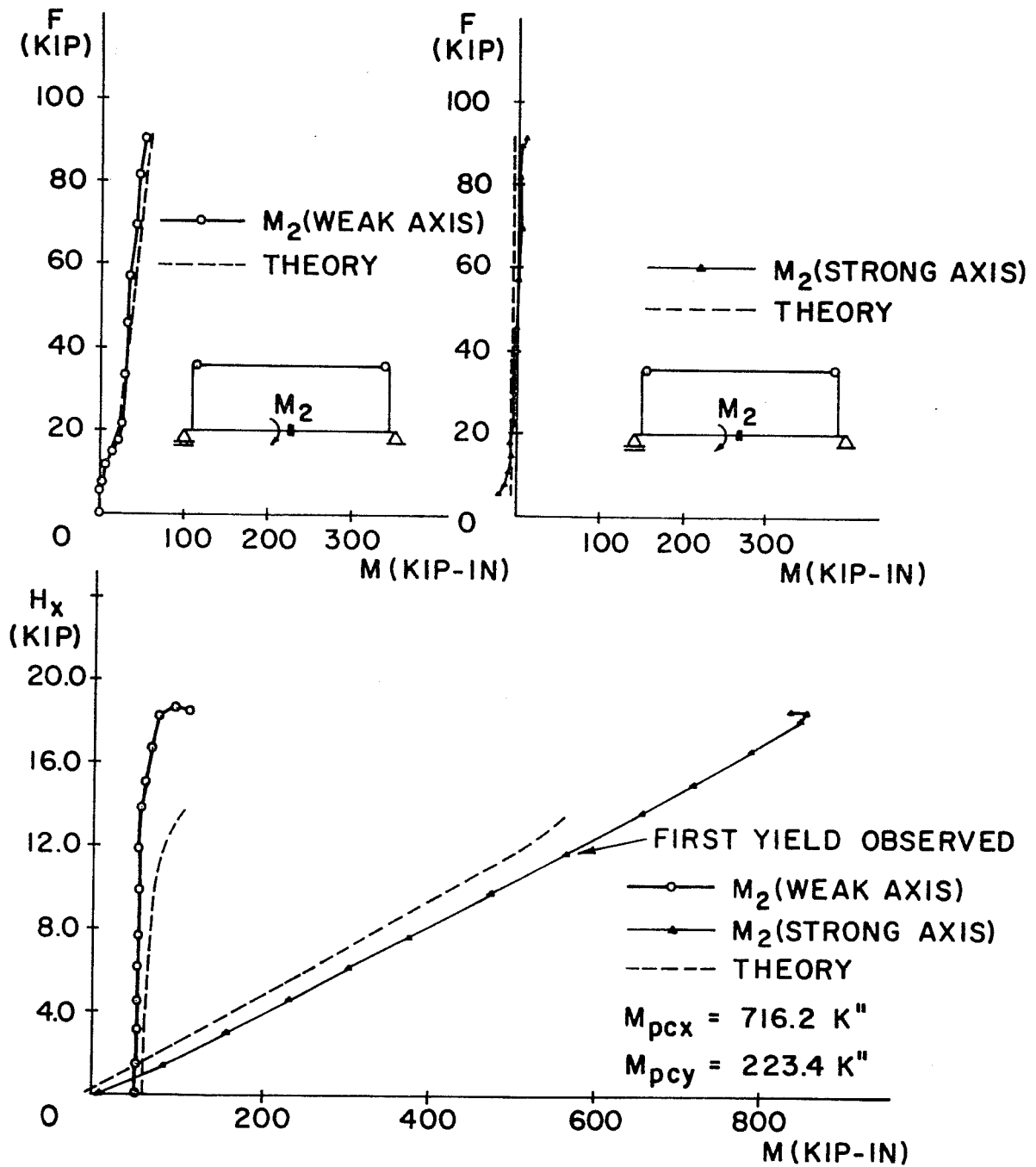


Fig. 5.23 (Continued)

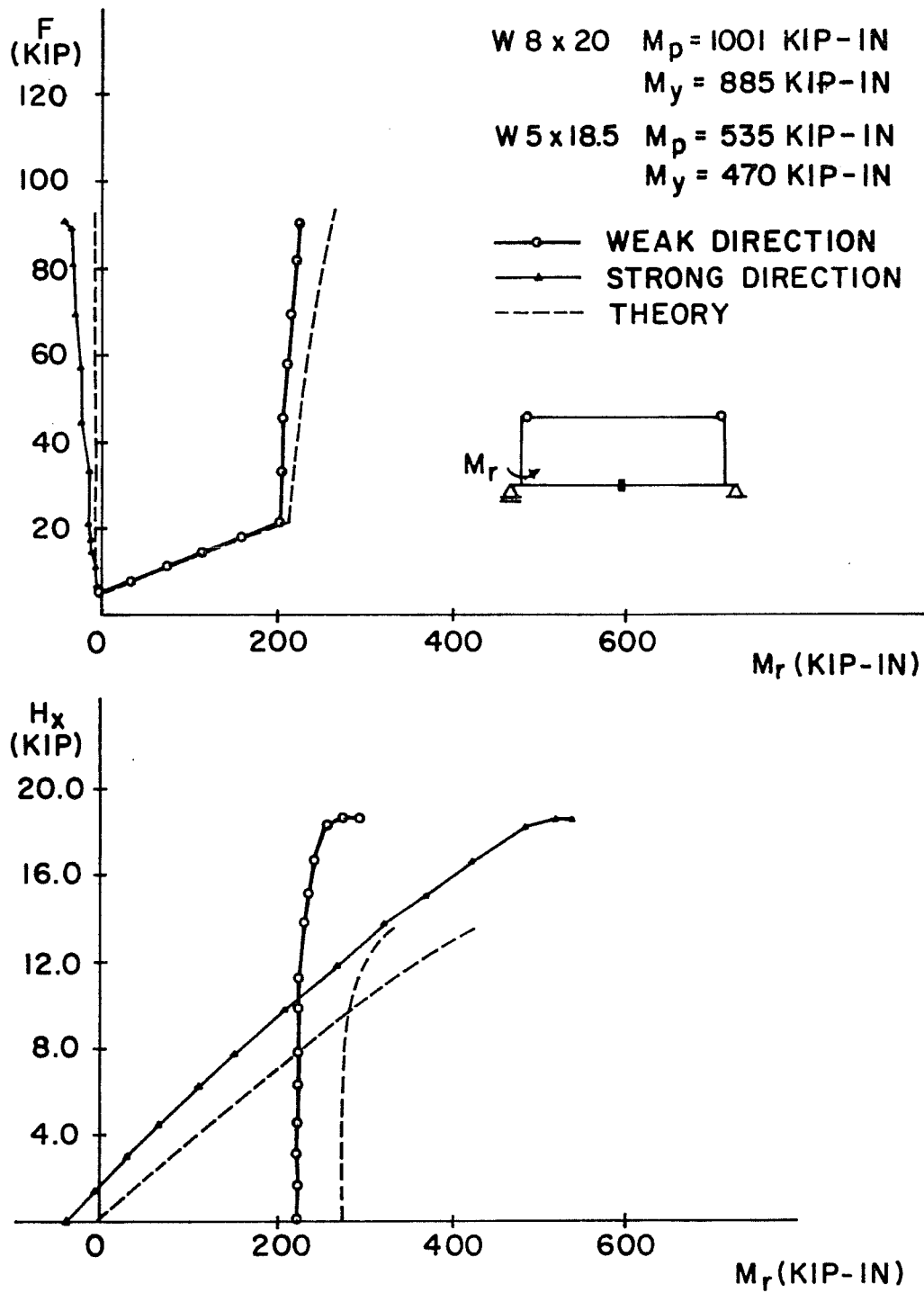


Fig. 5.24 Variation of restraining moments with loads (Specimen BC-3)

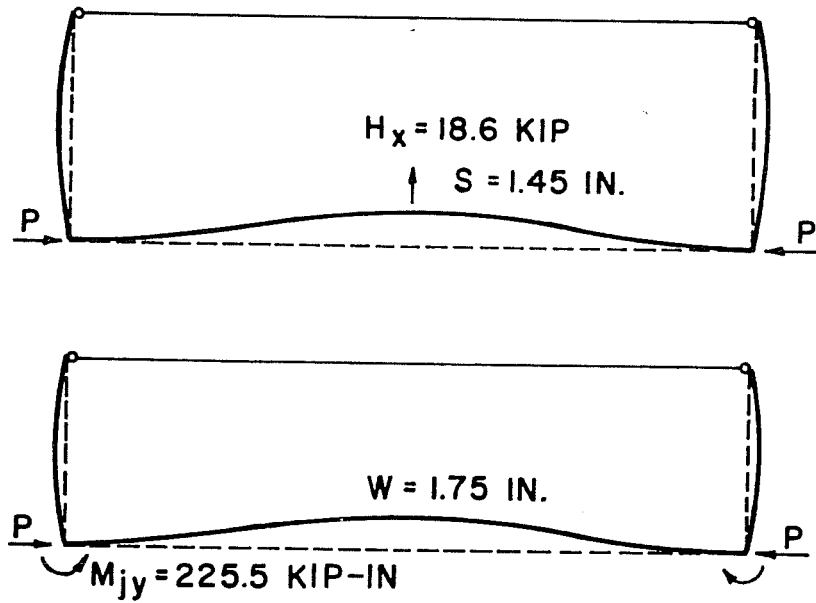


Fig. 5.25 Deflected shapes of Specimen BC-3 at the maximum load

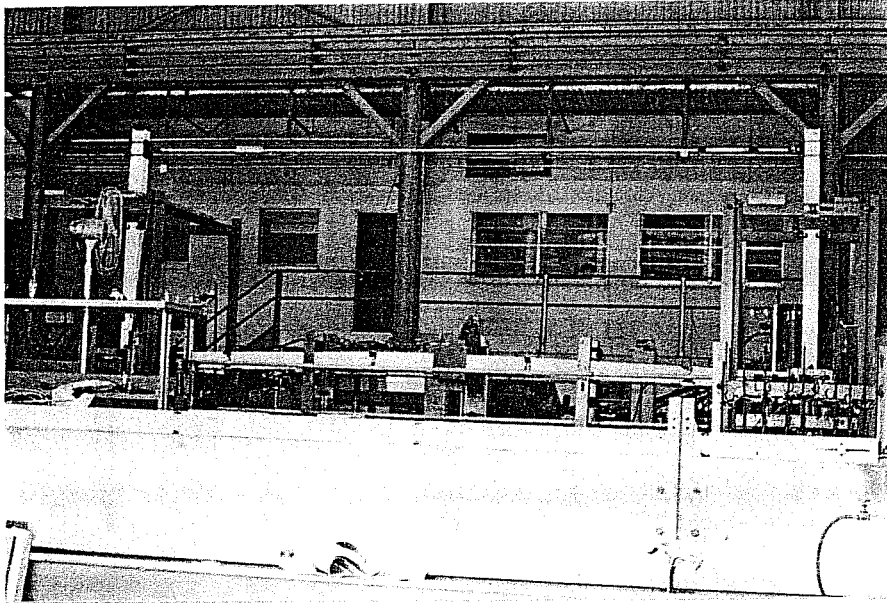


Fig. 5.26 Specimen BC-1 after failure

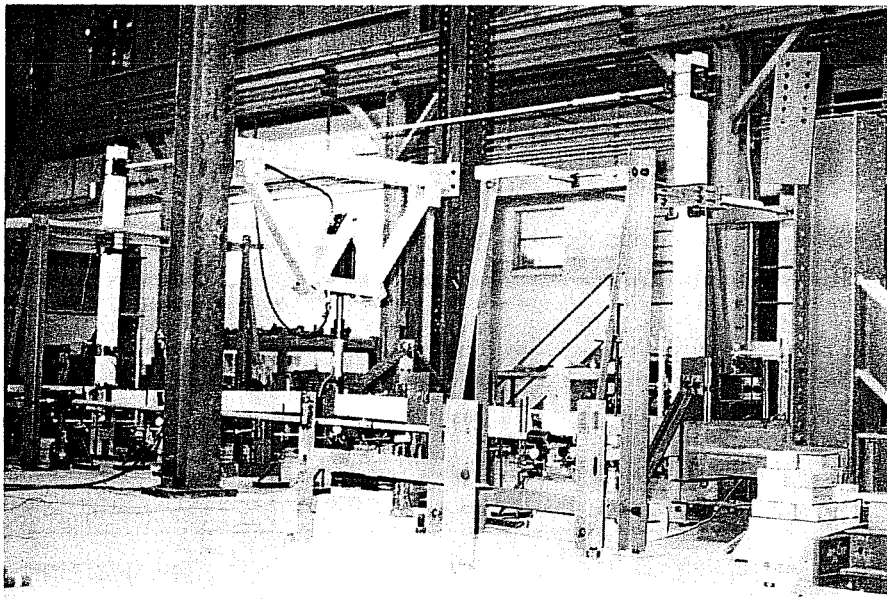


Fig. 5.27 Specimen BC-2 after failure

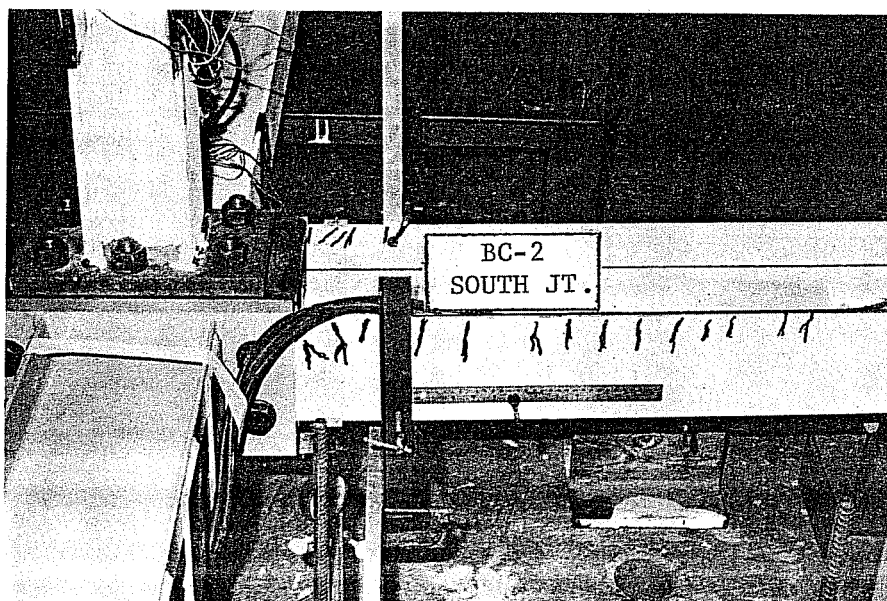


Fig. 5.28 Yielded zone at south joint after failure, Specimen BC-2

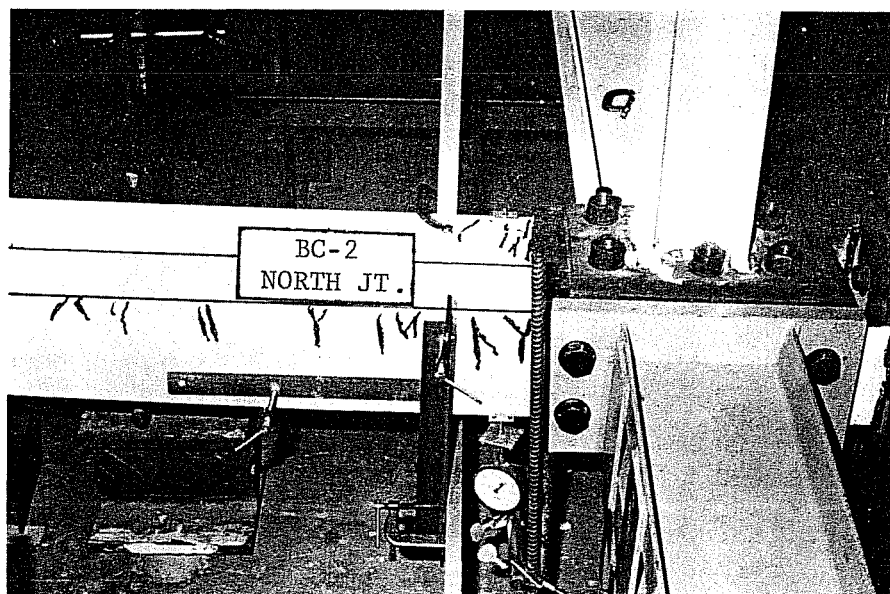


Fig. 5.29 Yielded zone at north joint after failure, Specimen BC-2

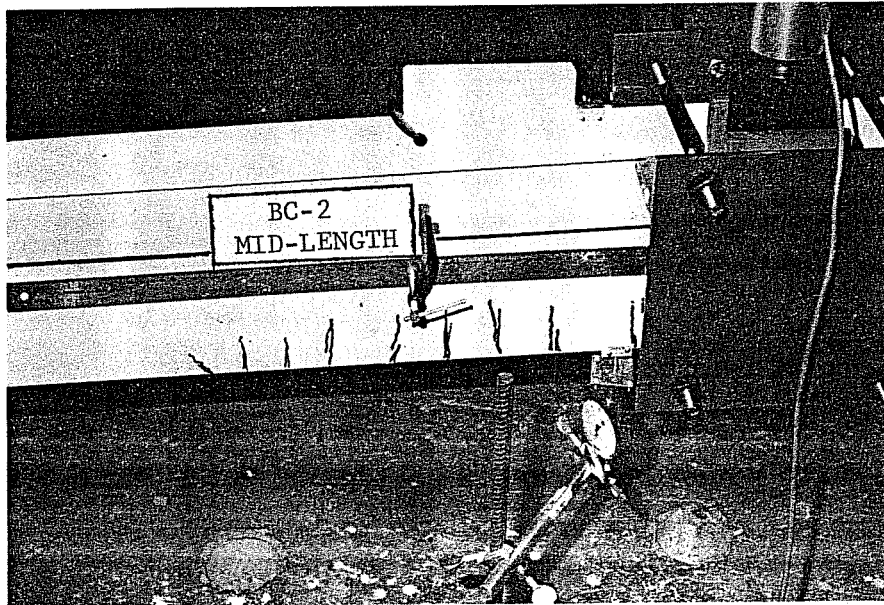


Fig. 5.30 Yielded zone at midlength after failure, Specimen BC-2

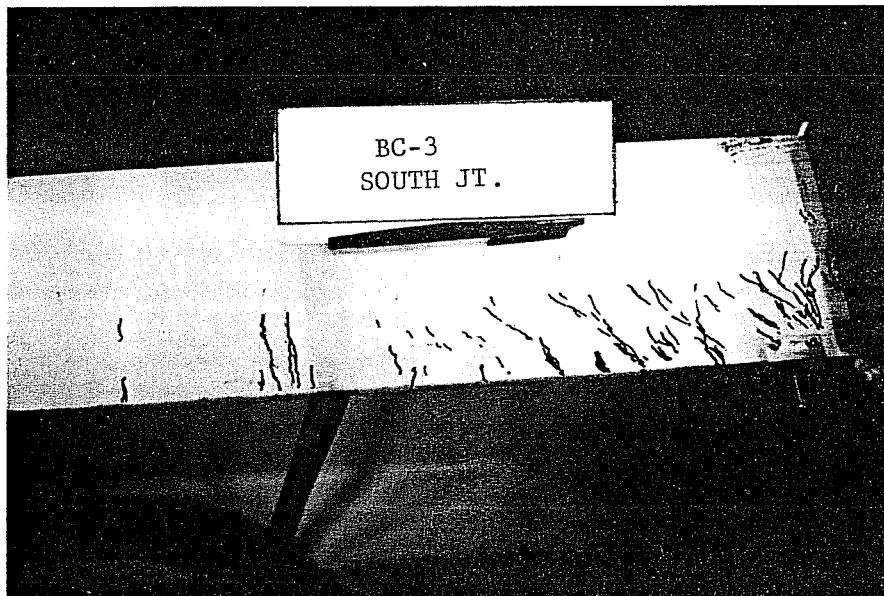


Fig. 5.31 Yielded zone at south joint after failure, Specimen BC-3

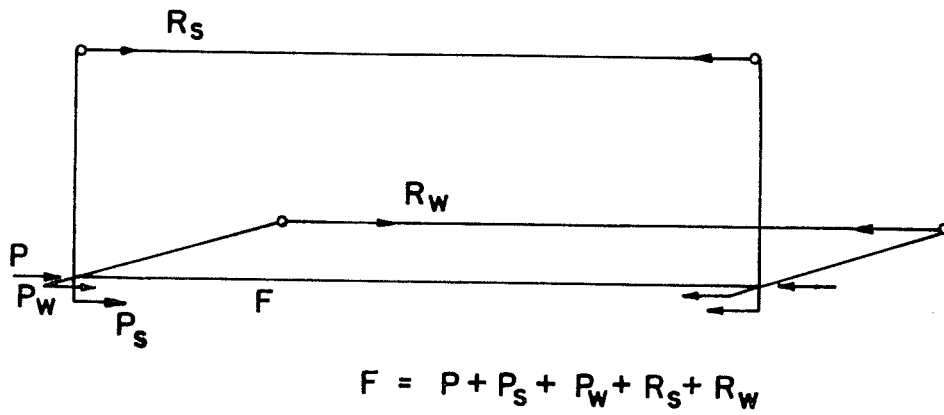


Fig. 5.32 Axial force in test specimens

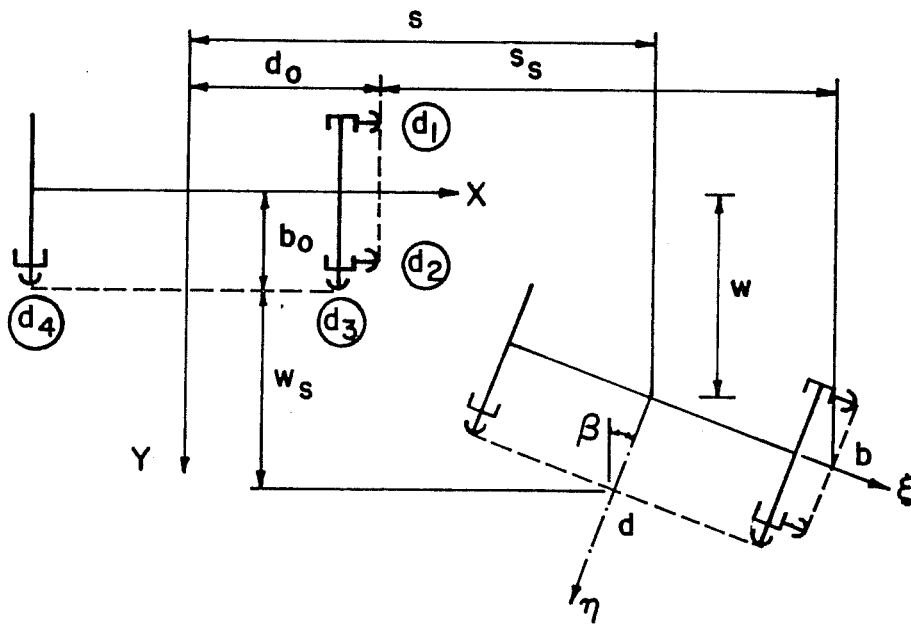


Fig. 5.33 Displacement components of a cross section

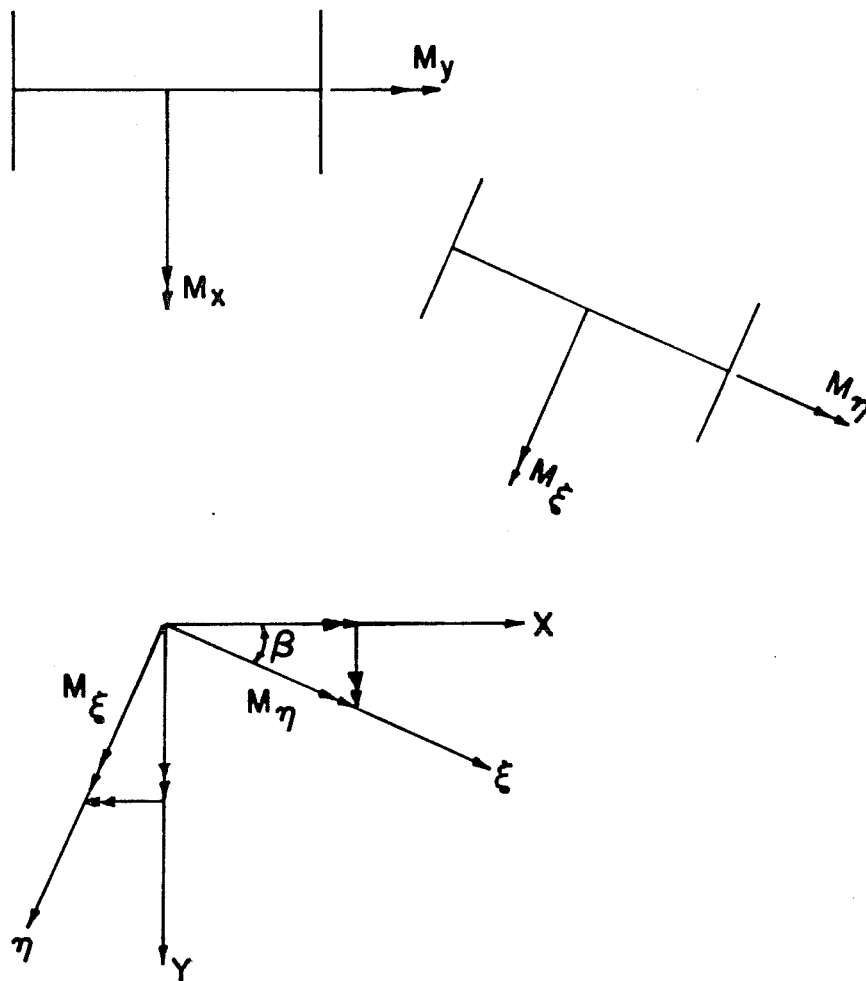


Fig. 5.34 Moments at a cross section in untwist and twist coordinates

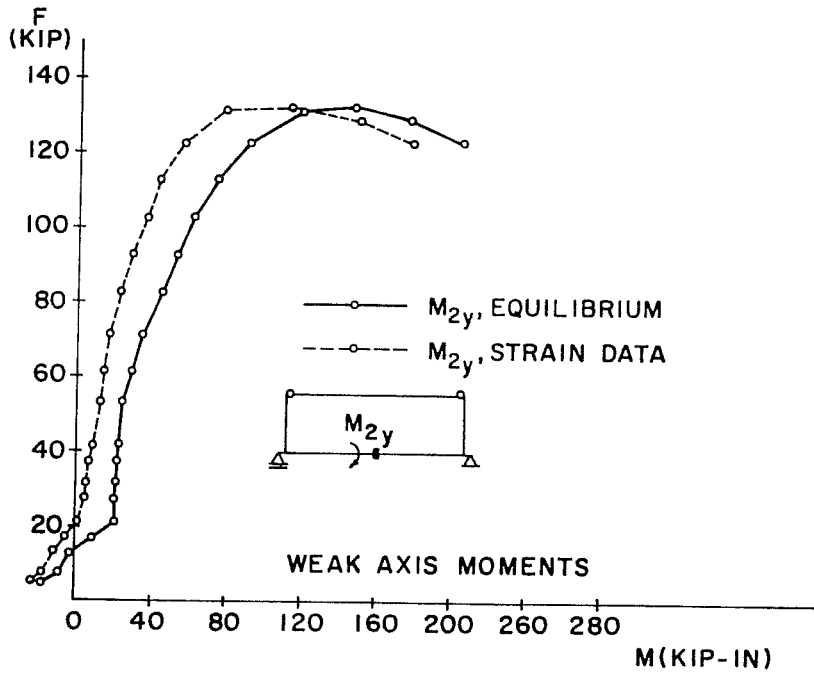
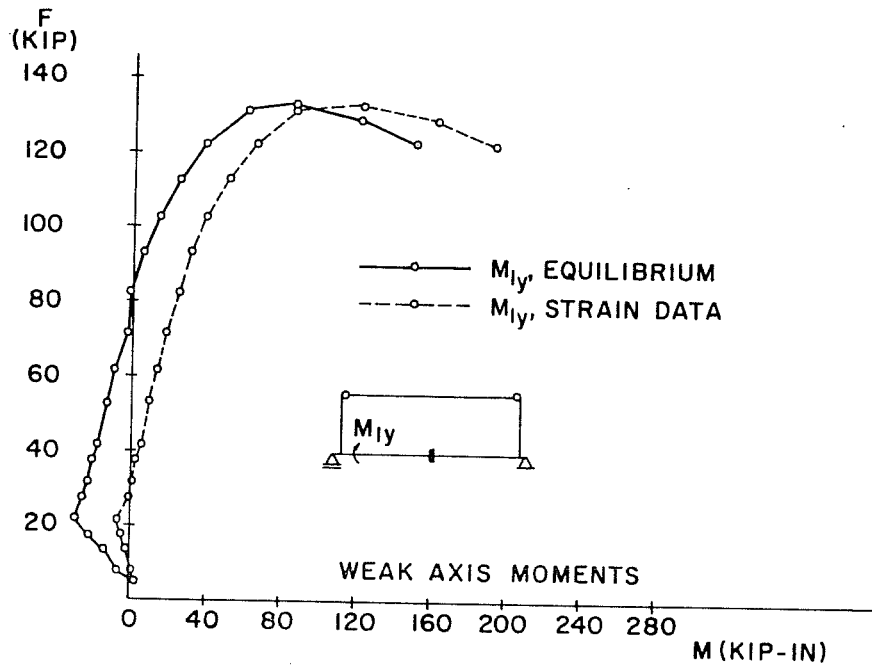


Fig. 5.35 Comparison of column moments based on the equilibrium and strain data analysis (Specimen BC-1)

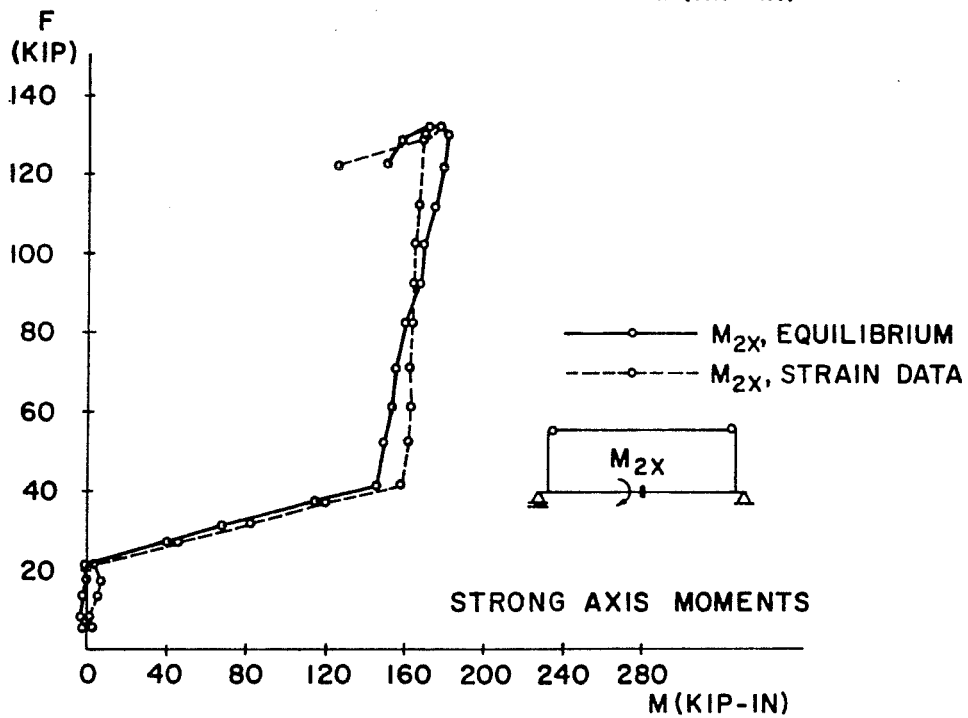
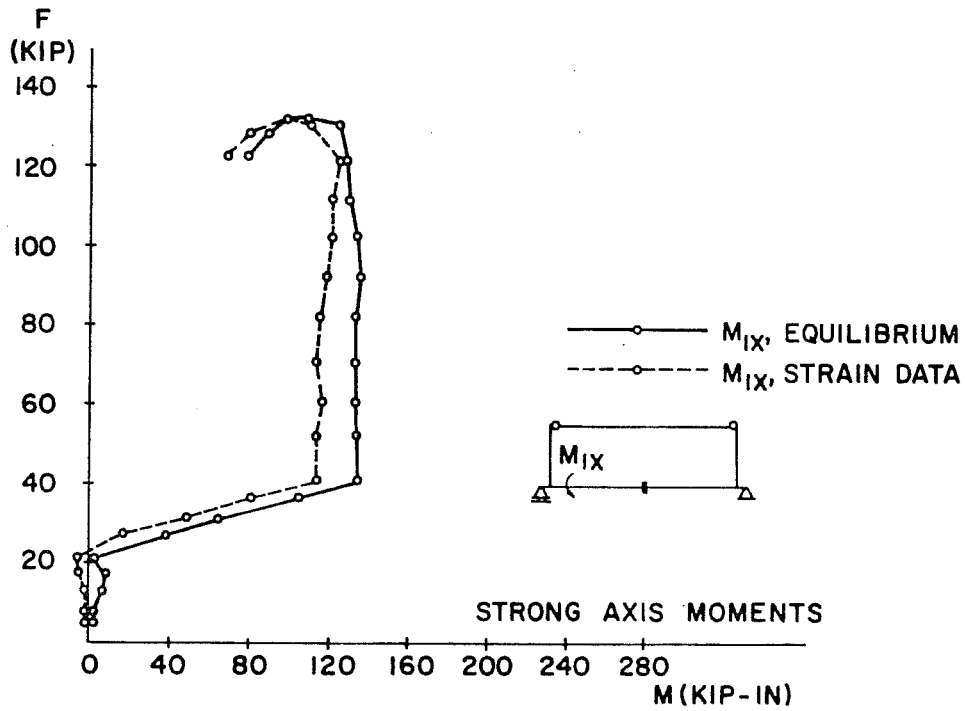


Fig. 5.35 (Continued)

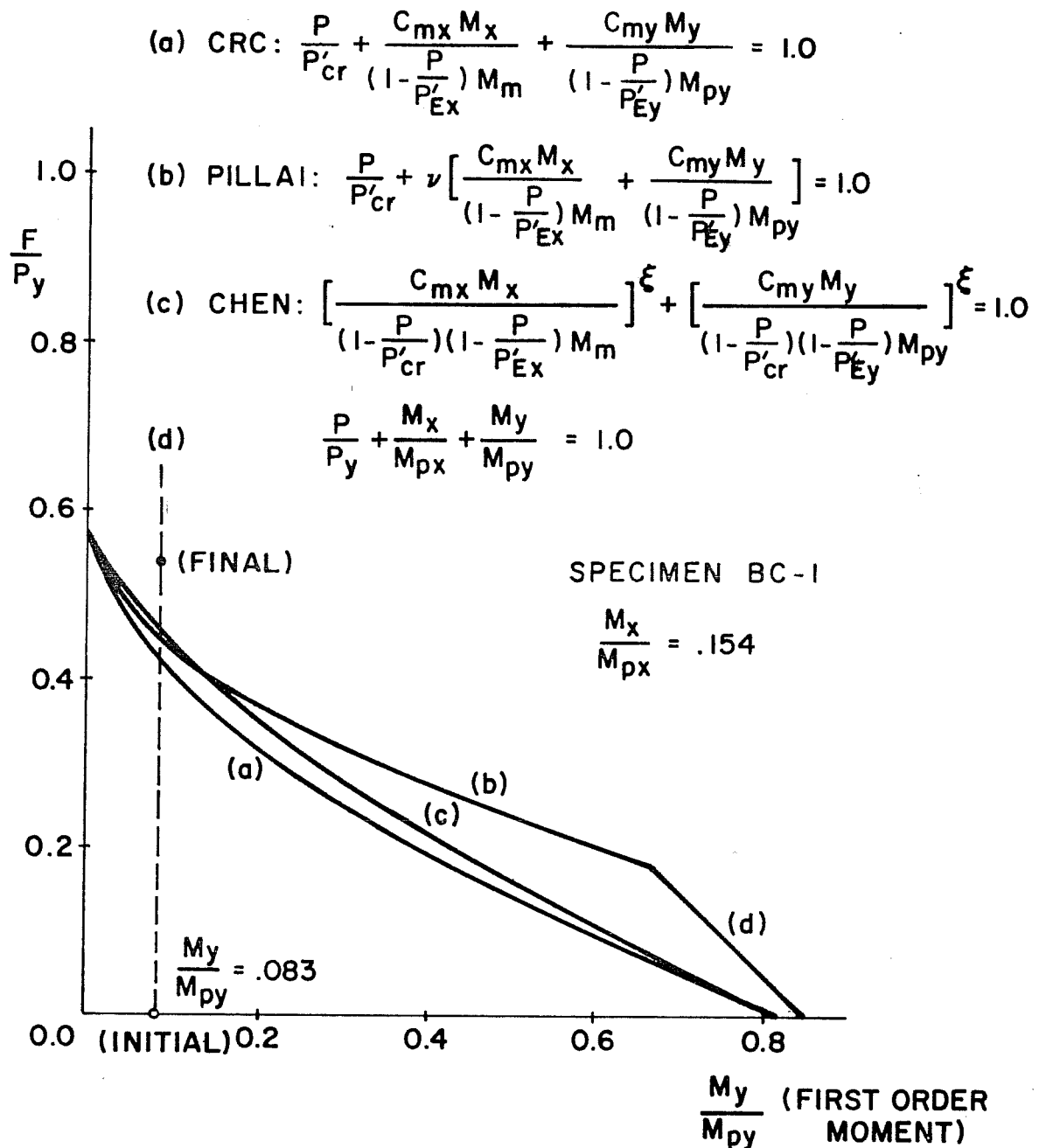


Fig. 5.36a Comparison of test and predicted results (Specimen BC-1)

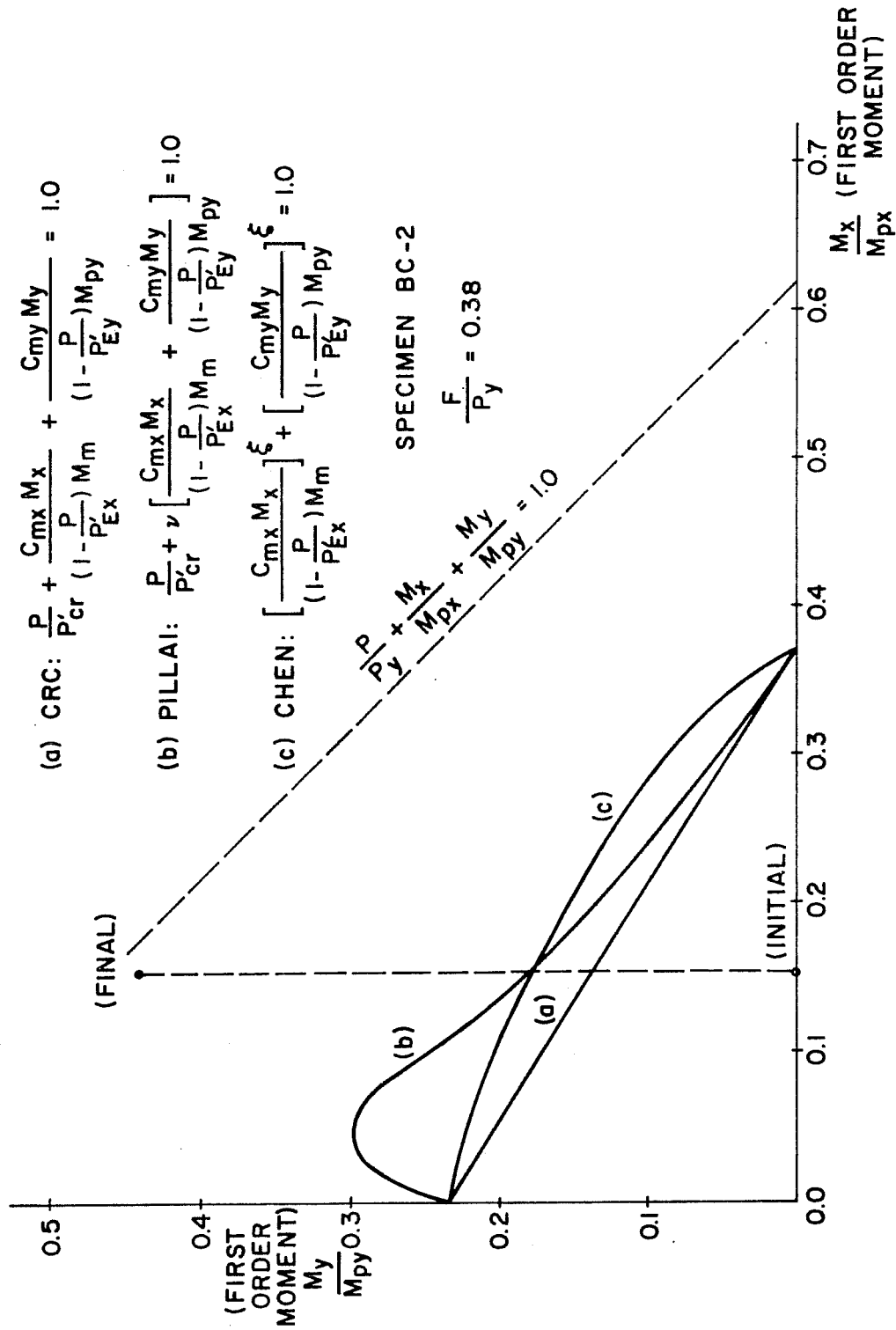


Fig. 5.36b Comparison of test and predicted results (Specimen BC-2)

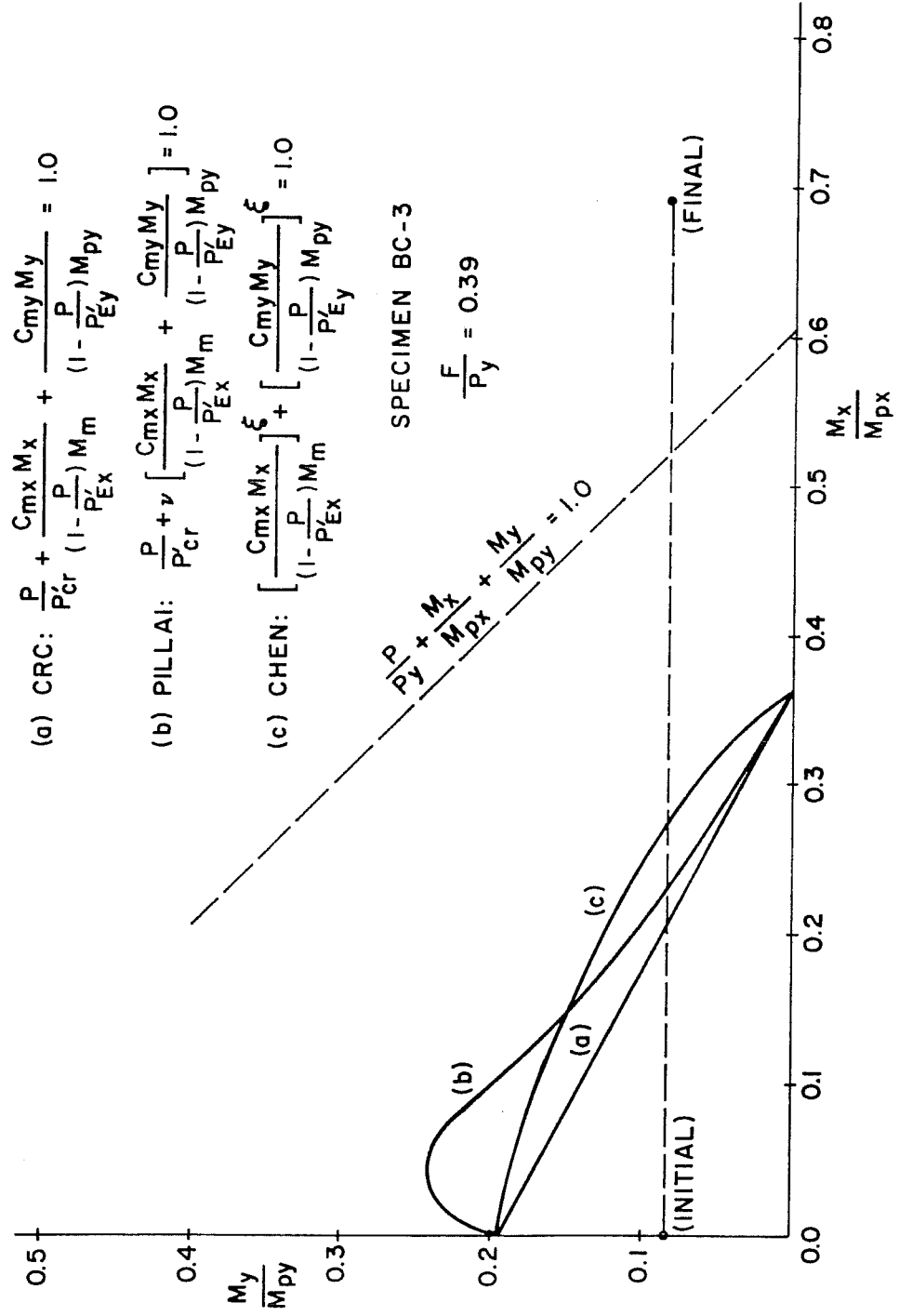


Fig. 5.36c Comparison of test and predicted results (Specimen BC-3)

A P P E N D I X A

MOMENT-THRUST-CURVATURE RELATIONSHIPS

In order to compute the moment-thrust-curvature relationships numerically, a wide flange section is divided into finite grid elements. The coordinate system is chosen to pass through the centroid of the section. Under the action of bending moment and axial thrust, the strain at element i with residual stress can be expressed in the nondimensional form

$$\frac{\epsilon_i}{\epsilon_y} = \frac{\epsilon_o}{\epsilon_y} + \varphi \frac{c_i}{c} + \frac{\epsilon_{ri}}{\epsilon_y} \quad (\text{A.1})$$

where ϵ_i is the total strain at element i , positive for tensile strain; ϵ_o the strain at the centroid of the section; φ is the curvature nondimensionalized by the curvature at initial yielding for pure bending moment, $\varphi = \epsilon_y/c$; c_i is the distance of the center of element i from the centroidal axis; ϵ_{ri} is the residual strain at element i ; ϵ_y is the strain at yield point; and c is the half depth or half width of the cross section for bending about the strong or weak axis, respectively.

Assuming an elastic-perfectly plastic stress-strain relationship for the steel, the strain in Eq. A.1 is related to the stress by

$$\frac{\sigma_i}{\sigma_y} = \frac{\epsilon_i}{\epsilon_y} \quad \text{for} \quad \left| \frac{\epsilon_i}{\epsilon_y} \right| < 1 \quad (\text{A.2a})$$

$$\frac{\sigma_i}{\sigma_y} = \pm 1 \quad \text{for} \quad \left| \frac{\epsilon_i}{\epsilon_y} \right| \geq 1 \quad (\text{A.2b})$$

in which σ_i and σ_y are the normal stress at element i and the yield stress, respectively, σ_i being positive for tensile stress.

The axial thrust and moment are then determined from the following two equilibrium equations in nondimensionalized form,

$$p = \frac{1}{A} \sum_{i=1}^n \frac{\sigma_i}{\sigma_y} \Delta A_i \quad (\text{A.3})$$

$$m = \frac{1}{Z} \sum_{i=1}^n \frac{\sigma_i}{\sigma_y} c_i \Delta A_i \quad (\text{A.4})$$

where p and m are the axial thrust and moment nondimensionalized by the yield load, $P_y = \sigma_y A$, and the fully plastic moment, $M_P = \sigma_y Z$, of the section, respectively; A is the area and Z the plastic modulus of the section; ΔA_i denotes the area of element i and n the total number of elements.

The moment-thrust-curvature relationships are obtained from Eqs. A.3 and A.4, together with Eqs. A.1 and A.2, by specifying the residual stress distribution; hence, the residual strain distribution, and systematically varying ϵ_0 and ϕ . For simplicity, it is assumed that the residual stress is constant across the thickness and that equilibrium is maintained within each plate components.

B I B L I O G R A P H Y

1. American Institute of Steel Construction, Specification for the Design, Fabrication, and Erection of Structural Steel for Buildings, New York, 1969.
2. Arnold, P., Adams, P. F., and Lu, L. W., "Strength and Behavior of an Inelastic Hybrid Frame," Journal of the Structural Division, ASCE, Proc. V. 94, ST1, January 1968.
3. American Society of Civil Engineers, Plastic Design in Steel, A Guide and Commentary, No. 41, ASCE Manuals and Reports on Engineering Practice, New York 1971.
4. Austin, W. J., "Strength and Design of Metal Beam-Columns," Journal of the Structural Division, ASCE, Proc. V. 87, ST4, April 1961.
5. Baker, J. F., Horne, M. R., and Heyman, J., The Steel Skeleton Vol. II, Plastic Behavior and Design, Cambridge University Press, 1956.
6. Birnstiel, C., and Michalos, J., "Ultimate Load of H-Columns under Biaxial Bending," Journal of the Structural Division, ASCE, Proc. V. 89, ST2, April 1963.
7. Birnstiel, C., Leu, K. C., Tesoro, J. A., and Tomasetti, R. L., "Experiments on H-Columns under Biaxial Bending," Department of Civil Engineering, New York University, January 1967.
8. Bleich, F., Buckling Strength of Metal Structures, McGraw-Hill Book Company, New York, 1952.
9. Carpenter, E. F., "Experimental and Analytical Study of Beam-Column Subassemblages," unpublished MS thesis, University of Delaware, June 1967.
10. Chen, W. F., "Further Studies of an Inelastic Beam-Column Problem," Fritz Engineering Laboratory Report No. 331.6, Lehigh University, January 1970.
11. Chen, W. F., and Santathadaporn, S., "Review of Column Behavior under Biaxial Loading," Journal of the Structural Division, ASCE, Proc. V. 94, ST12, December 1968.

12. Chubkin, G. M., "Experimental Research on the Stability of Thin Plate Steel Members with Biaxial Eccentricity," Paper No. 6, Analysis of Spatial Structures, Vol. 5, Moscow, 1959, G.I.L.S.
13. Driscoll, G. C., Jr., et al., "Plastic Design of Multistory Frames," Lecture Notes, Fritz Engineering Laboratory Report No. 273.20, Lehigh University, 1965.
14. English, G. W., and Adams, P. F., "The Experiments on Laterally Loaded Steel Wide-Flange Beam-Columns," Structural Engineering Report No. 33, University of Alberta, Edmonton, Canada, May 1971.
15. Fukumoto, Y., "Inelastic Lateral Torsional Buckling of Beam-Columns," unpublished Ph.D. dissertation, Lehigh University, 1963.
16. Galambos, T. V., "Inelastic Lateral Torsional Buckling of Eccentrically Loaded Wide-Flange Columns," unpublished Ph.D. dissertation, Lehigh University, 1959.
17. Galambos, T. V., "Review of Tests on Biaxially Loaded Steel Wide-Flange Beam-Columns," Fritz Engineering Laboratory Report No. 278.4, Lehigh University, April 1963.
18. Galambos, T. V., Structural Members and Frames, Prentice-Hall, Inc., Englewood Cliffs, New Jersey, 1968.
19. Galambos, T. V., and Ketter, R., "Columns under Combined Bending and Thrust," Journal of the Engineering Mechanics Division, ASCE, Proc. V. 85, EM2, April 1959.
20. Galambos, T. V., and Prasad, J., "Ultimate Strength Tables for Beam-Columns," WRC Bulletin No. 78, Welding Research Council, June 1962.
21. Gaylord, E. H., and Gaylord, C. N., Design of Steel Structures, Second Edition, McGraw-Hill Book Company, New York, 1972.
22. Gent, A. R., "Elastic-Plastic Column Stability and the Design of No-Sway Frames," Proceedings of the Institution of Civil Engineers, Vol. 34, June 1966.
23. Gent, A. R., and Milner, H. R., "The Ultimate Load Capacity of Elastically Restrained H-Columns under Biaxial Bending," Proceedings of the Institution of Civil Engineers, Vol. 41, December 1968.

24. Harstead, G. A., Birnstiel, C., and Leu, K. C., "Inelastic H-Columns under Biaxial Bending," Journal of the Structural Division, ASCE, Proc. V. 94, ST10, October 1968.
25. Hill, H. N., and Clark, J. W., "Lateral Buckling of Eccentrically Loaded I-Section Columns," Transactions, ASCE, Vol. 116 1951.
26. Huber, A. W., and Beedle, L. S., "Residual Stress and the Compressive Strength of Steel," The Welding Journal Research Supplement, Vol. 33, No. 12, December 1954.
27. Isbell, D., "Comparison of Approximate Methods of Second Order Analysis," unpublished M.S. report, Department of Civil Engineering, The University of Texas at Austin, January 1973.
28. Johnston, B. G., Guide to Design Criteria for Metal Compression Members, Second Edition, John Wiley and Sons, Inc., New York, 1966.
29. Johnston, B. G., Guide to Stability Design Criteria for Metal Structures, Third Edition, John Wiley and Sons, Inc., New York, 1976.
30. Ketter, R., "Further Studies of the Strength of Beam-Columns," Journal of the Structural Division, ASCE, Proc. V. 87, ST6, August 1961.
31. Kloppel, K., and Winkelmann, E., "Experimentelle und Theoretische Untersuchungen uber die Traglast von Zweiachsig Aussermittig Gedruckten Stahlstaben," Der Stahlbau, Vol. 31, No. 2, February 1962.
32. Laosirichon, V., "The Effect of Beam Yielding on Steel Column Strength," unpublished Ph.D. dissertation, The University of Texas at Austin, 1975.
33. Lay, M. G., and Galambos, T. V., "The Experimental Behavior of Restrained Columns," WRC Bulletin No. 110, Welding Research Council, November 1965.
34. Lay, M. G., Aglietti, R. A., and Galambos, T. V., "Tests on A36 and A441 Steel Beam-Columns," Fritz Engineering Laboratory Report No. 278.14, Lehigh University, June 1964.
35. Levi, V., Driscoll, G. C., Jr., and Lu, L. W., "Structural Sub-assemblages Prevented from Sway," Journal of the Structural Division, ASCE, Proc. V. 91, ST5, October 1965.

36. Levi, V., Driscoll, G. C., Jr., and Lu, L. W., "Analysis of Restrained Columns Permitted to Sway," Journal of the Structural Division, ASCE, Proc. V. 93, ST1, February 1967.
37. Lim, L. C., "The Strength and Behavior of Laterally Unsupported Columns," unpublished Ph.D. dissertation, Lehigh University, 1970.
38. Lu, L. W., "Stability of Frames under Primary Bending Moments," Journal of the Structural Division, ASCE, Proc. V. 89, ST3, June 1963.
39. Lu, L. W., "Inelastic Buckling of Steel Frames," Journal of the Structural Division, ASCE, Proc. V. 91, ST6, December 1965.
40. Lu, L. W., and Kamalvand, H., "Ultimate Strength of Laterally Loaded Columns," Journal of the Structural Division, ASCE, Proc. V. 94, ST6, June 1968.
41. Marshall, P. J., and Ellis, J. S., "Ultimate Biaxial Capacity of Box Steel Columns," Journal of the Structural Division, ASCE, Proc. V. 96, ST9, September 1970.
42. Massonnet, C., "Stability Considerations in the Design of Steel Columns," Journal of the Structural Division, ASCE, Proc. V. 85, ST7, September 1959.
43. McNamee, B., and Lu, L. W., "Inelastic Multistory Frame Buckling," Journal of the Structural Division, ASCE, Proc. V. 98, ST7, July 1972.
44. Milner, H. R., and Gent, A. R., "Ultimate Load Calculations for Restrained H-Columns under Biaxial Bending," Civil Engineering Transactions, The Institution of Engineers, Australia, April 1971.
45. Mitchell, J. S., "A Nonlinear Analysis of Biaxial Loaded Beam-Columns Using a Discrete Model," unpublished Ph.D. dissertation, The University of Texas at Austin, 1973.
46. Ojalvo, M., "Restrained Columns," Journal of the Engineering Mechanics Division, ASCE, Proc. V. 86, EM5, October 1960.
47. Ojalvo, M., and Fukumoto, Y., "Nomographs for the Solutions of Beam-Column Problems," WRC Bulletin No. 78, Welding Research Council, June 1962.

48. Oral, A., "Inelastic Analysis of Planar Steel Frames," unpublished Ph.D. dissertation, The University of Texas at Austin, 1974.
49. Pillai, S. U., "Review of Recent Research on the Behavior of Beam-Columns under Biaxial Bending," Civil Engineering Research Report No. CE70-1, Royal Military College of Canada, Kingston, Canada, January 1970.
50. Pillai, S. U., and Ellis, J. S., "Hollow Tubular Beam-Columns in Biaxial Bending," Journal of the Structural Division, ASCE, Proc. V. 97, ST5, May 1971.
51. Salem, A. H., Discussion of "Buckling Analysis of One-Story Frames," by A. Zweig, Journal of the Structural Division, ASCE, Proc. V. 95, ST5, May 1969.
52. Salvadori, M. G., "Lateral Buckling of I-Beams," Transactions, ASCE, Vol. 120, 1955.
53. Salvadori, M. G., "Lateral Buckling of Eccentrically Loaded I-Columns," Transactions, ASCE, Vol. 121, 1956.
54. Santathadaporn, S., and Chen, W. F., "Analysis of Biaxially Loaded H-Columns," Journal of the Structural Division, ASCE, Proc. V. 99, ST3, March 1973.
55. Sheninger, E. L., and Lu, L. W., "Experiments on Nonsway Structural Subassemblages," Journal of the Structural Division, ASCE, Proc. V. 96, ST3, March 1970.
56. Springfield, J., "Design of Columns Subjected to Biaxial Bending," AISC Journal, June 1975.
57. Springfield, J., and Adams, P. F., "Aspects of Column Design in Tall Steel Buildings," Journal of the Structural Division, ASCE, Proc. V. 98, ST5, May 1972.
58. Springfield, J., and Hegan, B., "Comparison of Test Results with Design Equations for Biaxially Loaded Steel Wide-Flange Beam-Columns," Canadian Steel Industries Construction Council, Toronto, Canada, 1973.
59. Tebedge, N., and Chen, W. F., "Design Criteria for H-Columns under Biaxial Loadings," Journal of the Structural Division, ASCE, Proc. V. 100, ST3, March 1974.
60. Timoshenko, S. P., and Gere, J. M., Theory of Elastic Stability, McGraw-Hill Book Company, New York, 1961.

61. Vinnakota, S., and Aoshima, Y., "Spatial Behavior of Rotationally and Directionally Restrained Beam-Columns," IABSE Publication, Vol. 34, Part II, 1974.
62. Wood, B. R., Beaulieu, D., and Adams, P. F., "Column Design by P-Delta Method," Journal of the Structural Division, ASCE, Proc. V. 102, ST2, February 1976.
63. Wood, B. R., Beaulieu, D., and Adams, P. F., "Further Aspects of Column Design by P-Delta Method," Journal of the Structural Division, ASCE, Proc. V. 102, ST3, March 1976.
64. Yarimci, E., "Incremental Inelastic Analysis of Framed Structures and Some Experimental Verifications," unpublished Ph.D. dissertation, Lehigh University, 1966.
65. Yarimci, E., Yura, J. A., and Lu, L. W., "Techniques for Testing Structures Permitted to Sway," Fritz Engineering Laboratory Report No. 273.4, Lehigh University, May 1966.
66. Yen, Y. C., Lu, L. W., and Driscoll, G. C., Jr., "Tests on the Stability of Steel Frames," Fritz Engineering Laboratory Report No. 276.9, Lehigh University, September 1961.
67. Yura, J. A., "The Effective Length of Columns in Unbraced Frames," AISC Journal, April 1971.
68. Yura, J. A., Discussion on "The Effective Length of Columns in Unbraced Frames," AISC Journal, January 1972.
69. Yura, J. A., "Stability of Structures," C.E. 397 Lecture Notes, Department of Civil Engineering, The University of Texas at Austin.
70. Yura, J. A., and Galambos, T. V., "Strength of Single Story Steel Frames," Journal of the Structural Division, ASCE, Proc. V. 91, ST5, October 1965.
71. Zoetmeijer, P., "A Design Method for the Tension Side of Statically Loaded Bolted Beam to Column Connections," Heron, Joint Publication of Stevin Laboratory and IBBC Institute, Vol. 20, No. 1, The Netherlands, 1974.
72. ACI Committee 318, "Building Code Requirements for Reinforced Concrete (ACI 318-71), American Concrete Institute, Detroit, 1971.

73. MacGregor, J. G., Breen, J. E., and Pfrang, E. O., "Design of Slender Concrete Columns," Journal of the American Concrete Institute, Proc. V. 67, No. 1, January 1970.